AD-A062 433 CIVIL ENGINEERING LAB (NAVY) PORT HUENEME CALIF F/G 8/11
SEISMIC LIQUEFACTION POTENTIAL.(U)
SEP 78 J M FERRITTO, J B FORREST
UNCLASSIFIED CEL-TN-1530 NL

1 OF 2
AD
A062433

LEVEL II

AD A062433

Technical Note

CEL

TN no. N-1530

DDC FILE COPY

title: SEISMIC LIQUEFACTION POTENTIAL

author: J. M. Ferritto and J. B. Forrest

date: September 1978

sponsor: Naval Facilities Engineering Command

program nos: YF53.534.091.01.423

CIVIL ENGINEERING LABORATORY
NAVAL CONSTRUCTION BATTALION CENTER
Port Hueneme, California 93043

78 12 18 017

Unclassified

SECURITY CLASSIFICATION OF THIS PAGE *(When Data Entered)*

REPORT DOCUMENTATION PAGE

READ INSTRUCTIONS BEFORE COMPLETING FORM

1. REPORT NUMBER: TN-1530	2. GOVT ACCESSION NO.: DN687101
3. RECIPIENT'S CATALOG NUMBER:	
4. TITLE *(and Subtitle)*: SEISMIC LIQUEFACTION POTENTIAL,	5. TYPE OF REPORT & PERIOD COVERED: Not Final; Oct 1977 – Mar 1978
	6. PERFORMING ORG. REPORT NUMBER:
7. AUTHOR(s): J. M. Ferritto and J. B. Forrest	8. CONTRACT OR GRANT NUMBER(s):
9. PERFORMING ORGANIZATION NAME AND ADDRESS: CIVIL ENGINEERING LABORATORY, Naval Construction Battalion Center, Port Hueneme, California 93043	10. PROGRAM ELEMENT, PROJECT, TASK AREA & WORK UNIT NUMBERS: 62760N; YF53.534.091.01.423
11. CONTROLLING OFFICE NAME AND ADDRESS: Naval Facilities Engineering Command, Alexandria, Virginia 22332	12. REPORT DATE: September 1978 13. NUMBER OF PAGES: 187
14. MONITORING AGENCY NAME & ADDRESS *(if different from Controlling Office)*: CEL-TN-1530	15. SECURITY CLASS. *(of this report)*: Unclassified 15a. DECLASSIFICATION/DOWNGRADING SCHEDULE:

16. DISTRIBUTION STATEMENT *(of this Report)*

Approved for public release; distribution unlimited.

Technical note, Oct 77-Mar 78,

17. DISTRIBUTION STATEMENT *(of the abstract entered in Block 20, if different from Report)*

F53534

YF53534091

18. SUPPLEMENTARY NOTES

192 p.

19. KEY WORDS *(Continue on reverse side if necessary and identify by block number)*

Liquefaction, earthquake, soil dynamics.

20. ABSTRACT *(Continue on reverse side if necessary and identify by block number)*

This report presents a summary of the factors causing seismically induced soil liquefaction. The report presents the current procedures in use to compute the liquefaction potential of a site. Risk analysis procedures are presented to better estimate the probability of liquefaction.

DD FORM 1 JAN 73 1473 EDITION OF 1 NOV 65 IS OBSOLETE

Unclassified

SECURITY CLASSIFICATION OF THIS PAGE *(When Data Entered)*

Library Card

Civil Engineering Laboratory
SEISMIC LIQUEFACTION POTENTIAL, by J. M. Ferritto and J. B. Forrest
TN-1530 187 pp illus September 1978 Unclassified

1. Soil liquefaction 2. Earthquakes I. YF53.534.091.01.423

This report presents a summary of the factors causing seismically induced soil liquefaction. The report presents the current procedures in use to compute the liquefaction potential of a site. Risk analysis procedures are presented to better estimate the probability of liquefaction.

PREFACE

The purpose of this report is to provide guidance to design engineers and planners to minimize the damage from seismically induced soil liquefaction. The report treats liquefaction in detail and presents a guide for evaluation of liquefaction risk potential. It is not the intent of the report to be a design manual nor to be a state-of-the-art review. Hopefully, it lies somewhere between the two. Much data have been reviewed and presented to give the reader an appreciation of the complexity of the problem. Guidance and recommendations are given to assist in the interpretation and use of the information. Significant portions of this report have been previously published by the U.S. Department of Transportation, Federal Highway Administration, Washington, D.C. in FHWA-RD 77-127, "Determination of Seismically Induced Soil Liquefaction Potential at Proposed Bridge Sites," by J. M. Ferritto and J. B. Forrest.

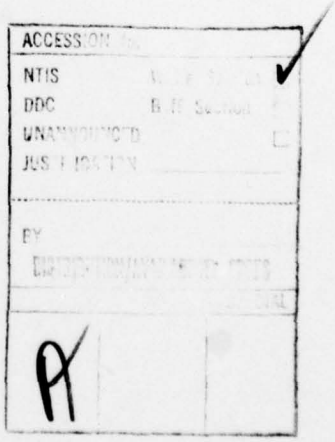

CONTENTS

Page

Chapter 1

INTRODUCTION

Cohesionless soils that may provide adequate structural support under ordinary circumstances may liquefy and settle during an earthquake. When liquefaction occurs, settlements may be increased by at least one order of magnitude over static settlements. The design engineer is particularly interested in the differential ground settlement caused by earthquakes. When a loose sand is subjected to seismically induced vibratory motion, it tends to decrease in volume. If it is saturated and drainage is impeded due to permeability limitations, then some of the interparticle stress is transferred to the water. The transferred load causes a rise in the pore water pressure (generally, the higher the intensity of vibration, the greater the potential for increase in pore water pressure). As the pore pressure approaches the confining pressure on a cohesionless soil, all shear resistance is lost. As a consequence the soil may settle, causing severe structural damage.

Soil borings taken at a site to provide information on existing soil conditions can, with proper analysis, give an indication of the liquefaction potential in earthquake-prone regions. However, a foundation system is normally designed to support the structure only under static loads. When soil liquefaction potential exists, the engineer generally has no means by which to evaluate the associated structural hazard (risk assessment) that could be caused by the earthquake.

Early quantitative studies of liquefaction generally pertained to natural earth slopes which became unstable from a gradual rise in the water table or tidal fluctuations which caused excess seepage pressures. Generally, a massive flow slide would begin, and the soil would come to rest only when the slope angle had been reduced to a few degrees. To explain this phenomenon Casagrande (1936) proposed the "critical void ratio" concept. Subsequently, following extensive studies of numerous flow slides along the banks of the Mississippi River, empirical rules were developed by the Corps of Engineers to predict the likelihood of occurrence of such flow slides.

During the last 10 to 15 years, the term "liquefaction" has been extended to include soil behavior under cyclic loading conditions caused by earthquake vibrations. While the end result - loss of soil strength - is the same whether caused by static or dynamic loading, the shear stresses leading to liquefaction under cyclic loading conditions may be much lower than those required to cause liquefaction under static loading conditions. Under continuous vibrations cyclic stresses cause an incremental buildup of pore pressure which progressively reduces the effective strength.

The strength that a sand can mobilize to resist shearing along a given plane depends on the effective or intergranular pressure on the plane and the effective coefficient of friction. The shearing resistance or strength τ_f may be written

$$\tau_f = \sigma' \tan \phi'$$

in which σ' is the effective stress and ϕ' is the effective angle of internal friction. In a saturated sand the intergranular normal stress σ' is defined as

$$\sigma' = \sigma - u$$

where σ = the total normal stress

u = the pore water pressure

Then

$$\tau_f = (\sigma - u) \tan \phi'$$

If water pressure u increases, while the total stress σ remains constant, the shear strength τ_f across any plane of failure decreases independent of the friction angle ϕ'. When $u = \sigma$, the $\tau_f = 0$; the sand has lost all its shear strength and is said to have liquefied. The sand is sometimes considered to have liquefied when large strains occur under applied loads. In soil mechanics practice, the term "soil liquefaction" may be defined by two criteria. One defines liquefaction in terms of loss of strength and material transformation of a granular material into a fluid. An alternate definition is expressed in terms of the amount of strain or deformation that is unacceptable from a structural viewpoint.

GENERAL PROCEDURE FOR EVALUATING SOIL LIQUEFACTION POTENTIAL

The method proposed by Seed and Idriss (1970) summarizes the usual engineering approach.

1. After establishing the soil conditions and the design earthquake, determine the time history of shear stresses induced by the earthquake ground motions at different depths within the deposits.

2. By appropriate weighting of the stress levels involved in the various stress cycles throughout the earthquake, convert the stress history into an equivalent number of uniform stress cycles and plot the equivalent uniform stress level as a function of depth as shown in Figure 1-1. By this means the intensity of ground shaking, the duration of shaking, and the variation of shear stress with depth within the deposit are taken into account.

3. By means of laboratory soil tests data, determine the cyclic shear stresses which would have to be developed at various depths to cause liquefaction in the same number of stress cycles as that determined in step (2), representative of the particular earthquake under consideration. The stress level required to cause failure under the equivalent number of cycles may then be plotted as a function of depth as shown in Figure 1-1.

4. By comparing the shear stresses induced by the earthquake with those required to cause liquefaction, determine whether any zone exists within the deposit where liquefaction can be expected to occur (induced stresses exceed those causing failure).

REFERENCES, CHAPTER 1

Casagrande, A. (1936) "Characteristics of cohesionless soils affecting the stability of slopes and earth fills," Contributions to Soil Mechanics, 1925-1940. Boston, Mass., Boston Society of Civil Engineering, 1940.

Seed, H. B., and Idriss, I. M. (1970) "A simplified procedure for evaluating soil liquefaction potential," Journal of the Soil Mechanics and Foundations Division, ASCE, vol 97, no. SM9, Sep 1970, pp 1249-1274.

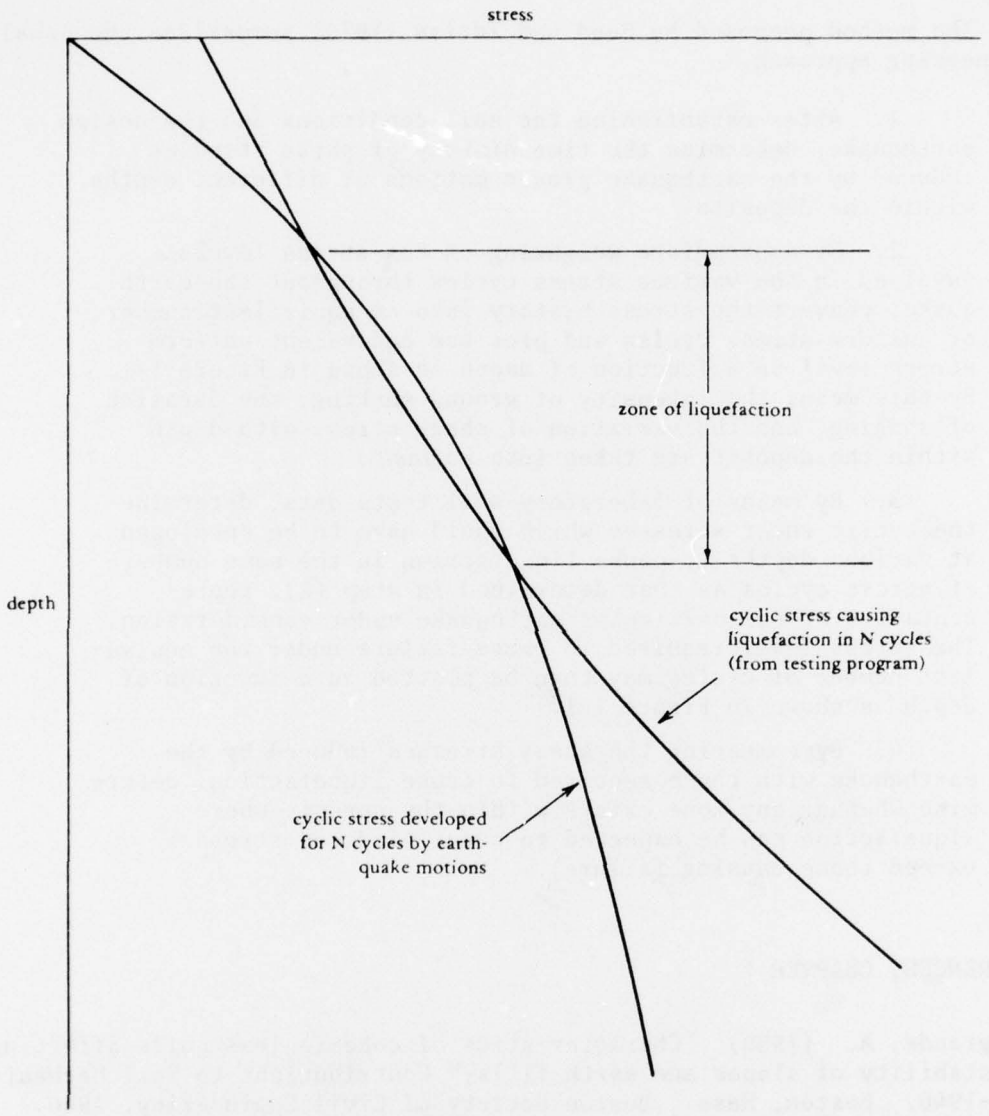

Figure 1-1. Method of evaluating liquefaction potential (after Seed and Idriss, 1970).

Chapter 2

SOIL PARAMETERS AFFECTING LIQUEFACTION

LIQUEFACTION PHENOMENA

The introductory portion of this chapter is directed toward the reader who does not have first-hand familiarity with soil response. To provide a better understanding of the behavior of saturated granular soils under load, typical test data on both quasi-static (monotonic) and cyclically loaded soil specimens are discussed. This will provide insight into the undrained shear behavior and liquefaction of saturated sands and provide an understanding of the liquefaction phenomenon more satisfactorily than that communicated by attempts at generalized or abstract definitions.

Monotonic Loading

Consider first the response of a saturated sand under monotonic loading in a standard undrained triaxial compression test. Three different types of material response (such as that presented by Castro 1969) will be illustrated qualitatively (Figures 2-1 and 2-2) to show the behavior of three specimens of sand at low, moderate, and high relative densities. Under increasing vertical (deviator) stress, each of these specimens exhibits a different type of behavior, depending upon its volumetric strain-shear stress coupling which is, in turn, a function of its initial density. The densest sample, test 3, does not undergo liquefaction, but exhibits an initial sharp rise in pore pressure with axial strain (Figure 2-1b); this corresponds to a decrease in effective stress (Figure 2-2) and a reduction in stiffness (deviator stress) (Figure 2-1a). The pore pressure rise and loss in stiffness is related to the tendency for the sand to initially compress under applied shear stress. At larger strains, the volumetric strain-shear strain coupling inherent in granular materials causes volume dilation to occur with attendant reduction in pore pressures (Figure 2-1b), increase in effective stress (Figure 2-2), and some increase in stiffness (see Figure 2-1a).

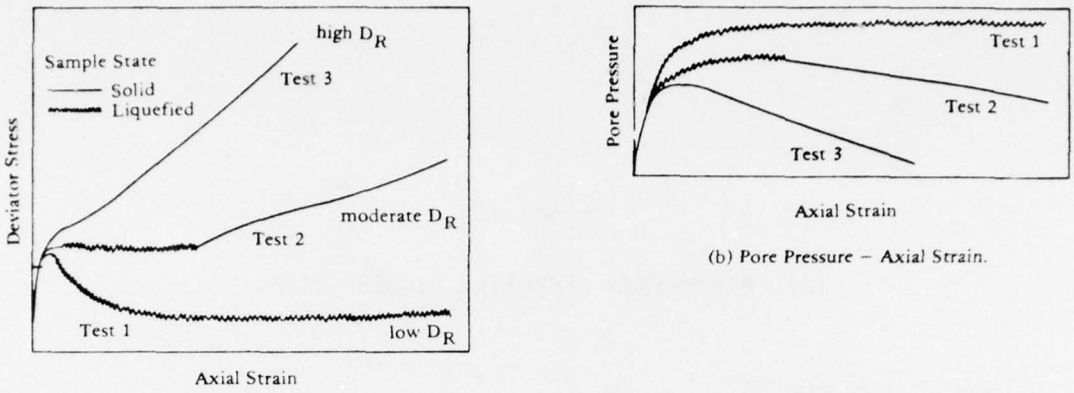

(a) Deviator Stress – Axial Strain.

(b) Pore Pressure – Axial Strain.

Figure 2-1. Stress-strain curves for three monotonically loaded triaxial compression tests on undrained sample of sand.

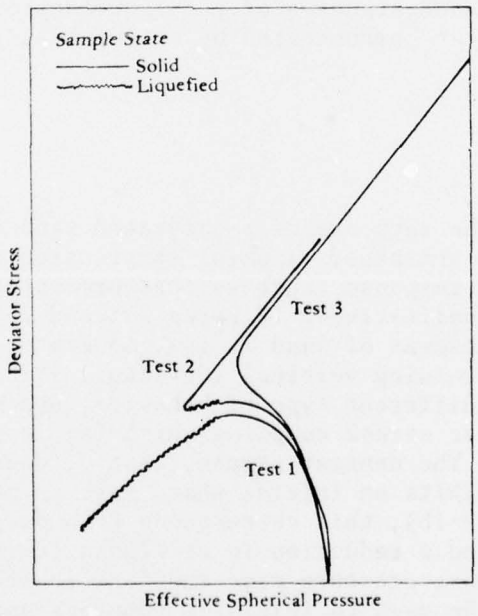

Figure 2-2. Stress paths for the three triaxial compression tests plotted in Figure 2-1.

Test 1 is an example of "unlimited flow." The specimen exhibits response behavior similar to that shown in test 3 up to the commencement of yielding (Figure 2-1a). Beyond this point, the specimen in test 1, because of its loose condition, does not dilate; hence, the pore water pressure approaches the initial confining chamber pressure, and the strength falls off dramatically.

The phenomenon of "limited flow" is demonstrated in test 2. In this test, initial specimen yielding (Figure 2-1a) did not occur until a considerable amount of strain (volumetric dilation) had occurred. This behavior is attributed to the fact that the density of the specimen was slightly looser than the specimen of test 3. At large axial strain, the test 2 specimen starts to dilate, causing a recovery of effective stress (Figure 2-2) and a re-establishment of some vertical load stiffness (Figure 2-1a).

Cyclic Loading Without Stress Reversal

Cyclically loaded tests demonstrate a different type of pore pressure generation and strength loss from those of monotonic tests. Figure 2-3 shows complete loss of effective stress, or unlimited flow, during cyclic loading of two triaxial specimens without stress reversal. With each application and release of the deviator stress, a residual pore pressure is generated, which results in an incremental reduction in the effective confining pressure. Following a certain number of cycles, depending upon the initial value of effective confining stress and the deviator (shear) stress level, a liquefaction condition is encountered, where the effective confining pressure is reduced to zero. It is interesting to note that the wavy lines in Figure 2-3 represent the yield envelope for these soil specimens; that is, the maximum obliquity or the shear-stress/normal-stress relationship for the material at failure. Such tests can also demonstrate "limited flow." The results of such a test are shown in Figure 2-4. During the first cycle of deviator loading (Path 0-ℓ-s-1) the specimen liquefied at a deviator stress of about 100 kN/m^2 and then restabilized by a dilation-associated increase in effective confining stress. Thereafter, the specimen remained within the stable domain as indicated by later load cycles (shown by numbers on the diagram). The reduction in deviator stress noted between successive cycles in Figure 2-4 is a result of the constant deviator load applied to a cross-sectional area that is increasing due to specimen deformation.

Information such as the foregoing has been used to support the conclusion that shear-stress reversals are necessary to produce repeated occurrences of liquefaction during cyclic loading (Seed and Lee, 1969).

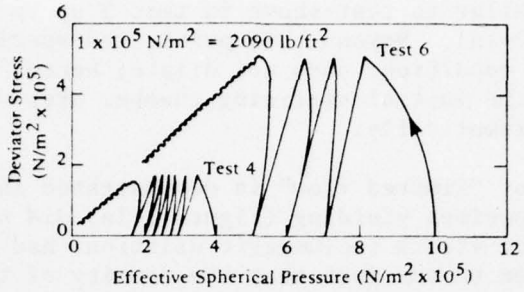

Figure 2-3. Liquefaction and unlimited flow generated by cyclic loading (stress paths from cyclically loaded triaxial compression tests without stress reversals). (Data from L. T. Youd, 1975, in work published by Earthquake Engineering Research Institute.)

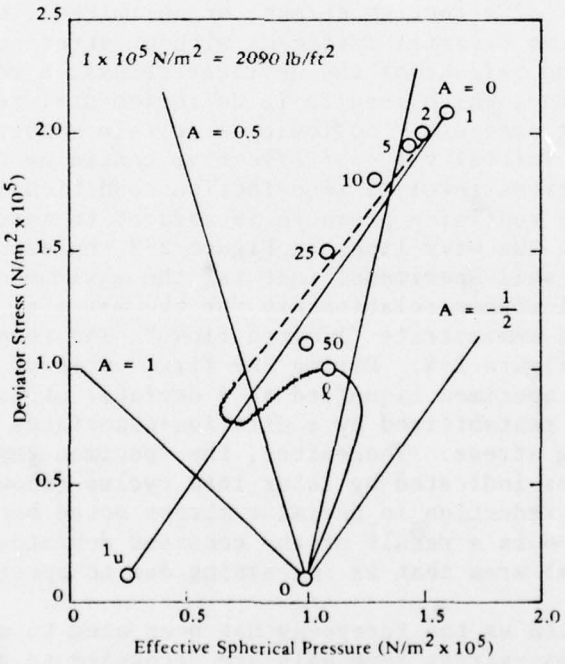

Figure 2-4. Stress path from a cyclically loaded triaxial compression test without stress reversals; liquefaction and limited flow occurred only during first loading (data found in L. T. Youd, 1975, in work published by Earthquake Engineering Research Institute).

It is interesting to consider Figure 2-4 in another context; the straight lines sloping upward from point 0 represent constant values of a parameter equivalent to Skempton's pore pressure parameter A. It is noted that, under initial loading, the value of A is approximately 0 (no pore pressure generation) and then increases to a value >1.0 (pore pressure generated faster than applied deviator stress) just prior to liquefaction (the specimen is attempting to compress). Thereafter, the specimen maintains an A value of about -0.5 during continued cycling. This latter implies that during application of compressive deviator load, the specimen is, in fact, dilating - hence, causing a negative change or reduction in pore pressure. During the unloading portion of the cycle, the specimen recovers some of its volume expansion, causing an increase in pore pressure. This is interesting in that it is not the normal behavior experienced under monotonic triaxial shear testing.

Cyclic Loading With Stress Reversal

In cyclic triaxial tests with stress reversals (i.e., those incorporating alternating tensile and compressive deviator stress), a type of limited flow referred to by Castro (1969) as cyclic mobility, is exhibited. A record from this type of test is shown in Figure 2-5. In this test the effective confining stresses are incrementally reduced by the increases in residual pore pressure with each load cycle. At some point, often during an extensional cycle, the effective confining stresses approach zero and liquefaction occurs. The specimen deforms rapidly, but then resolidifies from a dilatency-associated decrease in pore pressure. Upon the ensuing compressional cycle, the specimen again undergoes a period of limited flow, generally near peak deviator stress level, following which the specimen may again regain strength by a dilation-associated increase in effective stress. In this manner cyclic triaxial tests may undergo increasingly larger alternating vertical strain increments with each half-cycle, until the integrity of the specimen is completely destroyed.

The response of the soil specimen shown in Figure 2-5 suggests an initial value of an equivalent Skempton pore pressure coefficient A* during a double-amplitude strain cycle of about 0.2. This factor then increases progressively up to about 0.5 at large strain amplitudes. Replotting the data of Figure 2-5 in Figure 2-6 shows one interpretation of what is occurring in detail. The specimen, initially under an effective stress σ_3 undergoes a gradual increase in pore pressure, resulting in a decrease in average effective confining stress. At the same

*Skempton's A was not defined for situations involving stress reversals. The use of an equivalent "A" is introduced here as an aid to characterizing the soil response.

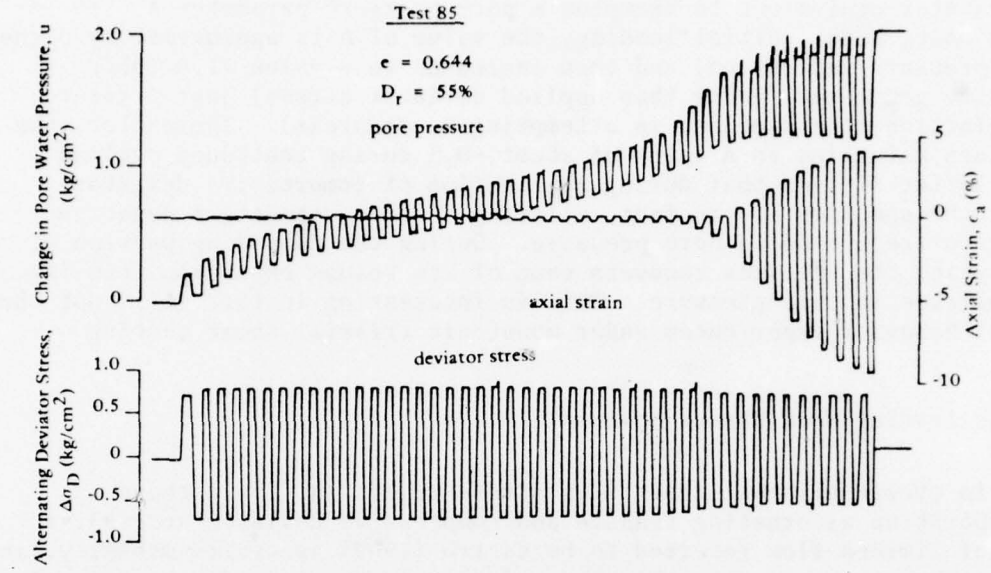

Figure 2-5. Data from a triaxial test on medium-dense Ottawa sand (from "Soil Dynamics Liquefaction of Sands," by W. L. Finn, p. 104, Figure 3, in Proceedings, International Conference on Microzonation for Safer Construction Research and Application, sponsored by American Society of Civil Engineers, 30 Oct-2 Nov 1972).

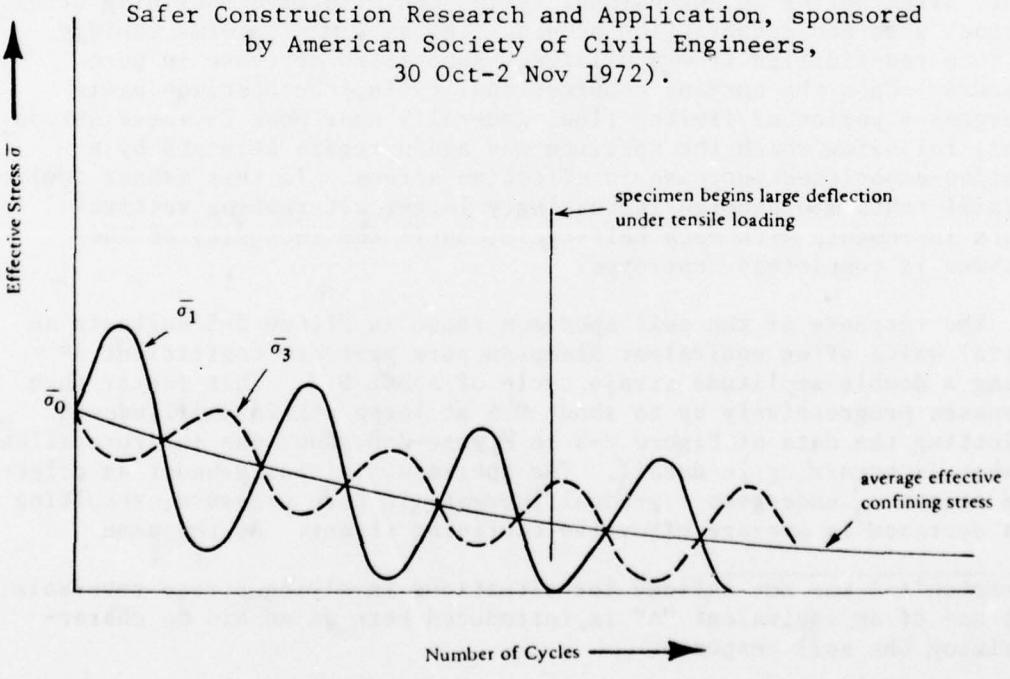

Figure 2-6. Plot of data in Figure 2-5.

time, the pore pressure coefficient A is gradually increasing, reducing the amplitudes of the vertical stress oscillations but increasing the magnitude of the lateral stress oscillations. At some point (noted in Figure 2-6 and in this example during an extensional cycle), the effective stress value attempts to go into tension. Since granular material has no effective tensile strength, unrestrained deformation commences.

This way of looking at deformations during cyclic loading can provide additional insight into the complexity of soil response. For example, traditional interpretation of triaxial test results has indicated a strong relationship between strength and ratio of effective principal stresses. This ratio is a direct function of the total applied stress levels and the pore water pressure parameter A. For example, for typical cyclic triaxial tests (Seed and Lee, 1966) values of equivalent A less than 0.5 would mean a greater effective principal stress ratio during the extensional phase of the loading cycle than during the compressional phase. Hence, such specimens would be expected to commence undergoing large deformations first in tension. Figure 2-7 shows results from shake table tests (DeAlba, Chan, and Seed, 1975) on a medium dense sand layer under a uniform vertical surcharge following the occurrence of cyclic mobility. The motion of the table is shown in Figure 2-7, and the reponse of the specimen may be visualized in terms of the relative ballast displacement, Figure 2-7c. The pore pressure level, as well as the total of confining pressure and back pressure for reference, is shown in Figure 2-7a. This test illustrates the following behavior, commencing our observation with the ballast and the table off center at an extreme position. The table motion changes direction; and, since dilation has caused a temporary reduction in pore pressure, the soil behaves as a solid and imparts a motion on the ballast. As the table commences to catch up with the ballast, shear strain magnitude is reduced, the pore pressure rises, and liquefaction recurs. The ballast then remains essentially stationary until the table has passed through its center position and has again exerted a large relative deformation upon the sand – causing dilation, reduction of pore pressure, and regain of strength. The reverse of the table motion then imparts a new impulse to the ballast through the resolidified soil, and the reverse portion of the loading cycle occurs. Thereafter the cycle is repeated.

Although various other types of apparatus are available for studying liquefaction, the foregoing explanations serve to illustrate the most pertinent characteristics of laboratory behavior.

PARAMETERS DIRECTLY ASSOCIATED WITH LIQUEFACTION

The foregoing discussion dealt with some of the characteristics of liquefaction behavior. Some of the specific soil parameters involved will be considered individually.

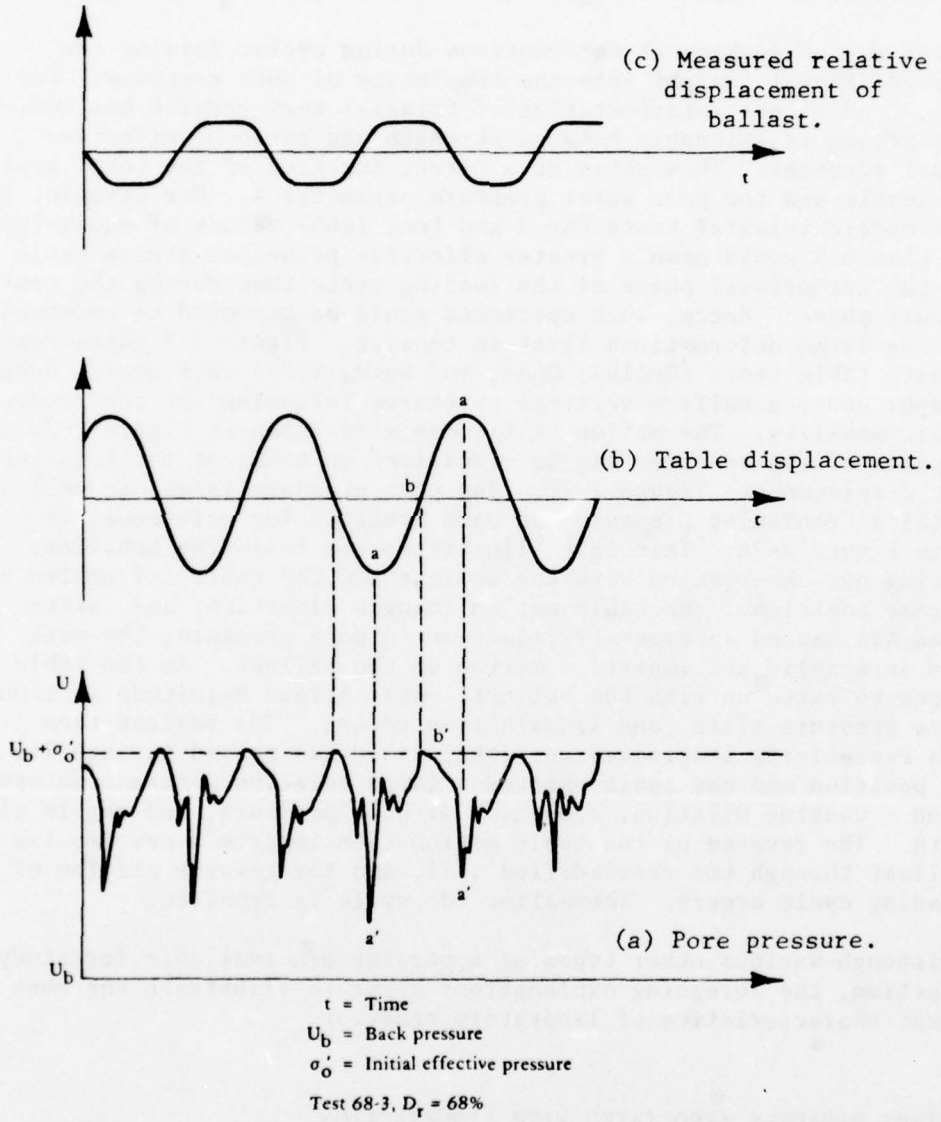

Figure 2-7. Specimen behavior after liquefaction (from DeAlba, Chan, and Seed, 1975).

The major factors associated with the liquefaction of saturated cohesionless soils appear to be: initial relative density, cyclic shear stress level, initial (static) shear stress level, initial effective confining pressure, drainage conditions, and number of cyclic shear stress applications, or duration of shaking. Of lesser importance are soil grain characteristics such as particle size, shape, and gradation. Soil structure, or fabric, as a result of previous history is known to be a significant parameter, but it is difficult to define or sometimes even recognize and, hence, its effects are difficult to quantify.

The foregoing factors reflect the physical properties of the soil, the initial stress conditions, stratigraphy in the ground, and the characteristics of the applied earthquake motions. Many of these items are difficult to control precisely in the laboratory and impossible to evaluate reliably in the field. A brief discussion follows on some of the more significant factors affecting liquefaction.

Dynamic Shear Stress Level

The fundamental concept of liquefaction is based upon the shear-strain/volumetric-strain coupling exhibited by soils. The process of pore pressure buildup, leading to liquefaction under cyclic loading, is dependent upon the volumetric strain response under applied shear stresses. The residual increment of pore water pressure generated by an applied dynamic shear stress cycle is, under undrained conditions, related to the shear strain which is, in turn, related to the magnitude of that stress cycle. In the field, the magnitude of dynamic shear stress may be ascertained from the acceleration levels, either by rough approximation or by more sophisticated computer analysis.

In the laboratory, the applied shear stress levels are defined according to the type of test. In triaxial testing the applied shear stress is taken as one-half the maximum deviator stress excursion (when symmetric stress reversals are used). This is the maximum dynamic shear stress experienced by the specimen and is exerted upon planes oriented 45 degrees from the vertical axis. For the simple shear test the applied shear stress is taken as that exerted on horizontal planes; this is not the maximum value of shear stress exerted upon the specimen. This situation is similar to that in other types of apparatus such as the hollow cylinder test. For shake table tests where shear stresses are applied by means of inertial forces, the horizontal shear stress varies slightly throughout the thickness of the specimen and usually is taken as the horizontal shear stress exerted at the bottom of the specimen.

Laboratory testing procedures generally simulate shaking in only one direction, whereas actual earthquake motions may have components in all three principal directions. The conclusion that the most critical stresses from a liquefaction viewpoint arise from vertically propagating horizontal shear waves appear to be relatively satisfactory. Vertical stress components are not considered significant since these are of a dilatational nature and completely absorbed by the pore water. For dynamic shear loading in a second horizontal direction, work by Pike, Chan and Seed (1974) have suggested that the allowable shear stress ratio should be reduced by 10%.

Characteristics of the Shear Stress Record

Earthquake ground motions generally consist of a number of randomly distributed peak stress cycles of varying shapes and magnitudes.

Difficulties involved in analyzing the various random earthquake ground motions have led to an attempt to express earthquake records in terms of an equivalent number of uniform stress cycles (Lee and Chan, 1972). The number of significant cycles in a particular earthquake record depends directly upon the frequency content and the duration of loading. These, in turn, are related to the magnitude of the earthquake, the distance to its epicenter, and the nature of the materials through which the stress waves must propagate.

It has been noted by Peacock and Seed (1968) and Yoshimi and Oh-Oka (1975) that the frequency of vibration, at least within 0.17 to 12 cps, which covers the range of earthquake motions in overburden, is of secondary importance. Actual shape of the stress pulse used in laboratory test simulations has been found not to be critical; i.e., whether or not it is in the form of a sine wave, a saw tooth, or other form. It is common to present soil susceptibility to liquefaction in terms of number of uniform stress cycles causing liquefaction under a specified level of applied shear stress, as in Figures 2-8 and 2-9. As noted in these figures the number of stress cycles a specimen can withstand increases almost exponentially with a decrease in shear stress level for any constant confining stress level and relative density.

There are some weaknesses in simulating random earthquake motions in terms of uniform cycles. For example Martin, Finn and Seed (1975) note that the tendency for dry sands to undergo volume changes is a direct function of dynamic shear strain level. But dynamic shear strain level is a function of soil modulus of rigidity G, which in turn depends upon the effective confining stress level and, hence, the pore water pressure generated. Since the pore pressure level existing at the time of application of a specific peak is very important, the relative position

of any peak in a sequence of loading cycles is significant. The previous discussion on the effects of stress reversals also suggests that the peculiar characteristics of the loading history (i.e., the symmetry of the stress record, etc.) may be significant. Ishihara, Tatsuoka and Yasuda (1975) note that ground motion inputs in which the maximum peak occurs early are less critical than input records for which the peaks are more uniformly distributed (i.e., vibratory as opposed to shock loadings).

Relative Density

The relative density of a soil appears to be one of the major factors regarding liquefaction potential of cohesionless sands. Relative density is stressed here rather than absolute density since it is actually the pore volume of the soil compared to its minimum and maximum possible pore volumes that is of significance. The denser a soil, the lower is its tendency toward volume contraction during shearing; the lower is the pore pressure which will be generated; hence, the more unlikely to liquefy. This increased liquefaction resistance with increased density is illustrated in Figure 2-8.

Relative density can be controlled in the laboratory using reconstructed samples; however, in typical field situations with complex stratification, relative density may lose its meaning. (A factor such as relative density has meaning only in uniform soil conditions; actual experience shows that natural soil deposits are quite often very heterogeneous.)

It is also conceivable that there is an upper limit of relative density D_R, above which a soil under field behavior will either no longer tend to compress and generate pore pressures or will, immediately upon commencing yielding, undergo volume increases which prohibit liquefaction. Based on specific site data taken from the 1964 Niigata earthquake, Kishida (1969) concludes that these soils are not likely to liquefy at relative densities above 75%. Although cyclic mobility (temporary loss of strength) can occur at relative densities up to 100%, it is thought that negligible distortions occur in this range at least prior to any drainage or pore water redistribution (Castro and Poulos, 1976).

It is impossible to define an upper limit to D_r beyond which liquefaction will not occur; nevertheless, it appears realistic that for a value of D_r above about 80%, liquefaction damage could be considered improbable.

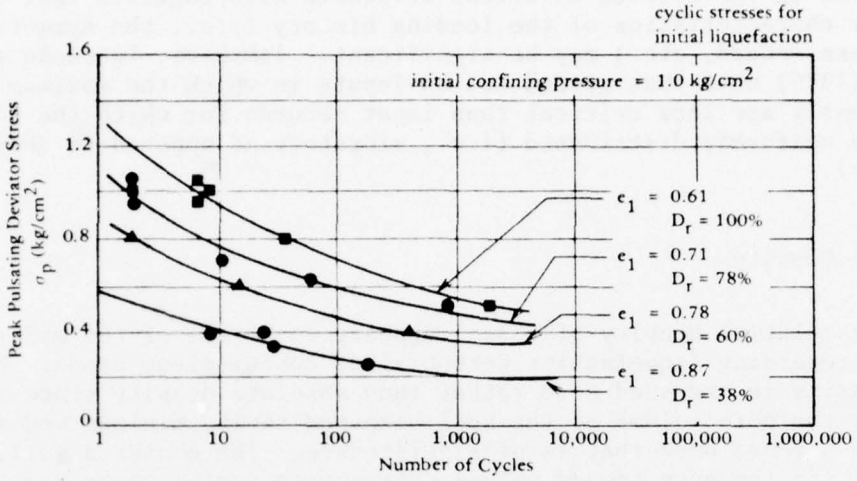

Figure 2-8. Effect of void ratio (from "Cyclic Stress Conditions Causing Liquefaction of Sand," by K. L. Lee and H. B. Seed, 1967, in Journal of Soil Mechanics and Foundations, ASCE, vol. 93, no. SM1, Jan 1967).

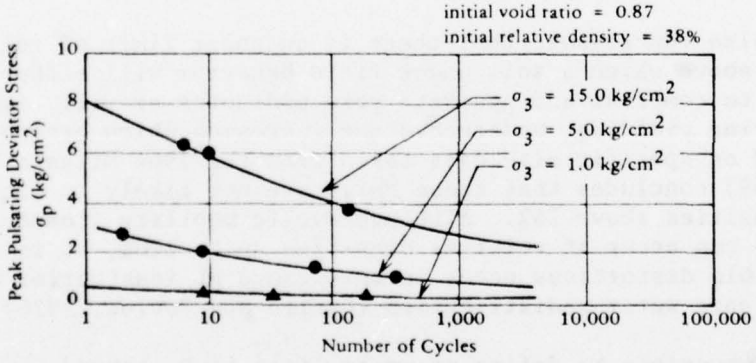

Figure 2-9. Effect of confining pressure (from "Cyclic Stress Conditions Causing Liquefaction in Sand," by K. L. Lee and H. B. Seed, 1967, in Journal of Soil Mechanics and Foundations, ASCE, vol. 93, no. SM1, Jan 1967).

Initial Effective Confining Stress

The resistance of a soil to liquefaction under cyclic loading has been noted to be a function of the effective confining pressure, prior to application of shear (see Figure 2-9). Although larger confining stresses would seem to enhance volume decrease and, hence, liquefaction (at least under monotonic loading conditions), under cyclic loading this is apparently more than offset by other factors such as the increased level to which the pore pressure must be generated to achieve instability; i.e., the increased strength.

Perhaps, for this reason, field observations of liquefaction of level ground have generally been limited to relatively shallow depths, in few cases below 50 or 60 feet. This is in agreement with Kishida (1969) who observed in the 1964 Niigata earthquake that liquefaction did not occur where effective overburden stress exceeds $2 kg/cm^2$ (27 psi). Although there is a trend toward reduced liquefaction potential at higher stresses, the observed field cases are very limited and cannot be expected to apply in all situations. Liquefaction evaluations must not omit regions simply because the effective pressure exceeds some empirical value.

In the isotropically consolidated triaxial test the effective confining stress prior to application of shear stress is the difference between the chamber pressure σ_3 and any back pressure applied to the pore fluid. For the simple shear test, the vertical effective pressure is generally used to represent the confining stress level. For the hollow cylinder tests, all components of the stress vector can, at least theoretically, be controlled so the effective confining stress level is often defined in terms of the effective volumetric stress, $1/3(\sigma_1' + \sigma_2' + \sigma_3')$.

Because of the difficulty of estimating lateral stress levels in the field, the vertical effective stress is used to define the level of confinement, but much work is available (Seed and Peacock, 1971) to indicate that the ratio of lateral to vertical stress K_o and, hence, the true degree of confinement actually existing in the field are of major importance.

The shear stress level required to cause liquefaction in remolded sand specimens at relative density less than 50% has been found to vary linearly with confining stress levels (Seed and Lee, 1966, and Peacock and Seed, 1968). Therefore it has been found convenient to normalize the effects of dynamic cyclic shear stress level with the value of initial effective confining stress. It is important to recognize that the use of this normalized ratio may not always be applicable to field conditions, particularly where strongly developed structure or cementation is present.

Thus, this simplification in treatment of liquefaction potential may not be valid in all circumstances. Soils near the ground surface, under very small degrees of confinement could have resistance to liquefaction in excess of that suggested from test results acquired at higher confining stress levels. This might be associated with material fabric or structure, or, in effect, equivalent to a previous stress history or over-consolidation pressure. That this exists for hydraulic fill sands has been suggested by Meehan (1976). For the above reasons, recovered soil samples as opposed to reconstituted specimens are preferred for cyclic shear testing, where possible. Where acquisition and testing of undisturbed samples are not possible, normalizing shear stress level with confining stress, based upon reconstituted samples is conservative in the surface layers and now forms a part of most simplified liquefaction treatments. This form of normalizing will be continued herein.

Drainage Conditions

The rate at which pore water pressure is permitted to dissipate from within a soil body has a major influence upon whether or not liquefaction can occur, particularly under cyclic loading (Wong, Seed, and Chan, 1974). Since the rate of pore pressure dissipation is known to be a function of the square of the longest drainage path, the detailed geometry of the soil profile is also important. A study of the interrelationships between different layer compressibilities and permeabilities on the occurrence of liquefaction has been presented by Yoshimi and Kuwabara (1973). This analytical study, based upon solutions to the Terzaghi one-dimensional consolidation problem, illustrates that liquefaction will propagate easily from a lower liquefied layer to an overlying one if the upper layer has a considerably lower compressibility or permeability than the initially liquefied stratum.

A useful tool for investigating the influence of drainage on potentially liquefiable soil strata is discussed by Seed, Martin and Lysmer (1975). A computer code, APOLLO, discussed in Chapter 4 provides a numerical, one-dimensional solution of the diffusion equation with a pore-pressure-generating term included to represent the earthquake-generated pore pressure increases. With this code it is possible to investigate the influence of length of drainage path, stratification, water table and saturation level variations, different permeabilities, compressibilities, densities, and other conditions.

Grain Characteristics

Under normal triaxial test conditions, fine silty sands appear to be most susceptible to liquefaction (Lee and Fitton, 1969). That fine-grained soils, with cohesive strength, are less vulnerable to liquefaction,

seems reasonable. With regard to coarser soils, however, this observation is apparently influenced by system compliance. For example, coarser materials permit greater membrane indentation into the specimen under the influence of the confining pressure σ_3. Upon generation of pore pressure under cyclic loading, some of this membrane indentation is reduced, permitting, in effect, a degree of internal drainage. Work by Wong, Seed, and Chan (1974), which attempts to account for system compliance, shows that grain size is of little significance in the liquefaction of soils under undrained conditions. Thus, the fact that coarser materials perform much better even in the laboratory is probably due to membrane indentation permitting some internal drainage and, hence, pore pressure reduction (see also Martin, Finn, and Seed, 1975). Nevertheless, since coarser soils permit a much more rapid dissipation of excess pore pressure when drainage is possible in the field (due to their greater permeabilities), the potential for liquefaction is, in fact, reduced. This reduced liquefaction potential for coarser materials such as gravels was much in evidence during the Alaska earthquake of 1964 (Figure 2-10).

Alternatively, fine-grained materials such as cohesive soils get their strength primarily from intermolecular bonds rather than gravity forces; thus, liquefaction in the classical sense does not apply. Sensitive or highly structured clays can nevertheless undergo dramatic reductions in strength under cyclic loadings. Occasionally the percentage of fines is used to define limits beyond which liquefaction will not occur. For example, the Army Corps of Engineers has established the criterion - based upon the stability of point bar deposits in the Mississippi River - that those sands with more than 10% passing the 200 sieve are not apt to liquefy due to river fluctuations.

Grain shape does not appear to exert a significant influence upon liquefaction susceptibility within the narrow ranges of clean sands normally studied (Lee and Fitton, 1969; Rocker, 1968). However, Castro (1969) has reported sharp angular sands with higher liquefaction resistance than normally expected. Again, this might be somewhat due to the effect of membrane indentation as discussed in the previous paragraph in relation to the effects of grain size. Another variable closely associated with this might be surface texture of the grains, but this factor has been explored even less thoroughly.

The effects of soil gradation on liquefaction have not been studied to any extent, but it does not appear to be a significant variable. The gradation of critical soils shown on Figure 2-10 do not suggest any sensitivity to range of particle sizes. Although a well-graded soil exhibits frictional characteristics superior to those of a uniform soil, the graded soil can undergo a much broader range of volume changes than can uniform materials and is apt to be much less permeable. Thus, it is difficult to predict which material would be superior on an intuitive bases.

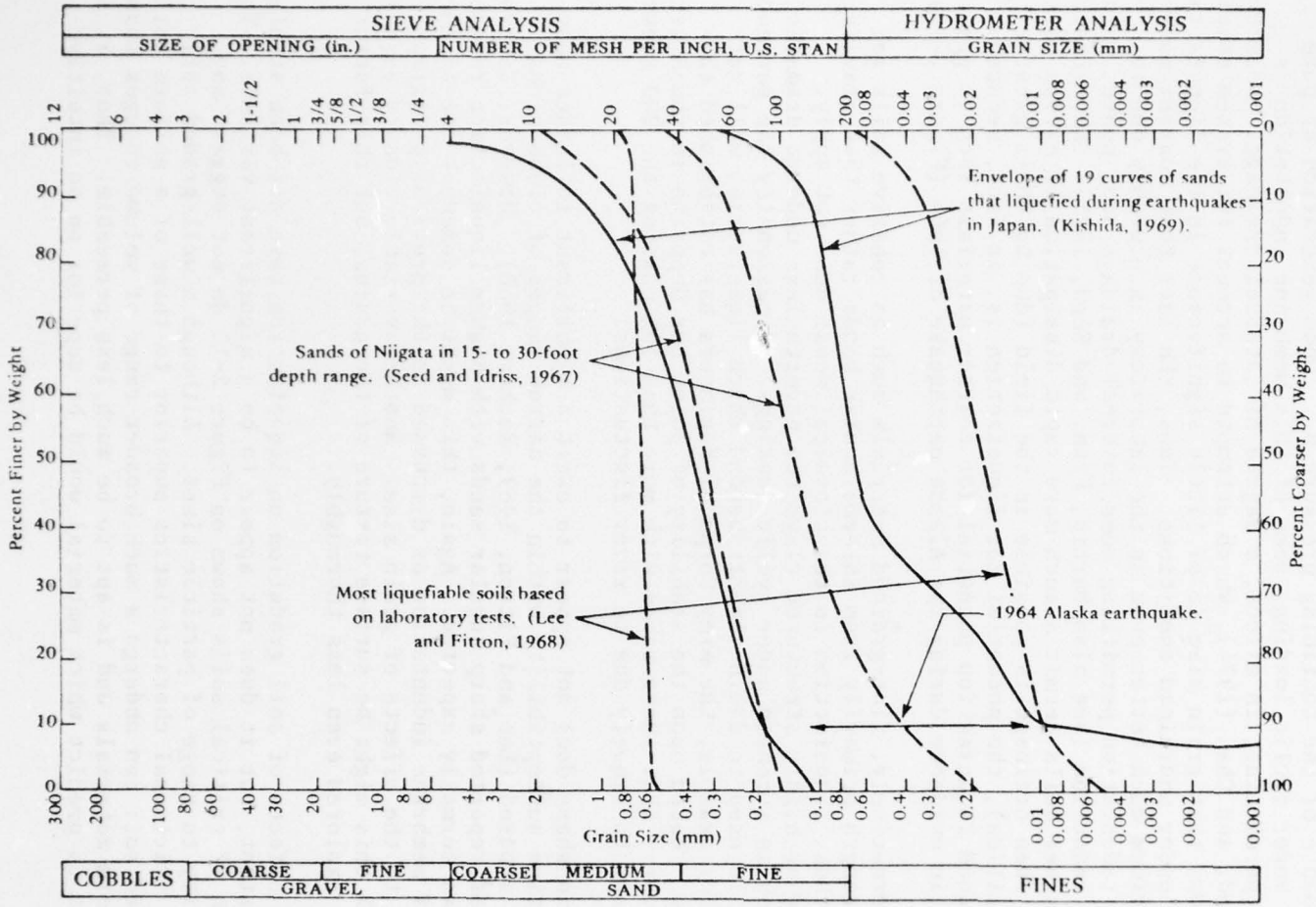

Figure 2-10. Soils susceptible to liquefaction (from "Evaluation of Soil Liquefaction Effects on Level Ground During Earthquake," by H. B. Seed, in a paper presented at the ASCE Annual Convention, Philadelphia, Pa., 27 Sep-1 Oct 1976).

Previous Stress History

The influence of previous stress history is of major interest in liquefaction studies. Finn, Bransby and Pickering (1970) present laboratory data showing that a sample, which has previously liquefied, is more susceptible to liquefaction. In Figure 2-11 data are shown on a specimen of sand at an initial relative density D_R of 50% and an initial effective isotropic confining pressure of 200 kN/m^2, which is subjected to cyclic loading with stress reversals. The specimen first underwent limited flow or cyclic mobility under the extensional portion of the 25th load cycle. This specimen then underwent several additional cycles wherein it reliquefied, flowed, and then restabilized (not shown in Figure 2-11). After a total of 29 load cycles, the specimen was permitted to drain, and was reconsolidated under an effective spherical pressure of 200 kN/m^2, which yielded a relative density D_R of 60%. Upon resumption of cyclic loading the specimen was noted as reliquefying during the extensional segment of its first loading cycle, in spite of its increased D_R value over that of the initial test squence. Based on such information, it is possible that the number of loading cycles required to cause liquefaction is substantially reduced by previous episodes of liquefaction.

This conclusion, which would appear to contradict intuition, is discussed herein to illustrate that judgment is necessary in interpreting test data. The foregoing test data might be explained in terms of the sample disturbance and material redistributions that can take place in laboratory tests due to local stress variation.

During the stress cycles leading up to initial liquefaction, the specimen would have developed weak zones which remained susceptible to liquefaction during later load applications. Seed, Mori, and Chan (1975) have provided data indicating that previous shear stress history can increase the resistance of a soil specimen to cyclic mobility.

Others have noted increases of up to 10 cycles to failure between reconstituted and undisturbed samples. Standard penetration tests taken by Kishida (1970) in the vicinity of the Tokachi Oki earthquake showed decreased dynamic penetration resistances in hydraulic fills immediately following the earthquake (probably due to pore pressure generation) but increased penetration resistance after 3 weeks. The most important conclusion that can be made is that the susceptibility to future liquefaction depends primarily upon the condition of the soil resulting from the past liquefaction and the intensity of the subsequent shaking. Less dense areas will be more susceptible; more dense areas less susceptible.

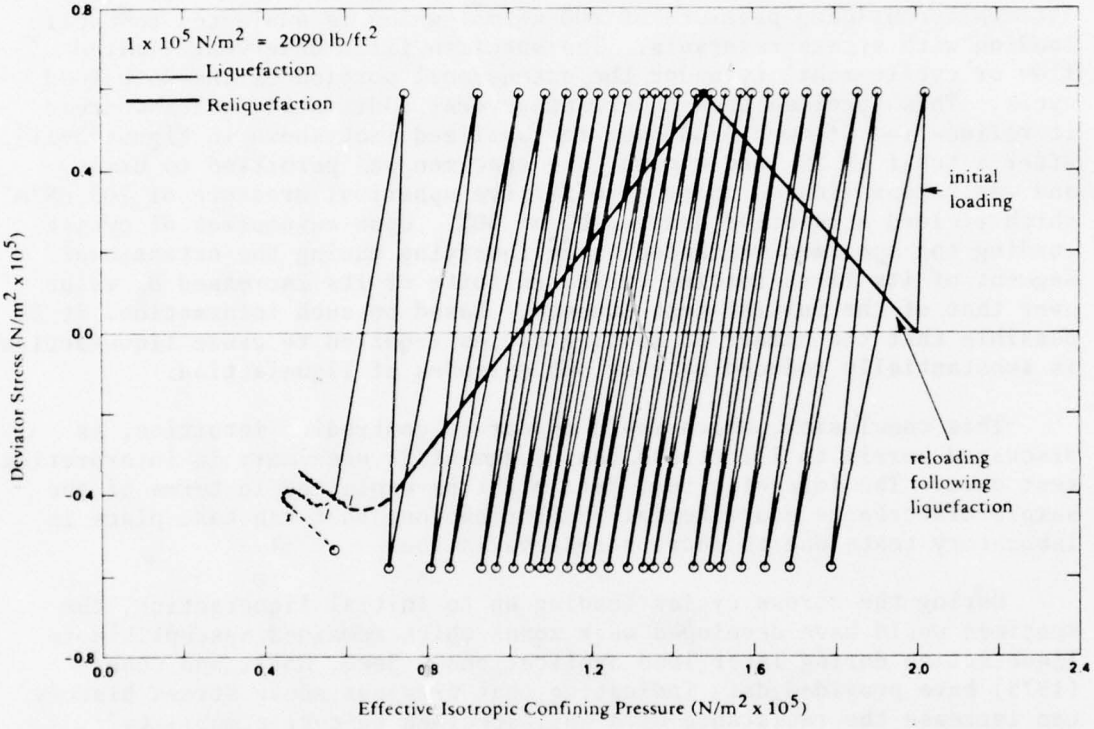

Figure 2-11. Stress paths from cyclically loaded liquefaction and reliquefaction tests on Ottawa sand sample (sample underwent liquefaction and limited flow in both tests)(from "Effect of Strain History on Liquefaction of Sand," by W. D. L. Finn et al. in Journal of Soil Mechanics and Foundations, ASCE, vol. 96, no. SM6, Figure 6, Jun 1970).

SUPERIMPOSED STATIC SHEAR LOADS

Current laboratory techniques for evaluating the liquefaction resistance of soils to earthquake loading (other than those directed toward specific dams) have considered only horizontal soil layers; i.e., situations where initial static shear stresses on the horizontal plane, due to any imposed loading, are minimal. Studies for evaluating the liquefaction potential of soils in dams have considered the effects of initial static shear stress. However, these studies are somewhat empirical, are site specific in nature, and involve extensive triaxial testing. Current laboratory techniques used for other liquefaction studies have considered it conservative and sufficiently accurate to neglect the effects of the initial static shear stresses caused by the foundation. Simple general methodologies for evaluating the effects of bridge foundations on liquefaction are not known to be in use.

Huang (1961) provides some insight into the behavior of sands during vibration by reporting pore water generation to be an inverse function of initial static principal stress ratio. This would suggest that at least for some levels of applied dynamic stress, an initial static stress ratio reduces the tendency for cyclic mobility to occur. Obviously this tendency can persist only within a narrow region. Otherwise, one is faced with the untenable conclusion that the greater the initial static shear stress level existing prior to application of cyclic shearing, the greater the resistance to cyclic mobility.

As long as one is interested only in the free field situation, where shake table or simple shear tests are directly applicable, standard test data, including empirical correction factors (Peacock and Seed, 1968; DeAlba, Chan, and Seed, 1975), is satisfactory for liquefaction analysis. However, should one desire insight into the liquefaction potential in regions of foundation load discontinuities, such as beneath footings or steep slopes, liquefaction criteria based more upon these latter situations are desirable. It is necessary that a general approach to defining liquefaction criteria be developed that can utilize the available body of triaxial and free field oriented experimental data, but that can still be applicable to the situation near foundations and structures, where static shear loads are acting. Any parameters selected for defining the liquefaction potential near load discontinuities should, if possible, be general enough to incorporate the bulk of experimental results that are available for the cases not involving concentrated loads.

The shear stress levels causing liquefaction in the triaxial test, simple shear and shake-table tests have generally been measured upon planes without any initial static shear stresses (principal planes). Thus, there has been no necessity to consider initial static shear

stresses. Where initial static shear loads are acting on the plane of interest, prior to cyclic loading, questions arise such as, what is the significant shear stress to use for liquefaction evaluation and what is the influence of varying degrees of maximum stress reversal (Yoshimi and Oh-Oka, 1975). It is suggested that by considering the dynamic shear stress $\Delta\tau_I$ applied on the new major principal plane following application of any static shear stress increments, all the foregoing problems are avoided, and available experimental data is still applicable to areas of load discontinuity, such as beneath foundations or earth structures.

This stress $\Delta\tau_I$ is defined (for the simple shear or ring-torsion test) in Figure 2-12. Consider the series of concentric Mohr circles in Figure 2-12. Let the Mohr's circle with radius r_o represent the initial effective stress conditions on a soil element with horizontal effective stress $\sigma'_h = K_c\sigma'_v$, and vertical effective stress σ'_v. Application of a static shear stress $\Delta\tau_s$ to the horizontal plane results in the stress in the specimen now being represented by the larger Mohr circle with radius r_s, showing a rotation of the principal plane (formerly the horizontal plane) through the angle ψ. Now, superposition of a dynamic (cyclic) shear stress increment $\Delta\tau_d$, upon the horizontal plane results in a new Mohr's circle of varying radius r_s. Since the soil is saturated, only shear stress would be added to this effective stress diagram, even in the field. This causes dynamic shear stress increment $\Delta\tau_I$ applied to what was the major principal plane prior to application of $\Delta\tau_d$. It may be seen from Figure 2-12 that:

$$\Delta\tau_I = r_d \sin\theta$$

where

$$\theta = \tan^{-1}\left(\frac{\Delta\tau_s + \tau_d}{r_o}\right) - 2\psi$$

and

$$\psi = \tan^{-1}\left(\frac{\Delta\tau_s}{r_o + r_s}\right)$$

Here $\Delta\tau_I$ is defined for a dynamic stress increase $\Delta\tau_d$; however, it may be shown that for a dynamic stress decrease ($-\Delta\tau_d$ on the horizontal plane), the shear stress $\Delta\tau_I$ on the principal plane is of equal magnitude, but in the opposite direction.

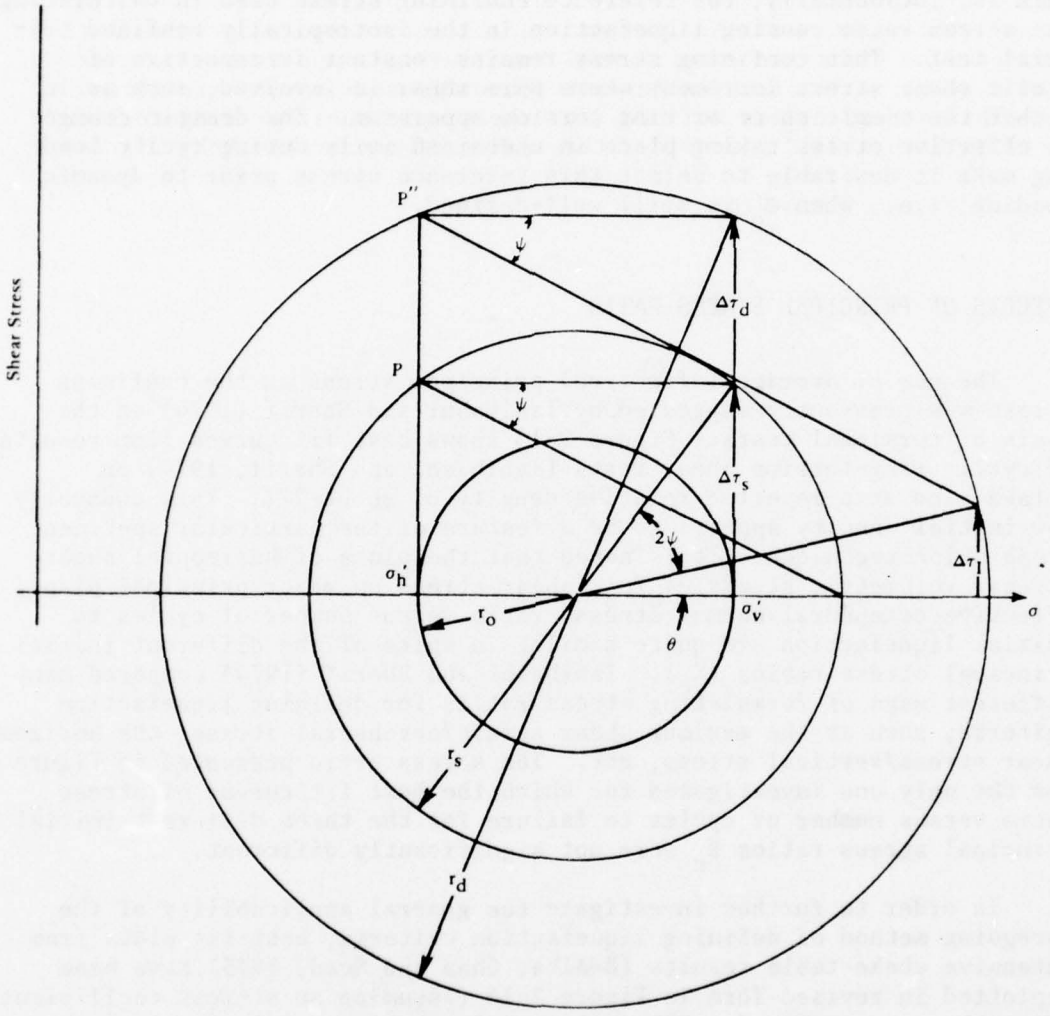

Figure 2-12. Illustration of critical shear stress $\Delta\tau_I$.

The reference plane for measurement of cyclic shear stress (i.e., the major principal plane) is established prior to dynamic loading. Therefore, it is desirable to select the reference confining stress at this stage also. To this end the average or volumetric effective stress $\sigma'_o = (\sigma'_1 + \sigma'_2 + \sigma'_3)/3$, acting prior to cyclic shearing, is selected. This is, incidentally, the reference confining stress used in calculating the stress ratio causing liquefaction in the isotropically confined triaxial test. This confining stress remains constant irrespective of static shear stress increment where pure shear is involved, such as in either the simple shear or ring torsion apparatus. The drastic changes in effective stress taking place in undrained soils during cyclic loading make it desirable to select this reference stress prior to dynamic loading; i.e., when σ'_o is still well-defined.

EFFECTS OF PRINCIPAL STRESS RATIO

The use of average (effective) principal stress as the confining stress was previously suggested by Ishibashi and Sherif (1974) on the basis of torsional tests. Figure 2-13 shows best fit curves from results of cyclic ring-torsion shear tests (Ishibashi and Sherif, 1974) on Ottawa sand at a reported relative density of about 27%. This unusually low initial density appears to be a feature of the particular specimen preparation technique. It is noted that the plots of horizontal shear stress/ volumetric stress, τ_d/σ'_o (shear stress on major principal plane/ effective octahedral normal stress) ratio versus number of cycles to initial liquefaction are quite similar in spite of the different initial principal stress ratios (K_c). Ishibashi and Sherif (1974) compared many different ways of formulating stress ratios for defining liquefaction criteria, such as the maximum shear stress/octahedral stress, the horizontal shear stress/vertical stress, etc. The stress ratio presented in Figure 2-13 was the only one investigated for which the best fit curves of stress ratio versus number of cycles to failure for the three different initial principal stress ratios K_c were not significantly different.

In order to further investigate the general applicability of the foregoing method of defining liquefaction criteria, best-fit plots from extensive shake-table results (DeAlba, Chan and Seed, 1975) have been replotted in revised form in Figure 2-14 (assuming an at-rest coefficient of earth pressure K_c of 0.45). Also shown in Figure 2-14 is the best-fit line from the triaxial data from Donovan (1974) (see Figure 2-15) for a relative density of 50%. The sands used for the bulk of the data appeared to be similar in grain size and angularity to the Monterey sand used by DeAlba, Chan, and Seed (1975). Although the shapes of the different data summaries differ slightly, the differences in stress ratios when calculated in the proposed way are negligible compared with the correction factors required for converting triaxial test data to the horizontal-shear/ vertical-stress ratio convention.

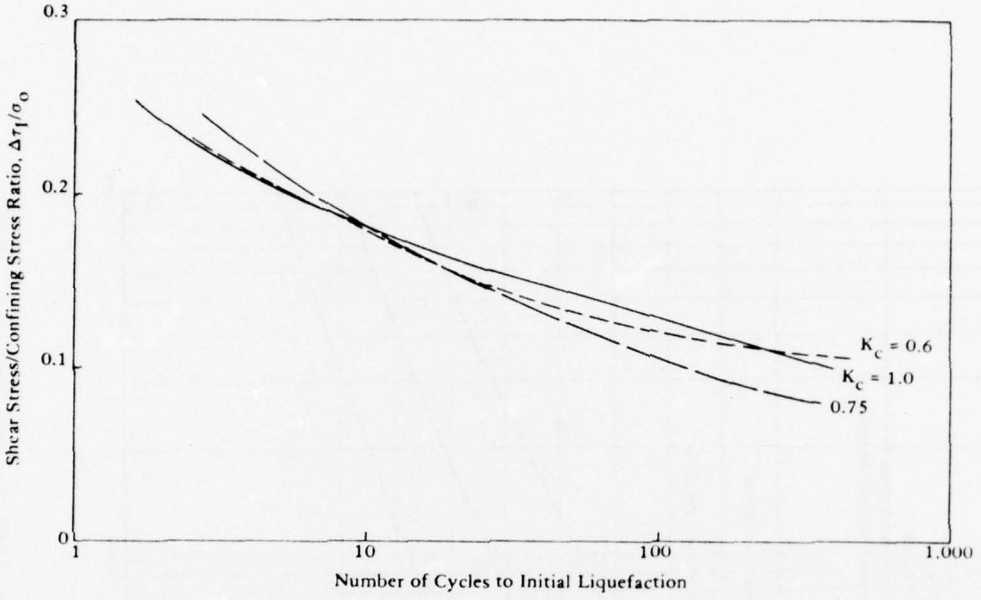

Figure 2-13. Results of ring-torsion shear tests on specimens having different initial principal stress.

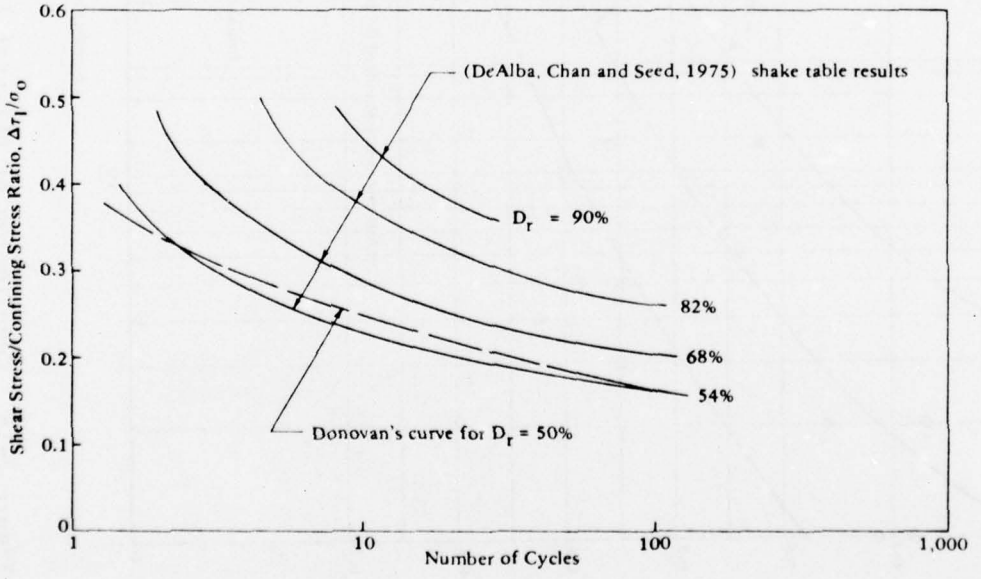

Figure 2-14. Comparison of stress ratios from triaxial and shake table testing.

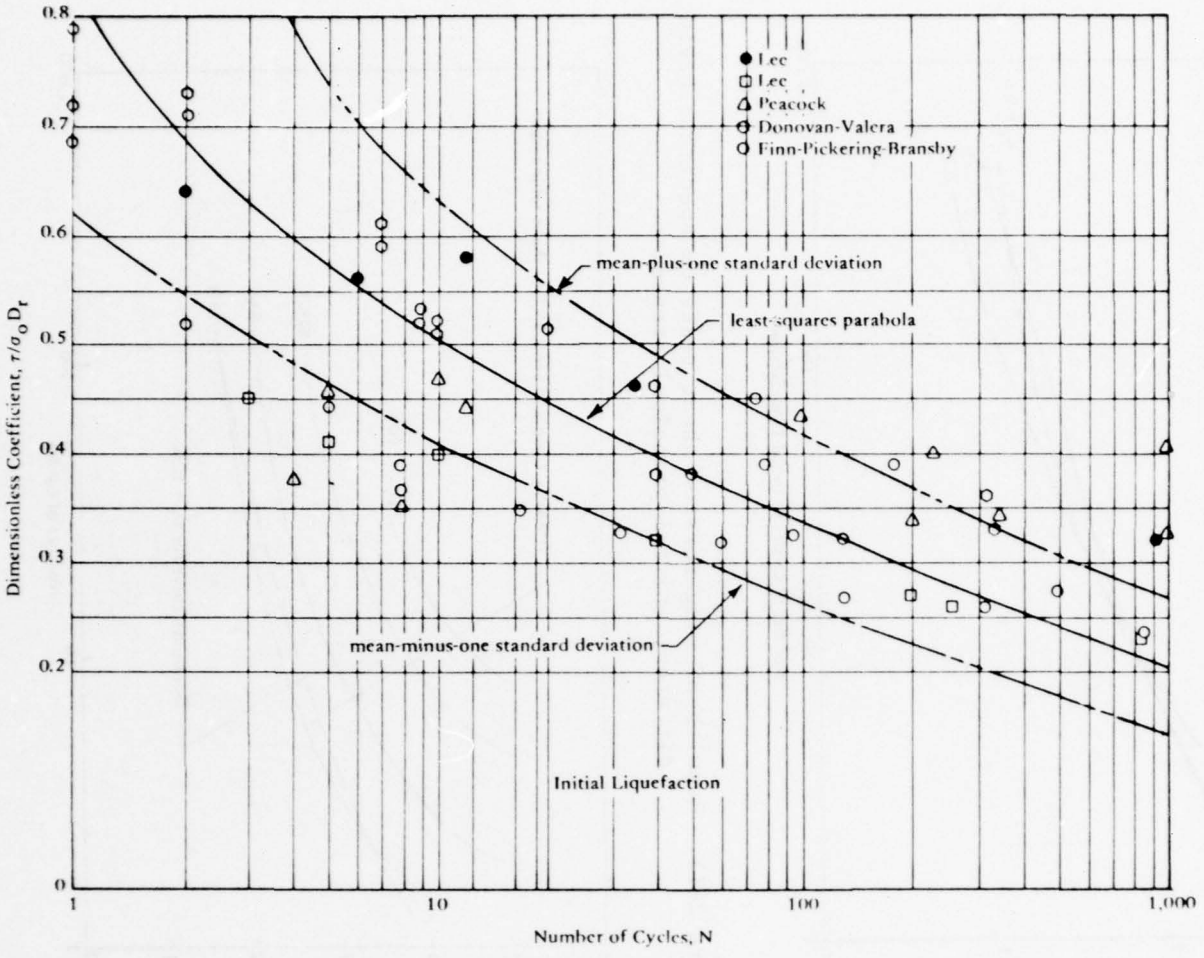

Figure 2-15. Compilation of triaxial liquefaction data (after Donovan, 1974).

The foregoing liquefaction data were generated for application to the free-field situation and deal with coefficients of earth pressure K_c from typical at-rest values of about 0.45 up to 1.0. It would be of major interest to study earth pressure coefficients of less than 0.45; i.e., approaching maximum obliquity or the failure envelope for the soil. Such cases can occur where initial static shear loads are applied. Unfortunately, little test data are available where cyclic loading is applied following an initial static load increment. One such paper dealing with this problem has been presented by Yoshimi and Oh-Oka (1975). Specimens of fine sand at a relative density of about 37% were cyclically loaded in a torsional shear device. Three series of tests were conducted; the first without an initially applied static shear stress increment and the other two with static shear stress increments sufficient to permit (1) only partial shear stress reversal and (2) no shear stress reversal on the plane of applied shear stress. Because of the different stress situations between the three series, conventionally calculated shear-stress/confining-pressure ratios (ratios calculated using shear stress level on the plane initially subjected to static shear stress increment) gave markedly different stress ratio versus numbers of cycles to failure relationships.

The best-fit curves from these data, plotted in terms of the stress ratio recommended herein, versus number of cycles to initial liquefaction are shown in Figure 2-16. Initial liquefaction has been taken as the point at which a major change in rate of shear strain commences. It was assumed that prior to application of the static shear stress increment the coefficient of earth pressure K_c was 0.45.

Following application of the static load increment it was assumed that the intermediate principal stress was unchanged but the minor principal stress was decreased by the same amount as the maximum principal stress was increased (Figure 2-12). This provided a reduction in the principal stress ratio K_c in the plane of maximum shear, and it is these revised values of K_c which are shown in Figure 2-16. Also shown on this figure are the curves from Figure 2-13 adjusted to the same relative density (D_r = 37%) as that of the Yoshimi and Oh-Oka (1975) data by multiplying the stress ratio by the factor 37/27. Although the plots on Figure 2-16 represent data on two different sands, both the reported gradations and the two testing devices appear quite similar.

The data in Figure 2-16 suggest that, for high K_c values, the use of the dimensionless coefficient recommended herein to define liquefaction provides an acceptable failure criterion for the various principal stress ratios. However, as the static K_c values fall below the normal free field situation (i.e., the Mohr circle representing the stress state approaches the yield envelope, as under a foundation), slightly reduced shear stress ratios may be required to cause liquefaction at a particular number of cycles. Yoshimi and Oh-Oka (1975) have noted that

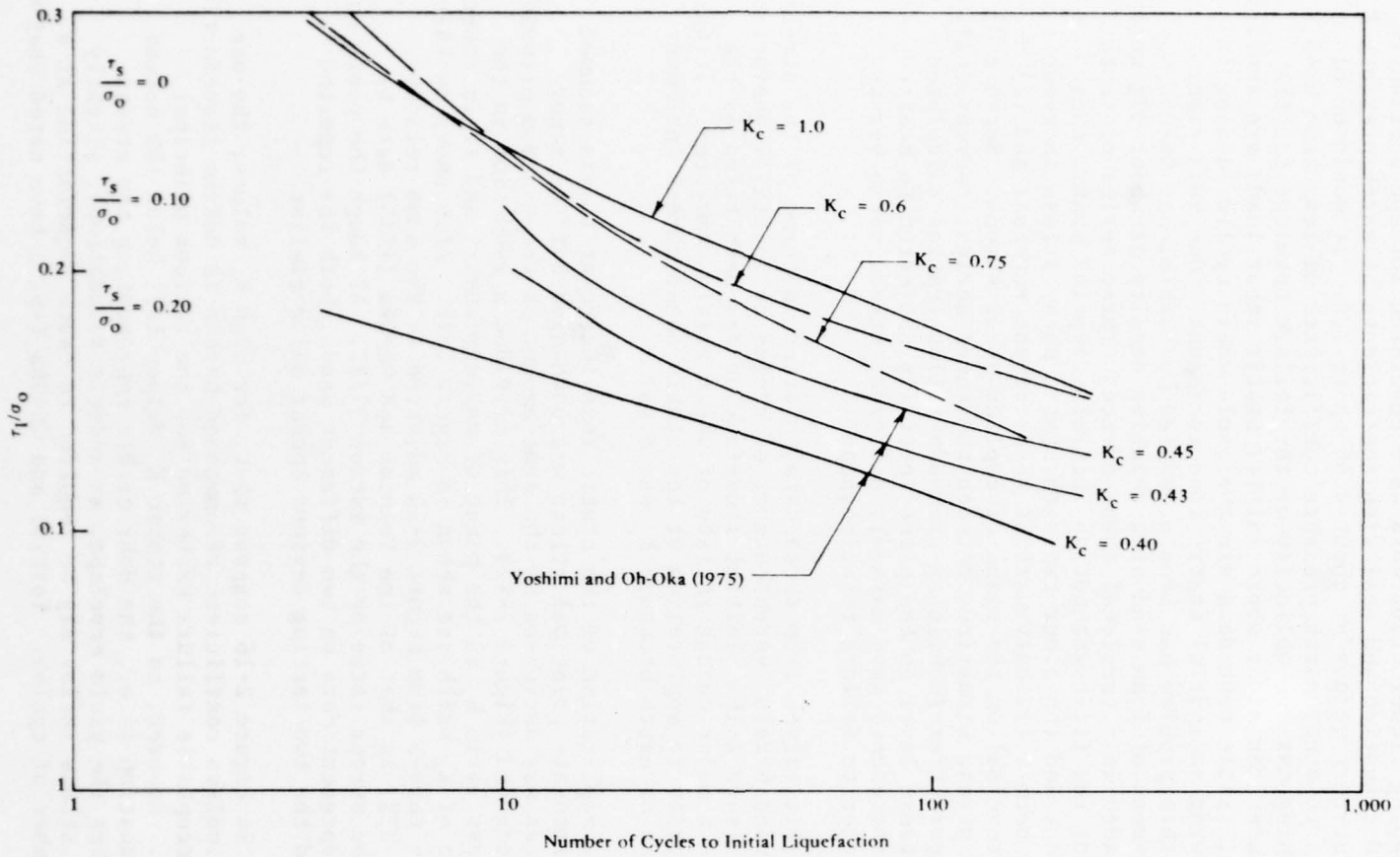

Figure 2-16. Liquefaction criteria applicable to regions with load discontinuities.

at the higher initial static stress levels, the number of cycles between initial liquefaction (marked increase in strain rate) and complete liquefaction (effective stress reduced to a negligible value) increases. Thus, the curves representing their data in Figure 2-16 would be in slightly better agreement with the Ishibashi and Sherif (1974) data were complete failure, rather than initial liquefaction, of concern. Actually, initial liquefaction by Ishibashi and Sherif (1974) appears to be closer to that defined as complete liquefaction by Yoshimi and Oh-Oka (1975).

Thus, liquefaction data can be presented in a format suitable to include the free field condition (away from concentrated loads) with horizontal soil layers, as has been generally considered, but also to include soil regions beneath load discontinuities. By plotting the ratio of dynamic shear stress generated on the major principal plane (prior to dynamic shearing) to average volumetric stress versus the number of stress cycles to liquefaction, cyclic triaxial tests can be used to provide an envelope of the liquefaction strength under fou ndation loads. By using the recommended format for plotting cyclic load data on specimens upon which initial static shear stresses are acting (K_c reduced to below a normal free field value of about 0.45), a more stringent criterion for liquefaction prediction may be identified for application beneath foundation loads.

The foregoing discussion attempted to provide insight into the liquefaction phenomenon. Various factors influencing the liquefaction potential were discussed with the aim of providing background to enable the engineer to use judgment in carrying out liquefaction hazard evaluations. The following portion of this chapter will deal with general soil reponse characterizations. These latter soil properties are those commonly used to define soil behavior from an engineering mechanics point of view.

PARAMETERS INDIRECTLY AFFECTING LIQUEFACTION

There is a family of soil parameters which, while not related to the liquefaction process directly, do influence the liquefaction potential. These are the response parameters which dictate how a soil will respond to applied stress. For example, since volumetric changes and, hence, liquefaction potential can be related to the distortional strain levels which a soil undergoes (Martin, Finn, and Seed, 1975), the shear stiffness or modulus of rigidity G of a soil under a specific load level is of particular concern. Earthquake motions can be either amplified or attenuated, depending upon characteristics of the soil profile (and its interaction with the frequency content of the disturbing earthquake) which, in turn, depends upon the values of the stiffness and damping parameters involved.

Since many treatments of earthquake-induced liquefaction deal with vertically transmitted horizontal shear waves, one approach to analysis requires only a value for the shear modulus G, together with a damping coefficient, to account for the energy absorption of the soil. Extensive experimental work dealing with these two parameters has been carried out by Seed and Idriss (1970), and Hardin and Drnevich (1970). These studies permit characterizing the shear response parameters of soil in terms of the basic soil index properties and the existing stress and strain states. For example, the shear modulus value for clean granular soils is related to void ratio, mean effective stress, maximum cyclic shear strain amplitude, and number of loading cycles (some soils have an additional dependency upon overconsolidation ratio, degree of saturation, and plasticity index). Soil damping, particularly in cohesionless soils, is at least partially due to relative movements between soil particles and, hence, is hysteretic. The contribution by dry friction to the damping ratio should be substantially independent of strain rate. Nevertheless, for analytical expediency all damping is represented by an equivalent viscous damping. Thus, selection of a damping coefficient makes the damping ratio a function of frequency. As long as the ratio of applied frequency to resonant frequency is not much greater than one, this appears to be acceptable even though it is strictly true only at resonance. For soils, damping is generally specified as a percentage of critical damping, and measured in terms of specific damping capacity, related to the ratio of the area within a hysteretic loop during a load cycle and the maximum stored energy during the cycle. Seed and Idriss (1970) have derived expressions for damping ratio as a function of strain level, number of cycles, frequency, mean effective stress, and the other index properties mentioned in reference to shear modulus G.

A number of investigations done on sandy soils have been summarized in Table 2-1. Recent work on shear stiffness and damping, with particular reference to sands, is being pursued by Silver and Park (1975) at the University of Illinois.

In all of this work, shear modulus G is noted as increasing with density and confining pressure and decreasing with shear strain amplitude. Damping coefficients on the other hand increase with shear strain amplitude and appear to decrease with confining stress and increased density.

Previous stress history is noted as increasing shear stiffness value and decreasing damping. One application of the use of the foregoing soil parameters to earthquake response analysis has been incorporated into a computer program SHAKE (Schnabel, Lysmer and Seed, 1972) in which the shear modulus of granular materials is treated as:

$$G = A\, K_2 (\sigma_n)^a$$

where A and a are constants, normally having values of 1,000 and 0.5, respectively, and K_2 is a function of the index properties of the soil and is an inverse function of the shear strain amplitude.

Typical variation of K_2 for sands based upon the results of various workers is presented in Figures 2-17 and 2-18, and a composite series of relationships for various relative densities is shown in Figure 2-19 (Seed and Idriss, 1970). Shear modulus measurements at very low strain levels are usually measured by shear wave velocity studies. For higher strain amplitudes, resonant column and cyclic triaxial, simple shear and hollow cylinder torsion tests are commonly employed.

It has been found (Seed and Idriss, 1970; Hardin and Drnevich, 1970) that shear modulus values at any strain level may be normalized in terms of maximum shear modulus to permit a generalized relationship for many soil materials to be collapsed into a single relationship. Such a relationship is presented in Figure 2-20 (Seed and Idriss, 1970).

Damping ratios, as mentioned, were found to vary as functions of soil index properties as well as the stress and strain states. Figure 2-21 shows the influence of friction angle, void ratio, coefficient of lateral earth pressure, and degree of saturation on a clean sand under a vertical effective stress of 1,000 psf (70 psi), based upon work by Hardin and Drnevich (1970). The influence of effective confining pressure is shown on Figure 2-22. Average values of damping ratio for an effective vertical stress of about 1 to 1-1/2 kg/cm^2 have been presented in Figure 2-23.

Although cohesive materials have been treated in the same format as granular materials, their soil models have not been found quite as satisfactory in this context. It is more expedient to normalize the shear modulus of clays in terms of the undrained shear strength S_u in the form of G/S_u versus shear strain amplitude. Data obtained by various investigations have been compiled in Table 2-2 and plotted in Figure 2-24. Again, it is possible to collapse the various shear modulus relationships into a single curve by normalizing them by the maximum value of shear modulus at infinitesimal strain (Figure 2-25). In this way, modulus values determined at very small strain levels, such as by measuring shear wave velocities in the field, can be used to predict the shear modulus under design loading conditions. Damping ratios for clays have been studied less extensively than for granular materials. However, a summary of the results of past studies is shown in Figure 2-26.

Little data are available for materials other than sands and clays, but available information indicates that coarser grained materials such as gravels may be expected to behave as sands (Seed and Idriss, 1970; Hardin and Drnevich, 1970). Figure 2-27 shows tentative modulus values for gravelly soils, but damping data is essentially nonexistent.

Table 2-1. Summary of Laboratory Investigations of Shear Moduli and Damping Ratios for Sandy Soils (from H.B. Seed and I.M. Idriss, 1970)

Type of Test	Soil Tested	Range of Strain		Range of Confining Pressure (psf)
		Shear	Axial	
Forced Vibration: Longitudinal Vibration	Sand		$<5\times10^{-3}$%	600 to 7,200
	Sand		$<5\times10^{-3}$%	450 to 7,500
	Sand		$<5\times10^{-3}$%	600 to 7,400
	Sand		$<5\times10^{-3}$%	600 to 7,200
	Sand, silty sand and clayey sand		$<5\times10^{-3}$%	1,000 to 3,500
Forced Vibration: Torsional Vibrations Solid Sample	Sand	$<10^{-2}$%		600 to 7,200
	Sand	$<10^{-2}$%		600 to 7,400
	Sand	$<10^{-2}$%		450 to 7,500
	Sand	$<10^{-2}$%		600 to 7,200
	Sand	$<10^{-2}$%		600 to 8,500
Forced Vibration: Torsional Vibration Hollow Sample	Sand	10^{-3} to 6×10^{-2}%		600 to 8,500
	Sand	10^{-3} to 6×10^{-2}%		500 to 1,800
Free Vibration: Cylindrical Sample	Sand		10^{-3} to 10^{-4}%	400 to 6,400
Triaxial Compression	Sand and gravel, silt and sand		2×10^{-3} to 5×10^{-3}%	400 to 1,800
	Sand, silty sand and clayey sand		5×10^{-3} to 0.1%	1,000 to 3,500
	Sand		10^{-1} to 1%	3,000 to 3,400
Simple Shear	Sand	3×10^{-2} to 0.5%		2,000
	Sand	10^{-2} to 0.5%		500 to 4,000

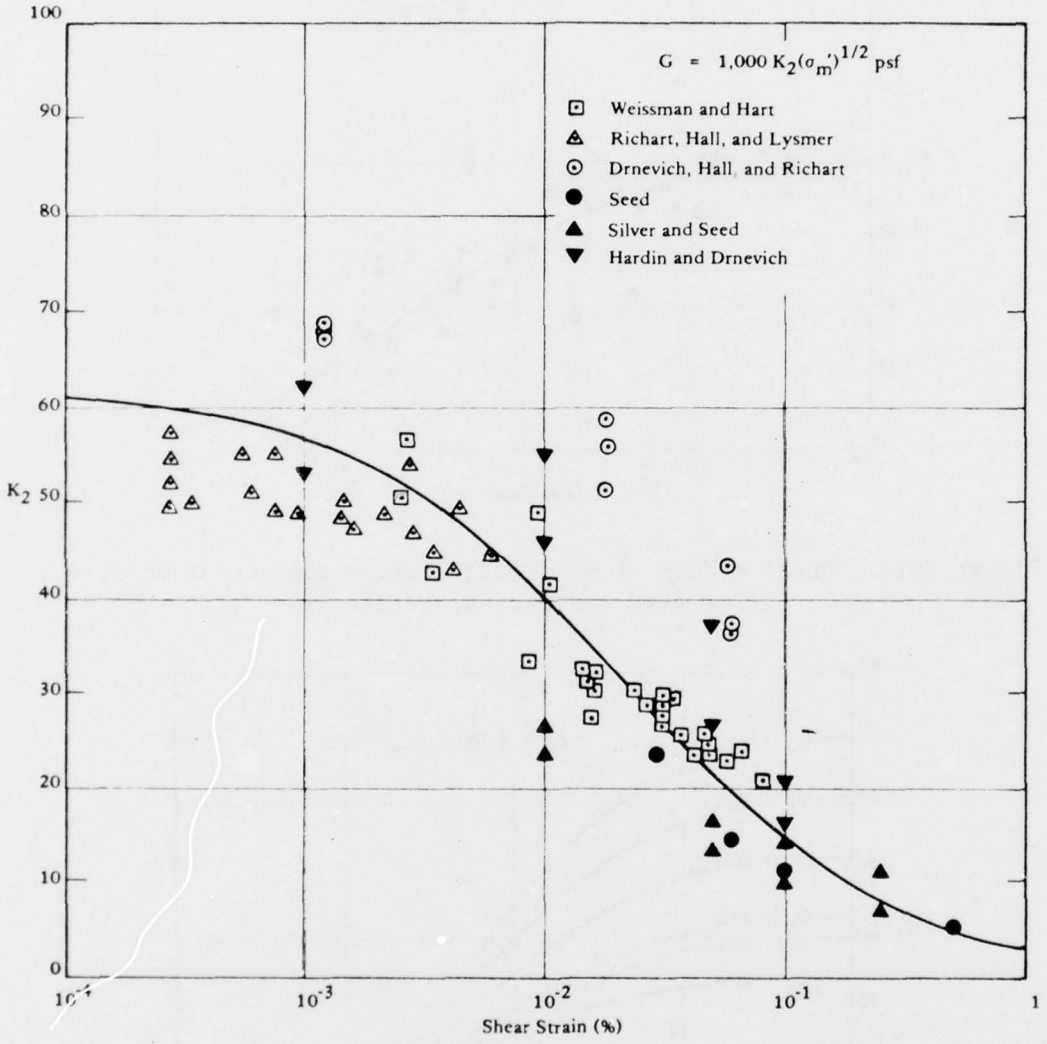

Figure 2-17. Shear moduli of sands at relative density of about 75% (from Seed and Idriss, 1970).

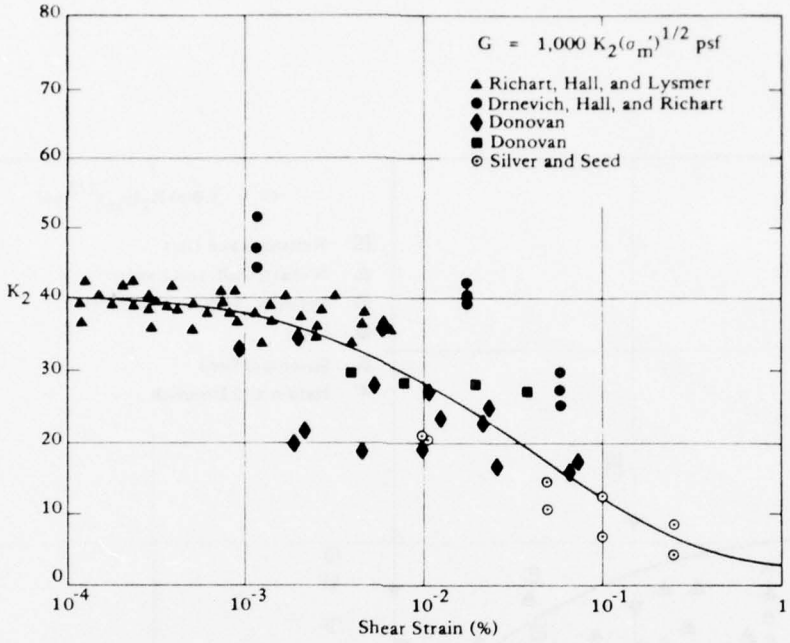

Figure 2-18. Shear moduli of sands at relative density of about 40% (from Seed and Idriss, 1970).

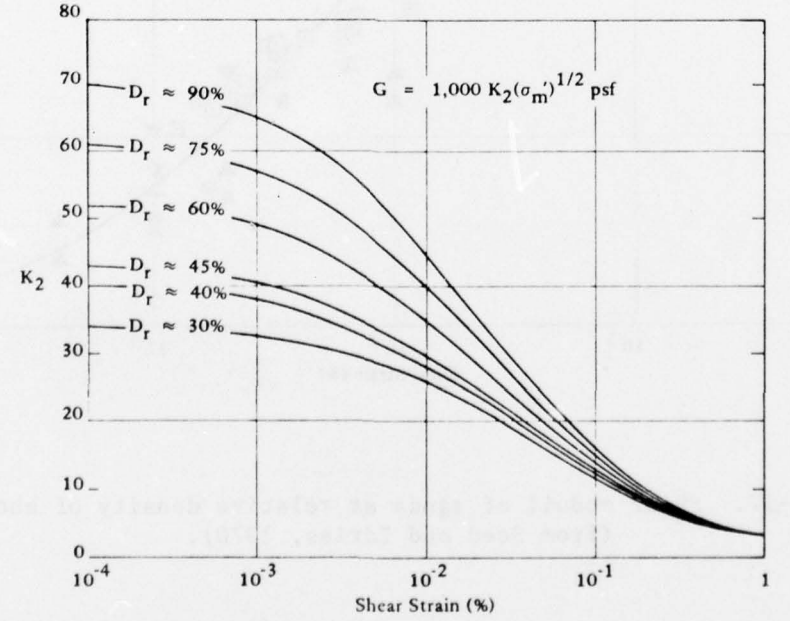

Figure 2-19. Shear moduli of sands at different relative densities (from Seed and Idriss, 1970).

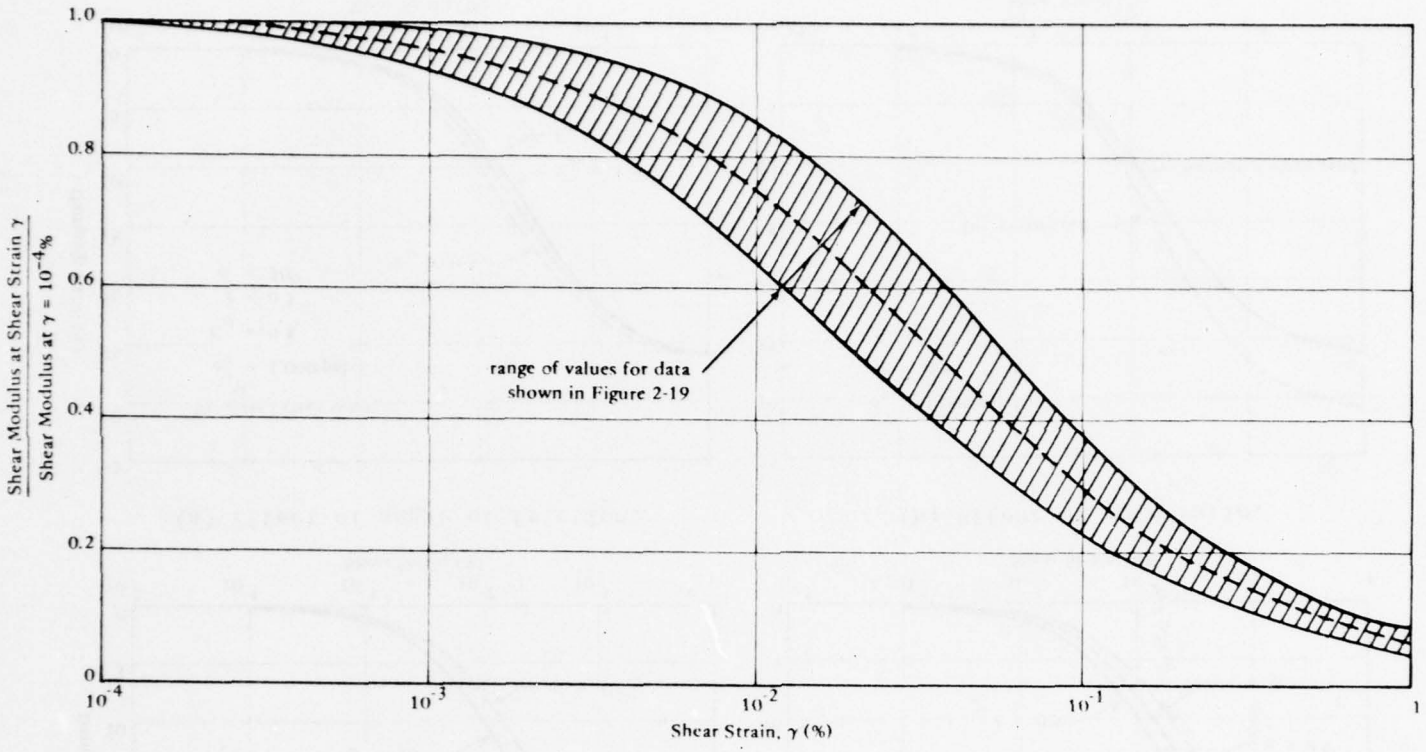

Figure 2-20. Variation of shear modulus with shear strain for sands (from Seed and Idriss, 1970).

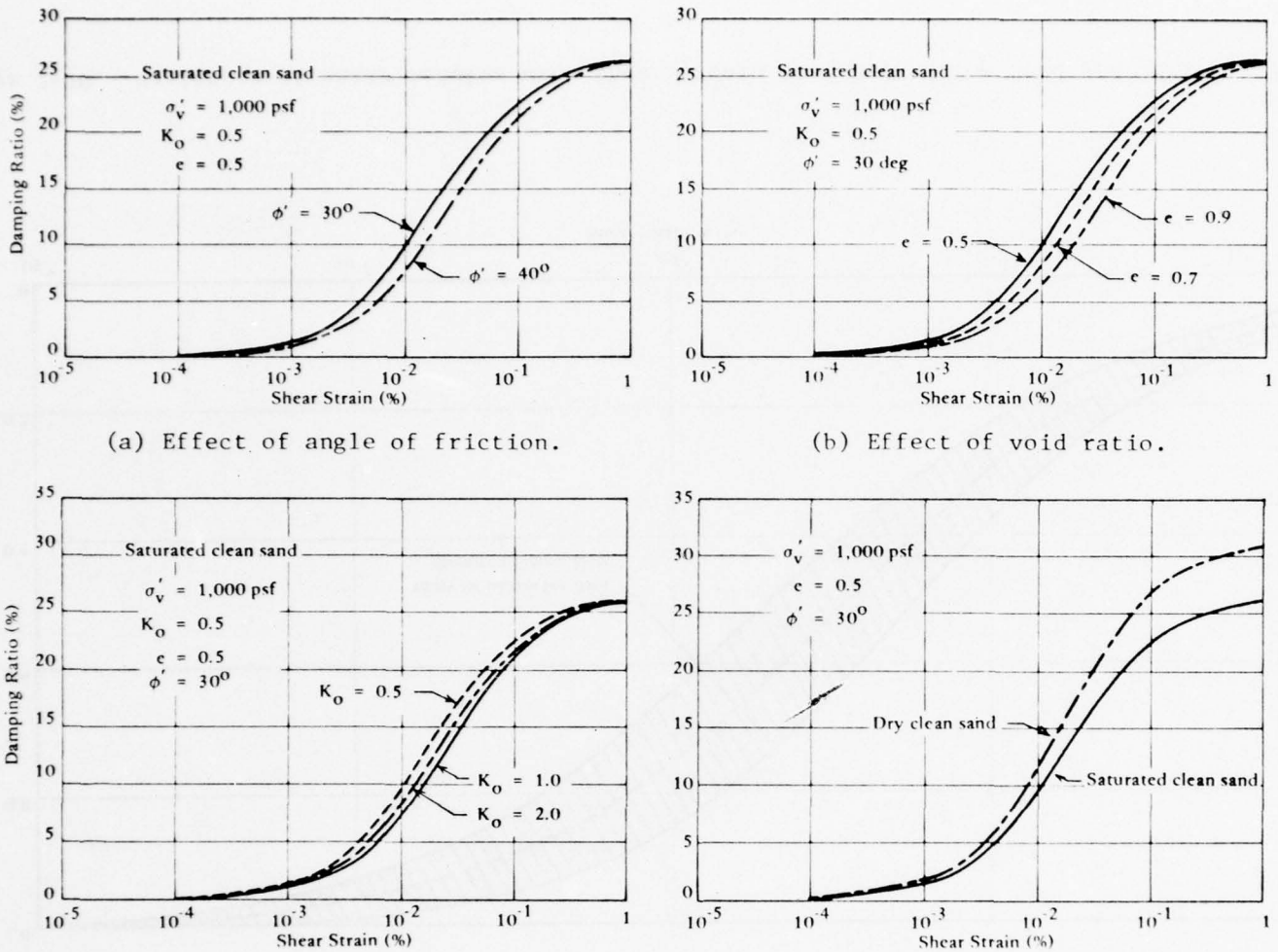

(a) Effect of angle of friction.

(b) Effect of void ratio.

(c) Effect of K_o.

(d) Effect of saturation.

Figure 2-21. Influence of various factors on the damping ratios for sands (from Seed and Idriss, 1970; based on Hardin and Drnevich expressions).

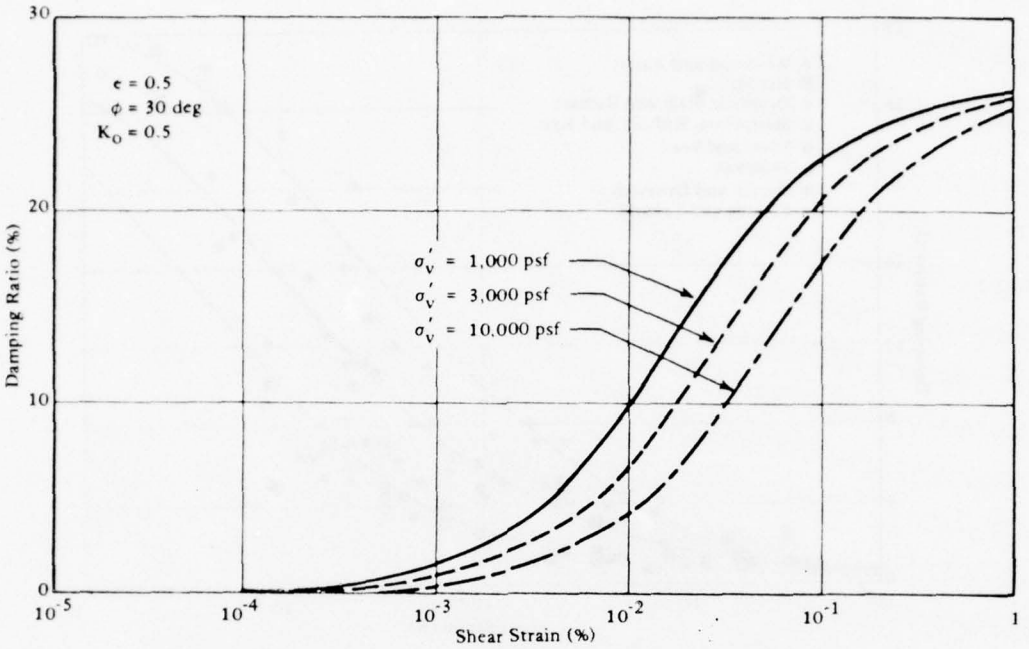

(a) Saturated sand (based on Hardin and Drnevich expressions).

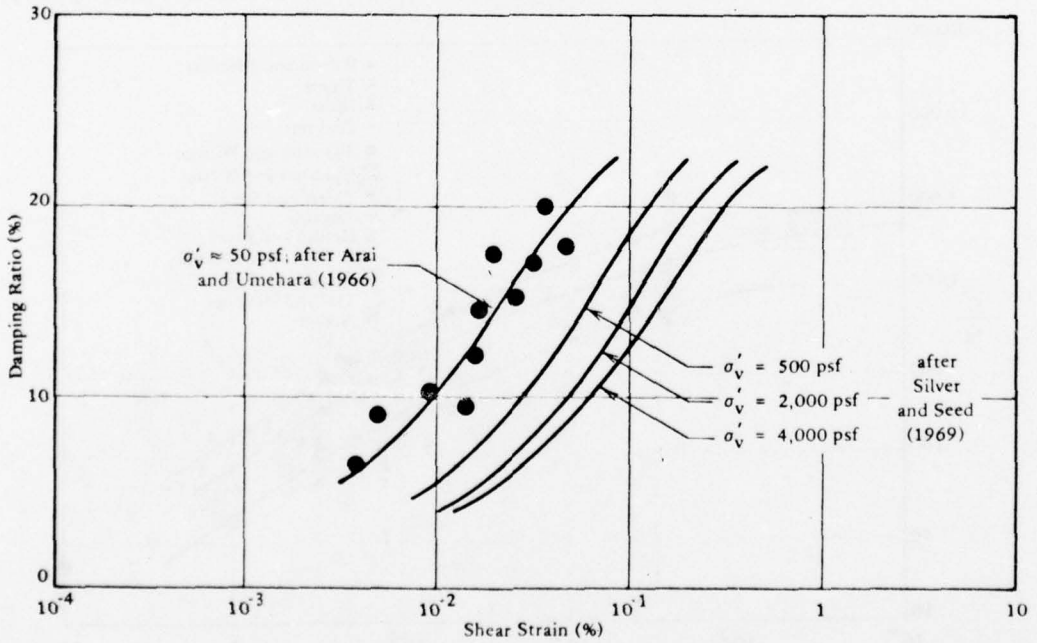

(b) Dry sand.

Figure 2-22. Influence of confining pressure on damping ratio (from Seed and Idriss, 1970).

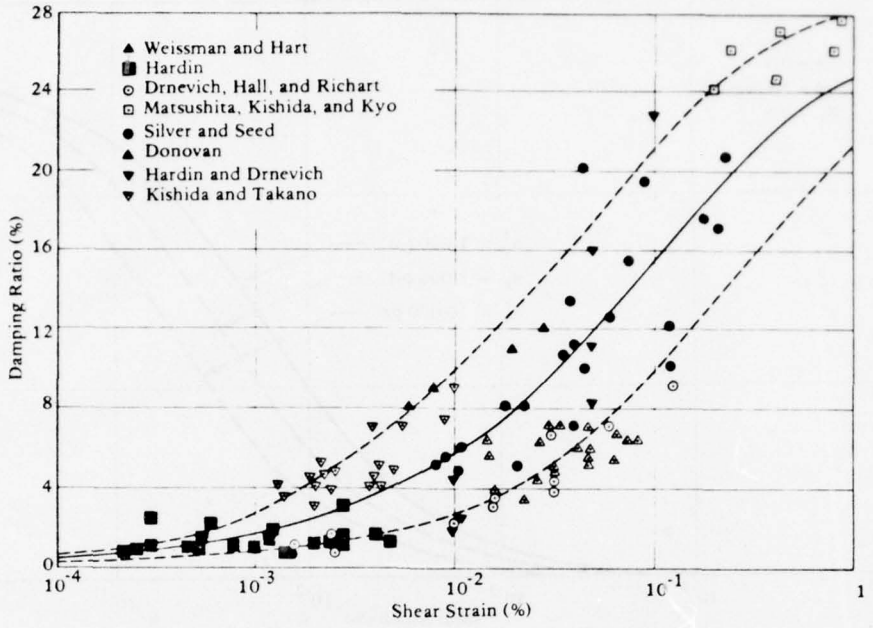

Figure 2-23. Damping ratios for sands (from Seed and Idriss, 1970).

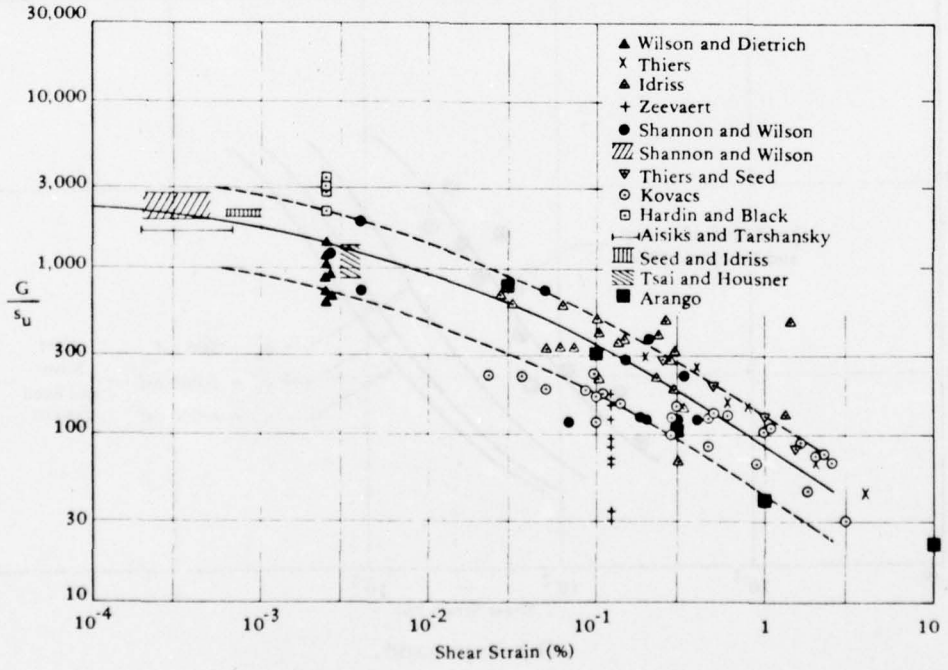

Figure 2-24. In situ shear moduli for saturated clays (from Seed and Idriss, 1970).

Table 2-2. Summary of Laboratory Investigations of Shear Moduli and Damping Ratios for Saturated Clays (from H.B. Seed and I.M. Idriss, 1970)

Type of Test	Soil Tested	Range of Strain		Range of Shear Strength (psf)	Data Correction Factor[a]
		Shear	Axial		
Field Tests					
Shear Wave Velocity	San Francisco Bay mud	$<10^{-3}$%		200 to 500	1.0
Compression Wave Velocity	Union Bay clay		$<10^{-3}$%		1.0
Laboratory Tests					
Free Vibration					
Longitudinal	Elkhorn Slough silty clay		3×10^{-2} to 2%	300 to 1,100	2.5
Shear	San Francisco Bay mud	2×10^{-2} to 0.5%		300	2.5
	Kaolinite/Bentonite mixture	5×10^{-2} to 2%		44 to 85	2.5
Forced Vibration					
Longitudinal	Cambridge clay		$\approx 2.5\times10^{-3}$%	1,080	2.5
	Mississippi gravels		$\approx 2.5\times10^{-3}$%	520	2.5
Torsional	Birch Bay clay	$\approx 2.5\times10^{-3}$%		1,000 to 2,420	2.5
	Montana clay	$\approx 2.5\times10^{-3}$%		6,000	2.5
Torsional (consolidated samples)	Whidbey Bay clay	$\approx 2.5\times10^{-3}$%		230 to 1,800	1.5[b]
	Silty clay	0.125%		800 to 1,500	1.0
	Edgar Plastic Kaolin	$\approx 2.5\times10^{-3}$%		1,400 to 1,800	1.0
Triaxial Compression	Ardmore clay		0.1 to 0.5%	–	–
	Ardmore clay		0.5 to 1%	–	–
	Union Bay clay		3×10^{-3} to 0.3%	200 to 880	2.5
	Silty clay		10^{-2} to 0.1%	–	–
	Webb Mark IV clay		0.2 to 1%	–	–
Torsional Shear	Georgia Kaolinite	3×10^{-2} to 0.2%		–	–
Simple Shear	San Francisco Bay mud	0.2 to 4%		300 to 400	2.5
	Kaolinite/Bentonite mixture	0.1 to 2.5%		44 to 85	2.5
	San Francisco Bay mud	0.1 to 3%		300	2.5

[a] Applied to modulus values to allow for sample disturbance.

[b] Sample disturbed slightly after consolidation.

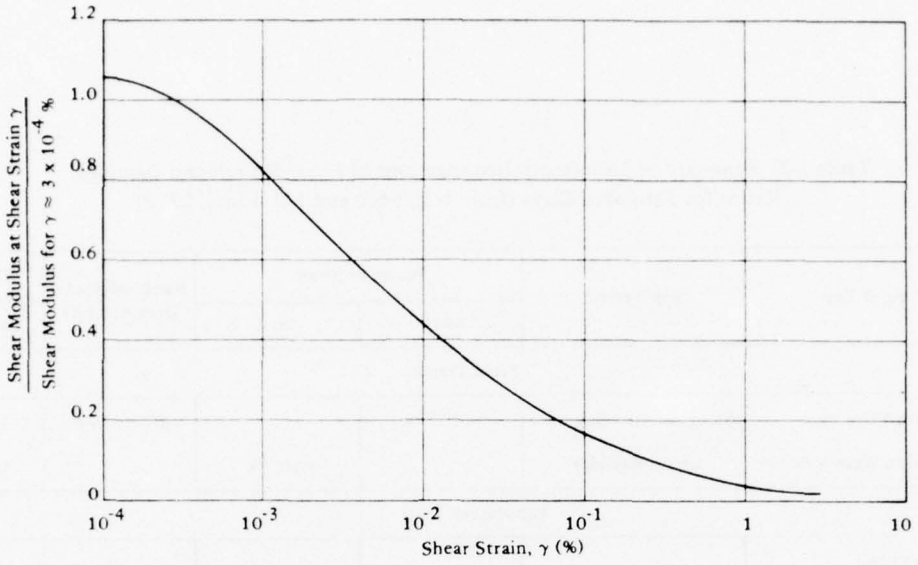

Figure 2-25. Typical reduction of shear modulus with shear strain for saturated clays (from Seed and Idriss, 1970).

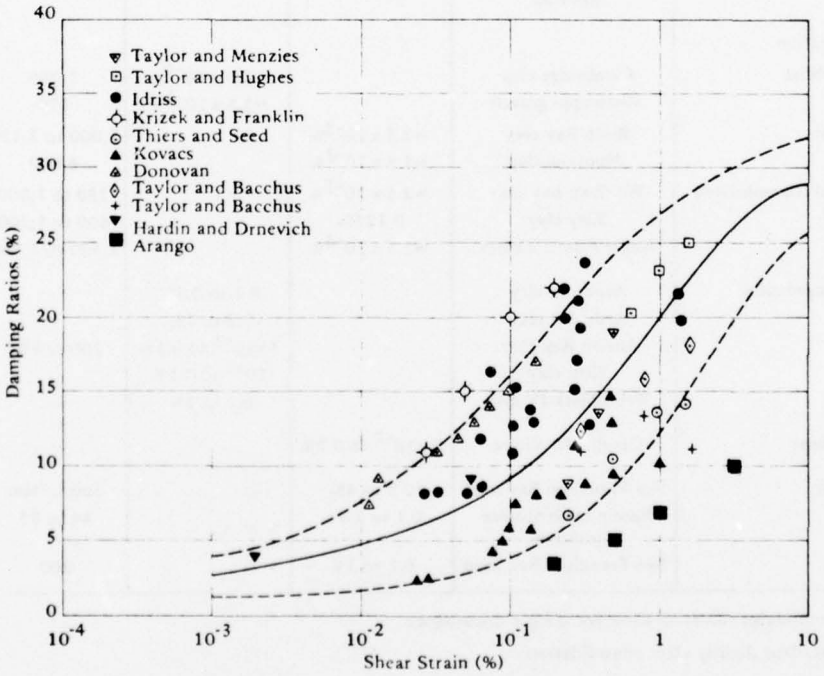

Figure 2-26. Damping ratios for saturated clays (from Seed and Idriss, 1970).

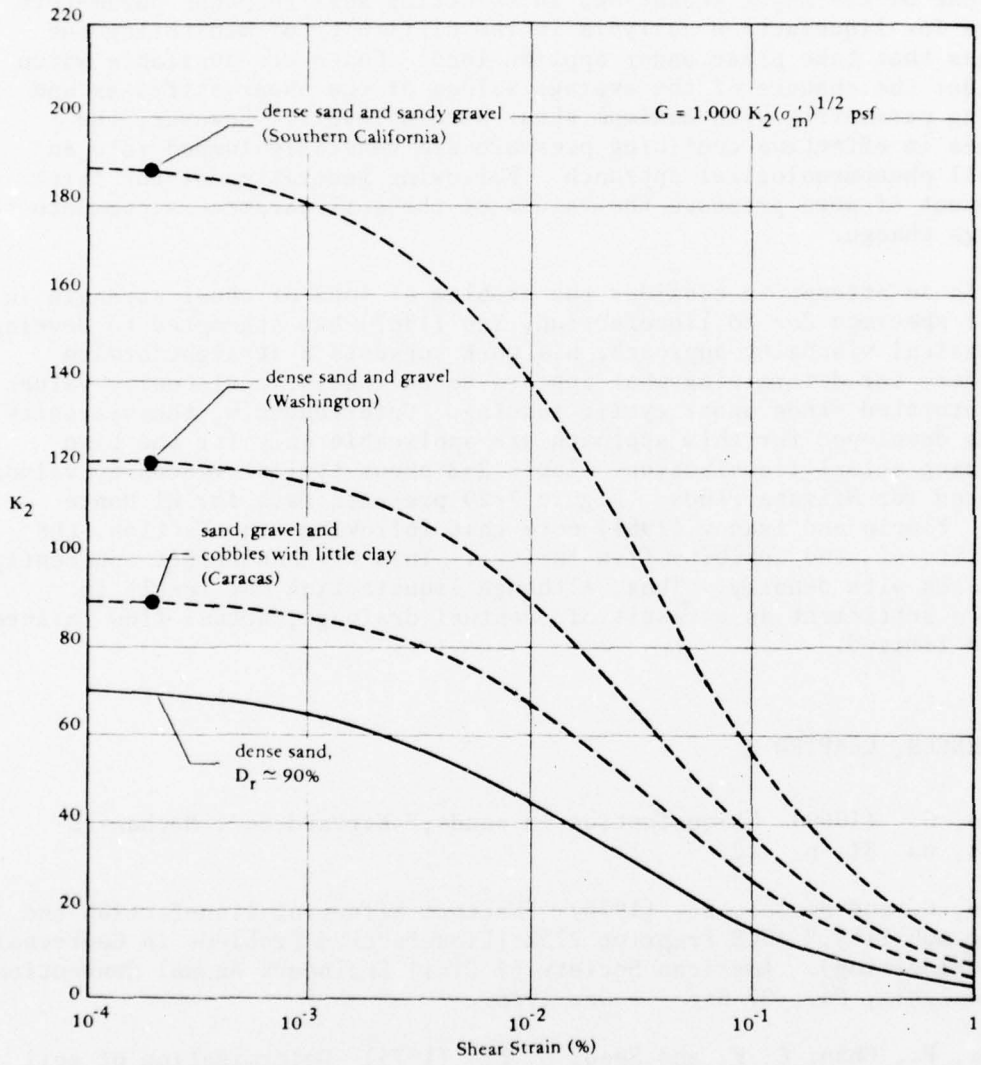

Figure 2-27. Modulus determinations for gravelly soils (from Seed and Idriss, 1970).

Peats are generally treated in the same format as clays. Available data on peats based upon field seismic wave velocities, laboratory studies, and earthquake ground response evaluations are shown in Figure 2-28.

One of the major weaknesses in selecting soil response parameters to use for liquefaction analysis is the difficulty of monitoring the changes that take place under applied load. Codes are available which consider the changes of the average values of the shear stiffness and damping parameters with maximum shear strain levels. However, the changes in effective confining pressure are generally lumped into an overall phenomenological approach. Following generation of the first increment of pore pressure the values of the soil parameters commence to undergo change.

In an attempt to consider the problem of loss of shear strength in a soil specimen due to liquefaction, Yen (1967) has attempted to develop a classical viscosity approach; his work suggests a straightforward procedure for determining what appears to be realistic viscosity values for saturated sands under cyclic loading. Unfortunately, the viscosity values developed for this approach are applicable only for the time preceding actual liquefaction. Table 2-3 shows typical viscosity values measured for Niigata sands. Figure 2-29 presents data for El Monte sand. Florin and Ivanov (1961) note that following liquefaction, the viscosity of sand inhibits flow failure. This viscous effect apparently increases with density. Thus, although liquefaction may result in surface settlement as a result of eventual drainage, actual flow failures may be limited.

REFERENCES, CHAPTER 2

Castro, G. (1969) "Liquefaction in sands," Harvard Soil Mechanics Series, no. 81, p. 112.

Castro, G. and Poulos, S. (1976) "Factors affecting liquefaction and cyclic mobility," ASCE Preprint 2752 (Liquefaction Problems in Geotechnical Engineering). American Society of Civil Engineers Annual Convention, Philadelphia, Pa., 27 Sep – 1 Oct 1976.

DeAlba, P., Chan, C. K. and Seed, H. B. (1975) Determination of soil liquefaction characteristics by large-scale laboratory test. University of California, Earthquake Engineering Research Center, EERC Report No. 75-14. Berkeley, Calif., 1975.

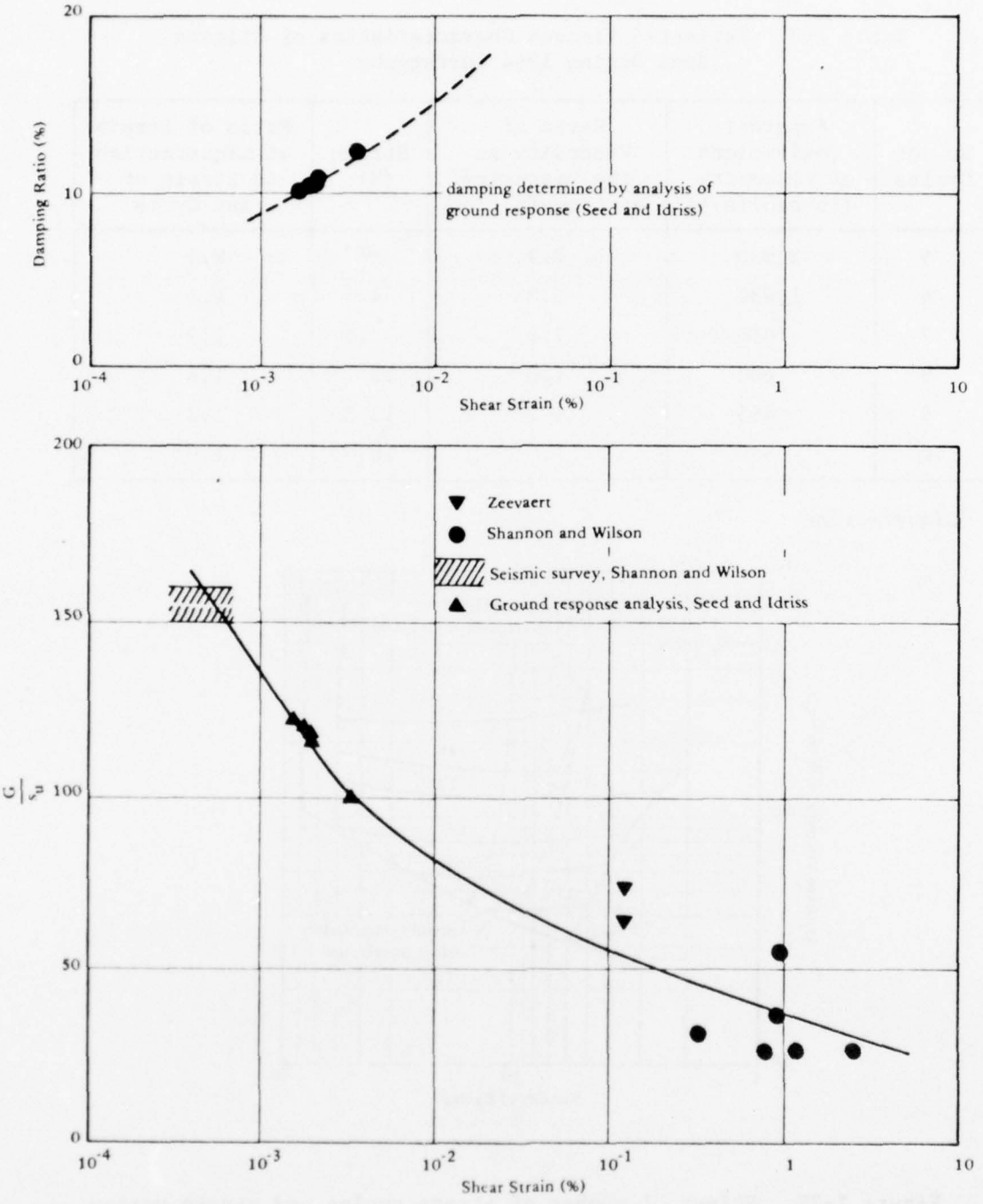

Figure 2-28. Moduli and damping determinations for peats (from Seed and Idriss, 1970).

Table 2-3. Estimated Viscous Characteristics of Niigata Sand During 1964 Earthquake

No. of Cycles	Apparent Coefficient of Viscosity (lb-sec/in.^{2})	Ratio of Viscosity to the Viscosity at Liquefaction	Strain (%)	Ratio of Strain at Liquefaction to Strain of Any Cycle
5	3,000	7.9	2$^+$	8.5
6	1,450	3.8	4	4.1
7	850	2.2	7.5	2.2
8	600	1.6	10	1.6
9	465	1.2	13.5	1.2
10[a]	380	1.0	16.5	1.0

[a]Liquefaction.

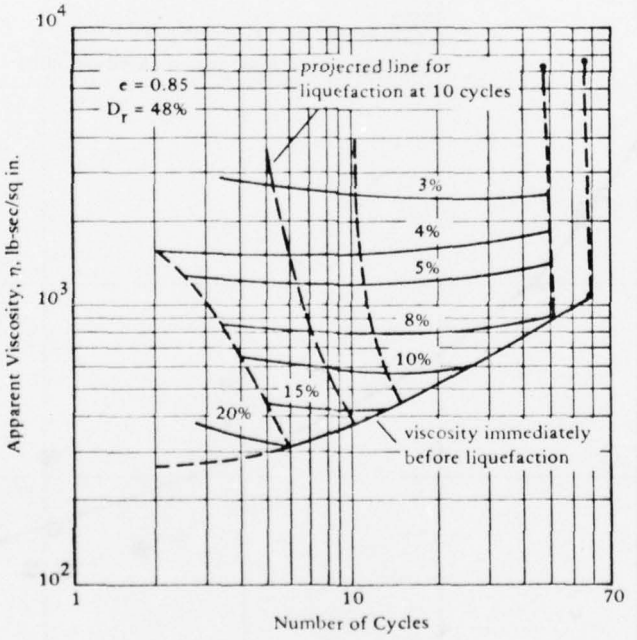

Figure 2-29. Effect of number of stress cycles and strain versus viscosity in El Monte sand (from "Viscosity of Saturated Sands Near Liquefaction," by B. C. Yen, copyrighted by The University of New Mexico Press, Albuquerque, N. M., 1967).

Donovan, N. C. (1974) CUMLIQ: Evaluation of potential for liquefaction of a soil deposit using random vibration procedures, University of California, Earthquake Engineering Research Center, National Information Service Earthquake Engineering. Berkeley, Calif., Jul 1974.

Finn, W. L. (1972) "Soil dynamics liquefaction of sands," in Proceedings of International Conference on Microzonation for Safer Construction Research and Application, 30 Oct - 2 Nov 1972. Seattle, Wash., 1972.

Finn, W. D. L., Bransby, P. L. and Pickering, D. J. (1970) "Effect of strain history on liquefaction of sand," Journal of Soil Mechanics and Foundation Division, ASCE, vol 96, no. SM6, Jun 1970, pp 1917-1934.

Florin, V. A. and Ivanov, P. L. (1961) "Liquefaction of saturated sandy soils," in Proceedings of Fifth International Conference on Soil Mechanics and Foundations, Paris, France. New York, N.Y., United Nations Educational Scientific and Cultural Organization, Jul 1961.

Hardin, B. and Drnevich, V. (1970) Shear modulus and damping in soils, University of Kentucky, College of Engineering, Technical Report UKY 26-70-CE2, Soil Mechanics Series. Lexington, Ky, Jul 1970.

Huang, W. (1961) "Investigations on stability of saturated sand foundations and slopes against liquefaction," in Proceedings of Fifth International Conference on Soil Mechanics Foundation Engineering, Paris, France, vol 11, 1961, pp 629-632.

Ishibashi, I. and Sherif, M. A. (1974) "Soil liquefaction by torsional simple shear device," Journal of the Geotechnical Division, ASCE, vol 100, no. GT8, Aug 1974, pp 871-808.

Ishihara, K., Tatsuoka, F. and Yasuda, S. (1975) "Undrained deformation and liquefaction of sand under cyclic stresses," Soils and Foundations, (Japan), vol 15, no. 1, Mar 1975.

Kishida, H. (1969) "Characteristics of liquefied sands during Mino-Owari, Tohnankai, and Kikui earthquakes," Soils and Foundations (Japan), vol 9, no. 1, Mar 1969.

Kishida, H. (1970) "Characteristics of liquefaction of level sandy ground during the Tokachioki earthquakes," Soils and Foundations (Japan), vol 10, no. 2, Jun 1970.

Lee, K. L. and Chan, K. (1972) "Number of equivalent significant cycles in strong motion earthquakes," in Proceedings of the International Conference on Microzonation for Safer Construction Research and Application, 30 Oct - 2 Nov 1972, vol II. Seattle, Wash., 1972, pp 609-627.

Lee, K. L. and Fitton, J. A. (1969) "Factors affecting the cyclic loading strength of soil," Symposium on Vibration Effects of Earthquakes on Soils and Foundations, Special Technical Publication No. 450, ASTM, pp 71-95.

Lee, K. L. and Seed, H. B. (1967) "Cyclic stress conditions causing liquefaction of sand," Journal of the Soil Mechanics and Foundations Division, ASCE, vol 93, no. SM1, Jan 1967, pp 47-70.

Martin, G., Finn, L. and Seed, H. (1975) "Fundamentals of liquefaction under cyclic loading," Journal of the Geotechnical Division, ASCE, no. GT5, May 1975.

Meehan, R. L. (1976) "Dynamic strength of hydraulic fill," Journal of the Geotechnical Division, ASCE, vol 102, no. GT6, Jun 1976.

Peacock, W. H. and Seed, H. B. (1968) "Sand liquefaction under cyclic loading simple shear conditions," Journal of the Soil Mechanics and Foundations Division, ASCE, vol 94, no. SM3, May 1968.

Pike, R., Chan, C. K. and Seed, H. B. (1974) Settlement and liquefaction of sands under multi-directional shaking, University of California, Earthquake Engineering Research Center, EERC Report No. 74-20. Berkeley, Calif., Feb 1974.

Rocker, K., Jr. (1968) The liquefaction behavior of sands subjected to cyclic loading; Progress Report no. 3, Repeated load and vibration tests upon sand, Massachusetts Institute of Technology, Department of Civil Engineering, Research Report R68-36, Soils Publ. no. 221. Cambridge, Mass., Jun 1968.

Schnabel, P. B., Lysmer, J. and Seed, H. B. (1972) SHAKE: a computer program for earthquake response analysis of horizontally layered sites, University of California, Earthquake Engineering Research Center, EERC Report No. 72-12. Berkeley, Calif., Nov 1972.

Seed, H. B. (1976) "Evaluation of soil liquefaction effects on level ground during earthquakes," ASCE Preprint 2752 (Liquefaction Problems in Geotechnical Engineering), American Society for Civil Engineers Annual Convention and Exposition, Philadelphia, Pa., 27 Sep-1 Oct 1976.

Seed, H. B. and Idriss, I. M. (1970) Soil moduli and damping factors for dynamic responses analysis, University of California, Earthquake Engineering Research Center, EERC Report no. 70-10. Berkeley, Calif., Nov 1970.

Seed, H. B. and Lee, K. L. (1966) "Liquefaction of saturated sands during cyclic loading," Journal of the Soil Mechanics and Foundations Division, ASCE, vol 92, SM6, Jun 1966.

Seed, H. B. and Lee, K. L. (1969) "Pore-water pressure in earth slopes under seismic loading conditions," in Proceedings of Fourth World Conference on Earthquake Engineering, Association Chilena de Sismologia e Ingenieria Anti-Sismica Impreso en Editorial Universelaria, Santiago, Chile, vol 3, 1969.

Seed, H. B., Martin, P. P. and Lysmer, J. (1975) The generation and dissipation of pore water pressures during soil liquefaction, University of California, College of Engineering, Earthquake Engineering Research Center, EERC Report No. 75-26. Berkeley, Calif., Aug 1975.

Seed, H. B., Mori, K. and Chan, C. K. (1975) Influence of seismic history on liquefaction characteristics of sands, University of California, Earthquake Engineering Research Center, EERC Report No. 75-25. Berkeley, Calif., 1975.

Seed, H. B. and Peacock, W. H. (1971) "Test procedures for measuring soil liquefaction characteristics," Journal of the Soil Mechanics and Foundations Division, ASCE, vol 97, no. SM8, Aug 1971.

Silver, M. L. and Park, T. K. (1975) "Testing procedure effects of dynamic soil behavior," Journal of the Geotechnical Division, ASCE, vol 101, no. GT11, Oct 1975.

Wong, T., Seed, H. B. and Chan, C. (1974) Liquefaction of gravelly soils under cyclic loading conditions, University of California, Earthquake Engineering Research Center, EERC Report No. 74-11. Berkeley, Calif., Nov 1974.

Yen, B. C. (1967) "Viscosity of saturated sand near liquefaction," in Proceedings of International Conference on Wave Propagation and Soil Mechanics, ASCE, University of New Mexico Press. Albuquerque, N.M., Aug 1967.

Yoshimi, Y. and Kuwabara, F. (1973) "Effect of subsurface liquefaction on the strength of surface soils," Soils and Foundations (Japan), vol 13, no. 2, Jun 1973.

Yoshimi, Y. and Oh-Oka, H. (1975) "Influence of degree of shear stress reversal on the liquefaction potential of saturated sand," Soils and Foundations (Japan), vol 15, no. 3, Sep 1975.

Youd, L. Y. (1973) Liquefaction flow and associated ground failures, U.S. Geodetic Survey, National Center, Circular 688. Reston, Va., 1973.

Youd, T. L. (1975) "Liquefaction, flow and associated ground failure," in Proceedings of the U. S. National Conference on Earthquake Engineering, Ann Arbor, Mich., Jun 1975. Earthquake Engineering Research Institute, Oakland, Calif., 1975, pp 146-155.

Chapter 3

PROCEDURES FOR ANALYSIS OF LIQUEFACTION OF SOILS

Earthquake ground motions are capable of causing a loss of shear strength of sand deposits below the water table. Field and laboratory tests have been performed to evaluate the liquefaction potential of soils. This chapter will present field standard penetration test interpretation, a summary of the void ratio concept, Seed's (1976) simplified hand computation procedure, a simple computer analysis, a more complex computer analysis, finite element analysis techniques, and some interesting research in progress.

STANDARD PENETRATION TEST USED FOR LIQUEFACTION PREDICTION

Standard penetration tests can be used directly to give an in situ evaluation of soil behavior. Seed (1976) presents Figure 3-1 which is an evaluation of the Niigata, Japan 1964 earthquake. Several lines divide regions of light damage (no liquefaction) from heavy damage (liquefaction). Such a correlation is applicable only to the Niigata soil and earthquake; however, the methodology may be extended. Castro (1975) has compiled earthquake field observations of liquefaction in terms of an effective shear stress ratio

$$\tau_e/\sigma'_v$$

where τ_e is defined* as

$$\tau_e = 0.7 \times A_{max} \times \sigma_v$$

*This will be discussed in more detail in the section entitled SIMPLE HAND COMPUTATION.

and

σ'_v = effective overburden pressure

A_{max} = maximum horizontal acceleration, g's

σ_v = total overburden pressure

and a corrected blow count N' defined as

$$N' = \frac{50N}{\sigma'_v + 10}$$

where N = standard penetration resistance measured in the field

The relationship is shown in Figure 3-2.

Christian and Swiger (1975) utilized discriminant analysis techniques to analyze the data from 39 earthquakes. They define a parameter A as

$$A = \frac{a\ \sigma_v}{\sigma'_v}$$

where a = site surface accelerations

The parameter A is a measure of the stress-strength ratio t/s'_v. Relative density is determined by use of the Gibbs and Holtz (1957) relation from standard penetration tests (Chapter 4). This value is not used as an absolute but rather as an intermediate correlation. Figure 3-3 shows the results of their analysis. The probability numbers are the confidence indicators that the line shown is the dividing line separating liquefiable from non-liquefiable cases. Thus, a P = 0.10 means that the location of the line is associated with a 90% confidence that all liquefiable cases are above the line. (Note: it is not to be confused with the probability of occurrence of liquefaction.) These curves give estimates of the standard penetration resistance required at a site to preclude liquefaction for a given confidence level.

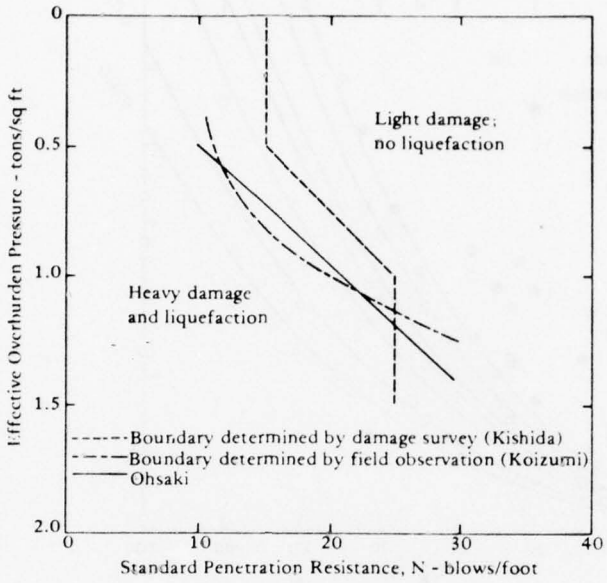

Figure 3-1. Analysis of liquefaction potential at Niigata for earthquake of June 16, 1964 (from "Liquefaction and Cyclic Mobility of Saturated Sands," by G. Castro in ASCE Geotechnical Journal, GT6, Jun 1975).

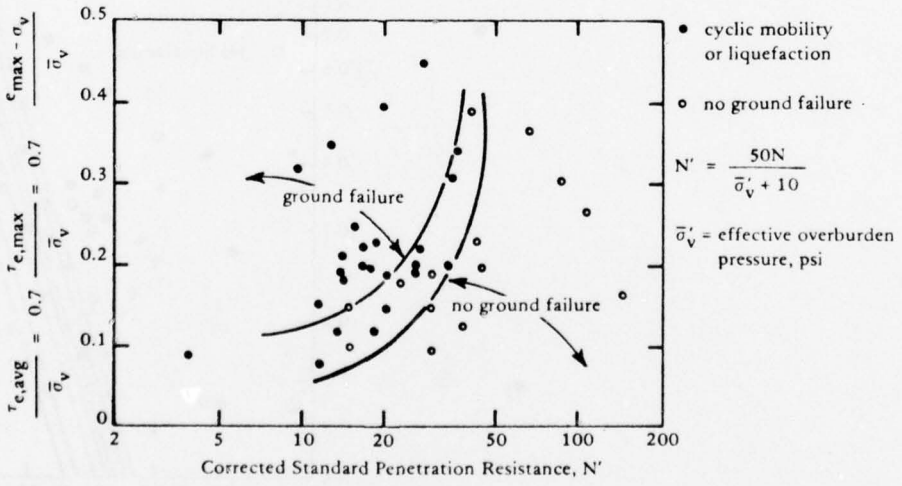

Figure 3-2. Performance of saturated sands at earthquake sites (from "Liquefaction and Cyclic Mobility of Saturated Sands," by G. Castro in Journal of the Geotechnical Division, ASCE vol. 101, no. GT6, Jun 1975).

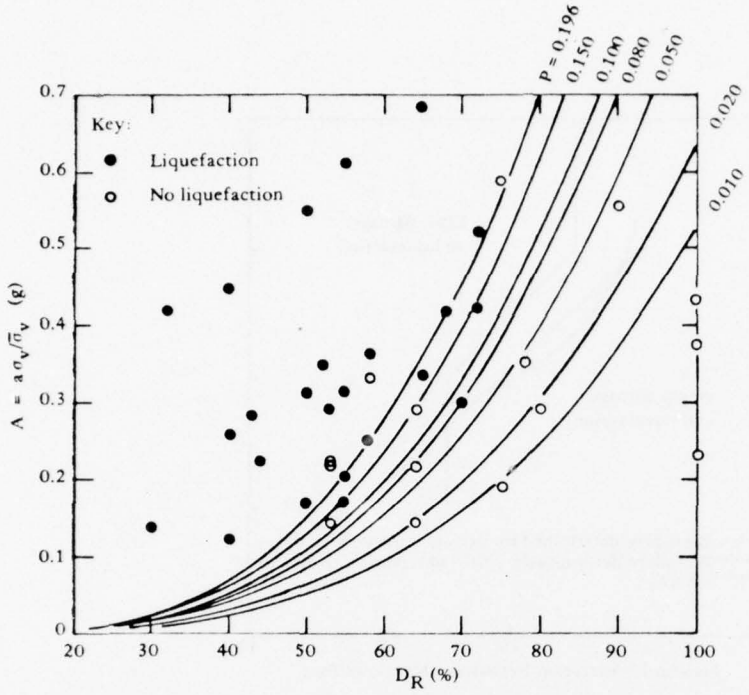

(a) Arithmetic scales.

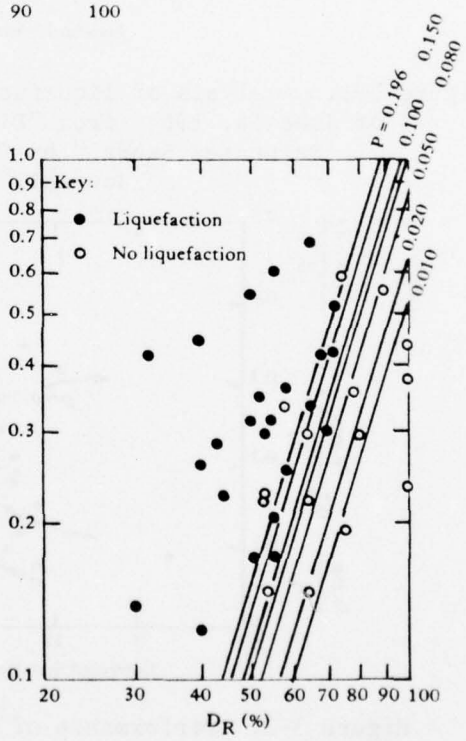

(b) Logarithmic scales.

Figure 3-3. Historical observations of liquefaction and discriminant curves (from "Statistics of Liquefaction and SPT Results," by J. T. Christian and W. F. Swiger in Journal of the Geotechnical Division, ASCE, vol. 101, no. GT11, Nov 1975 and discussion, vol. 102, no. GT12, Dec 1976).

Seed (1976) gives the results of a detailed study on penetration resistance in Figure 3-4. To use the information presented in Figure 3-4, the value of the standard penetration resistance should be corrected to an effective overburden pressure of 1 ton/ft^2 by means of the following expression

$$N_1 = C_N N$$

where C_N is taken from Figure 3-4c and

N_1 = corrected penetration resistance

N = standard penetration resistance as measured at the depth under consideration

σ'_o = effective overburden pressure in ton/ft^2 (where the penetration resistance has the value N)

σ'_1 = 1 ton/ft^2

Liquefaction studies in mainland China conducted independently but along similar lines to those developed in this country have also led to a correlation between earthquake shaking conditions causing liquefaction and the standard penetration resistance of sands. In this correlation, the critical value of the standard penetration resistance, N_{crit}, separating liquefiable from nonliquefiable conditions is determined by the following expression

$$N_{crit} = N\{1 + 0.125\ (d_s - 3) - 0.05\ (d_w - 20)\}$$

where d_s = depth to sand layer under consideration in meters

d_w = depth of water table below ground surface in meters

N = a function of the shaking intensity as follows:

Modified Mercelli Intensity	N (blows/ft)
7	6
8	10
9	16

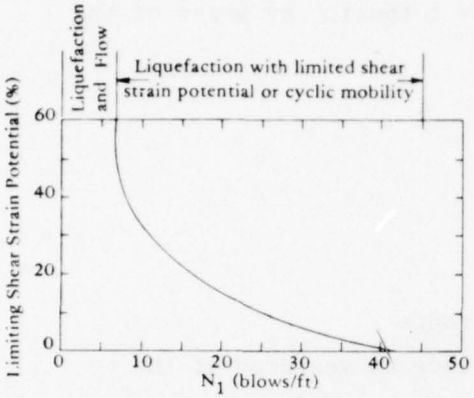

(a) Strain potential.

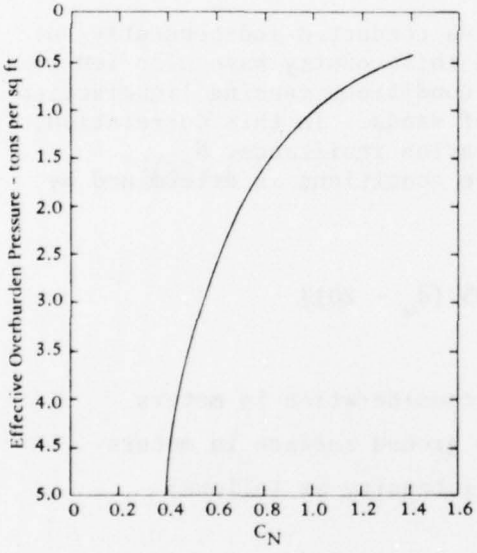

(b) Stress ratio.

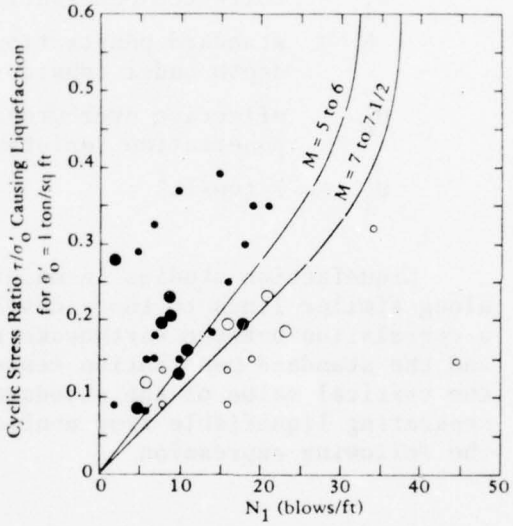

(c) Relationship between C_N and effective overburden pressure.

Figure 3-4. Use of standard penetration for liquefaction evaluation (from "Evaluation of Soil liquefaction Effects on Level Ground During Earthquake," by H. B. Seed, in a paper presented at the ASCE Annual Convention, Philadelphia, 27 Sep-1 Oct 1976).

This correlation was found by Seed (1976) to agree with data in Figure 3-4.

The data presented in this section can be used to give an approximate estimate of the liquefaction potential at a site. Clearly the number of observations is limited and the scatter in the data large. This method is well-suited for preliminary evaluation of alternative sites when detailed tests are not possible.

CRITICAL VOID RATIO CONCEPT

Castro (1975) differentiates between liquefaction (occurring as a result of loss of shear resistance under monotonic loading) and cyclic mobility, which he defines as progressive softening of a saturated sand under cyclic load. Castro (1975) questions the belief that cyclic mobility can occur in dilative sands in situ during earthquakes, at least to the same degree as has been observed in the laboratory. He presents data to suggest that the large strains exhibited in laboratory cyclic tests are due to redistribution of void ratios.

In order to better understand this approach, it is of interest to briefly review typical monotonic triaxial test data for cohesionless material. Figure 3-5a and b shows drained triaxial test results for a loose sand, a dense sand, and a sand at critical void ratio. Here, critical void ratio is defined as that value of initial void ratio that corresponds to the void ratio that would be reached at the maximum shear stress level for a specific soil under a particular confining stress level. As can be seen at failure, the net volumetric strain of a specimen at critical void ratio is zero at maximum shear loading. Loose and dense may be determined in relation to this. Figure 3-5c and d shows this more clearly for another series of tests at different initial void ratios and confinements. In Figure 3-5c volume change at maximum shear stress level is plotted versus initial void ratio for three series of triaxial tests under three different confining stresses. Figure 3-5d shows volume change versus confining pressure for three series of tests at different initial void ratios.

Information from the foregoing tests may be applied to undrained triaxial tests to predict their behavior. Since drainage is not allowed, volume change – and, thus, void ratio – is essentially unchanged. Figure 3-5e shows a plot of volume change versus initial confining pressure for drained triaxial tests on sand, similar to Figure 3-5d. Also shown are state paths for both a dense sand (point A) and a loose sand (point B) undergoing shear under undrained conditions.

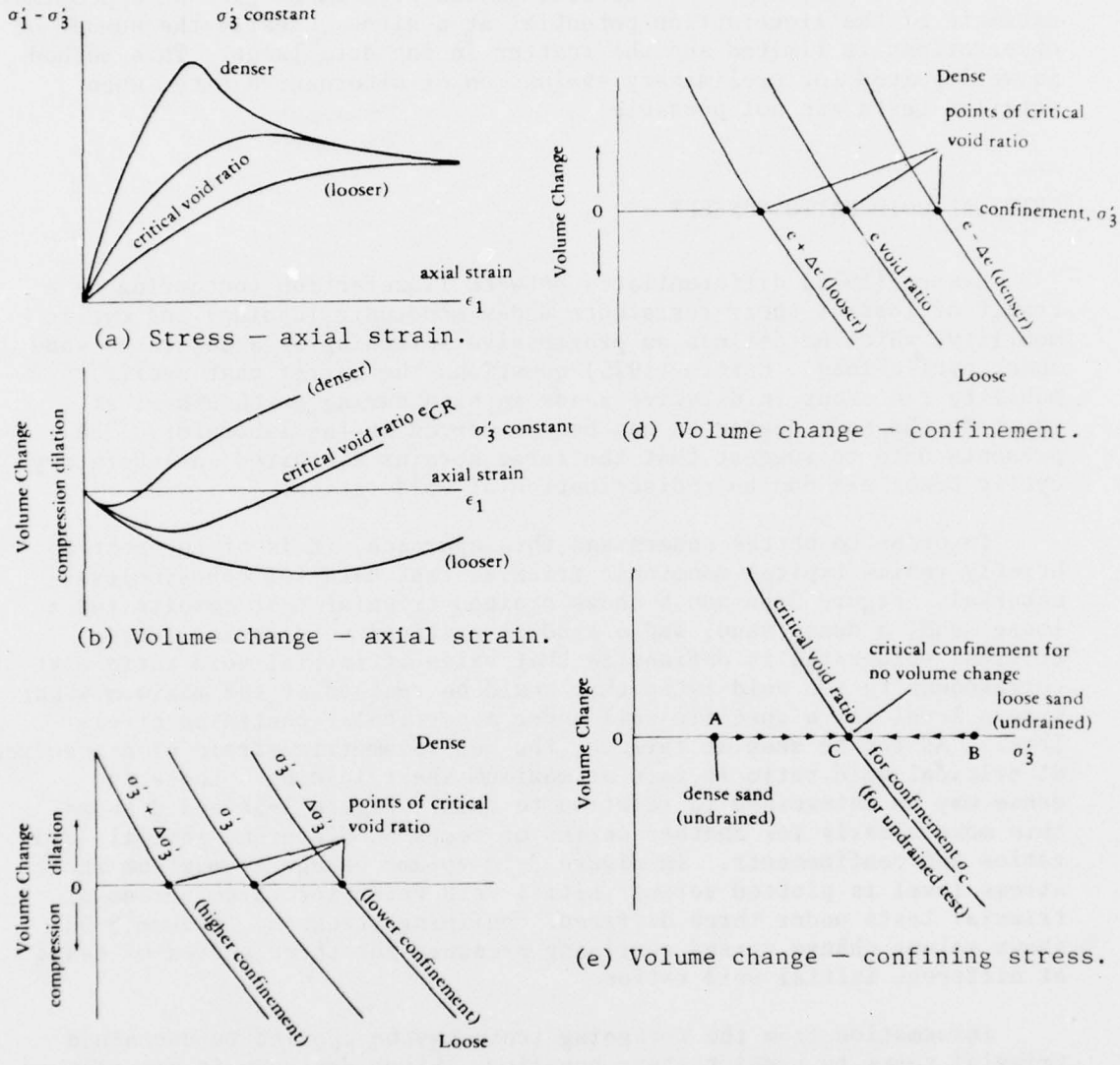

Figure 3-5. Drained triaxial test data.

Since drainage is not permitted, the dense sand trying to dilate reduces pore pressure, thereby increasing effective confinement under monotonic loading. The opposite is noted for the loose soil which increases pore pressure as it tends to try to compress. Figure 3-6 compares drained and undrained triaxial test data for a dense sand. It should be noted that although the dense sand does tend to dilate at failure strains, it initially undergoes compression at lower strain levels. These strain levels, although lower than failure, may be within the strain level noted in some earthquakes. Thus, pore pressure might build up even in dense undrained sands.

Castro (1975) in Figure 3-7 makes use of a state diagram to explain liquefaction under monotonic or cyclic loading. Under loading, a loose soil responds by an increase in pore pressure (reducing confinement) moving from point C toward point A. At point A, unlimited flow occurs at some small residual stress level.

In order to have a quicksand condition, defined by Castro (1975) as complete loss of strength, the soil would require a void ratio greater than Q. Dense sands may also respond by increase in pore pressure moving from point D toward point B. Should the cyclic load repetitions be vigorous enough, the sand state reaches point B, where the effective confining stress becomes zero. However, upon shearing, the specimen commences to deform, thereby dilates, and the state of the sand moves toward point D. With further loading the sand state continues to move to the right until, presumably with high enough loading, it meets the steady-state line and commences to deform at constant shear stress level.

This state diagram is used to define a liquefaction potential

$$L_p = \frac{\bar{\sigma}_{3c} - \bar{\sigma}_{3f}}{\bar{\sigma}_{3f}} \quad \text{(after Casagrande)}$$

where $\bar{\sigma}_{3c}$ = the initial effective minor principal stress

$\bar{\sigma}_{3f}$ = the effective minor principal stress at yielding

Since it is assumed that the friction angle of the sand is fully mobilized at steady-state yielding, the liquefaction potential may be defined by using Mohr-Coulomb theory as:

$$L_p = \frac{\bar{\sigma}_{3c} - \bar{\sigma}_{3f}}{\bar{\sigma}_{3f}} = \frac{\Delta u}{\sigma_{3f}} = \frac{\Delta u}{\sigma_{df} \frac{1 - \sin \phi}{2 \sin \phi}}$$

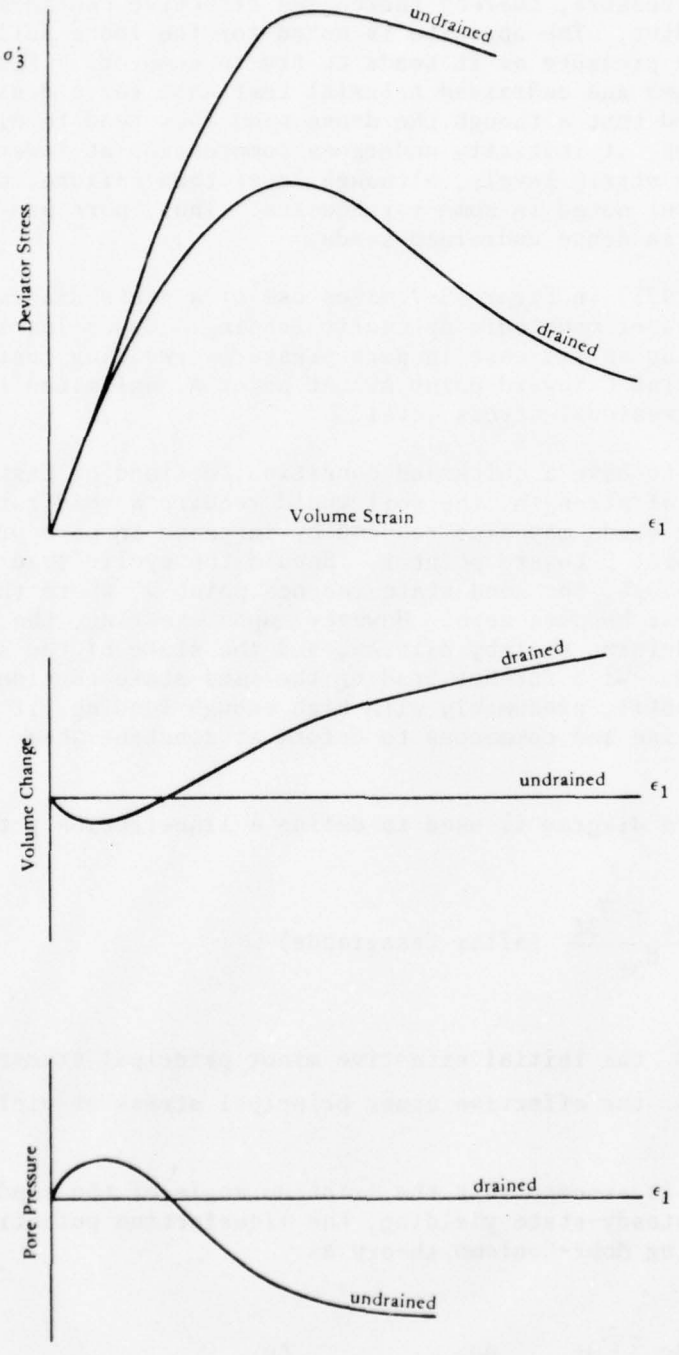

Figure 3-6. Comparison of drained and undrained triaxial test data.

where Δu = the pore pressure generated in reaching the critical state line

σ_{df} = the deviator stress existing at this state

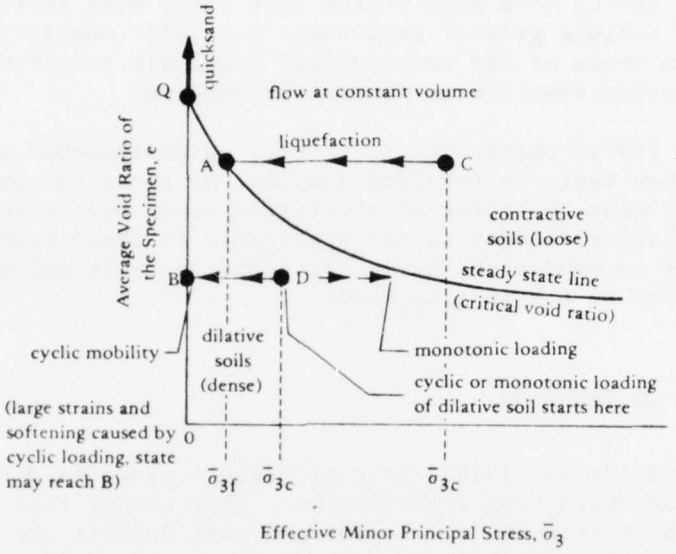

Figure 3-7. Undrained tests on fully saturated sands depicted on state diagram (from "Liquefaction and Cyclic Mobility of Saturated Sands," by G. Castro in ASCE Journal of the Geotechnical Division, vol. 101, no. GT6, Jun 1975).

The pore pressure Δu can be related to deviator stress σ_{df} by means of Skempton's parameter A_f

$$L_p = A_f \times \frac{2 \sin \phi}{1 - \sin \phi}$$

Although Castro (1975) applies this liquefaction potential value qualitatively (i.e., higher L_p's suggest higher liquefaction tendency), no quantitative criteria are given. Further, a sand classified as dense by this approach would have a negative L_p. Although the implication is that this would not liquefy, no specific statements to this effect are made.

Castro (1975) also shows state diagrams for various sands which show the steady-state lines to be functions of very subtle changes in particle shape, size, and gradation. In some cases these latter parameters are noted to exert an influence on the liquefaction potential as great, for example, as that of relative density.

The foregoing work also states that soils with initial static shear loading may exhibit greater resistance to cyclic mobility. This is explained in terms of the reduced load reversals resulting in reduced void ratio redistribution on laboratory samples.

Castro (1975) points out that tests on undisturbed samples are more realistic than tests on remolded samples; he feels the use of average density specimens to represent stratified sands may introduce large errors. Relative density is not applicable to these types of deposits, and there is no equivalent basis for comparing unit weights of remolded sand with that of the in situ sand.

SIMPLE HAND COMPUTATION

Seed and Idriss (1970a) have proposed a simplified hand computation procedure for evaluating liquefaction. They assume that the liquefaction producing shear stresses developed in a soil deposit are caused by upward propagating shear waves. The depth to the soil region under liquefaction investigation is defined as h. The soil column within a depth h is assumed to behave as shown in Figure 3-8. The maximum shear stress at a depth h is related to the ground acceleration by equilibrium

$$\tau_{max} = \frac{\gamma h}{g} (A_{max})\ r_d$$

where γ = total unit weight of soil

h = depth to region where liquefaction is expected

A_{max} = maximum surface acceleration

r_d = acceleration correction factor

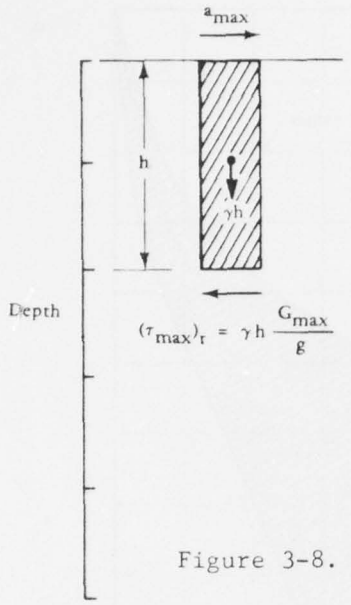

Figure 3-8. Approximate equilibrium representation.

The factor r_d is used to reduce the surface acceleration for depth since the soil is a deformable body rather than a rigid one. Figure 3-9 gives a range of values for r_d with depth. The actual time history of motion will have an irregular form (Figure 3-10), and an equivalent average stress is taken as 65% of the maximum which corresponds to an equivalent number of uniform cycles. Thus, the average stress τ_{av} is

$$\tau_{av} = 0.65 \left(\frac{\gamma h}{g} \right) A_{max} \, r_d$$

Evaluation of earthquake data has provided information on the equivalent number of significant stress cycles that can be expected as a function of earthquake magnitude, which will be presented later in this chapter.

Having the number of cycles, the average applied shear stress and the effective confining stress (s'_v, vertical stress), a simple procedure can be used to determine the liquefaction factor of safety. The number of cycles causing liquefaction can be determined by a laboratory test program using cyclic loading triaxial compression tests. Correction factors have been developed by DeAlba, Chan, and Seed (1975) (Figure 3-11a) to relate triaxial tests to (free-field) field observation.

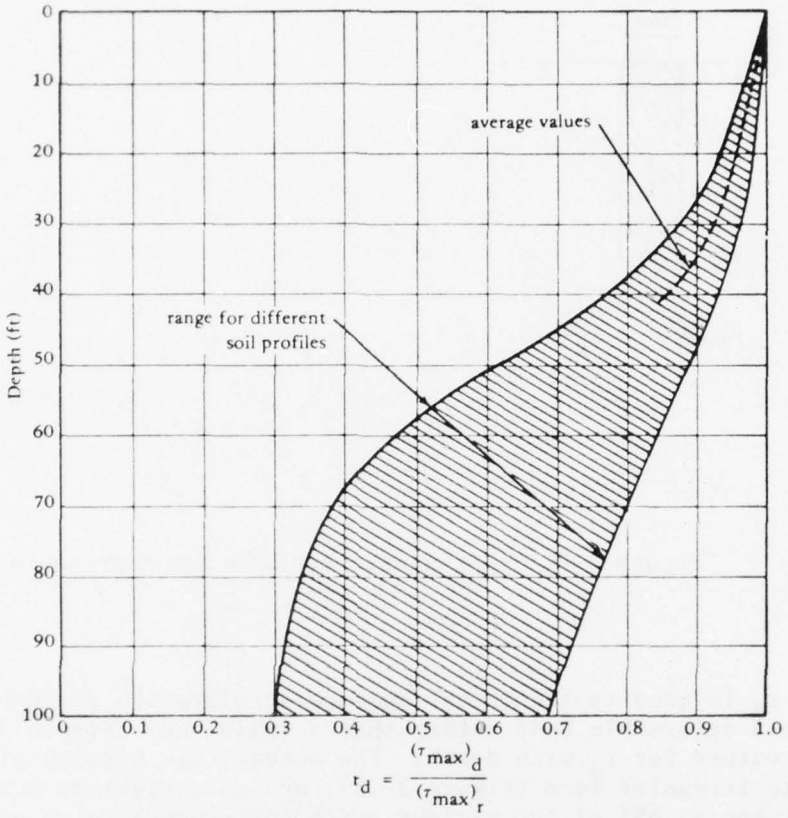

Figure 3-9. Range of value of r_d for different soil profiles.

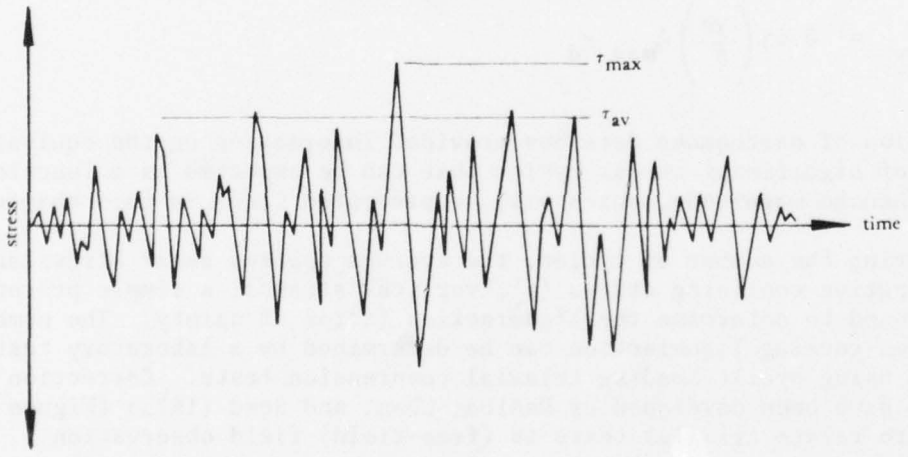

Figure 3-10. Time history of shear stresses during earthquake.

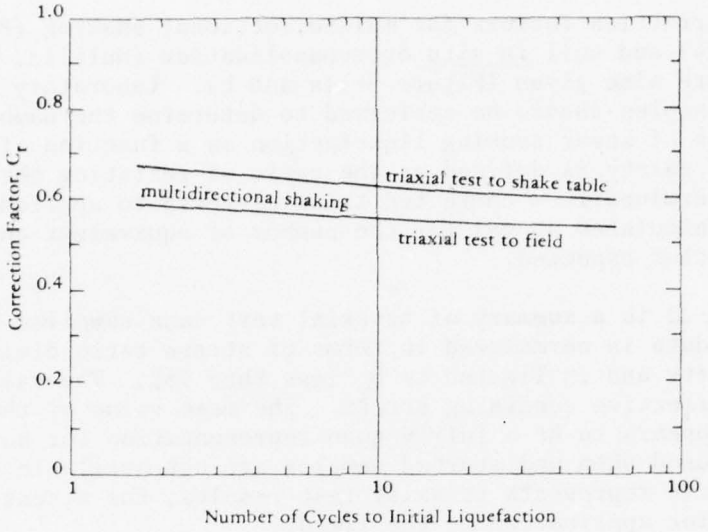

(a) $K_o = 4.$

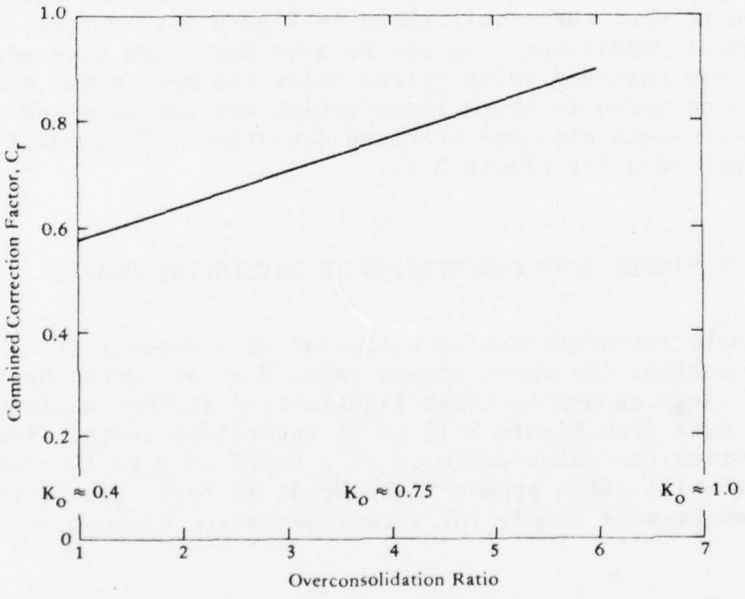

(b) Combined correction factor for cyclic triaxial compression tests accounting for multidirectional shaking and overconsolidation.

Figure 3-11. Correction factors for triaxial test results (from P. DeAlba, C. K. Chan, and H. B. Seed, 1975).

Additional correction factors for multidirectional shaking (Pyke, Chan and Seed, 1974) and soil in situ overconsolidation (Mulilis, Chan, and Seed, 1975) are also given (Figure 3-11a and b). Laboratory tests on undisturbed samples should be performed to determine the number of uniform cycles of shear causing liquefaction as a function of τ_{av}/σ_v. The factor of safety is defined as the ratio of resisting shear stress capacity (determined from corrected triaxial test) to applied shear stress (τ_{av} calculated above) for the number of equivalent uniform earthquake cycles expected.

Figure 3-12 is a summary of triaxial test data compiled by Donovan (1974). The data is normalized in terms of stress ratio divided by relative density and is limited to D_r less than 75%. The value of σ_3 is used as the effective confining stress. The mean value of the data in Figure 3-12 appears to be a fairly good representation for uniform sands and could be used when undisturbed samples are not available for testing. Since this curve represents triaxial test results, the stress ratio must be corrected for application to the field.

There are 34 cases of observed liquefaction where data of ground motion and site profile were estimated (Seed and Peacock, 1970). This data was used to plot the points shown in Figure 3-13 correcting field data to triaxial conditions. As can be seen there are no cases in which liquefaction was observed which extend below the mean minus one standard deviation and no cases in which liquefaction was not observed which extend above the mean plus one standard deviation. Thus additional validity is provided for Figure 3-12.

APPLICATION OF SIMPLE HAND COMPUTATION IN DEVELOPING CHARTS

To evaluate the liquefaction potential of a deposit it is necessary to determine whether the shear stress induced at any depth by the earthquake τ_{av} is large enough to cause liquefaction at that depth as indicated by corrected data from Figure 3-12 or by laboratory tests. For uniform deposits in which the water table is at a depth of 0 to 10 feet, the critical depth will often appear to be about 20 feet. Thus, the evaluation can often be made simply for a representative element at one of these depths.

Consider for example, a deposit of sand for which the water table is 5 feet below the ground surface and which is subjected to 10 cycles of ground shaking. The average shear stress induced will be:

$$\tau_{av} = 0.65\left(\frac{\sigma_v}{g}\right)(A_{max})\, r_d$$

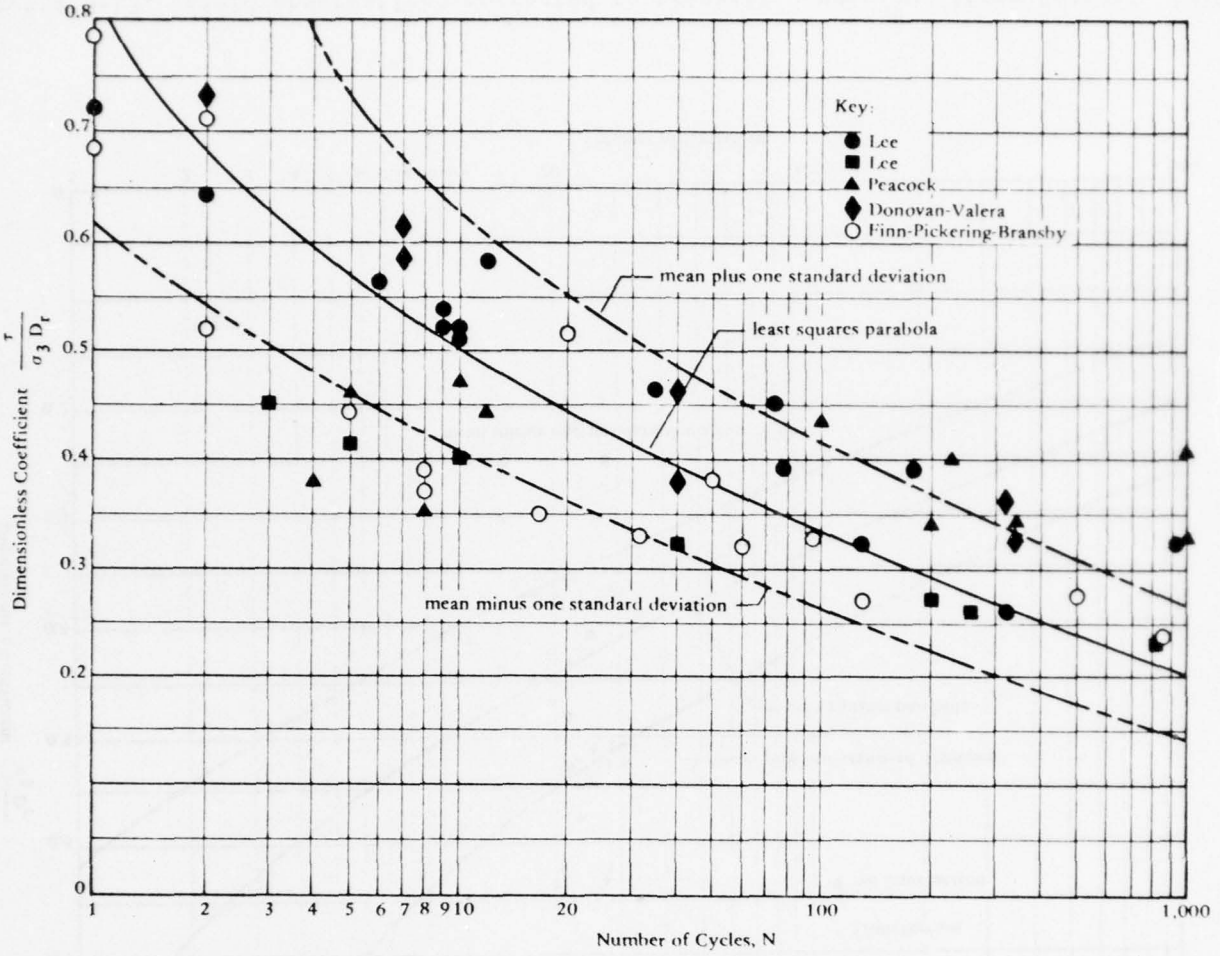

Figure 3-12. Soil strength for initial liquefaction (triaxial test data) (from Donovan, 1974).

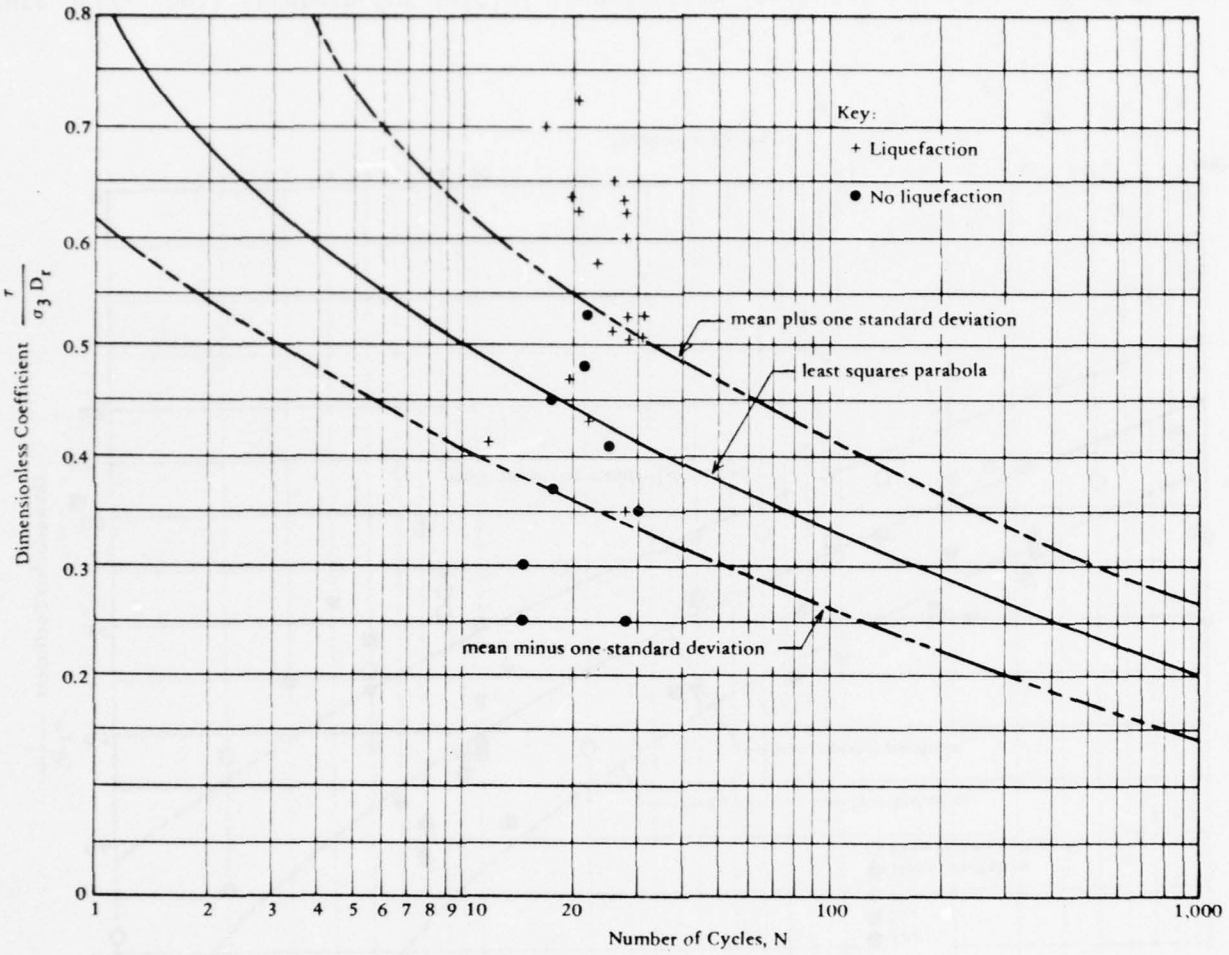

Figure 3-13. Field observations corrected to triaxial conditions (from Donovan, 1974).

At a depth of 20 feet, $r_d = 0.95$ (see Figure 3-9) giving

$$\tau_{av} = 0.65 \times 0.95 \times \frac{\sigma_v}{g} A_{max}$$

From Figure 3-12 the shear stress required to cause initial liquefaction for 10 cycles is

$$\tau/(\sigma_3' D_r) = 0.5$$

and

$$\tau_{av}/\sigma_v' = \frac{\tau C_r}{\sigma_3'}$$

Thus,

$$\tau_{av} = 0.5 \sigma_v' C_r D_r$$

where D_r is expressed as a decimal value and C_r is obtained from Figure 3-11.

Equating the applied τ_{av} with τ_{av} to give initial liquefaction gives

$$0.65 \times 0.95\left(\frac{\sigma_v}{g}\right) A_{max} = 0.5 \sigma_v' C_r D_r$$

$$\frac{A_{max}}{g} = 0.81\left(\frac{\sigma_v'}{\sigma_v}\right) C_r D_r$$

where $\sigma_v = \gamma h$

Assume a total saturated density of 132 lb/cu ft, a total density above the water table of 117 lb/cu ft, and a buoyant density of 69 lb/cu ft. This reduces to

$$\frac{A_{max}}{g} = 0.81 \times \frac{1620}{2565} \times C_r D_r$$

$$\frac{A_{max}}{g} = 0.512\ C_r\ D_r$$

For 10 cycles, $C_r = 0.57$

$$\frac{A_{max}}{g} = 0.29\ D_r$$

Thus, the following can be determined:

D_r	A_{max}/g*
0.40	0.116
0.50	0.145
0.60	0.174
0.70	0.203

The above values give the acceleration required to cause initial liquefaction at a depth of 20 feet with the water table at 5 feet, subject to 10 cycles of ground shaking.

Observed cases of liquefaction from Seed and Peacock (1970) are summarized in Figure 3-14 from which the following may be stated:

*Causing liquefaction in 10 cycles.

Maximum Ground Surface Acceleration	Liquefaction Very Likely	Liquefaction Potential Depends on Soil Type and Earthquake Magnitude	Liquefaction Very Unlikely
0.10 g	$D_r < 33$	$33 < D_r < 54$	$D_r > 54$
0.15 g	$D_r < 48$	$48 < D_r < 73$	$D_r > 73$
0.20 g	$D_r < 60$	$60 < D_r < 85$	$D_r > 85$
0.25 g	$D_r < 70$	$70 < D_r < 92$	$D_r > 92$

The data from Seed and Peacock may also be plotted to give Figure 3-15.

The values of relative density may be converted to values of standard penetration as a function of depth (see Chapter 4). Charts have been prepared by Seed and Idriss (1970a) giving the range of penetration resistance values in which liquefaction might be expected, Figures 3-16a and b.

SIMPLE COMPUTER ANALYSIS

Donovan (1974) has developed a computer program based in part on the simple soil model described in the previous section. The earthquake record is represented in terms of the peak acceleration, duration, and predominant frequency. The number of cycles at various acceleration levels is determined by a Rayleigh distribution. Miner's Linear Damage criteria are used to convert the different stress levels to an average stress for computation of a factor of safety. Donovan (1974) has compiled various triaxial test data, Figure 3-12. This data is used in the program as a measure of the soil shear strength. The input to the program requires a soil profile, limited knowledge of soil material and limited knowledge of the earthquake. The input to the program is simple and straightforward, consisting of the following:

1. Relative density of the soil layer of interest
2. Depth to center of the layer
3. Correction factor for triaxial test data (Figure 3-11)
4. Pressure produced by total weight of material above center of layer

(continued)

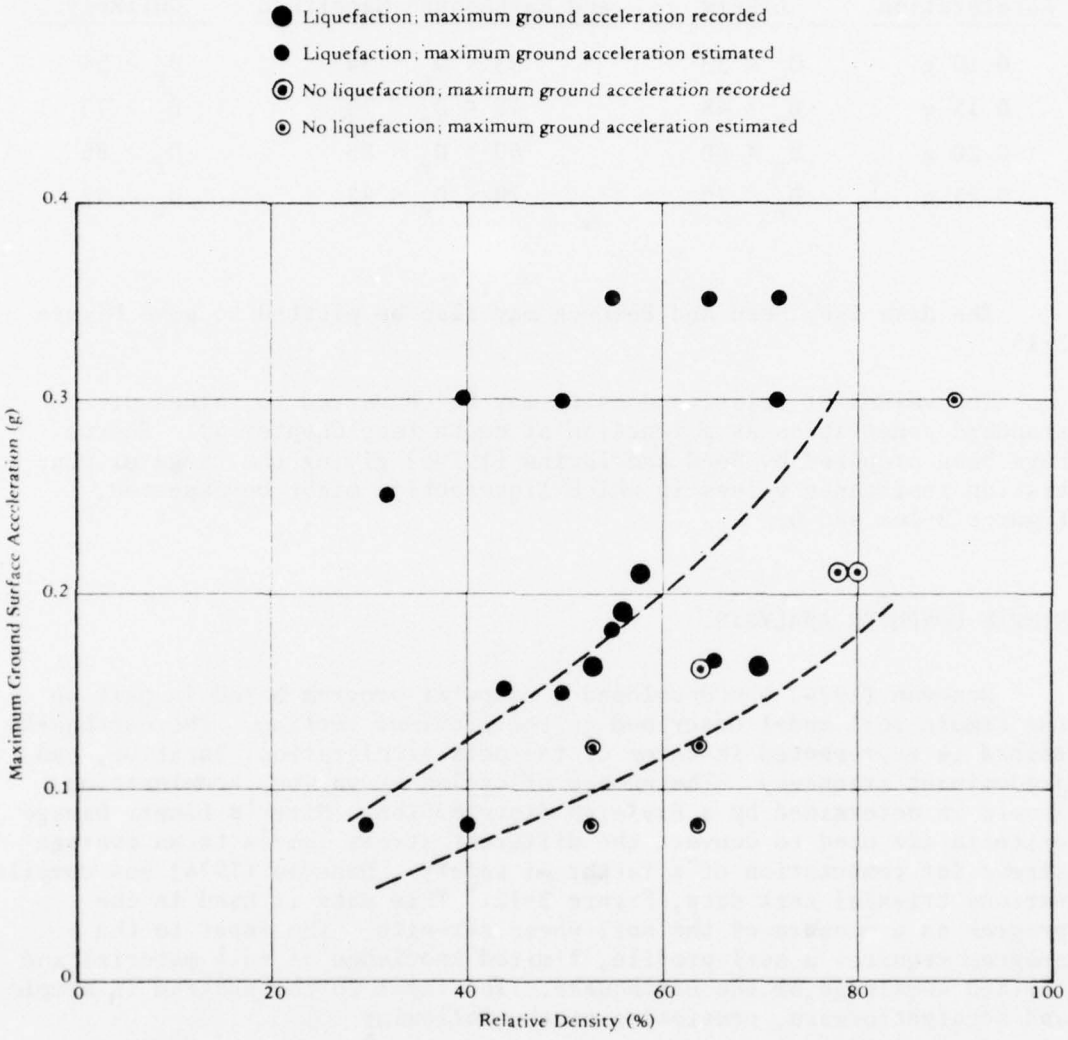

Figure 3-14. Evaluation of liquefaction potential for sands (water table 5 feet below ground surface) ("Evaluation of Soil Liquefaction Effects on Level Ground During Earthquakes," by H. B. Seed, in ASCE Preprint 2752 of Liquefaction Problems in Geotechnical Engineering, ASCE Annual Convention, Philadelphia, Pa., 27 Sep-1 Oct 1976).

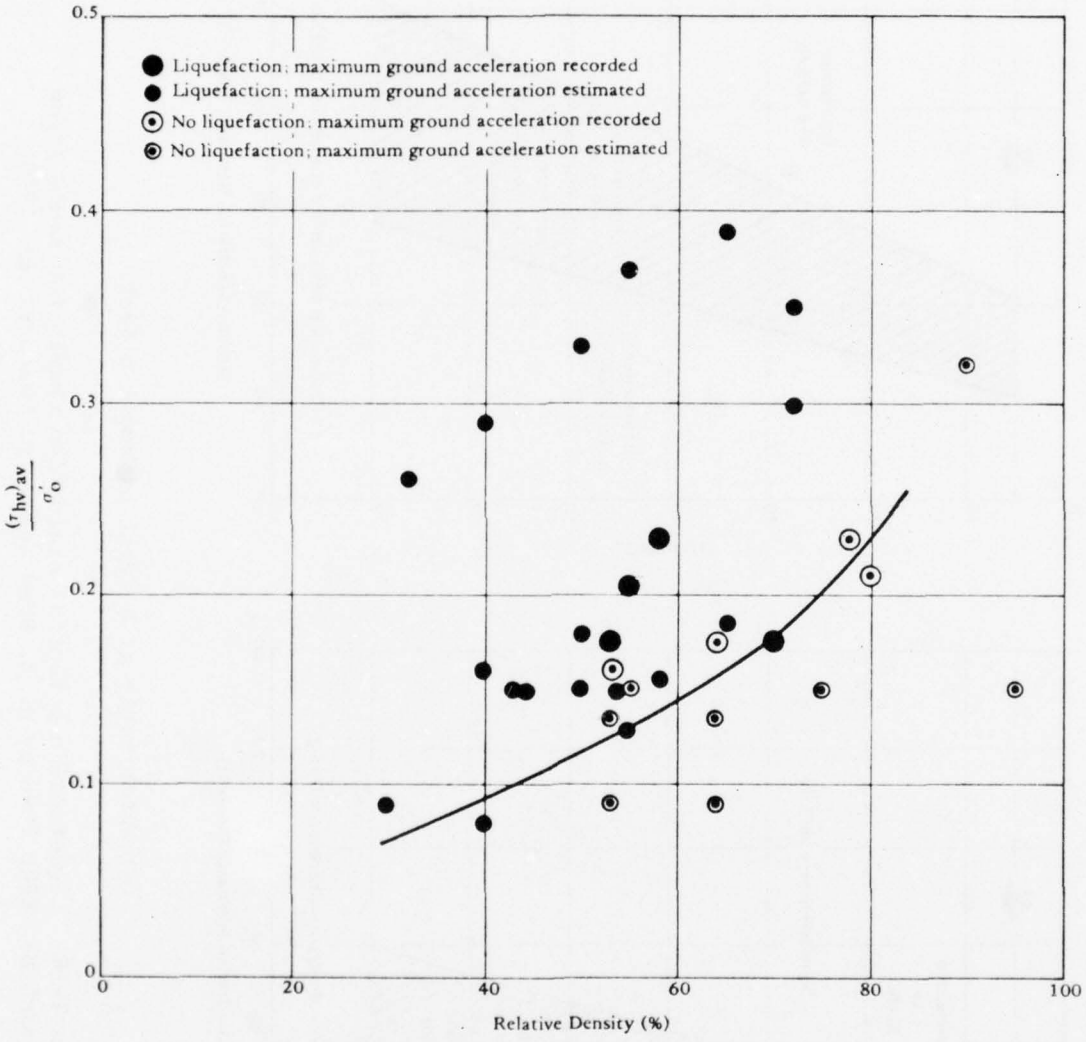

Figure 3-15. Relationship between $(\tau_{hv})_{av}/\sigma'_o$ and relative density for known cases of liquefaction and nonliquefaction (from Report No. EERC 70-8 by H. B. Seed and W. H. Peacock, Nov 1970).

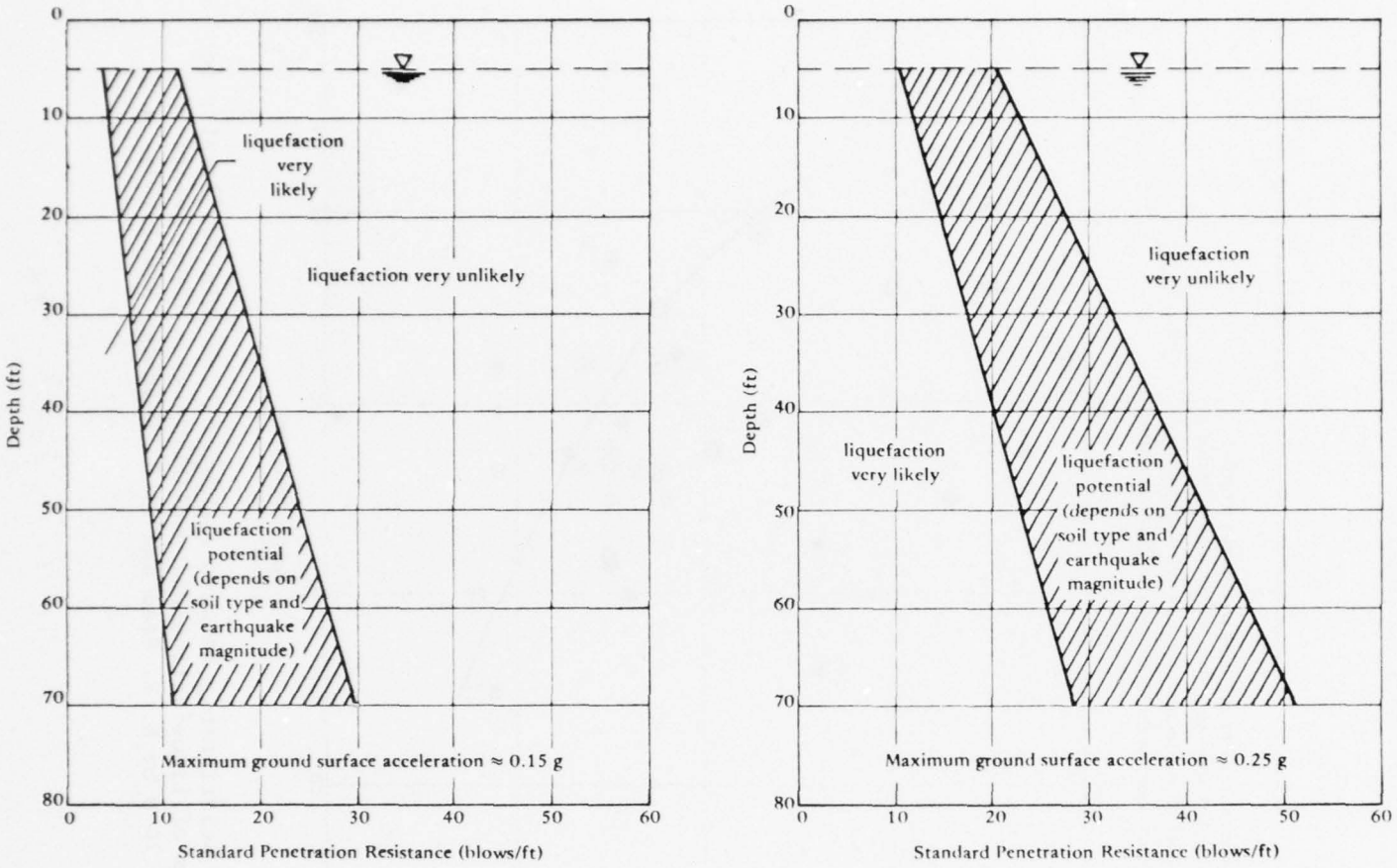

(a) Water table at a depth of about 5 feet.

Figure 3-16. Liquefaction potential evaluation charts for sands (from Report No. EERC 70-8 by H. B. Seed and W. H. Peacock, Nov 1970).

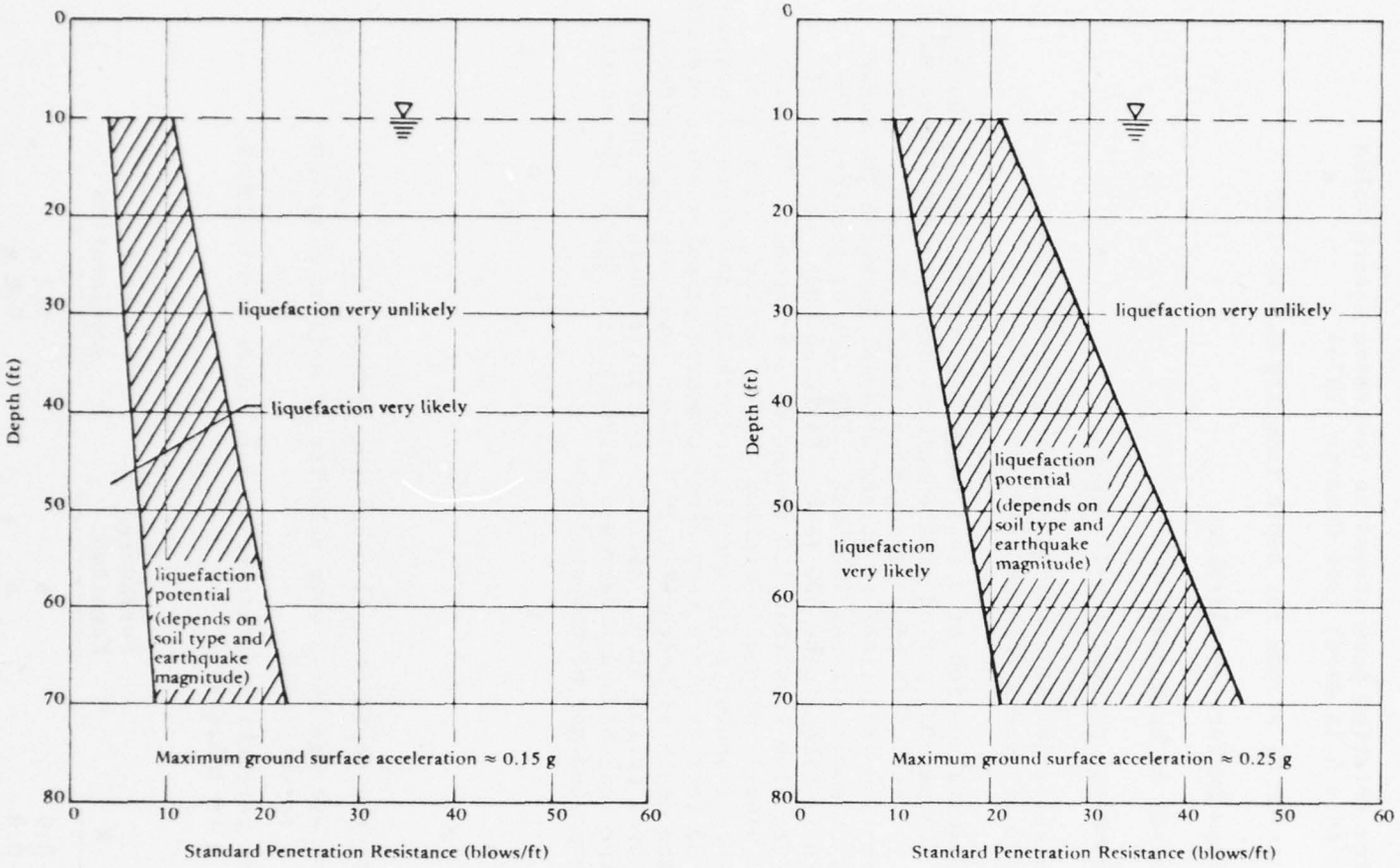

(b) Water table at a depth of about 10 feet.

Figure 3-16. Continued.

5. Effective stress at center of layer

6. Factor relating peak stress to root-mean-square value (3.5 to 4.5 is used) (see Donovan, 1974)

7. Reduction of stress for depth (usually 0.9 to 1.0)

8. Maximum surface acceleration

9. Duration of earthquake

10. Fundamental period of soil deposit

11. Data pairs defining the τ_{av}/σ'_v ratio versus the number of cycles (Figure 3-12)

The fundamental period of a soil deposit given as item 10 above is equal to the fundamental period of the soil overlying rock-like formations when subject to vertically propagating shear waves. For this usage, a rock-like formation is defined to be any material in which the shear wave velocity at small strains is about 2,500 ft/s or greater. The limit to depth is taken to be 500 feet. Based on this, the natural period will vary from less than 1.0 second to 2.5 seconds. The value 0.5 second is usually used as a minimum natural period. Firm sites, where only dense granular soils overlie bedrock and the depth to bedrock is less than 30 feet or where very dense cemented granular soils overlie bedrock and the depth of bedrock is 70 feet or less, may be considered to have a natural period of 0.5 second. For soils where the shear wave velocity of the soil does not decrease markedly with depth, the characteristic site period may be computed by:

$$T = \frac{4\,H}{R\,V_s}$$

where H = the depth of soil overlying bedrock

V_s = average shear wave velocity of soil as measured in the field

R = correction factor to V_s for higher strain levels as follows:

R	Earthquake Magnitude	Peak Acceleration
0.9	6	0.1 g
0.8	6	0.2 g
0.67	7	0.3 g
0.67	7	0.4 g

The program computes the number of cycles by dividing the duration of the earthquake by the period of the soil deposit.

An example problem is given in Figure 3-17.

COMPLEX COMPUTER ANALYSIS, ONE-DIMENSIONAL MODELS

A soil profile may be analyzed as a one-dimensional shear wave problem assuming the stress wave to be only a vertically propagating shear wave. The differential equations of motion can be solved in closed form for linear elastic soil properties. This has been done by Seed and Idriss (1969) and Kanai (1961) to provide a one-dimensional analysis of sites of simple geometry. However, the stress-strain characteristics of a site are highly nonlinear, hysteretic, and strain-dependent as shown in Chapter 2.

Streeter, et al. (1974) developed a computer program using the method of characteristics for calculating one-dimensional dynamic behavior of soils. A soil profile is divided into layers down to bedrock. Dynamic excitation of the soil is introduced at the rock-soil interface. The response of the soil can be evaluated on the basis of elastic, viscoelastic, or nonlinear (Ramberg-Osgood) soil behavior. The program determines shear, velocity, and displacement information.

An analytical technique for analyzing the response of horizontal soil profiles to earthquake motion is described by Seed and Idriss (1969, 1970b) and Idriss and Seed (1968, 1970). The soil profile is idealized by a series of discrete masses and springs with linear viscous dampers. The nonlinear and hysteretic stress-strain characteristics of the soil are introduced by using an equivalent shear modulus and an equivalent viscous damping factor which can vary with each layer of soil profile and with the strain level within the layer. The equivalent shear modulus for a given strain level is taken as the slope of the diagonal line (average slope) drawn through the hysteresis loop, which is shown in Figure 3-18 for a cyclically loaded laboratory specimen. The average equivalent viscous damping coefficient is proportional to the ratio of area of the hysteretic loop, as shown in the figure, to the maximum stored energy during the cycle.

An iterative procedure is used to obtain strain compatible values of shear modulus and damping. The response of the soil profile modeled as discrete masses is computed, and strains are determined.

```
EXAMPLE DATA SET FOR LIQUEFACTION BY STOCHASTIC PROCEDURES:  NCD  6-74
EL CENTRO EARTHQUAKE OF 1940.  LIQUEFACTION IN BRAWLEY, CALIF. (M=7.0)

LIQUEFACTION EVALUATION BY DONOVAN≠S STOCHASTIC PROCESS FOR LAYER
NUMBER 1 AT DEPTH OF 15.0 FEET,    NARROW BANDWIDTH USING ASSUMED
RAYLEIGH DISTRIBUTION

LIQUEFACTION POTENTIAL ESTIMATION BASED ON INTERPOLATION OF A
SERIES OF POINTS ON A (TAU/SIGMA) VS LOG10(NUMBER OF CYCLES)
RELATIONSHIP.  DATA FOR A RELATIVE DENSITY OF  55 PERCENT

       TAU/SIGMA  NUMBER OF CYCLES

  1       .421          1.00
  2       .359          3.00
  3       .332          5.00
  4       .297         10.00
  5       .265         20.00
  6       .225         50.00
  7       .198        100.00
  8       .173        200.00

    AVERAGE MAXIMUM SHEAR STRESS    =    180.0 PSF
    PEAK VALUE SIGMA LEVEL          =      4.0
    SIMPLE SHEAR CORRECTION FACTOR  =      .59
    DEPTH EFFECT REDUCTION FACTOR   =     1.00
    PEAK SURFACE ACCELERATION       =     .100 G
    EFFECTIVE NORMAL STRESS         =   1800.0 PSF
    FUNDAMENTAL PERIOD              =     .50 SECONDS
    DURATION OF STRONG SHAKING      =    30.0 SECONDS
    MOST PROBABLE NUMBER OF CYCLES  =      60
    RELATIVE DENSITY                =   55.000

      ALL STRESS VALUES REPRESENT THE  4.00 TIMES SIGMA LEVEL

      LIQUEFACTION WILL NOT OCCUR AT A RELATIVE DENSITY OF 55.000

    ITERATION NUMBER      =  1
    PEAK SHEARING STRESS  =  180.00 PSF

        STRESS    CUMULATIVE
          PSF       DAMAGE

        180.00   15.154E-03

    ITERATION NUMBER      = 17
    PEAK SHEARING STRESS  =  487.69 PSF
    FACTOR OF SAFETY      =   2.709

        STRESS    CUMULATIVE
          PSF       DAMAGE

        487.69   99.977E-02
```

Figure 3-17. Example problem using simple computer program.

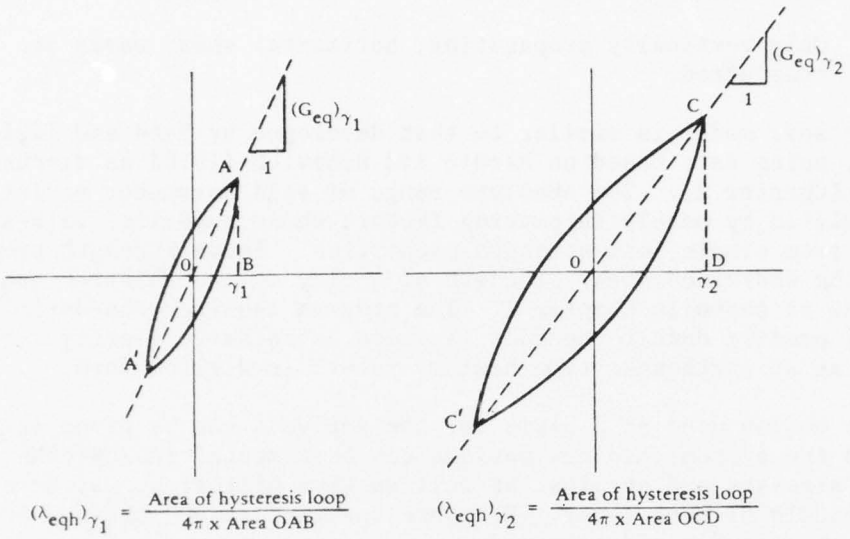

Figure 3-18. Equivalent linear shear moduli and damping used in discrete mass model (from H. B. Seed and I. M. Idriss, Jan 1969).

Another automated-analysis technique, more widely used today for treating horizontal soil layers, has been developed by Schnabel, Lysmer, and Seed (1972), based on the one-dimensional wave propagation method. This program, SHAKE, can compute the responses for a given horizontal earthquake acceleration specified anywhere in the system. The analysis incorporates nonlinear soil behavior, the effect of the elasticity of the base rock, and variable damping. It computes the responses in a system of homogeneous viscoelastic layers of infinite horizontal extent, subject to vertically traveling shear waves. The program is based on the continuous solution of the wave-equation adapted for use with transient motions through the Fast Fourier Transform algorithm. Equivalent linear soil properties are obtained by an iterative procedure for values of modulus and damping compatible with the effective strains in each layer. The following assumptions are made:

1. The soil layers extend infinitely in the horizontal direction.

2. The layers are completely defined by shear modulus, critical-damping ratio, density and thickness.

3. The soil values are independent of frequency.

4. Only vertically propagating, horizontal shear waves are considered.

The soil model is similar to that developed by Seed and Idriss (1970c), using data based on Hardin and Drnevich (1970) as discussed earlier (Chapter 2). The absolute range of soil parameter variation may be stipulated by merely in-putting factors whose numerical values may be derived from simple soil strength properties. These strength properties may be the undrained shear strength of a clay or the relative density for sands as shown in Chapter 2. The program requires the definition of the soil profile down to bedrock (assumed as seismic velocity 2,500 ft/s) as well as an earthquake time history record in digital form.

The motion used as a basis for the analysis can be given in any layer in the system, and new motions can be computed in any other layer. Maximum stresses and strains, as well as time histories, may be obtained in the middle of each layer. Response spectra may be obtained and amplification spectra determined.

For liquefaction analysis of a soil profile the stress history of the various layers is compared to their susceptibility to liquefaction.

The calculated shear stress history is used to determine a number of equivalent cycles of load at an average stress level from which τ_{av}/σ'_v is determined. The liquefaction susceptibility may be measured directly by cyclic loading test or estimated on the basis of Figure 3-12.

For laboratory cyclic load tests, soil specimens are prepared to represent the in situ conditions and are subjected to stress cycles of various magnitudes to determine the number of actual cycles necessary to cause liquefaction. The triaxial test information corrected to field conditions is used to estimate the shear stress level to cause liquefaction for the number of cycles determined in the computer analysis. The factor of safety is the ratio of the resisting shear strength from the triaxial test data to the applied shear stress level from the computer analysis.

Lee and Chan (1972) have developed a procedure for computing the equivalent number of cycles. The term equivalent number of significant cycles N_{eq} refers to that number of uniform cycles of stress intensity τ_{av} which, if applied to an element of soil, would have the same effect in terms of the soil strength or deformation as if the actual train of irregular cyclic shear stresses were applied (see Figure 3-19). The value of τ_{av} is usually taken to be equal to 0.65 τ maximum. To convert the actual stress time history into an equivalent number of uniform cycles, divide the stress range (0 to τ maximum) into a convenient number of levels and note the stress within each level or increment, τ_i, as shown in Figure 3-20. The actual number with peaks in the computed

stress history which fall within each of these levels is counted n_{τ_i}. Since the actual time history is not symmetric about the zero stress axis, the number of peaks on both sides are counted, and two peaks are equivalent to one cycle. A shear strength curve from laboratory tests or Figure 3-12 is corrected to field conditions. This curve represents a factor of safety of 1.0; theoretically the values on the curve should be divided by the estimated factor of safety to correctly show the true relationship for the soil under the specific earthquake.

The number of cycles N_{τ_i} and $N_{\tau_{av}}$ corresponding to the incremental stress levels and τ_{av} level are obtained. The ratio of the number of cycles at the τ_{av} stress level to cause liquefaction $N_{\tau_{av}}$ to the number of cycles at the incremental stress levels to cause liquefaction N_{τ_i} is used to multiply the actual number of counted cycles at that incremental stress level n_{τ_i}. These ratios are summed for all n increments of stress from 0 to τ_{max}

$$N_{eq} = \sum_{i=1}^{n} \left(\frac{N_{\tau_{av}}}{N_{\tau_i}} \text{ from test data or Figure 3-12} \right) \left(n_{\tau_i} \begin{matrix} \text{actual} \\ \text{SHAKE} \\ \text{data} \end{matrix} \right)$$

If the estimated factor of safety is correct, N_{eq} determined from the summation would equal $N_{\tau_{av}}$ from the laboratory test data or Figure 3-12 at the average stress level. If it does not, revise the estimate of the factor of safety and repeat. In practice it has been found that it is not necessary to multiply the strength curve by the estimated factor of safety. In this case the factor of safety would then be the ratio of τ at N_{eq} from test data divided by τ_{av}.

Seed, et al. (1975) have proposed Figure 3-21 as an average shape representation of the relationship between stress ratio and number of cycles to liquefaction. Using Figure 3-21, Figure 3-22 is generated; a factor of safety of 1.5 is applied to produce the lower curve. From this curve, Table 3-1 is obtained which gives conversion factors for equivalent stress levels. An example is given in Figure 3-23. Seed, et al. (1975) have also evaluated the equivalent number of uniform stress cycles based on strong motion data (Figure 3-24).

EFFECTS OF SOIL AND SITE PARAMETERS

Frequently, the parameters needed in the response studies are poorly defined at a given location. Often, the values of these parameters must be assumed in order to perform the ground response analyses. Experience has shown that variations in the value of any one of the parameters may affect the solution differently from site to site, and no general rules may be formulated at this time to establish the influence of the variables.

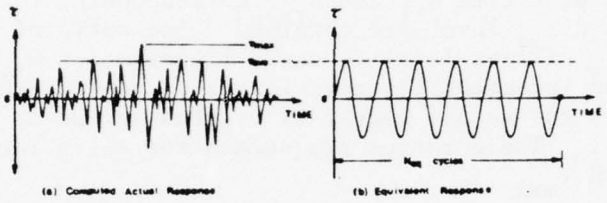

Figure 3-19. Actual and equivalent earthquake stress history.

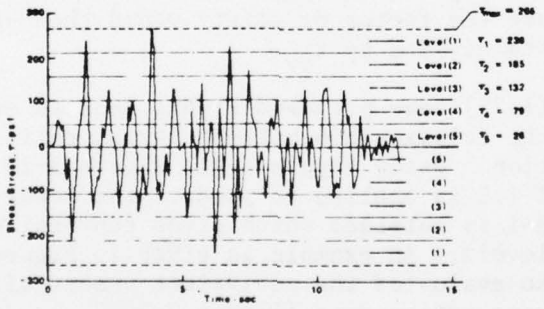

Figure 3-20. Steps in calculating N_{eq} from seismic stress history.

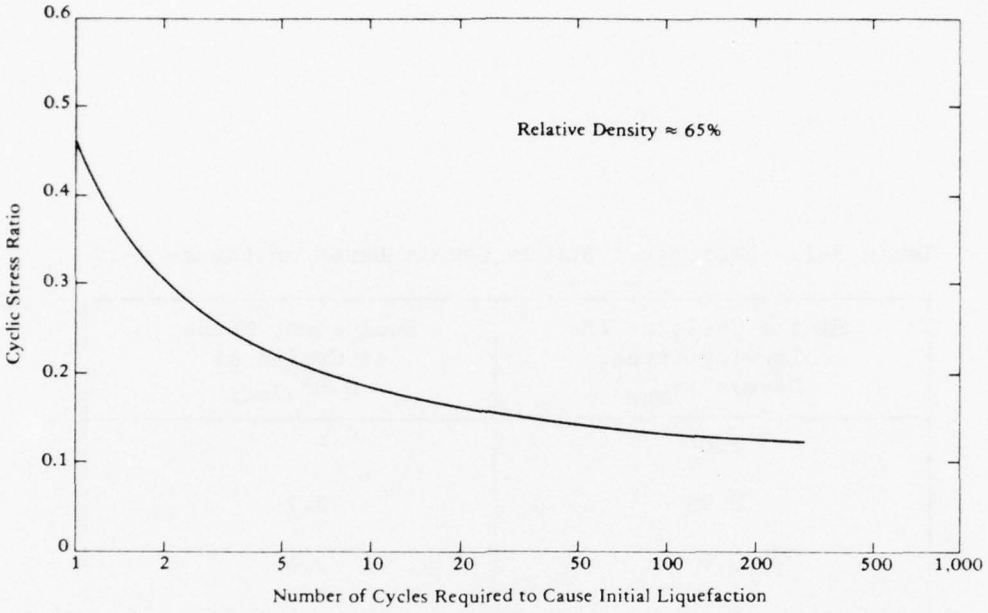

Figure 3-21. Representative curve for relationship between cyclic stress ratio and number of cycles to liquefaction (from H. B. Seed, 1976).

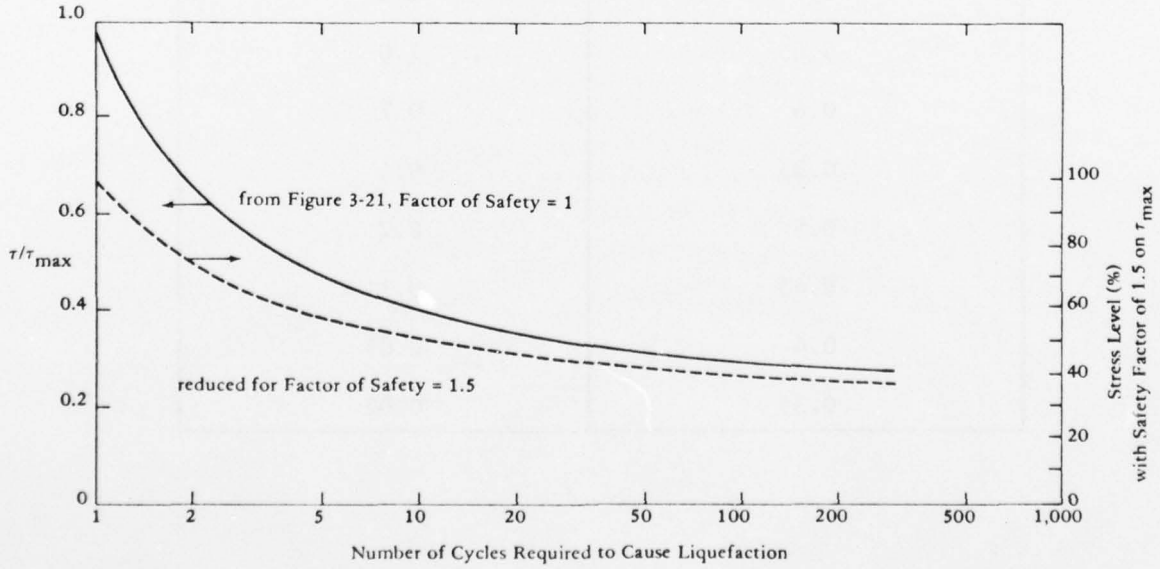

Figure 3-22. Representative relationship between τ/τ_{max} and number of cycles required to cause liquefaction (from H. B. Seed, 1976).

Table 3-1. Equivalent Stress Levels Based on Figure 3-17

Single Cycle at the Following Stress Levels (τ_{max})	Equivalent Number of Cycles at 0.65 τ_{max}
1.0	3
0.95	2.7
0.9	2.4
0.85	2.05
0.8	1.7
0.75	1.4
0.7	1.2
0.65	1.0
0.6	0.7
0.55	0.4
0.5	0.2
0.45	0.1
0.4	0.04
0.35	0.02

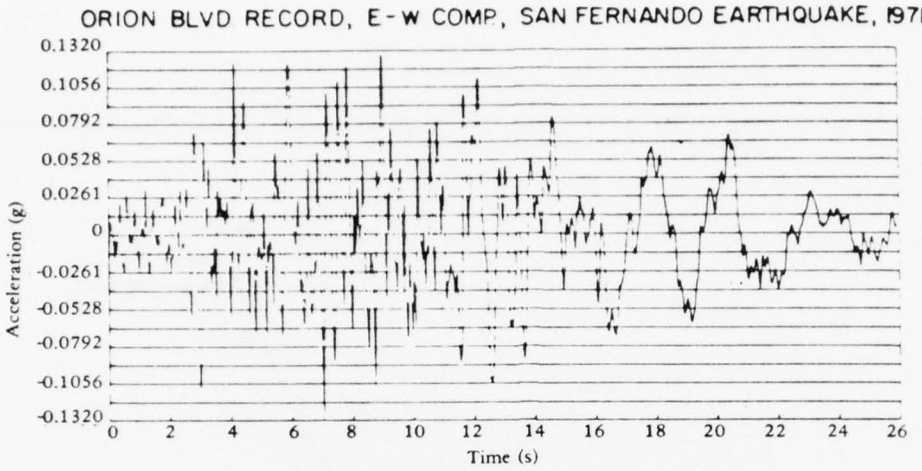

	ABOVE HORIZONTAL AXIS			BELOW HORIZONTAL AXIS		
Stress Level: Fraction of τ_{max}	Number of Stress Cycles	Conversion Factor	Equivalent No of Cycles at 0.65 τ_{max}	Number of Stress Cycles	Conversion Factor	Equivalent No of Cycles at 0.65 τ_{max}
τ_{max}	—	—	—	1	3.00	3.00
0.95 "	3	2.70	8.10	—	—	—
0.90 "	1	2.40	2.40	—	—	—
0.85 "	2	2.05	4.10	1	2.05	2.05
0.80 "	—	—	—	2	1.70	3.40
0.75 "	3	1.40	4.20	—	—	—
0.70 "	—	—	—	2	1.20	2.40
0.65 "	1	1.00	1.00	1	1.00	1.00
0.60 "	2	0.70	1.40	1	0.70	0.70
0.55 "	3	0.40	1.20	3	0.40	1.20
0.50 "	1	0.20	0.20	5	0.20	1.00
0.45 "	3	0.10	0.30	5	0.10	0.50
0.40 "	3	0.04	0.12	—	—	—
0.35 "	5	0.02	0.10	7	0.02	0.14
0.30 "	—	—	—	—	—	—
		Total	23.12		Total	15.39
		Average number of cycles at 0.65 τ_{max} = 19.30				

Figure 3-23. Evaluation of equivalent uniform cyclic stress series, Orion Boulevard record, east-west component (from H. B. Seed, 1976).

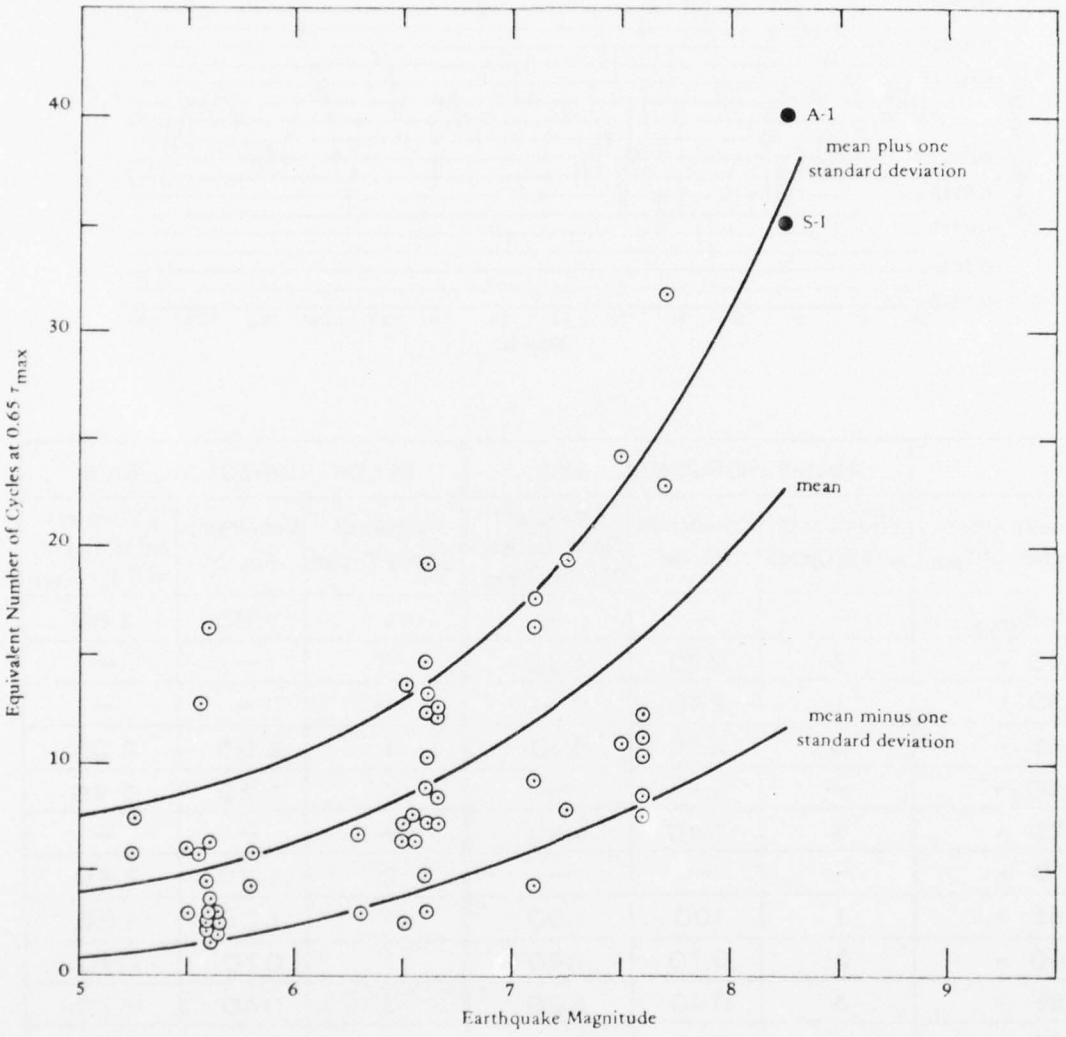

Figure 3-24. Equivalent numbers of uniform stress cycles based on all components of ground motion (from H. B. Seed, 1976).

Earthquake motions are produced by a stress wave, which is transmitted more rapidly and with less energy loss through the bedrock than through the overlying soils. When the bedrock has a horizontal surface of great extent and the overlying soil layers are also horizontal, it is frequently assumed that the earthquake motion within the soil is produced essentially by horizontal shear waves which propagate upward through the soil from the bedrock surface. This assumption greatly simplifies the analysis since the problem can be reduced to a one-dimensional shear wave problem. This is a simplification, since vertical components of the earthquake motion are always present and the wave transmission problem may be more complex than can be simulated in a one-dimensional model.

When the bedrock or soil layers are inclined, a one-dimensional shear wave assumption is questionable, and a two-dimensional model may be required to account for the more complex geometry and wave motion.

Lysmer, Seed, and Schnabel (1970) have shown that under identical boundary conditions, the lumped mass solution and the wave propagation solution are basically the same. Arango and Dietrich (1972) have investigated the variation of parameters for the two methods. They note close agreement in peak levels of motion with some differences in computed time histories.

Depth to Bedrock

In many cases the depth to bedrock is not well-defined. A preliminary analysis may be required to assess the influence of depth to bedrock on the ground response. Dezfulian and Seed (1969) have shown that an increase in thickness of the deposit may or may not cause a substantial change in surface motion. Their studies show that for shallow deposits, an increase in thickness of medium sand from 38 feet (12 meters) to 50 feet (15.6 meters) reduced the response significantly. Increasing the thickness to 80 feet (25 meters) reduced the response still more, but a further increase from 80 to 100 feet (31.2 meters) did not produce any additional reduction in the response.

For much deeper deposits, 1,000 feet (330 meters), Kiefer, et al. (1970) analyzing the conditions at Osaka, found that the response was not very sensitive to the range of depths investigated.

Arango and Dietrich (1972) studied the variation for depths to bedrock equal to 600, 800, and 900 feet. The values of the maximum acceleration and the velocity and acceleration spectra are shown in Figure 3-25. The acceleration spectra for two depths to bedrock at Study Site A are also shown in Figure 3-25.

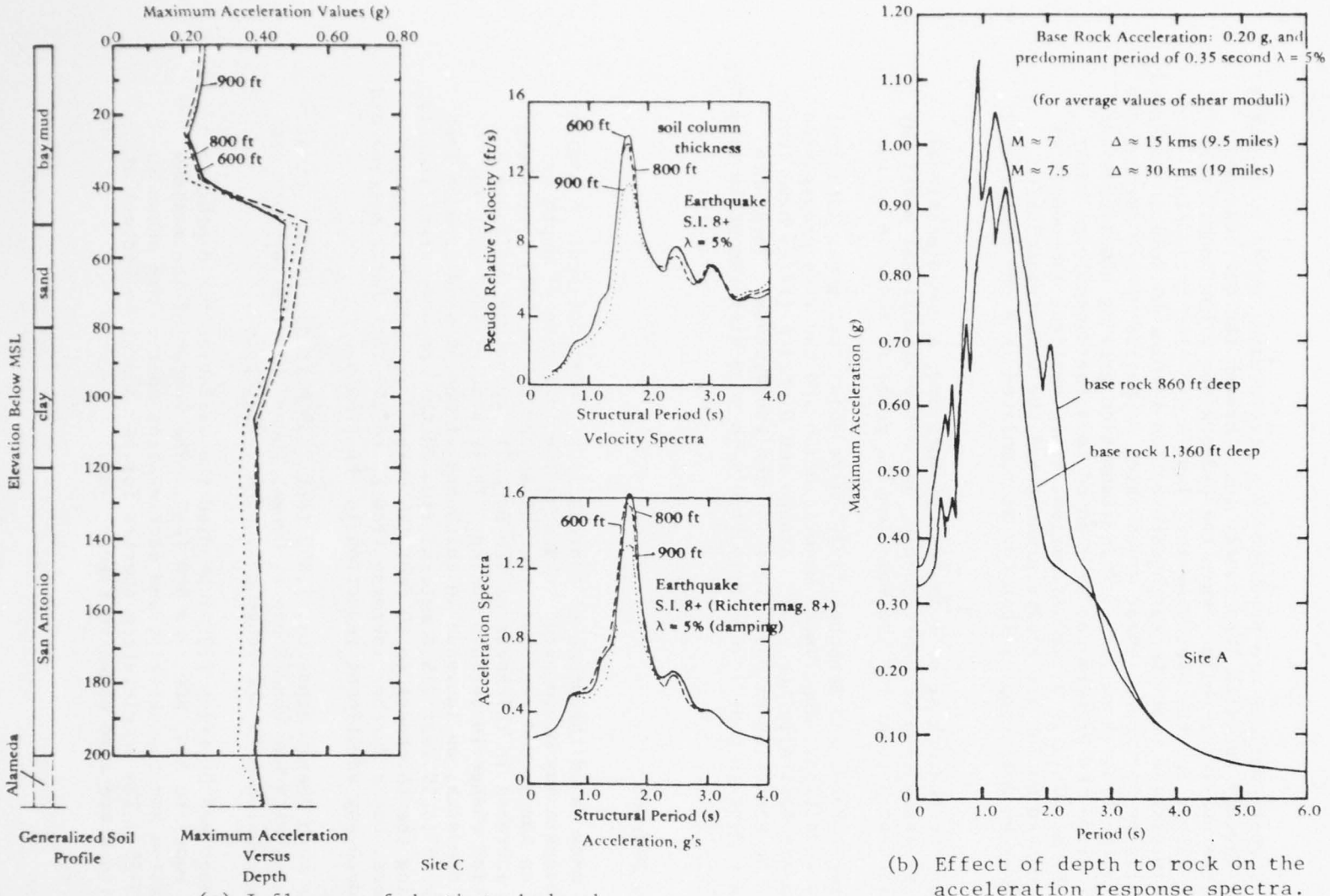

(a) Influence of depth to bedrock.

(b) Effect of depth to rock on the acceleration response spectra.

Figure 3-25. Response spectra and maximum surface accelerations (from "Soil and Earthquake Uncertainties on Site Response Studies," by I. Arango and R. J. Dietrich, in Proceedings of the International Conference on Microzonation for Safer Construction Research and Application, 30 Oct-3 Nov 1972).

The above examples show that for shallow soil deposits, the depth to bedrock may or may not significantly affect the response. Deep soil deposits are in general less sensitive. Preliminary studies using a reasonable range of depth to bedrock should precede any ground response calculation when uncertainties regarding the actual depth are present.

Influence of Soil Profile

The frequency characteristics of the ground motions and the form of the ground response spectra may be influenced by the nature of the soil conditions underlying the sites. This is illustrated by the studies by Arango and Dietrich (1972). Different soil profiles were used in the response analysis as shown in Figure 3-26. The values of the maximum acceleration and displacement obtained are shown in Figure 3-27. The corresponding response spectra are shown in Figure 3-28. Significant changes in response can result from variation in soil profile, and great care must be placed on the correct site stratigraphic representations. The importance of the time history of the ground motion on the response values is also apparent by comparing the spectra from Figure 3-28a to that of Figure 3-28b.

Soil Rigidity

Since the stiffness of the soil deposits can only be approximated, it is often desirable to run preliminary response analyses using the most reasonable values of the shear moduli for the various soils and values (say 50% to 100%) greater than those judged to be the most reasonable. Arango and Dietrich (1972) calculated the maximum ground surface acceleration, ground displacement, the fundamental period of the soil column, and the response spectra by using the average values of the shear moduli and values 50% higher. The results of the calculations are shown in Figure 3-29. In some cases, errors in the estimated shear moduli cause minor differences in the calculated ground response which have no practical significance for engineering purposes. In other cases, however, it has been found that great differences may occur as a consequence of varying the values of the shear moduli.

Amplitude of Rock Acceleration

Schnabel and Seed (1972) have indicated that spectral acceleration values are often not significantly influenced by substantial reductions in maximum acceleration levels in rock. It was found that generally a reduction of 15% to 25% in maximum rock acceleration values will affect the spectral acceleration by less than 10%.

Layer Classification	Layer Thickness (ft)	Unit Weight γT pcf	Strength Su (psf) or K_2*	Shear Modulus g x 10^6 (psf)	Shear Wave Velocity, Vs fps
Bay Mud	21	110	200	0.4	340
	21	110	250	0.5	380
Sand	15	125	K_2 = 80	3.0	880
	15	125	K_2 = 80	3.6	960
Clay	40	130	2,000	4.0	1,020
San Antonio	80	130	2,900	5.8	1,200
Alameda	100	130	12,000 clay	4.0	2,400
	100	130	K_2 = 115 gravel	12.8	1,800
	100	130	12,000 clay	24.0	2,440
	100	130	12,000 clay	24.0	2,440

*Shear modulus = $1{,}000\ K_2\ (\sigma'm)^{1/2}$
where $\sigma'm$ = mean effective stress.

(a) Model 1 C = 12,000 psf.

Layer Classification	Layer Thickness (ft)	Unit Weight γT pcf	Strength Su (psf) or K_2*	Shear Modulus g x 10^6 (psf)	Shear Wave Velocity, Vs fps
Bay Mud	21	110	200	0.4	340
	21	110	250	0.5	380
Sand	15	125	K_2 = 80	3.0	880
	15	125	K_2 = 80	3.6	960
Clay	40	125	2,000	4.0	1,020
San Antonio	80	130	2,900	5.8	1,200
Alameda	100	130	3,700 clay	7.4	1,350
	100	130	K_2 = 115 gravel	12.8	1,800
	100	130	7,300 clay	14.6	1,900
	100	130	9,000 clay	18.0	2,100

C = Su = Undrained clay strength.
P = Effective overburden pressure.

(b) Model 2 C/P = 1/4.

Figure 3-26. Four soil profile representations of same site (from "Soil and Earthquake Uncertainties on Site Response Studies," by I. Arango and R. J. Dietrich, in Proceedings of the International Conference on Microzonation for Safer Construction Research and Application, 30 Oct-3 Nov 1972).

AD-A062 433 CIVIL ENGINEERING LAB (NAVY) PORT HUENEME CALIF F/G 8/11
SEISMIC LIQUEFACTION POTENTIAL.(U)
SEP 78 J M FERRITTO, J B FORREST

UNCLASSIFIED CEL-TN-1530 NL

2 OF 2
AD
A062433

Layer Classification	Layer Thick-ness (ft)	Unit Weight γT pcf	Strength Su (psf) or K_2*	Shear Modulus g x 10^6 (psf)	Shear Wave Velocity, Vs fps
Bay Mud	21	110	200	0.4	340
	21	110	250	0.5	380
Sand	15	125	K_2 = 80	3.0	880
	15	125	K_2 = 80	3.6	960
Clay	40	130	2,000	4.0	1,020
San Antonia	80	130	2,900	5.8	1,200
Alameda	100	130	6,000 clay	12.0	1,730
	100	130	K_2 = 115 gravel	12.8	1,780
	100	130	10,000 clay	20.0	2,240
	100	130	10,000 clay	20.0	2,240

***Strength between Models 1 and 2.

(c) Model 3 intermediate properties.***

Layer Classification	Layer Thick-ness (ft)	Unit Weight γT pcf	Strength Su (psf) or K_2*	Shear Modulus g x 10^6 (psf)	Shear Wave Velocity, Vs fps
Bay Mud	21	110	200	0.4	340
	21	110	250	0.5	380
Sand	15	125	K_2 = 80	3.0	880
	15	125	K_2 = 80	3.6	960
Clay	40	130	2,000	4.0	1,020
San Antonio	80	130	2,900	5.8	1,200
Alameda	100	130	4,950 clay	9.9	1,560
	100	130	7,240 clay	14.5	1,900
	100	130	9,500 clay	19.0	2,170
	100	130	10,750 clay	21.5	2,320

(d) Model 4 C/P = 1/3.

Figure 3-26. Continued.

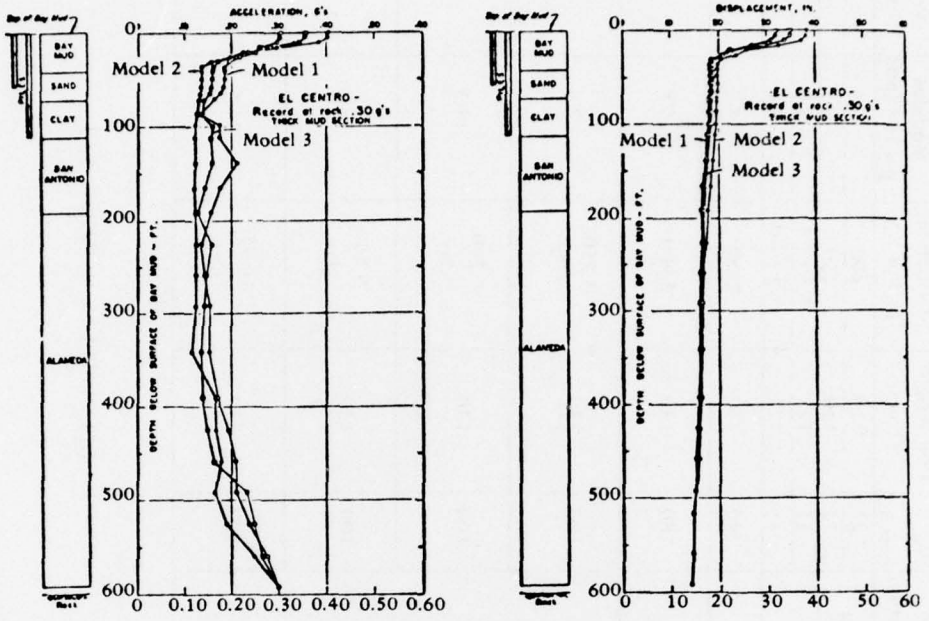

(a) El Centro earthquake.

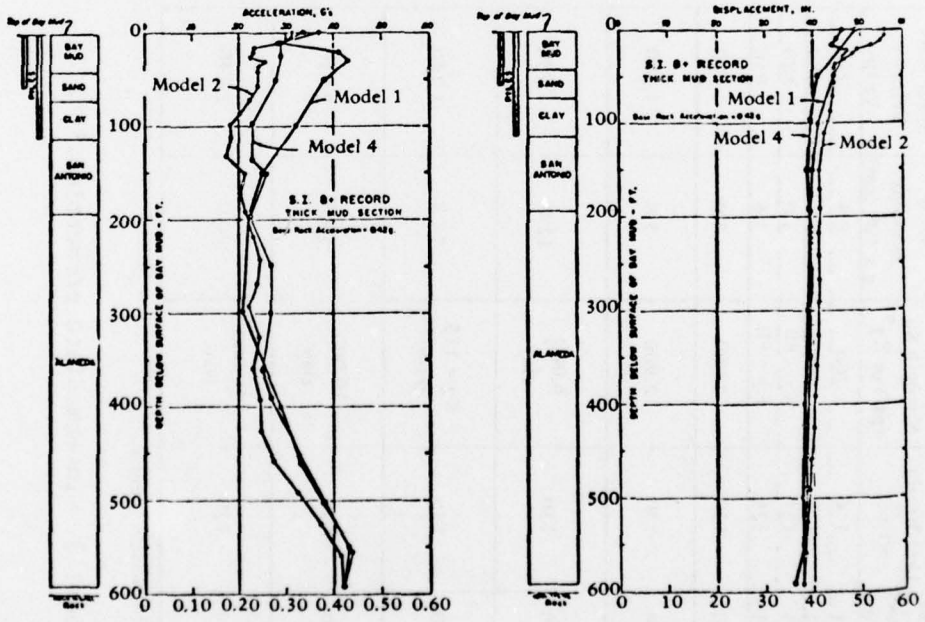

(b) Site intensity = 8+ earthquake.

Figure 3-27. Response of soil models (from "Soil and Earthquake Uncertainties on Site Response Studies," by I. Arango and R. J. Dietrich, in Proceedings of the International Conference on Microzonation for Safer Construction Research and Application, 30 Oct-3 Nov 1972).

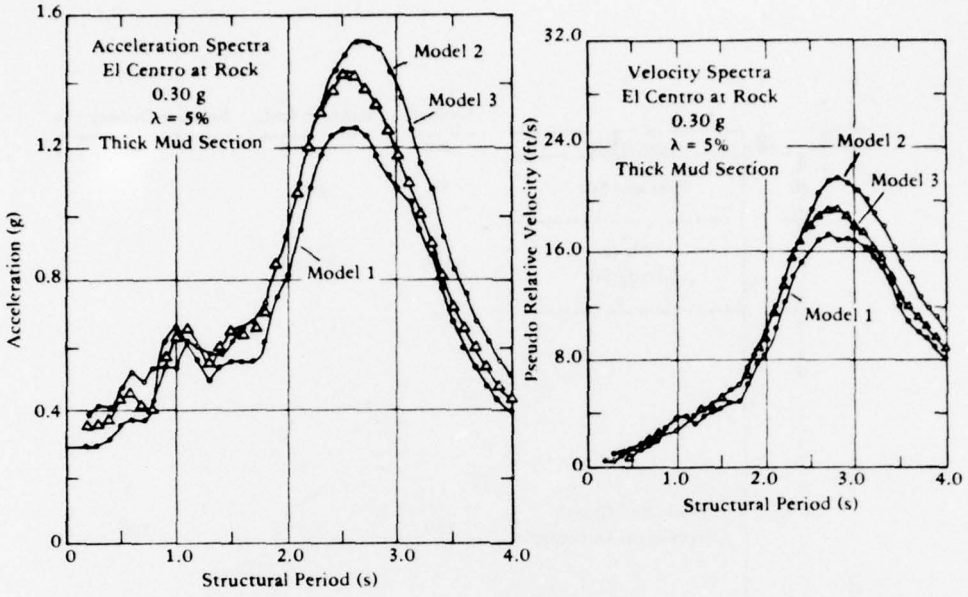

(a) El Centro earthquake.

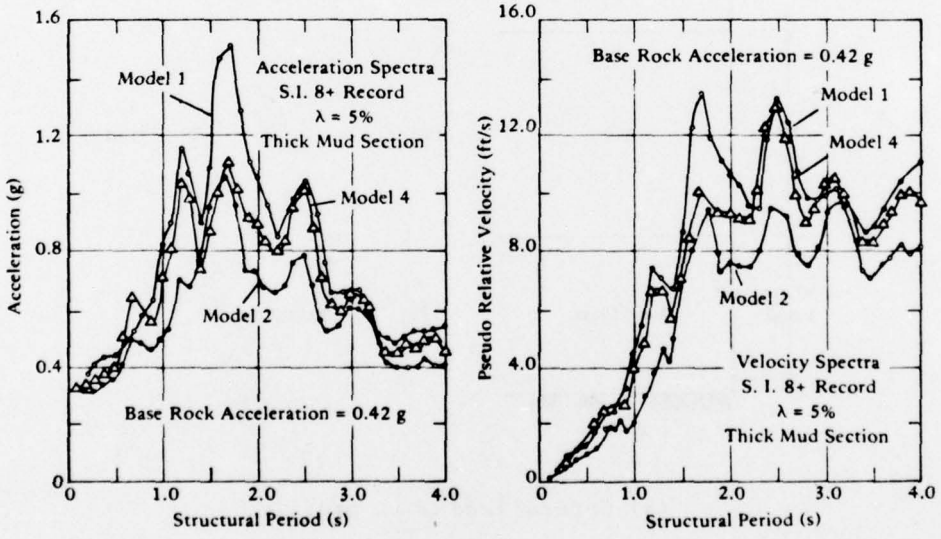

(b) S.I. 8+ earthquake.

Figure 3-28. Response spectra (from "Soil and Earthquake Uncertainties on Site Response Studies," by I. Arango and R. J. Dietrich, in *Proceedings of the International Conference on Microzonation for Safer Construction Research and Application*, 30 Oct-3 Nov 1972).

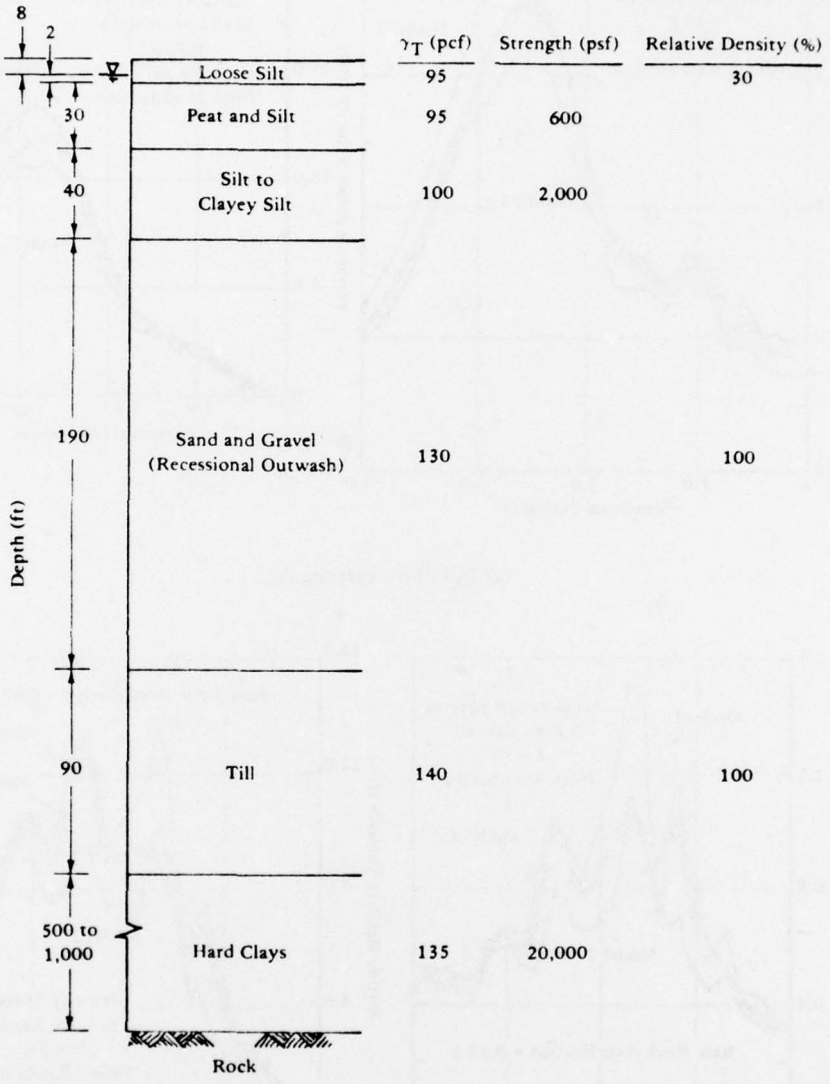

(a) Generalized soil profile.

Figure 3-29. Effect of variation of material properties (from "Soil and Earthquake Uncertainties on Site Response Studies," by I. Arango and R. J. Dietrich, in Proceedings of the International Conference on Microzonation for Safer Construction Research and Application, 30 Oct-3 Nov 1972).

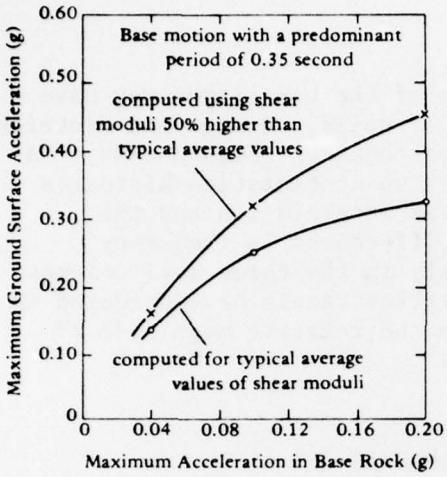

(b) Relationship between maximum ground surface displacement and maximum base rock acceleration.

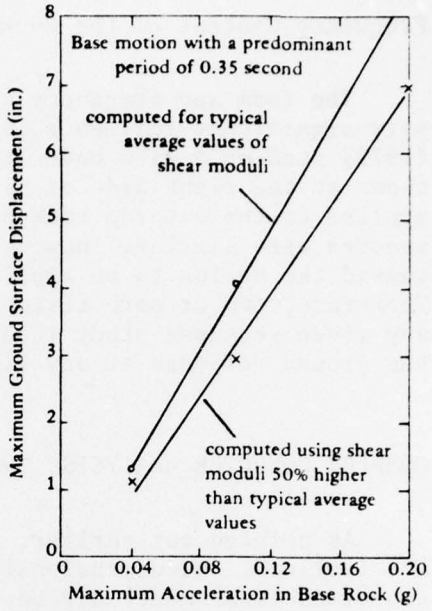

(c) Relationship between maximum ground surface displacement and maximum base rock acceleration.

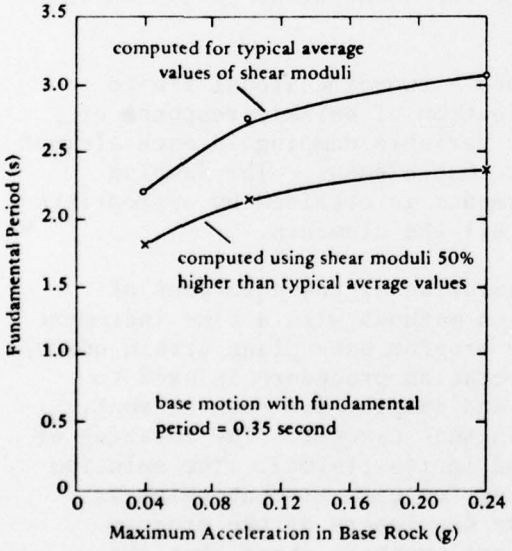

(d) Fundamental period of soil deposit.

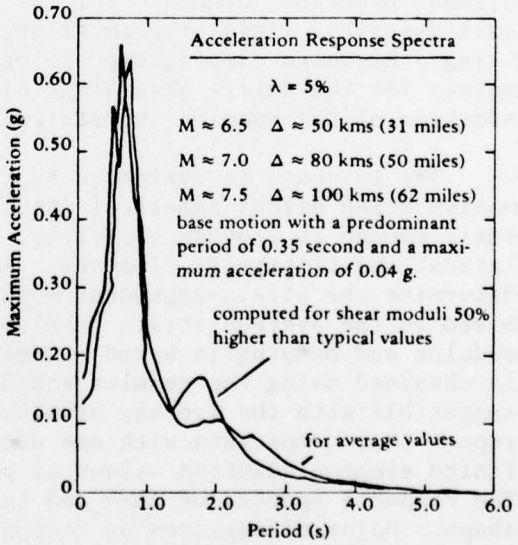

(e) Effect of soil moduli on the acceleration response spectra.

Figure 3-29. Continued

Frequency Content of the Rock Motions

The form and frequency characteristics of the base input may have a very significant influence on the response of soils. Arango and Dietrich (1972) studied a site under two different earthquakes (Figure 3-30). As shown at the right side of Figure 3-30, the two acceleration histories applied to the outcrop rock had the same peak acceleration and the spectra were similar. However, the small differences in frequency caused the motion to be amplified differently in the three soil columns. Therefore, two or more histories of acceleration should be considered in any given response study in order to define the relative magnitude of the ground response at any given location.

COMPLEX COMPUTER ANALYSIS, TWO-DIMENSIONAL MODELS

As pointed out earlier, when the ground surface or the soil layers are inclined, one-dimensional wave assumptions may not be valid and a two-dimensional model may be required to represent the more complex geometry. Although two-dimensional liquefaction analyses are not in routine soil practice, the same procedures for evaluation of a stress history can be utilized. Finite element representations have been used to study dams and embankments.

Idriss, et al. (1973) have developed a two-dimensional finite element program - QUAD-4 - for the evaluation of seismic response of soil deposits. This program allows for variable damping in each element using a Rayleigh damping expression for that element. The damping matrix for the entire assemblage of elements is obtained by appropriate addition of the damping submatrices of all the elements.

The response is evaluated by the solution of the equations of motion using direct numerical integration methods with a time increment small enough to provide stability. The program uses plane strain quadrilateral and triangular elements. An iteration procedure is used to determine the strain-dependent modulus and damping for each element, based on the average strain developed in that element. The relation of modulus and damping is based on Seed and Idriss (1970c). The solution is obtained using the modulus and damping for each element which is compatible with the average strain. The developers of the program report that comparison with one-dimensional methods shows that the finite element solution values of shear stress are about 10% greater. The response spectra of one- and two-dimensional methods are of similar shape. Major differences on response spectra occur only when the input motion has large amounts of high frequency components or when the finite element model is very coarse. The addition of variable damping makes the response calculation results in better agreement with recorded data.

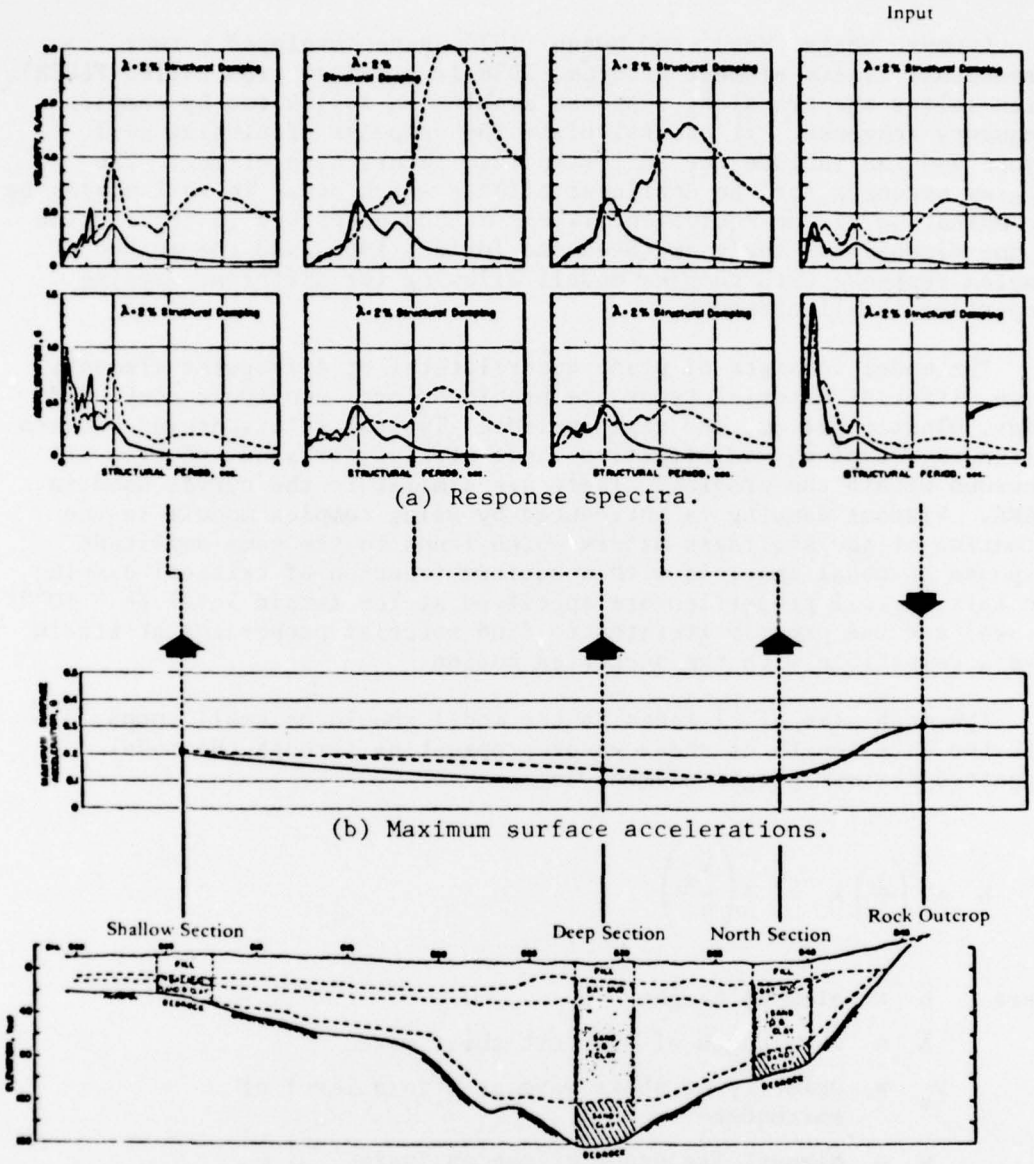

(a) Response spectra.

(b) Maximum surface accelerations.

(c) Generalized longitudinal soil profile.

Figure 3-30. Response spectra and maximum surface accelerations (from "Evaluation of Soil Liquefaction Effects on Level Ground During Earthquake," by H. B. Seed in ASCE Preprint 2752, Liquefaction Problems in Geotechnical Engineering, ASCE Annual Convention, Philadelphia, Pa., 27 Sep-1 Oct 1976).

Lysmer, Udaka, Seed, and Hwang (1974) have developed a two-dimensional finite element program, LUSH (revised version called FLUSH), which solves the transient response problem in soil sites by complex frequency response. It can calculate the response of sloping soil layers and can include the soil-structure interaction effect. The program accounts for the nonlinear effects which occur in soil masses by a combination of the equivalent linear method described in the section on one-dimensional analyses (Seed and Idriss, 1969) and the method of complex response with complex moduli allowing for different damping properties in all elements.

The model consists of plane quadrilateral or triangular elements. Three different material types are provided for: nonlinear clays and sands, elastic solids, and rigid solids. Typical relationships between stiffness, damping, and effective shear strains for sand and clay are provided within the program. These are similar to the curves used in SHAKE. Viscous damping is introduced by using complex moduli in the formation of the stiffness matrix which lends to the same amplitude response as nodal analysis with a uniform fraction of critical damping. The initial soil properties are specified at low strain level ($q = 10^{-4}\%$ strain) and the program iterates to find material properties at strain levels compatible with the specified motion.

The mesh size of elements in the model should be small compared with the wave length of shear waves propagating through the model. A suggested maximum height element is

$$h = \left(\frac{1}{5}\right)\lambda = \frac{1}{5}\left(\frac{V_s}{w}\right)$$

where h = element height

λ = wavelength of shortest shear wave

V_s = velocity of shear wave at strain level of earthquake

w = highest frequency of the analysis

The existing methods for liquefaction evaluation discussed above, including finite element programs, do not compute the pore pressure change with loading directly from the material properties and the actual shear strain produced by the actual time-dependent load. The process of liquefaction transforms an element of soil from a saturated granular solid to a viscous fluid. As a result of this change of material state, the soil in a liquefied zone has reduced shear strength and can undergo

large displacements. The actual in situ pore water pressure determination under dynamic field loading conditions is of major interest in the analysis of the liquefaction potentiality of a soil. The following paragraphs present some current research in progress.

Ghaboussi and Dikmen (1977) have proposed a method for determination of pore pressures and intergranular stresses by considering the soil as a two-phase medium. In the two-phase representationof saturated soils the granular solid skeleton and the fluid are treated as independent materials with individual material properties. The coupling between the volume changes of fluid and solid skeleton is taken into account through an additional material parameter. The flow of fluid with respect to the solid is assumed to be governed by a generalized form of Darcy's flow law, for which the material's parameter is the coefficient of permeability. The bulk modulus of the fluid, the coupling material parameter, and the coefficient of permeability is assumed to remain constant in the present dynamic analysis. The solid granular skeleton, in contrast, is a highly nonlinear material. A realistic constitutive relation for the solid skeleton of saturated granular soils must be capable of simulating the important nonlinear features such as dilatancy, compaction, shear failure and load reversal effects. Stress compaction, a factor in the pore pressure built up, is of special importance in liquefaction analysis.

The onset of liquefaction in an element of saturated soil is to be determined by a "liquefaction criterion" defined as reduction of the mean intergranular pressure. The initiation of liquefaction in any analysis, as determined by satisfying the liquefaction criterion, marks the boundary between two behavior conditions for an element of soil. In the pre-liquefaction state the soil is treated as a two-phase, fluid-saturated, porous solid. The important characteristic of a potentially liquefying soil at this stage is the increase of the pore pressures accompanied by the decrease of the mean intergranular pressure. After the initiation of liquefaction the behavior of an element of soil changes. A second material model is used to represent the post-failure behavior.

The analysis in the pre-liquefaction stage will lead to determination of the potentiality of liquefaction. If the extent of the development of the liquefaction, and the associated stress and pore pressure distribution are of interest, then the analysis should be carried into the post-liquefaction stage. Doing so requires accounting for the change in behavior from the fluid-saturated granular material to a viscous material in an element of soil which has satisfied the liquefaction criterion.

The key to success for liquefaction analysis of the type proposed by Ghaboussi and Dikmen (1977) lies in the appropriate mathematical modeling of the important features of the constitutive response of the granular solid skeleton of the soil. Loose sands are most susceptible to liquefaction under seismic loading conditions since they tend to compact

under shear deformation. This reduction of the volume in loose sands causes the pore pressure buildup and consequent reduction of the mean intergranular pressure, leading to liquefaction. Appropriate representation of the properties of granular soils requires special attention in a liquefaction analysis. Nonlinear material models are required to model the plastic behavior of the soil. This pre-liquefaction is under investigation using a soil model developed by Ishihara, et al. (1975).

Ishihara et al. (1975) have presented a model for liquefaction based upon studies of the cyclic deformation of sands. This model permits assessing pore pressures, shear strains, and the occurrence of liquefaction un undrained horizontal soil layers. This model, originally based on triaxial data, has been revised to fit torsion test results and incorporated into a computer code by Ishihara et al. (1976). The applied stress history for the in situ soil profile may be calculated by some of the foregoing computer programs, such as SHAKE (Schnabel, Lysmer and Seed, 1972). This stress history is then applied to the soil model to predict pore pressures and shear distortions.

Test data on undrained sands illustrate that for shearing loads below a particular shear stress/effective stress ratio q/p', reloading always retraces the unloading path. Plastic yielding, associated with the original application of shear stress, results in a buildup of residual pore pressure (and thus reduction in effective stress). Thus, it is possible to define for any particular soil density, a so-called virgin state, defined by a relationship such as that of Figure 3-31, in terms of shear stress, q versus effective mean principal stress p'. A series of such planes forms a vector surface in p' - q - e space (where e is void ratio or a measure of density). This "state" surface specifies the route or path in p' - q - e space along which stresses must be changed in order for deformations to be plastic. Plastic yielding occurs only when stresses are changed along paths lying on the state surface, and all other paths away from it are associated merely with elastic deformations. For undrained shearing of saturated sand, the stress paths can be defined for a specific state by a single slice or plane perpendicular to the e axis, such as Figure 3-32 (for a loose sand). This figure shows yield lines, or "equi-γ lines," which are curves in p' - q space at which yielding occurs whenever stress paths cross them. For stress paths within previously approached yield loci the deformations are assumed to be elastic, and no change in effective stress occurs.

With increase in the q/p' ratio, shear strains are generated with magnitudes equal to those values shown on the equi-γ lines in Figure 3-32.

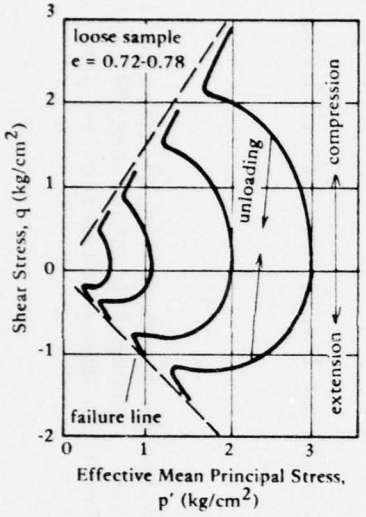

Figure 3-31. Typical undrained stress paths for loose samples (Fuji River Sand) (from K. Ishihara, 1975).

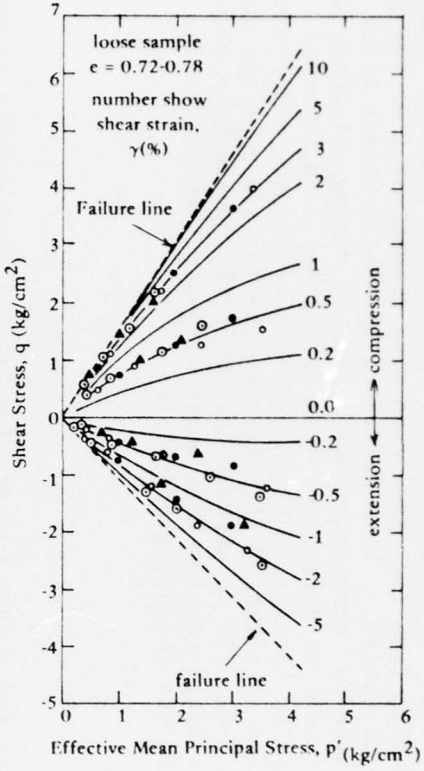

Figure 3-32. Equi-γ lines for loose samples (Fuji River sand) (from K. Ishihara, 1975).

Experimental results on saturated sands show that the shear in one direction below some limiting stress ratio does not influence the virgin state response for shearing in the opposite direction. However, beyond a certain q/p' ratio, the pore pressure commences to increase drastically during any unloading (and increases even more dramatically during loading in the opposite direction). This defines a threshold stress value which, if not exceeded, permits elastic response during unloading and provides plastic work-hardening response during any load increase. The angle defined by the threshold stress value is called the angle-of-phase transformation and is slightly flatter than the failure envelope as shown in Figure 3-32. It is assumed that initial liquefaction occurs where the stress ratio crosses this angle-of-phase transformation. This model is based on the following postulates.

Postulate 1

The tendency for volume change in saturated sand samples is expressed in development of residual pore pressures. State surfaces such as Figure 3-31 contain a series of concentric curves which represent the changing stress state of any specimen undergoing undrained deformation. Any loading path at stress ratios below the angle-of-phase transformation follows the curved state line passing through its point of initiation. Unloading (from stress values beneath the angle-of-phase transformation) is considered elastic; i.e., no change in effective stress with reduction in shear stress.

Postulate 2

The undrained shear strain levels are defined by the equi-γ lines.

Postulate 3

These equi-γ lines may be approximated by straight lines passing through the p' - q origin. (Changes in state caused by the very small volume changes associated with change in effective pressure are neglected.)

Postulate 4

The yield conditions for loading in one direction are independent of the stress history of loading in the opposite direction.

Postulate 5

Instability of the saturated sand occurs when q/p' reaches the angle-of-phase transformation θ^* (a state of initial liquefaction is assumed). It is noted that this model does not provide a reliable means of predicting response once the liquefaction state is reached.

In order to adapt the model for numerical computations, the stress paths in p' - q space must be expressed in terms of a mathematical function. These stress paths selected for virgin loading below the angle-of-phase transformation may be represented by circles with centers at p^* along the p-axis which intersect this axis at p'_o, the initial consolidation pressure. It is noted that the curvature for dense sands is less than for loose sands (the radius is greater).

To attempt to model the sand behavior beyond initial liquefaction – i.e., between initial and complete liquefaction (effective stresses are reduced to zero) – it is assumed that the loading stress path in the p' - q plane follows the angle-of-phase transformation θ^*. Upon load release, the developed pore pressure has been found to be proportional to the ratio of the shear stress level prior to unloading q_r, divided by that at initial liquefaction q_θ, or

$$\frac{p'_r}{p'_o} = K_r \frac{q_o}{q_r}$$

where p'_r = the effective pressure following unloading

p'_o = the effective pressure at initial liquefaction

K_r = a new material constant

This model, for undrained sand using only three parameters – θ^*, p'_o and K_r – may be used to determine pore-pressure buildup and shear strain for any prescribed stress path.

SELECTION OF METHODS

Various methods for prediction of liquefaction have been reviewed. Figure 3-4 may be used for preliminary analysis when data is limited. For the simple geometry of essentially horizontal ground, the simple hand computation procedure should be adequate. Figure 3-33 gives a comparison of the Simple Hand Method, the Simple Computer Program, and

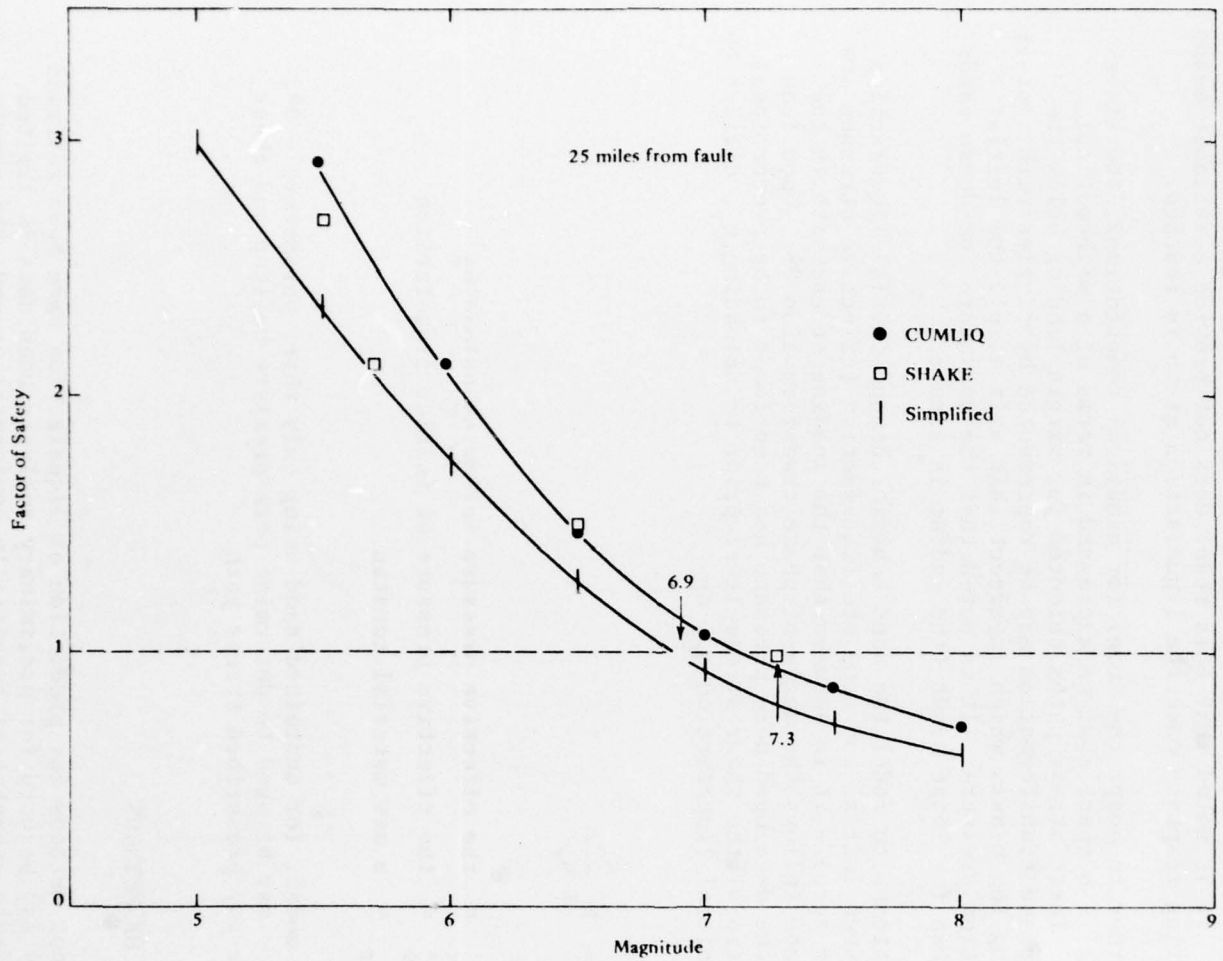

Figure 3-33. Comparison of prediction procedures.

SHAKE. For the profile used, the simple hand computation procedure provides a conservative estimate of the factor of safety when compared with the other procedures presently in use. This makes liquefaction analysis for simple sites possible without the use of a computer. Figures 3-11, 3-12, and 3-24 can be used as a guide to give the strength of the soil and the number of earthquake cycles. The τ/σ ratio used for soil strength should be reduced by 10% to account for multidirectional shaking and overconsolidation.

REFERENCES, CHAPTER 3

Arango, I. and Dietrich, R. J. (1972) "Soil and earthquake uncertainties on site response studies," in Proceedings of the International Conference on Microzonation for Safer Construction Research and Application, 30 Oct - 3 Nov 1972. Seattle, Wash., National Science Foundation.

Castro, G. (1975) "Liquefaction and cyclic mobility of saturated sands," Journal of the Geotechnical Division, ASCE, vol 101, no. GT6, Jun 1975, p. 55.

Christian, J. T. and Swiger, W. F. (1975) "Statistics of liquefaction and SPT results," Journal of the Geotechnical Division, ASCE, vol 101, no. GT11, Nov 1975.

DeAlba, P., Chan, C. K. and Seed, H. B. (1975) Determination of soil liquefaction characteristics by large-scale laboratory tests, University of California, Earthquake Engineering Research Center, EERC Report No. 75-14. Berkeley, Calif., May 1975.

Dezfulian, H. and Seed, H. B. (1969) Seismic response on soil deposits underlain by sloping rock boundaries, University of California, Earthquake Engineering Research Center, EERC Report No. 69-9. Berkeley, Calif., Jul 1969.

Donovan, N. C. (1974) CUMLIQ: Evaluation of potential for liquefaction of a soil deposit using random vibration procedures, University of California, Earthquake Engineering Research Center, National Information Service on Earthquake Engineering. Berkeley, Calif., Jul 1974.

Ghaboussi, I. and Dikmen, S. (1977) LASS II, computer program for analysis of seismic response and liquefaction of horizontally layered sands, University of Illinois, UILU-ENG 77-2010. Urban, Ill., Jun 1977.

Gibbs, H. J. and Holtz, W. G. (1957) "Research on determining the density of sand by spoon penetrator test," in Proceedings of Fourth International Conference on Soil Mechanics and Foundations Engineering, vol 1, London, England, 1957.

Hardin, B. and Drnevich, V. (1970) Shear modulus and damping in soils, University of Kentucky, College of Engineering, Soil Mechanics Series Technical Report UKY 26-70-CE2. Lexington, Ky., Jul 1970.

Idriss, I. M., et al. (1973) QUAD 4: A computer program for evaluating the seismic response of soil structures by variable damping finite element procedures, University of California, Earthquake Engineering Research Center, EERC Report No. 73-16. Berkeley, Calif., Jul 1973.

Idriss, I. M. and Seed, H. B. (1968) "Seismic response of horizontal soil layers," Journal of the Soil Mechanics and Foundations Division, ASCE, vol 94, no. SM4, Jul 1968, pp 103-1031.

Idriss, I. M. and Seed, H. B. (1970) "Seismic response of soil deposits," Journal of the Soil Mechanics and Foundations Division, ASCE, vol 96, no. SM2, Mar 1970, pp 631-638.

Ishihara, K., et al. (1975) "Undrained deformation and liquefaction of sand under cyclic stresses," *Soils and Foundations* (Japan), vol 15, no. 1, Mar 1975.

Ishihara, K., et al. (1976) "Prediction of liquefaction in sand deposits during earthquakes," Soils and Foundations (Japan), vol 16, no. 1, Mar 1976.

Kanai, K. (1961) "An empirical formula for the spectrum of strong earthquake motions," Bulletin, Tokyo University Earthquake Research Institute, vol 39, 1961.

Kiefer, F. W., Seed, H. B. and Idriss, I. M. (1970) "Analysis of earthquake ground motions at Japanese sites," Bulletin of the Seismological Society of America, vol 60, no. 6, Dec 1970, pp 2057-2070.

Lee, K. L. and Chan, K. (1972) "Number of equivalent significant cycles on strong motion earthquakes," in Proceedings of the International Conference on Microzonation for Safer Construction Research and Application, 30 Oct - 3 Nov 1972. Seattle, Wash., National Science Foundation, 1972.

Lysmer, J., et al. (1974) LUSH: A computer program for complex response analysis of soil structure systems, University of California, Earthquake Engineering Research Center, EERC Report No. 74-4. Berkeley, Calif., Apr 1974.

Lysmer, J., Seed, H. B. and Schnabel, P. B. (1970) Influence of base rock characteristics on ground reponse, University of California, Earthquake Engineering Research Center, EERC Report No. 70-7. Berkeley, Calif., Nov 1970.

Mulilis, J. P., Chan, C. K. and Seed, H. B. (1975) The effects of method of sample preparation on the cyclic stress-strain behavior of sands, University of California, College of Engineering, Earthquake Engineering Research Center, EERC Report No. 75-18. Berkeley, Calif., Jul 1975.

Pyke, R., Chan, C. K. and Seed, H. B. (1974) Settlement and liquefaction of sands under multi-directional shaking, University of California, College of Engineering, Earthquake Engineering Research Center, EERC Report No. 74-2. Berkeley, Calif., Feb 1974.

Schnabel, P. B., Lysmer, J. and Seed, H. B. (1972) SHAKE: A computer program for earthquake response analysis of horizontally layered sites, University of California, Earthquake Engineering Research Center, Report No. 72-12. Berkeley, Calif., Dec 1972.

Schnabel, P. B. and Seed, H. B. (1972) Accelerations in rock for earthquakes in the western United States, Unversity of California, College of Engineering, Earthquake Engineering Research Center, EERC Report No. 72-2. Berkeley, Calif., Feb 1972.

Seed, H. B. (1976) "Evaluation of soil liquefaction effects on level ground during earthquakes," ASCE Preprint 2752 (Liquefaction Problems in Geotechnical Engineering), American Society for Civil Engineers Annual Convention and Exposition, Philadelphia, Pa., 27 Sep - 1 Oct 1976.

Seed, H. B., et al. (1975) Representation of irregular stress time histories by equivalent uniform stress series in liquefaction analysis, University of California, College of Engineering, Earthquake Engineering Research Center, EERC Report No. 75-29. Berkeley, Calif., Oct 1975.

Seed, H. B. and Idriss, I. M. (1969) "Influence of soil conditions on ground motions during earthquakes," Journal of the Soil Mechanics and Foundations Division, ASCE, vol 95, no. SM1, Jan 1969, pp 99-137.

Seed, H. B. and Idriss, I. M. (1970a) A simplified procedure for evaluating soil liquefaction potential, University of California, Earthquake Engineering Research Center, EERC Report No. 70-9. Berkeley, Calif., Nov 1970.

Seed, H. B. and Idriss, I. M. (1970b) "Analysis of ground motions at Union Bay, Seattle, during earthquakes and distant nuclear blasts," Bulletin of the Seismological Society of America, vol 60, no. 1, Feb 1970, pp 125-136.

Seed, H. B. and Idriss, I. M. (1970c) Soil moduli and damping factors for dynamic response analysis, University of California, Earthquake Engineering Research Center, EERC Report No. 70-10. Berkeley, Calif., Dec 1970.

Seed, H. B. and Peacock, W. H. (1970) Applicability of laboratory test procedures for measuring soil liquefaction characteristics under cyclic loading, University of California, Earthquake Engineering Research Center, EERC Report No. 70-8. Berkeley, Calif., Nov 1970.

Streeter, V. L., Wylie, E. G. and Richart, F. E. (1974) "Soil motion computations by characteristics method," Journal of the Geotechnical Division, ASCE, vol 100, no. GT3, Mar 1974, pp 247-263.

Chapter 4

CONSEQUENCES OF LIQUEFACTION

The magnitude of the foundation problems associated with liquefaction are directly related to the amount of ground movement or ground failure. Ground failures may be of three basic types: flow landslides, landslides with limited displacement, and bearing capacity failures. Liquefaction of a layer at depth which does not undergo large displacements may actually act as an isolator impeding the transmission of vibration energy from underlying layers to structures at the surface. Seed and Idriss (1967) show an earthquake record at Niigata, Japan, in which the surface motion significantly changes from a predominantly short-period motion to a long-period motion after about 8 seconds of motion. Presumably this indicates the time of the onset of liquefaction (Figure 4-1).

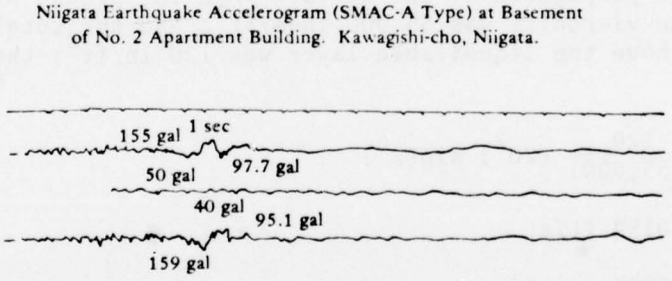

Figure 4-1. Record of ground accelerations during Niigata earthquake (from "Landslides During Earthquakes due to Soil Liquefaction," by H. B. Seed in Journal of Soil Mechanics and Foundations Division, ASCE, vol. 95, no. SM5, May 1968, Figure 6).

LIQUEFACTION FLOW LANDSLIDES

When the in situ relative density of the soil is low enough (D_r < 45%), unlimited flow may occur. If the soil is unrestrained, sizable masses of earth materials may travel long distances. The principal restraint is only a function of the viscous restraining forces. The flow velocity can be estimated by the following equation for a case where liquefaction propagates to the surface.

$$U = \frac{\gamma_t}{2N} (b^2 - S^2) \sin \Theta$$

where U = horizontal flow velocity (ft/s)

N = viscosity (lb-s/ft^2) (Chapter 2)

γ_t = total unit weight of soil

b = depth to bottom of liquefiable layer

S = depth to top of liquefiable layer

Θ = angle of slope

For example, if the depth to the bottom of a liquefiable layer was 20 feet and it propagated to the surface when the ground slope was 2 degrees, the viscosity was 55,000 lb-s/ft^2; and the total unit weight of the soil above the liquefiable layer was 120 lb/ft^2; then,

$$U = \frac{120}{2(55,000)} (20^2) \sin(2^o)$$

$$= 0.0152 \text{ ft/s}$$

$$= 0.18274 \text{ in./s}$$

If the liquefiable condition were to last for 7 minutes, the displacement would be over 6 feet.

The above methodology and example, although highly idealized, can be used to give qualitative evaluations of the amount of flow displacement. One of the problems here is that the viscosity data on real soils is limited. The example shows that very slight slopes are capable of causing large deformations; conversely, horizontal deformation would not

be expected on truly flat ground. Flow landslides have occurred under seismic conditions and have been reported in the literature (Crandall, 1908; Seed, 1968). Flow continues as long as pore pressures remain high enough to maintain liquefaction. This is a function of the drainage conditions of the site and porosity of the soil and will be discussed later. The duration of liquefaction will also be discussed later.

LIQUEFACTION WITH LIMITED DISPLACEMENTS

For relative densities greater than about 45%, the data tends to indicate that limited flow rather than unlimited flow might be expected. DeAlba, Chan, and Seed (1975) have conducted shake-table tests, Figures 4-2 and 4-3, which suggest limiting horizontal shear strain as a function of relative density. The value of 45% relative density is shown as the approximate division between limited and unlimited flow. Figure 4-3 could presumably be used to estimate shear strains within the soil layer undergoing liquefaction for use in predicting the horizontal transient displacement for level ground not experiencing flow (note that in Figure 4-3 shear strain is expressed independent of ground motion level). This fact and the paucity of data at this time make these results preliminary and in need of further verification.

On sloping ground, increments of finite downslope movements could cause dilatancy-induced solidification. Thus, flow could be interrupted by solidification stages which would limit the displacement. There have been numerous cases of limited displacements, also called lateral spreading, reported (Richter, 1958; McCulloch and Bonilla, 1970; Oldham, 1899; Youd, 1973a and b). Observed cases in these references noted movements of several feet on ground sloping from 0.5 to 2%. Youd (1975) deduces several points of interest based on laboratory soil behavior. Episodes of limited flow would be expected to be most prevalent where shear stress reversals occur; thus, limited flow would be expected to occur as long as strong ground shaking exists. The shear stress reversals associated with limited flow are more easily developed beneath mild slopes where static stresses are small, rather than steep slopes. At the conclusion of a series of limited flow cycles, the soil in the failure zone may be denser or looser or at the same condition as it was before the disturbance, depending on whether pore water migrated into or out of the liquefied soil during shear.

BEARING CAPACITY FAILURES

When liquefaction occurs in soils beneath structures, flow deformations may develop, allowing vertical motion to occur. Loss of foundation support and buoyant rise of buried tanks are possible types of failures.

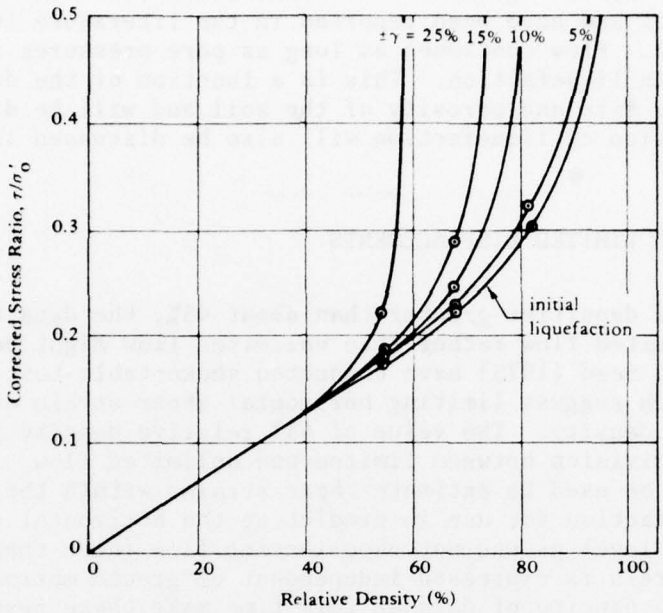

(a) Five stress cycles.

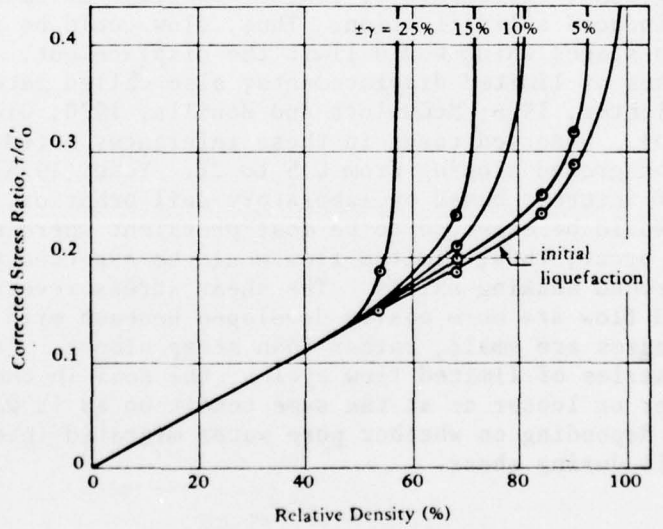

(b) Ten stress cycles.

Figure 4-2. Limiting shear strains (from H. B. Seed, P. P. Martin, and J. Lysmer, 1975).

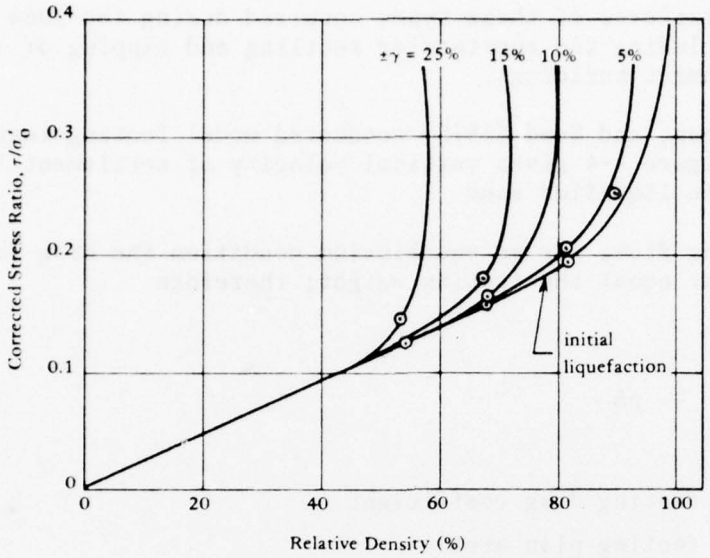

(c) Thirty stress cycles.

Figure 4-2. Continued

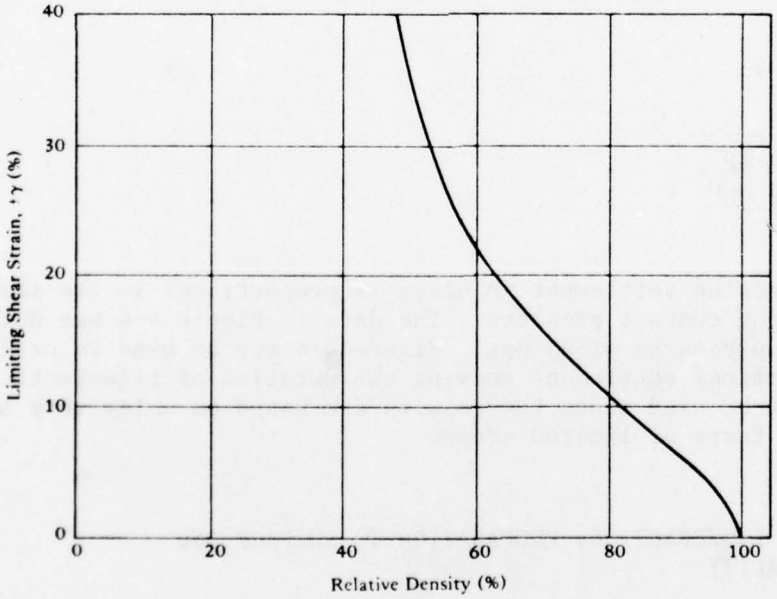

Figure 4-3. Limiting shear strains independent of loading.

Several major failures of these types occurred during the 1964 Niigata earthquake, including the spectacular settling and tipping of several high-rise apartment buildings.

DeAlba, Chan, and Seed (1975) conducted model footing tests on a shake table; Figure 4-4 gives vertical velocity of settlement for a model footing in liquefied sand.

Considering flow, for an equilibrium condition the drag force of the footing must equal the footing weight; therefore

$$C_D \, A \, \rho \frac{V^2}{2} = pA$$

where C_D = footing drag coefficient
A = footing plan area
ρ = soil density
V = footing velocity
p = footing contact pressure

Solving for V:

$$V = \sqrt{\frac{2p}{C_D \rho}}$$

Thus, the footing settlement velocity is proportional to the square root of the footing contact pressure. The data in Figure 4-4 was obtained for footing pressures of 25 psi. Figure 4-4 may be used to crudely estimate vertical settlement knowing the duration of liquefaction. Caution must be used since the results are base[illegible] few very small scale model tests of limited scope.

DURATION OF LIQUEFACTION, PROPAGATION TO SURFACE AND BEARING CAPACITY

The duration and propagation of liquefaction in a subsurface layer is controlled by the drainage path for the built-up pore pressure, the coefficients of permeability, and the coefficient of consolidation, which dictates the volume change characteristics of the soil layers.

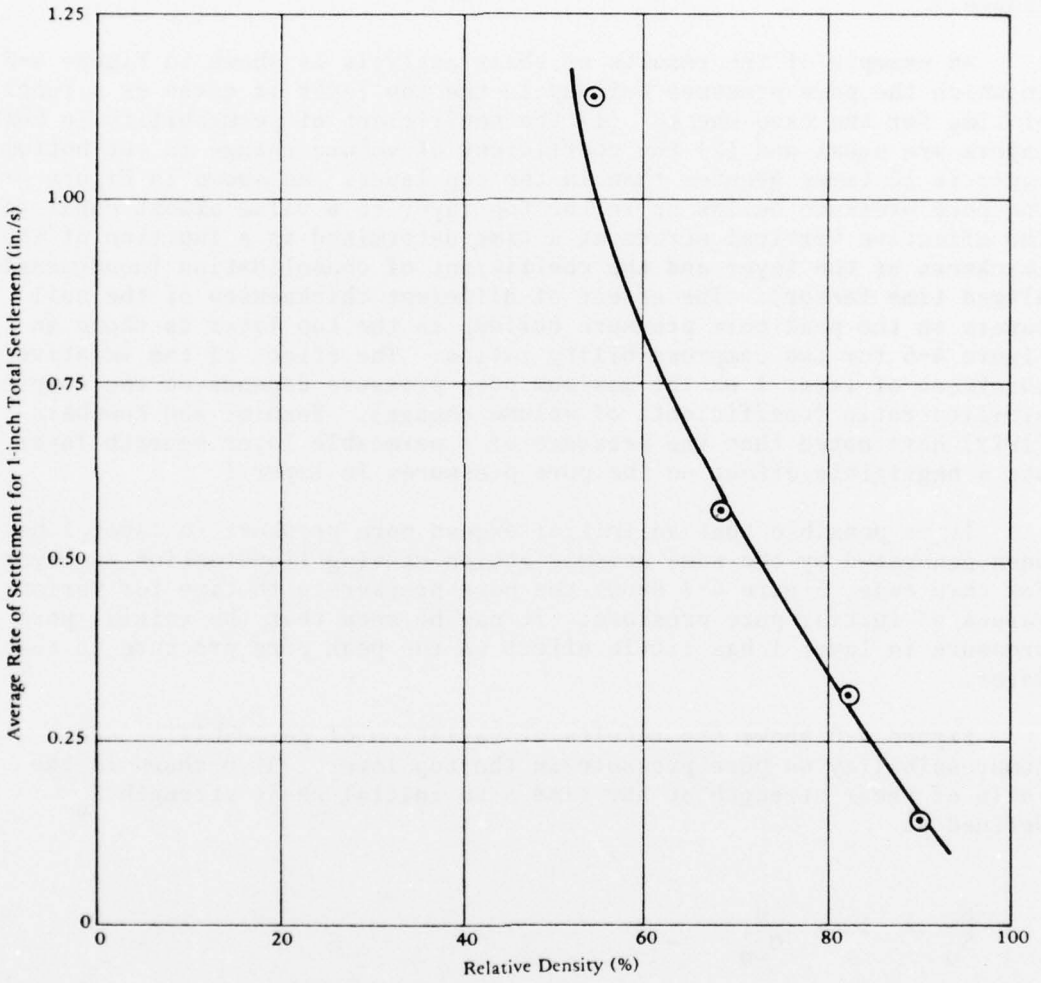

Figure 4-4. Average rate of footing settlement (from H. B. Seed, P. P. Martin, and J. Lysmer, 1975).

Yoshimi and Kuwabara (1973) have investigated pore pressure dissipation using a finite element analysis, assuming one-dimensional flow (using Darcy's law) and layer II undergoing liquefaction. They assumed that the induced seismic shear stress terminates at the onset of liquefaction, that the soil in layer I undergoes rebound and recompression with a constant coefficient of volume change, and that the soil in layer II undergoes virgin compression with a constant coefficient of volume change.

An example of the results of their analysis is shown in Figure 4-5 in which the pore pressure buildup in the top layer is given as a function of time for the case where: (1) the coefficient of permeability in both layers are equal and (2) the coefficient of volume change in the bottom layer is 10 times greater than in the top layer. As shown in Figure 4-5 the pore pressure builds up in the top layer to a value almost equal to the effective vertical stress at a time determined as a function of the thickness of the layer and the coefficient of consolidation (nondimensionalized time factor). The effect of different thicknesses of the soil layers on the peak pore pressure buildup in the top layer is shown in Figure 4-6 for two compressibility ratios. The effect of the relative thickness of layer I on the maximum pore pressure depends on the compressibility ratio (coefficients of volume change). Yoshimi and Kuwabara (1973) have noted that the presence of a permeable layer beneath layer II has a negligible effect on the pore pressures in layer I.

It is possible that an initial excess pore pressure in layer I has been generated by the same seismic action causing liquefaction in layer II. For this case, Figure 4-7 shows the pore pressure with time for various values of initial pore pressure. It can be seen that the initial pore pressure in layer I has little effect on the peak pore pressure in that layer.

Figure 4-8 shows the results of variation of permeability and compressibility on pore pressure in the top layer. Also shown is the ratio of shear strength at any time S to initial shear strength S_o defined as

$$\frac{S}{S_o} = 1 - \frac{u}{\sigma'_{vo}}$$

Since the maximum pore pressure varies nearly linearly with depth in layer I, the minimum strength ratio S_{min}/S_o corresponding to the maximum pore pressure may be considered a constant throughout layer I

$$\frac{S_{min}}{S_o} = 1 - \frac{u_{max}}{\sigma'_{vo}} = 1 - \frac{i_{max}}{i'_{cr}}$$

where i_{max} = maximum hydraulic gradient

i_{cr} = critical hydraulic gradient

Figure 4-9 shows the minimum strength in layer I for use in estimating the liquefaction of that layer. The data are replotted in Figure 4-10 to show areas where complete liquefaction in layer I occurs. It should be noted that the critical hydraulic gradient corresponding to $u_{max}/\sigma_{vo}' = 1$ in a field situation probably cannot be maintained without causing fissures and local eruption of sand and water. The presence of a foundation will affect the state of stress and seepage conditions; however, the strength ratio S_{min}/S_o may still give a crude indication of the bearing capacity. The time to the minimum strength as noted in Figure 4-8 depends upon the coefficient of permeability, the compressibility, and the thickness of the soil. These may be in seconds or in minutes, depending on site conditions. Observations during the Niigata earthquake of 1964 noted most of the surface movement occurred minutes after the earthquake strong motion ended. Note that densification causes a reduction in k_1 and m_{v1} of the top layer and a reduction of S/S_o, which is not favorable; however, densification will cause an increase in the initial shear strength S_o, which is beneficial. The net effect of densification of layer I may or may not be advantageous, depending on the initial soil properties and the degree of densification. Increasing the permeability of the top layer markedly increases the stability of the soil. Thus, vibroflotation, sand drains, or using a coarse backfill should be more effective than densification methods in which density alone is increased.

Seed, Martin, and Lysmer (1975) have more recently investigated the distribution of hydrostatic pore pressure in the soil by use of the equation

$$\frac{\partial u}{\partial t} = C_v\left(\frac{\partial^2 u}{\partial z^2}\right) + \frac{\partial u_g}{\partial t}$$

where C_v = coefficient of consolidation of the soil

z = depth within soil

$\partial u_g/\partial t$ = rate of pore pressure generation caused by earthquake

This is the diffusion equation used in Terzaghi's classical consolidation theory, with a pressure-generating term added. The solution of this equation is accomplished by the finite-difference technique using incremental time steps. The pore pressure generation is estimated by Figure 4-11 as a function of the number of cycles to cause liquefaction.

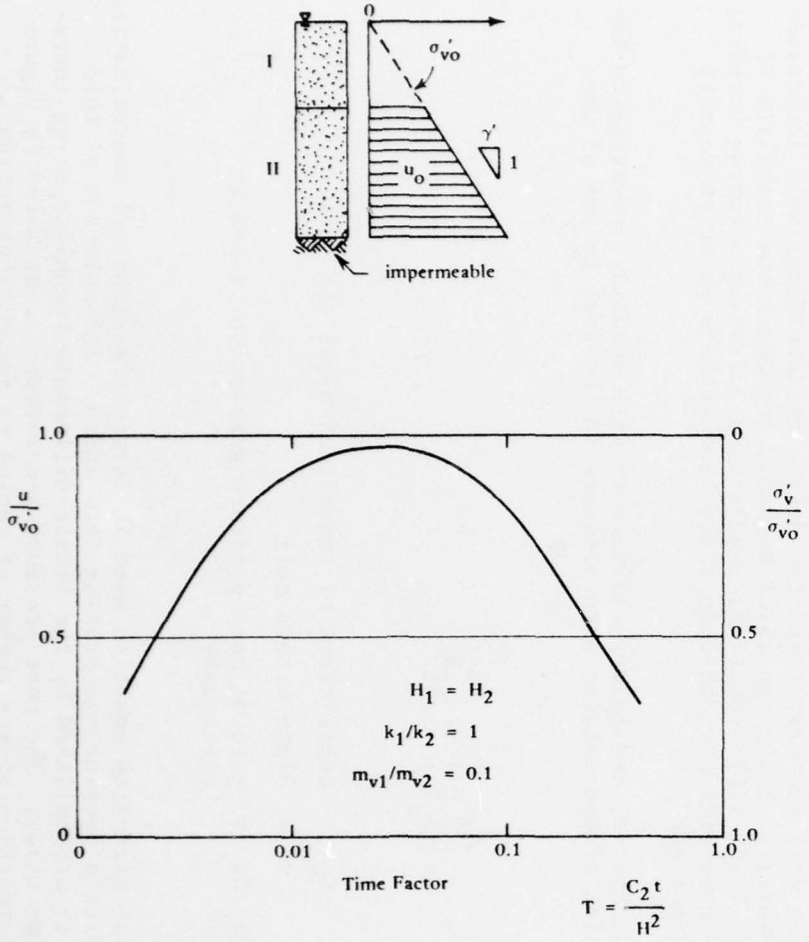

Figure 4-5. Pore pressure at middepth layer I (from Y. Yoshimi and F. Kuwabara, 1973).

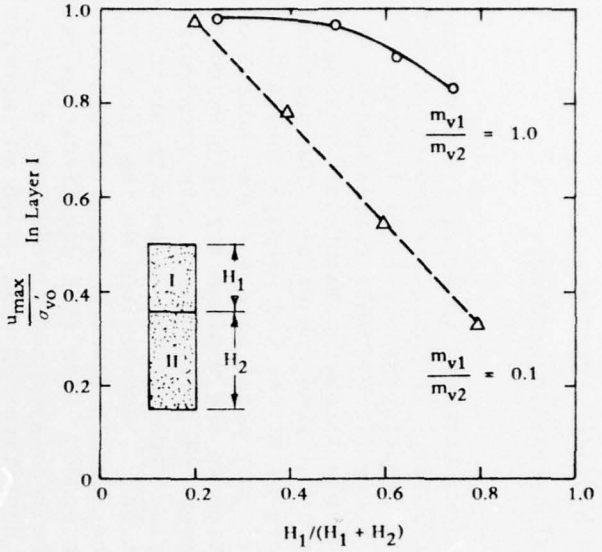

Figure 4-6. Effect of relative thickness of layer I on maximum pore pressure in layer I (from Y. Yoshimi and F. Kuwabara, 1973).

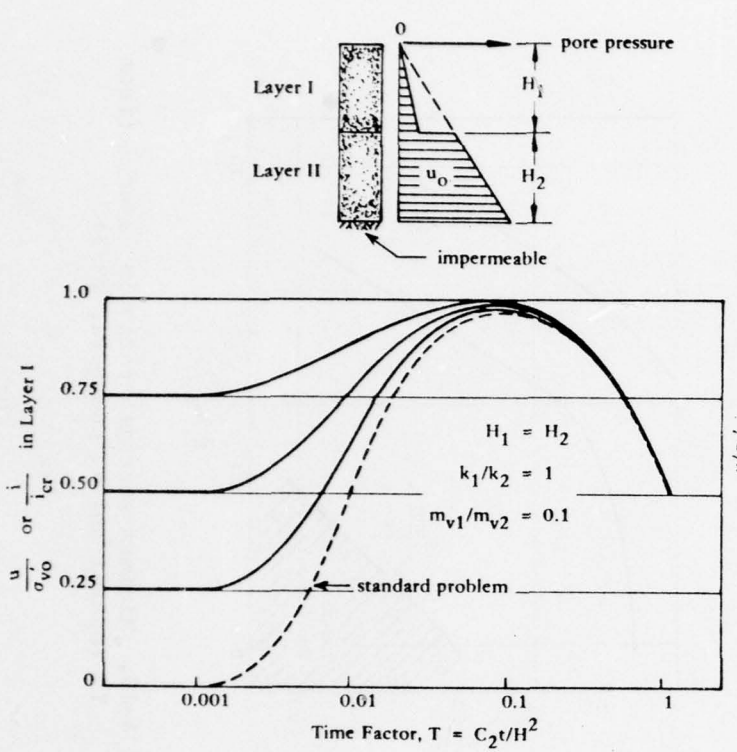

Figure 4-7. Effect of initial excess pore pressure in layer I (from Y. Yoshimi and F. Kuwabara, 1973).

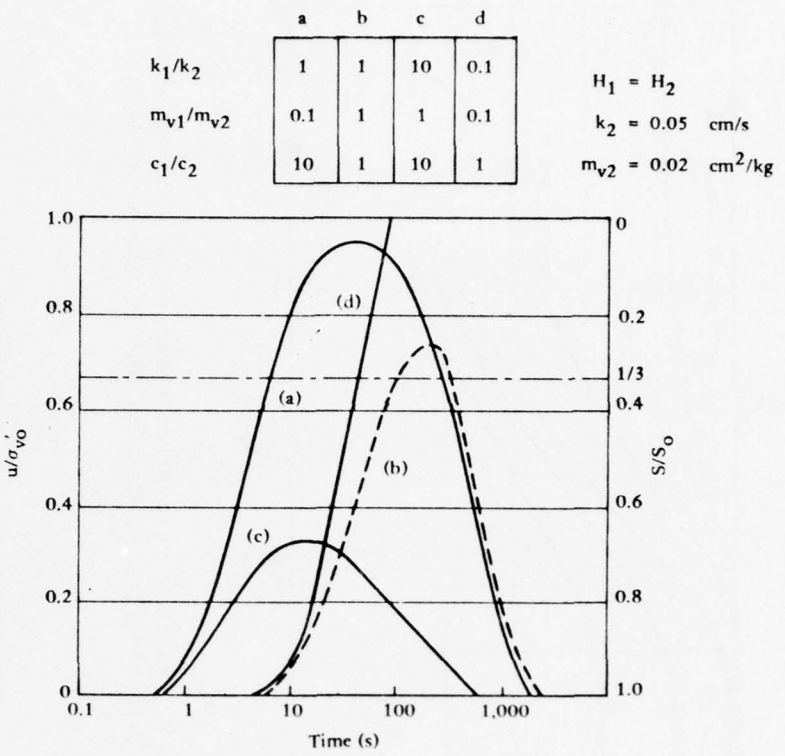

Figure 4-8. Time histories of excess pore pressure at middepth of layer I (from Y. Yoshimi and F. Kuwabara, 1973).

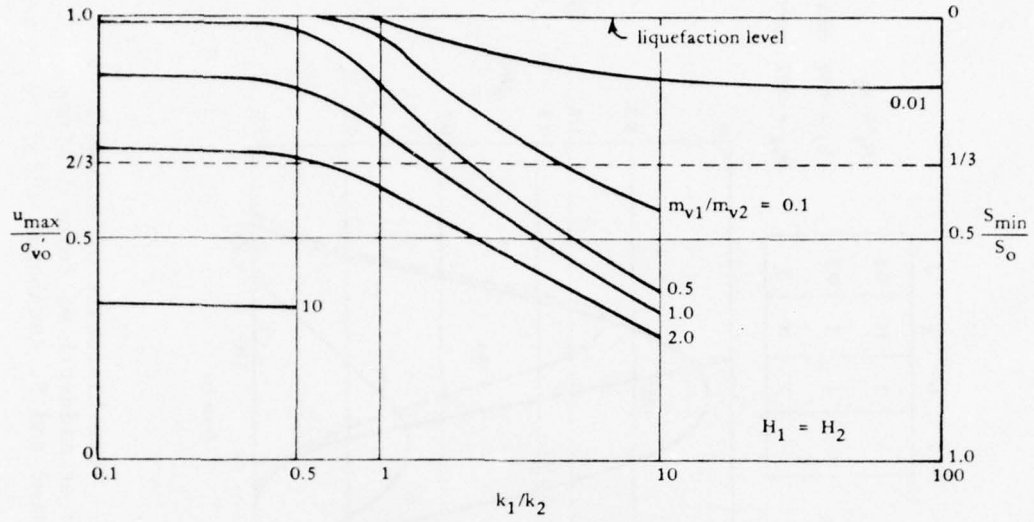

Figure 4-9. Maximum pore water pressure or minimum strength in layer I (from Y. Yoshimi and F. Kuwabara, 1973).

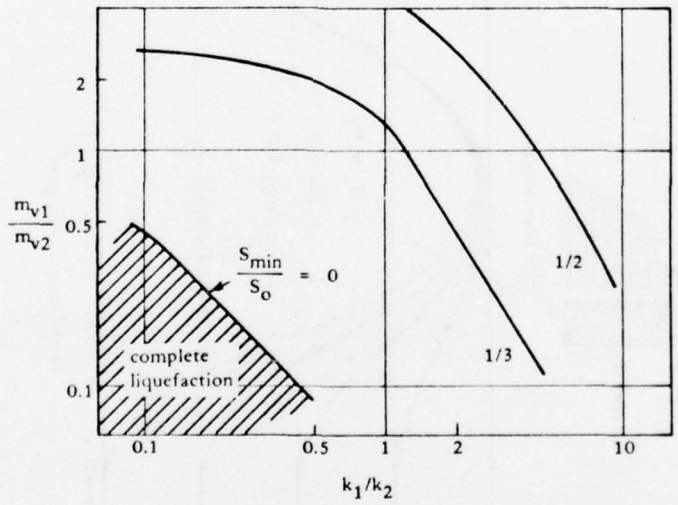

Figure 4-10. Minimum strength ratio in layer I (from Y. Yoshimi and F. Kuwabara, 1973).

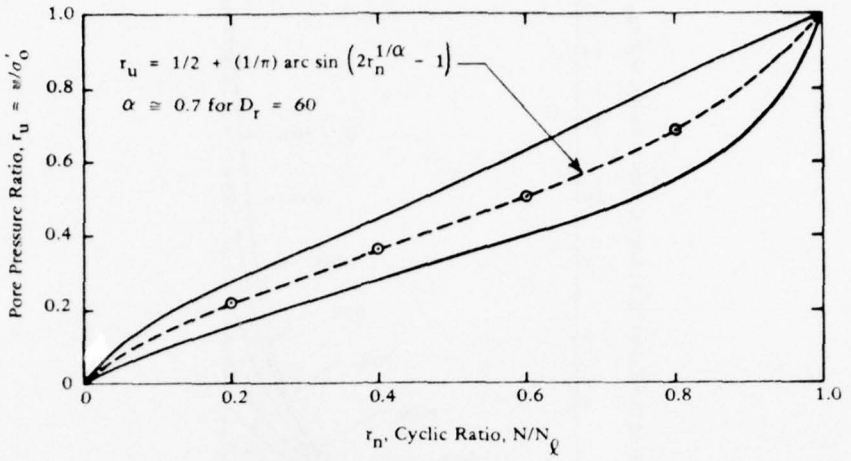

Figure 4-11. Rate of pore water pressure buildup in cyclic simple shear tests (after P. DeAlba, C. Chan, and H. B. Seed, 1975).

The coefficient of consolidation C_v, which is defined in terms of the coefficient of volume compressibility m_v and the coefficient of permeability k, may be estimated by means of Figures 4-12 and 4-13.

$$C_v = \frac{k}{m_v \gamma_w}$$

The rise in the water table is given by:

$$\Delta H = \frac{-k\left(\frac{\partial u}{\partial z}\right)\Delta t}{n_e}$$

where n_e = the effective porosity

This procedure has been automated in the form of the computer program APOLLO prepared by Martin (1975) and may be used in conjunction with the analysis using the computer program SHAKE described in Chapter 3. SHAKE is used to produce the equivalent uniform cyclic stress (τ_{eq}) and the equivalent number of uniform stress cycles (n_{eq}) for various depths

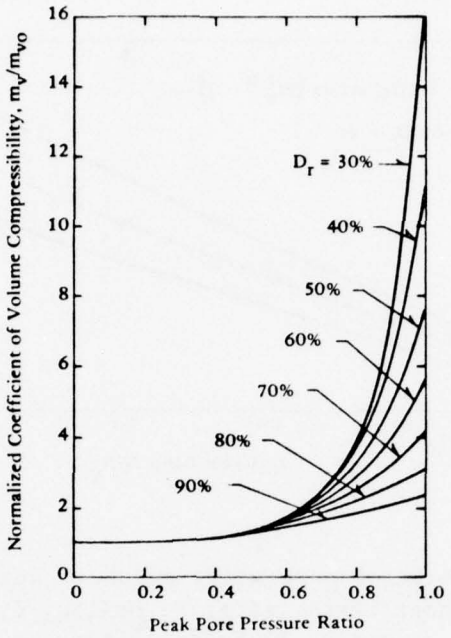

Figure 4-12. Theoretical relationships between compressibility of sands and pore pressure buildup (from H. B. Seed, P. P. Martin, and J. Lysmer, 1975).

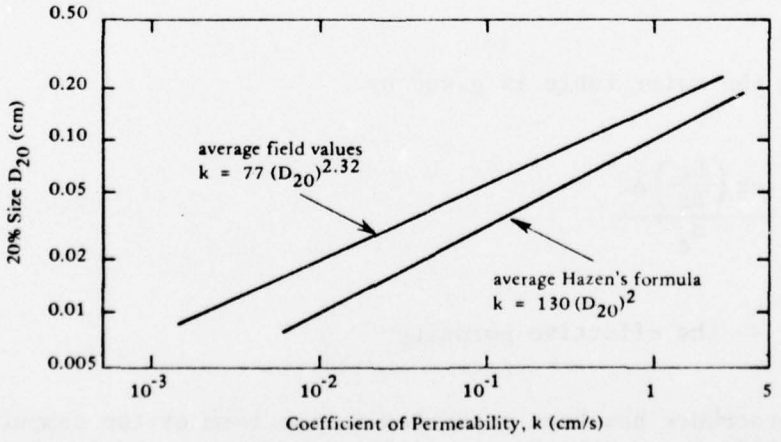

Figure 4-13. Relationships between grain size and coefficient of permeability for sands (from H. B. Seed, P. P. Martin, and J. Lysmer, 1975).

of soil. From strength data the number of cycles to cause liquefaction at each depth is determined. Using this information program APOLLO solves the pore pressure generation-dissipation equation.

The pore pressure generation function is based on undrained test data. This application is deemed sufficiently accurate when small time steps are used to properly account for drainage. The elastic response analysis used to determine the number of cycles to liquefaction can be made to consider the isolation effects of subsurface liquefaction on near surface shaking and the reduction in pore pressure generation when iteration techniques are used.

A typical example from Seed et al. (1975) from the Niigata earthquake of 1964 is shown in Figures 4-14 and Figure 4-15. The computed variations of pore water pressure with time are given. Figure 4-15 shows the buildup of pore pressures. It may be seen that the sand layer at a depth of 15 feet liquefies after about 21 seconds of shaking; liquefaction extends to depths of 20, 30, and 40 feet after about 23, 32, and 40 seconds of shaking. Although the layers above 15 feet depth continue to increase in pore pressure as the shaking progresses, the rate of increase is very low after the 15-foot level liquefies. It has been noted in Seed, Martin, and Lysmer (1975) that when the pore pressure ratio in the top foot of soil reaches 60%, the ground will become soft, and a man will sink. This occurs after about 8.5 minutes in the Niigata analysis. The pore pressure ratio at the ground surface begins to decrease after about 20 minutes but would not support a man until about 40 to 50 minutes after the earthquake. The results of the computer analysis are in general agreement with observed reports.

If the water table were located at a depth of 15 feet, no significant pore pressure increases would occur in the upper 10 feet of soil even though the soil is liquefied between 15 and 40 feet. Thus, in this situation the bearing capacity of small shallow footings near the surface might well be essentially unaffected by the dissipation of pore water pressures in the liquefied zone.

Program APOLLO has been expanded into a two-dimensional computer program called GADFLEA (Booker et al., 1976). The approach is very similar to the one-dimensional analysis requiring as input information the number of cycles causing liquefaction by soil element. The number of cycles causing liquefaction is a function of the applied shear stress loading and soil confinement. These may be determined from a conventional two-dimensional elastic or inelastic finite element analysis. Using the input data program GADFLEA computes the two-dimensional pore pressure generation and dissipation from the earthquake.

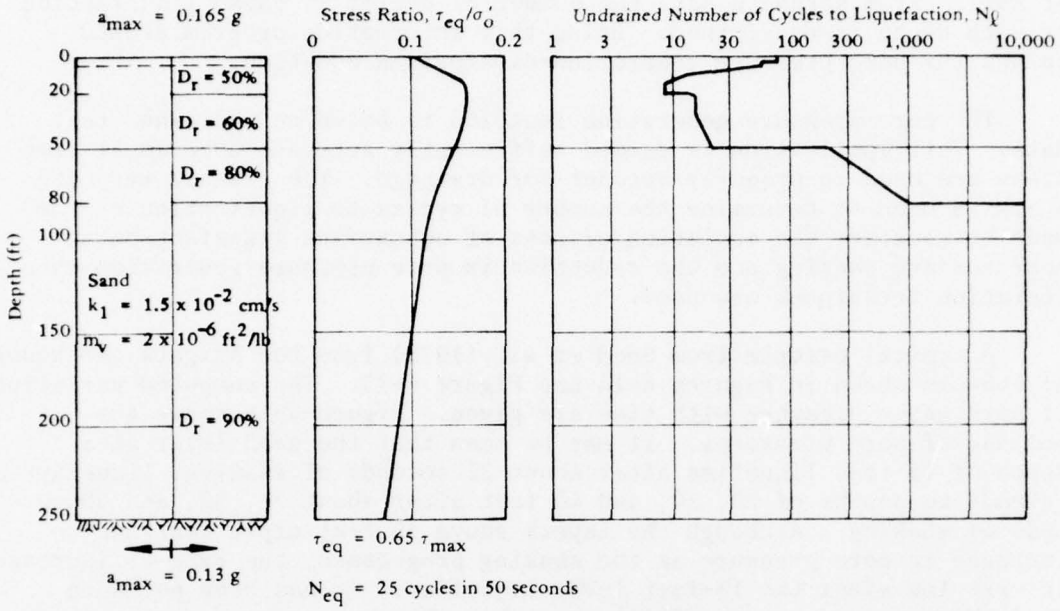

Figure 4-14. Soil profile and stress conditions used for analysis (from H. B. Seed, P. P. Martin, and J. Lysmer, 1975).

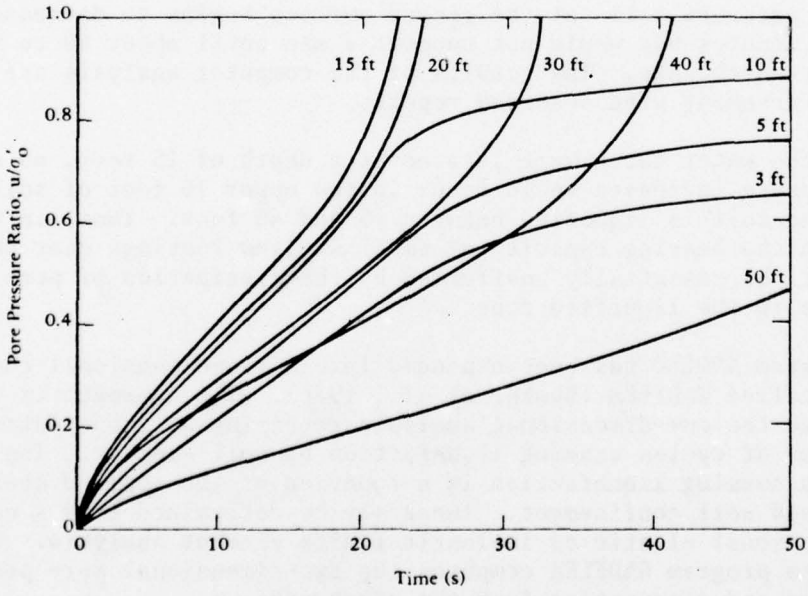

(a) During earthquake shaking.

Figure 4-15. Computed development and variation of pore water pressures for soil profile shown in Figure 7-8 (from H. B. Seed, P. P. Martin, and J. Lysmer, 1975).

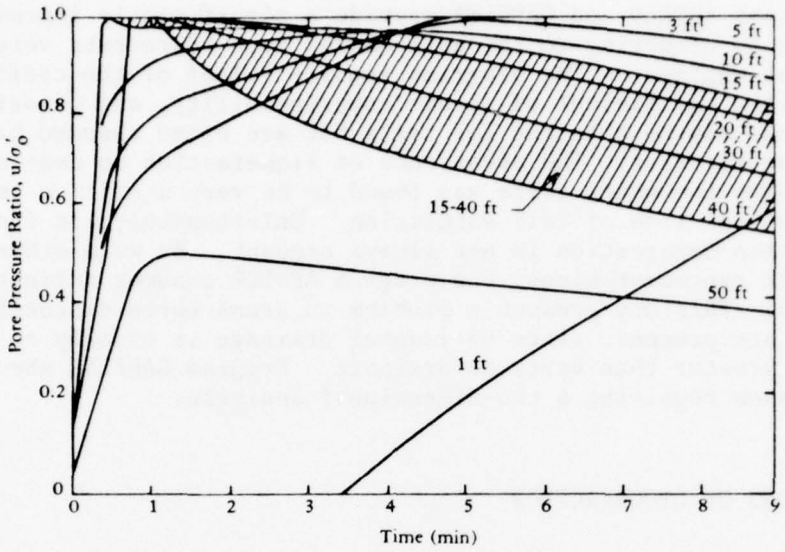

(b) In 8-minute period following earthquake.

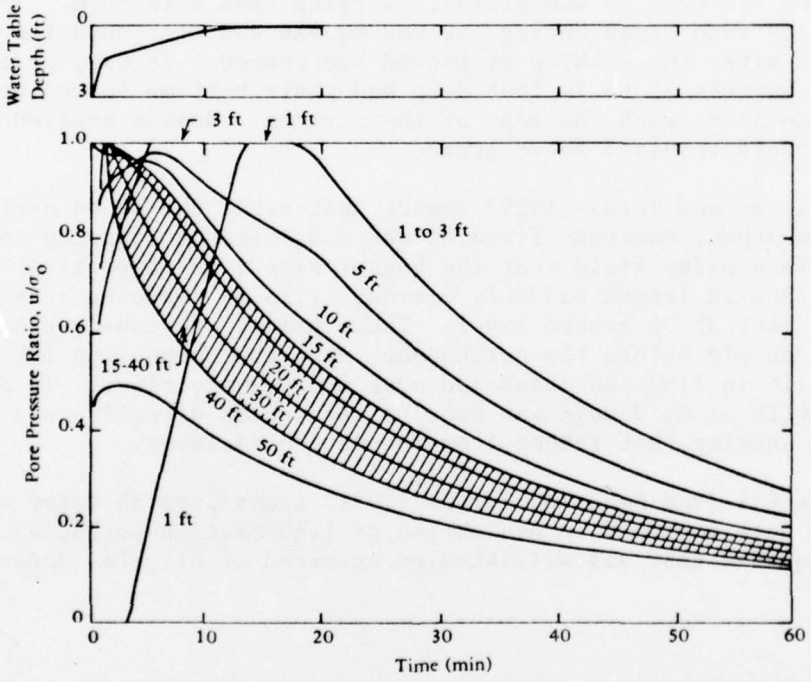

(c) In 60-minute period following earthquake.

Figure 4-15. Continued

Programs APOLLO and GADFLEA provide a significantly improved picture as to what is occurring to the soil and as such represents very useful tools to an engineer. The programs require values of the coefficient of permeability, coefficient of volume compressibility, and porosity. These values may be obtained for tests but are often assumed based on soil characteristics. The occurrence of liquefaction on near surface regions above the water table was found to be very sensitive to the location of the line of full saturation. Unfortunately, in field conditions a clean demarcation is not always present. As with other one-dimensional representations, the program APOLLO assumes infinite horizontal layers. This may present a problem in areas where discontinuities or slopes are present, since horizontal drainage is usually an order of magnitude greater than vertical drainage. Program GADFLEA should be used in cases requiring a two-dimensional analysis.

OBSERVATIONS OF LIQUEFACTION

Oldham (1899) reports that during the Assam, India, earthquake of 12 June 1897, a large number of jets of water rose to heights of 2 to 4 feet from fissures on the plains, carrying sand with them. The ejection of water and sand began during the earthquake and continued for 20 to 30 minutes after the shaking of ground had ceased. In many places drainage channels 15 to 20 feet deep had their bottoms forced up until they became level with the tops of their sides. Houses settled until only the roofs remained above ground.

Ambraseys and Sarma (1969) report that after the Kanto earthquake of 1923 in Japan, numerous fissures and mud volcanoes spurted intermittently. In a paddy field near the Sagami River, seven vertical wooden poles 20 feet in length suddenly emerged, finally reaching a height of about 4.5 feet above ground level. These piles, previously unknown to the local people before the earthquake, were the foundation for an old bridge built in 1182 and abandoned over 600 years earlier. In most cases, little or no damage was done to structures directly as a result of ground shaking, but rather from foundation failures.

Table 4-1 from Seed and Idriss (1971) summarizes 35 cases where available data was used in evaluation of liquefaction potential. One of the earthquakes that was well-studied occurred at Niigata, Japan in 1964.

Table 4-1. Site Conditions and Earthquake Data for Known Cases of Liquefaction and Nonliquefaction

Earthquake	Year	Magnitude	Site	Distance From Source of Energy Release (miles)	Soil Type	Depth of Water Table (ft)	Critical Depth (ft)	Average Penetration Resistance at Critical Depth, N	Relative Density (%)	Maximum Ground Surface Acceleration (g)	τ_{av}/σ'_o	Duration of Shaking (s)	Field Behavior
Niigata	1802	6.6	Niigata	24	Sand	3	20	6	53	0.12	0.135	~20	Nonliquefaction
			Niigata	24	Sand	3	20	12	64	0.12	0.135	~20	Nonliquefaction
Niigata	1887	6.1	Niigata	29	Sand	3	20	6	53	0.08	0.09	~12	Nonliquefaction
			Niigata	29	Sand	3	20	12	64	0.08	0.09	~12	Nonliquefaction
Mino Owari	1891	8.4	Ogaki	20	Sand	3	45	17	65	~0.35	0.39	~75	Liquefaction
			Ginan West	20	Sand	6	30	10	55	~0.35	0.37	~75	Liquefaction
			Unuma	20	Sand and Gravel	6	25	19	75	~0.35	0.35	~75	Nonliquefaction
			Ogase Pond	20	Sand	8	20	16	72	~0.35	0.35	~75	Liquefaction
Santa Barbara	1925	6.3	Sheffield Dam	7	Sand	~15	25	—	40	~0.2	0.16	15	Liquefaction
El Centro	1940	7.0	Brawley	5	Sand	~15	~15	—	58	~0.25	0.155	30	Liquefaction
			All-Am. Canal	5	Sand	~20	~25	—	43	~0.25	0.155	30	Liquefaction
			Solfatara Canal	5	Sand	5	~20	—	32	~0.25	0.26	30	Liquefaction
Tohnankai	1944	8.3	Komei	100	Sand	5	13	4	40	~0.08	0.08	~70	Liquefaction
			Meiko St.	100	Silt and Sand	2	8	1	30	~0.08	0.09	~70	Liquefaction
Fukui	1948	7.2	Takaya	4	Sand	11	23	18	72	~0.30	0.30	~30	Liquefaction
			Takaya	4	Sand	3	23	28	90	~0.30	0.32	~30	Nonliquefaction
			Shonenji Temple	4	Sand	4	10	3	40	~0.30	0.29	~30	Liquefaction
			Agr. Union	4	Sand and Silt	3	20	5	50	~0.30	0.33	~30	Liquefaction
San Francisco	1957	5.5	Lake Merced	4	Sand	8	10	7	55	~0.18	0.13	18	Liquefaction
Chile	1960	8.4	Puerto Montt	~70	Sand	12	15	6	50	~0.15	0.15	~75	Liquefaction
			Puerto Montt	~70	Sand	12	15	8	55	~0.15	0.15	~75	Liquefaction
			Puerto Montt	~70	Sand	12	20	18	75	~0.15	0.15	~75	Nonliquefaction
Niigata	1964	7.5	Niigata	32	Sand	3	20	6	53	0.16	0.175	40	Liquefaction
			Niigata	32	Sand	3	25	15	70	0.16	0.175	40	Liquefaction
			Niigata	32	Sand	3	20	12	64	0.16	0.175	40	Nonliquefaction
			Niigata	32	Sand	12	25	6	53	0.16	0.16	40	Nonliquefaction
Alaska	1964	8.3	Snow River	60	Sand	0	20	5	50	~0.15	0.18	180	Liquefaction
			Snow River	60	Sand	8	20	5	44	~0.15	0.15	180	Liquefaction
			Quartz Creek	70	Sandy Gravel	0	~25	40 - 80	100	~0.12	0.145	180	Nonliquefaction
			Scott Glacier	55	Sand	~20	~20	10	65	~0.16	0.185	180	Liquefaction
			Valdez	35	Sand and Gravel	5	~20	13	68	~0.25	0.25	180	Liquefaction
Tokachioki	1968	7.8	Hachinohe	45 to 110	Sand	3	12	14	78	0.21	0.23	45	Nonliquefaction
			Hachinohe	45 to 110	Sand	3	12	6	58	0.21	0.73	45	Liquefaction
			Hachinohe	45 to 110	Sand	5	10	15	80	0.21	0.185	45	Nonliquefaction
			Hakodate	100	Sand	3	15	6	55	0.18	0.205	45	Liquefaction

NIIGATA EARTHQUAKE OF 1964

Seed and Idriss (1967) describe the extensive damage from the magnitude 7.5 earthquake which occurred 35 miles north of the city of Niigata, Japan on 16 June 1964. The acceleration level at the city was about 0.16. Observed damage may be divided into four groups, as shown in Table 4-2.

Table 4-2. Niigata Earthquake

Damage to Foundation	Maximum Settlement (in.)	Angle of Tilt (deg)	Average Relative Density (%)	Range of Relative Density (%)
None	0-8	0-0.3	75	60-90
Slight	8-20	0.3-1	67	50-85
Intermediate	20-40	1-2.3	60	45-75
Heavy	>40	>2.3	45	30-60

The determination of the relative density of the in situ sands is extremely crude as extrapolated from the data presented by Seed and Idriss (1971).

It was noted that piles driven through loose zones into firm zones experienced significant horizontal displacement. When liquefaction occurs around the upper portion of the pile the pile loses its lateral resistance, producing movement. There were many cases of bending of piles supporting buildings in Niigata.

Kishida (1969) reports that the upper surface of the liquefied soil layer in the most severely damaged area was situated at a depth of less than 25 feet below the ground surface and that soils as deep as 75 feet were liquefied.

MINO OWARI EARTHQUAKE OF 1891

The Mino Owari earthquake of 28 October 1891 was a shock of 8.4 magnitude located 18.6 miles from the city of Gifu, Japan. Kishida (1969) has studied the effects of this earthquake and gives profiles of four locations (Figures 4-16 to 4-19) which show various degrees of liquefaction ranging from none to complete. Note that fine sands were most vulnerable.

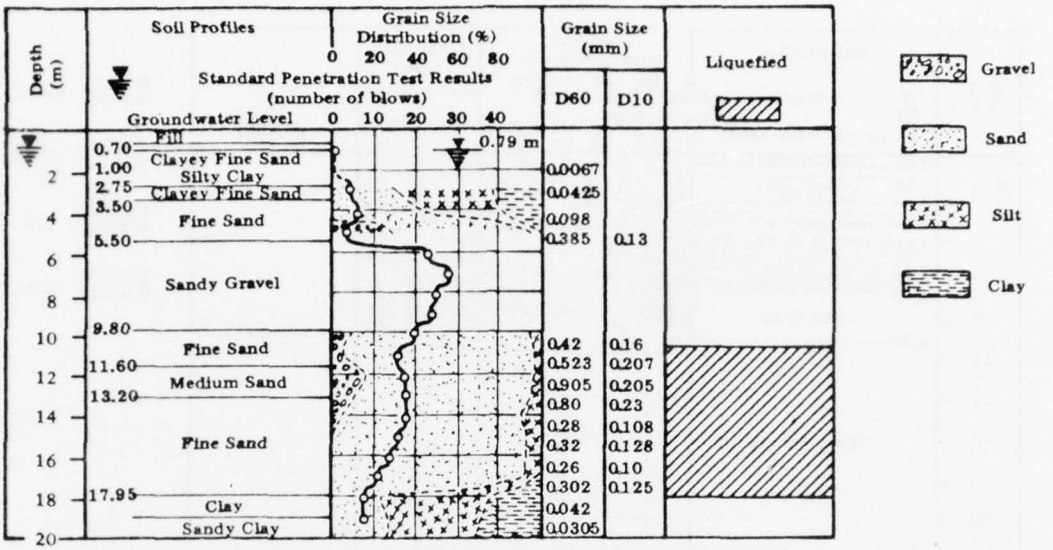

Figure 4-16. Soil profile, Ogaki City, Bangoku town (from H. B. Kishida, 1969).

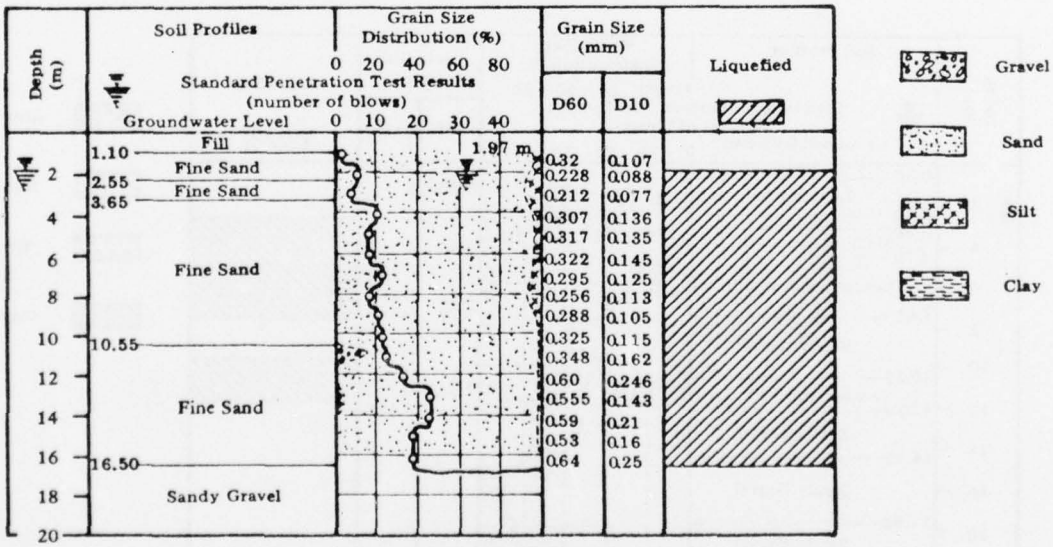

Figure 4-17. Soil profile, Ginan West Primary School (from H. Kishida, 1969).

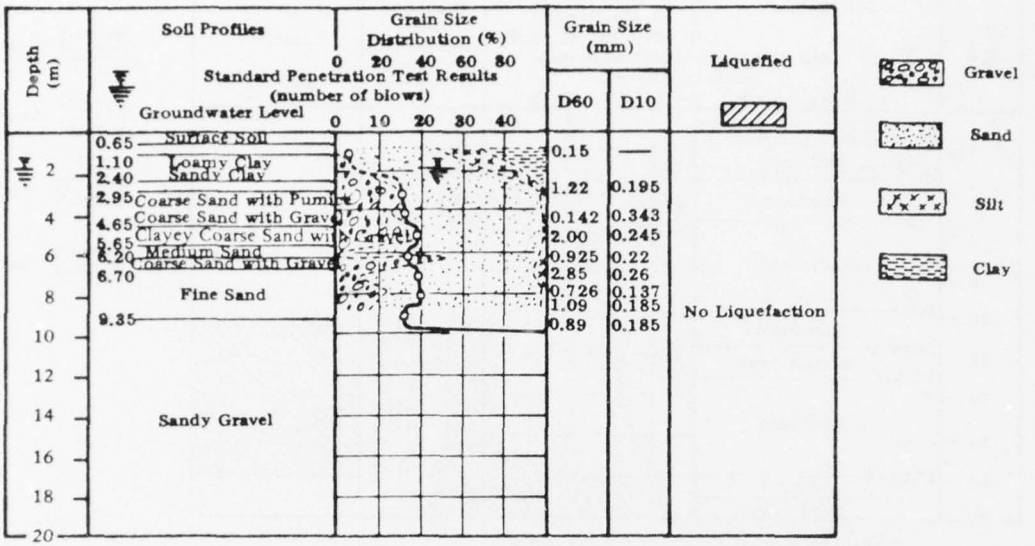

Figure 4-18. Soil profile, Unuma town (from H. Kishida, 1969).

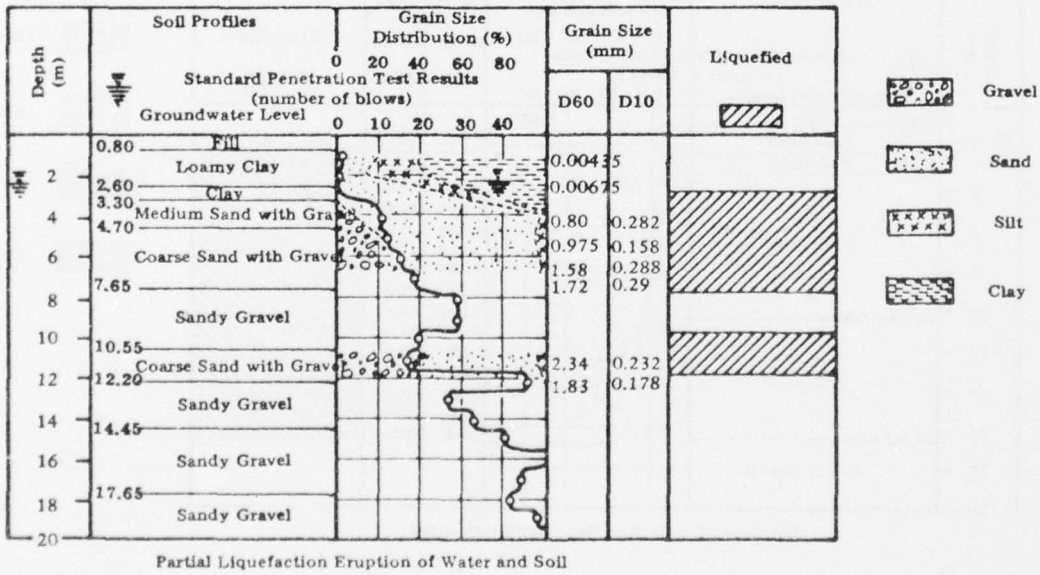

Figure 4-19. Soil profile, Ogase Pond (from H. Kishida, 1969).

TOHNANKAI EARTHQUAKE OF 1944

The Tohnanai earthquake of 7 December 1944 was a magnitude 8.3 earthquake located about 100 miles south-southwest of Nagoya City, Japan. Kishida (1969) studied the effects of this earthquake at three locations (Figure 4-20 to 4-22). At the location noted in Figure 4-20 a Buddhist Temple which was supported on piles did not show any settlement but the ground around the temple subsided about 1-1/3 feet, and water erupted during the earthquake. The tips of the piles were at a depth of about 5 meters below the surface (26.7 feet). Figure 4-21 shows a soil profile where houses settled as much as 3.3 feet. Fine sand was expelled from the ground. Figure 4-22 shows a soil profile where differential settlement occurred as a result of partial liquefaction.

FUKUI EARTHQUAKE OF 1948

The Fukui earthquake of 18 June 1948 was a magnitude 7.2 earthquake with its epicenter 3 miles east of Fukui City, Japan. Kishida (1969) studied the effects of this earthquake and gives four profiles (Figures 4-23 to 4-26) where liquefaction was observed in varying degrees. It is interesting to note that although the distance between locations of the soil profiles in Figure 4-23 and 4-24 was only about 1,800 feet, one underwent complete liquefaction with sand volcanoes noted on the surface and the other only partial limited liquefaction, the latter being an older area approximately 3.3 feet higher in elevation with more silt. Figure 4-25 shows a site where water and sand volcanoes were quite prevalent and the main building of a temple settled 1 foot. The distance between the locations shown in Figures 4-25 and 4-26 is about 1,800 feet. The site in Figure 4-26 did not show eruptions of sand and water and only partial liquefaction. This site is again in older ground slightly higher than that of Figure 4-25.

NONLIQUEFACTION (PRE-LIQUEFACTION) SUBSIDENCE

Lee and Albasia (1974), using cyclic triaxial tests, have investigated the settlements from volume change due to the dissipation of increased pore pressures. Their work is intended to represent general ground subsidence which might be expected from soil compaction and water drainage at stresses less than that required to induce complete liquefaction. Figure 4-27 shows a series of triaxial test results, considering the effects of confining pressure, relative density, and grain size on volumetric strain. Using Figure 4-11 or 4-28, the increase in pore pressure at any cycle less than N_L may be estimated. This increase in pore pressure can be used in conjunction with Figure 4-27 to estimate the volumetric strain from the rise in pore pressure and resulting drainage.

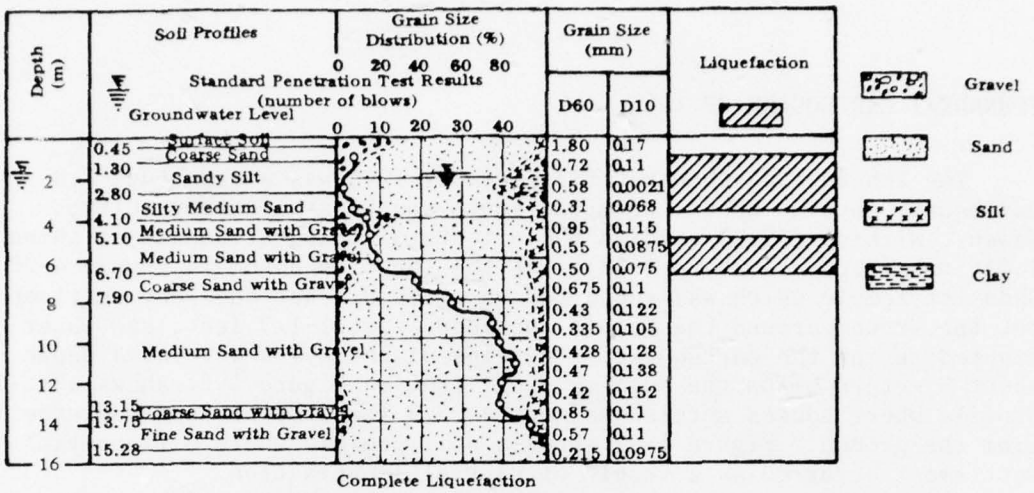

Figure 4-20. Soil profile, Komei town (from H. Kishida, 1969).

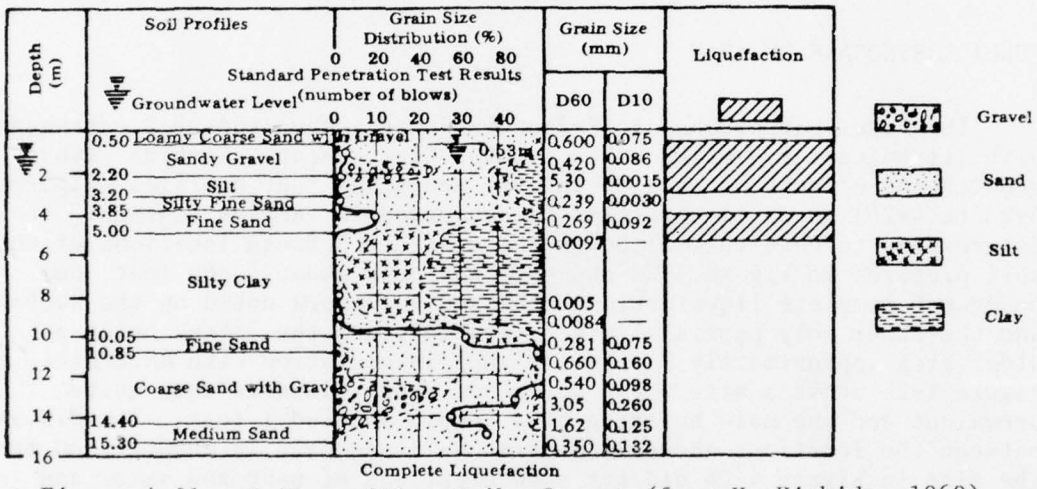

Figure 4-21. Soil profile, Meiko Street (from H. Kishida, 1969).

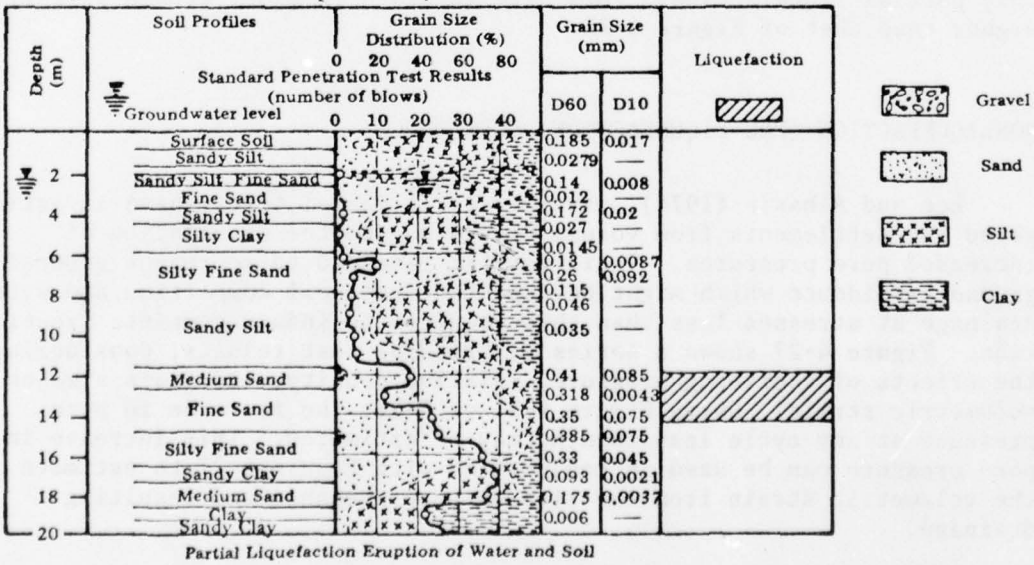

Figure 4-22. Soil profile, Ienaga Shinden (from H. Kishida, 1969).

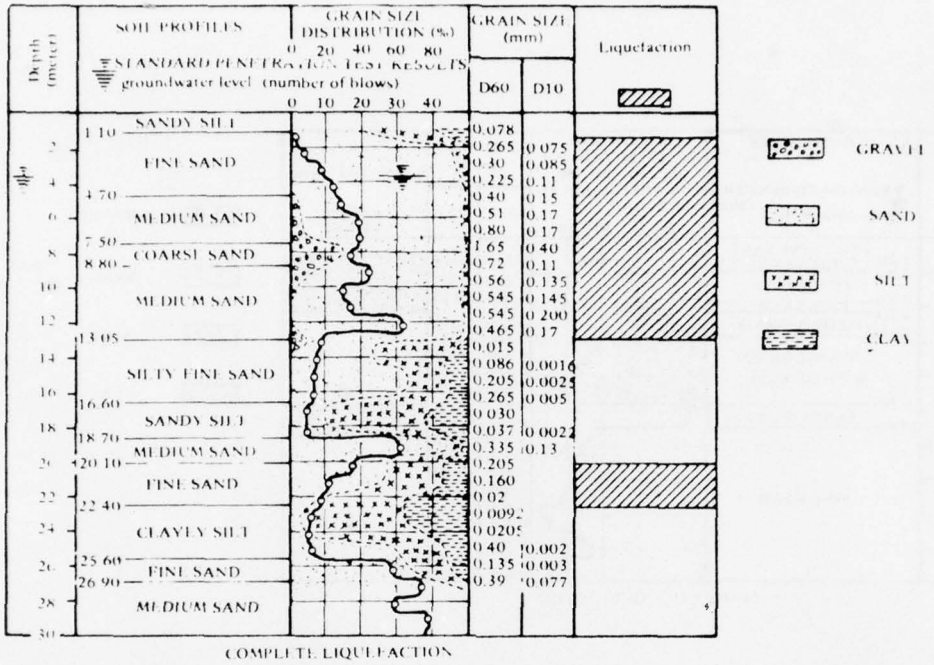

Figure 4-23. Soil profile, Takaya town 45-35 (from H. Kishida, 1969).

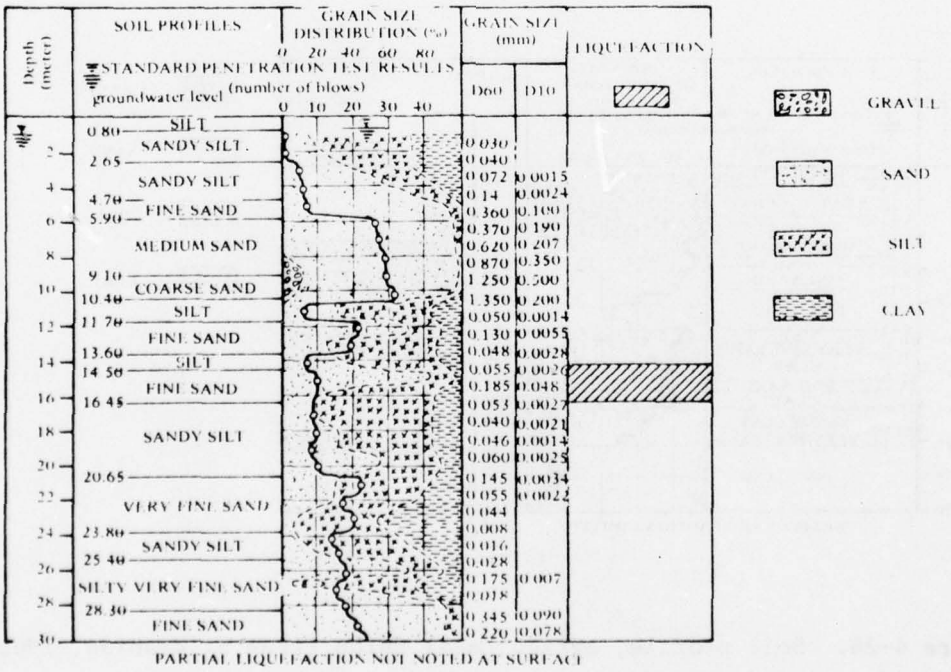

Figure 4-24. Soil profile, Takaya town 2-168 (from H. Kishida, 1969).

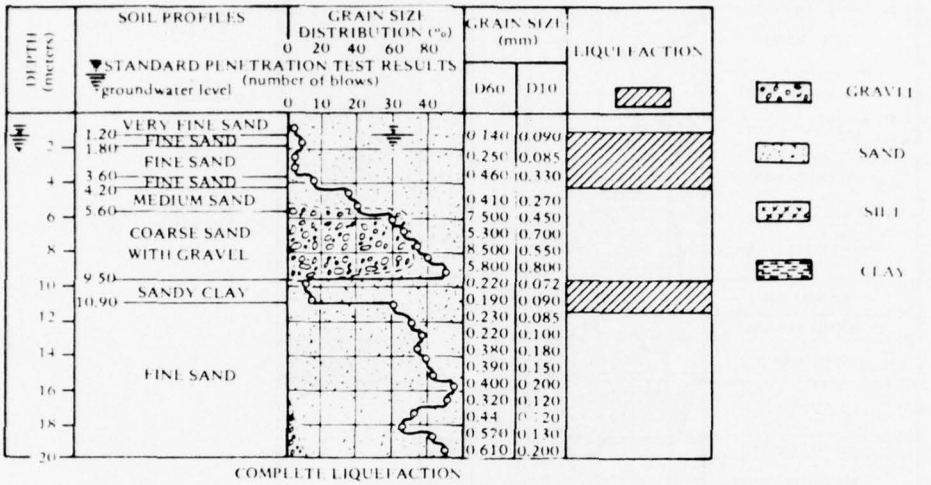

Figure 4-25. Soil profile, Shonenji Temple (from H. Kishida, 1969).

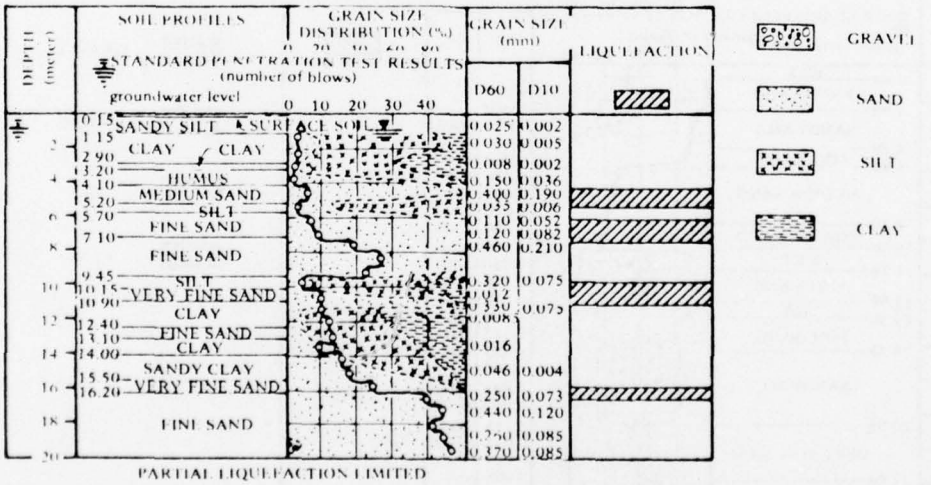

Figure 4-26. Soil profile, agricultural union (from H. Kishida, 1969).

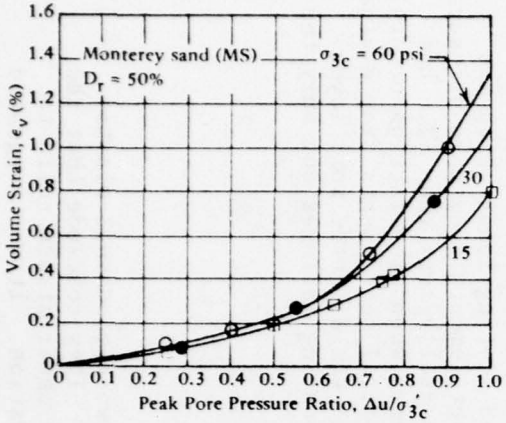

(a) Confining pressure on reconsolidation volumetric strain.

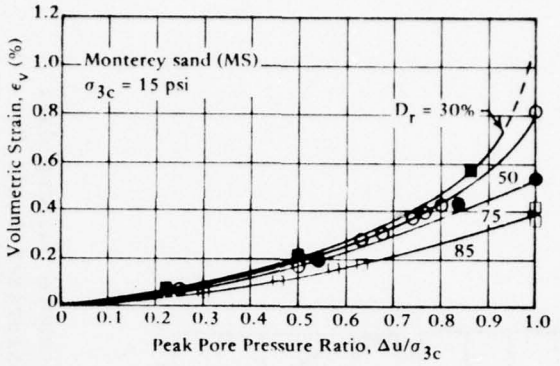

(b) Relative density on reconsolidation volumetric strain.

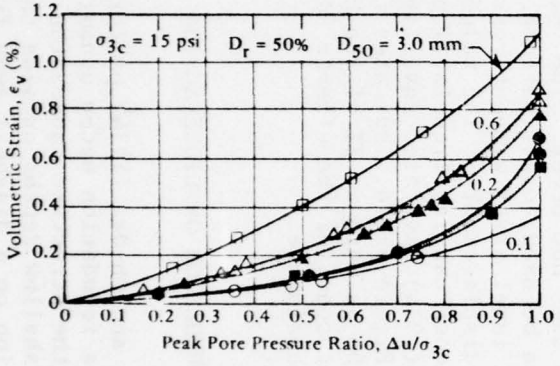

(c) Grain size on reconsolidation volumetric strain.

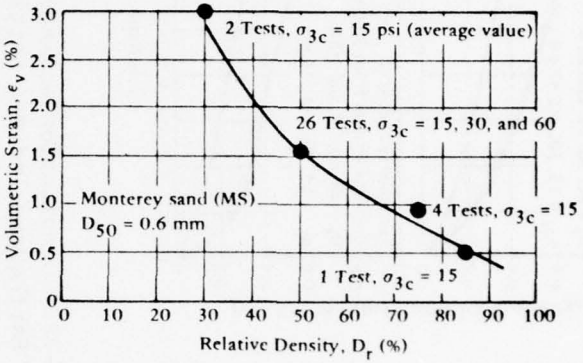

(d) Relative density on volumetric strain following complete liquefaction.

Figure 4-27. Effect of various factors on volumetric strain (from "Earthquake Induced Settlements in Saturated Sands," by K. L. Lee and A. Albasia, in Journal of the Geotechnical Division, ASCE, vol. 100, GT4, Apr 1974).

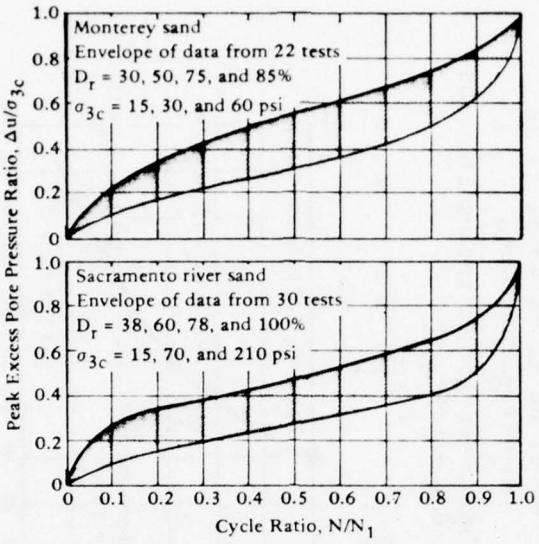

Figure 4-28. Compilation summary of pore pressure buildup data (from "Earthquake Induced Settlements in Saturated Sands," by K. L. Lee and A. Albasia, in Journal of the Geotechnical Division, ASCE, vol. 100, no. GT4, Apr 1974).

Figures 4-27a, b, and c are limited to conditions in which complete liquefaction does not occur. The volumetric strain and the thickness of the layer can be used to estimate the vertical settlement. This is intended for level areas without concentrated footing loads which may cause shear displacements. The volumetric settlements from pore pressures lower than those causing liquefaction are generally less than 1%. Lee and Albasia (1974) have also investigated cases when liquefaction occurs. Their data, Figure 4-27d, indicates that vertical settlements from drainage effects may be as much as 3% of the height of the affected soil layer. This does not consider the effects of soil bearing failures but only the "regional" subsidence.

EFFECT OF FOUNDATION ON LIQUEFACTION

Yoshimi and Oh-Oka (1974) performed a two-dimensional elastic analysis of a foundation under dynamic load. They conclude that the presence of the structure causes the dynamic shear stress ratio to increase at shallow depths outside the foundation. It was suggested that the region on a diagonal away from the edge of a footing would undergo liquefaction before the free field (area away from effects of the structure).

So significant is this hypothesis, if true, that this problem will be discussed here. It appears the gravity static stresses were not considered in the analysis of Yoshimi and Oh-Oka (1974). Furthermore, the choice of shear stress and confining stress were horizontal shear stress and vertical normal stress, rather than those of a principal stress orientation. The horizontal and vertical axis in the presence of initial static stress is an arbitrary choice.

In Chapter 2 a methodology was presented for computing an equivalent dynamic stress which would consider the effects of initial static shear stress from a foundation. In this analysis principal planes are used. This methodology was used in the following study.

To study the foundation problem, an elastic finite element analysis was performed. The soil was modeled by plane strain two-dimensional quadrilateral elements. The footing was also modeled using the same type of element with different material properties. To attempt to model the loading correctly, a typical column extended vertically above the footing. The top of the column was restrained by horizontal one-dimensional elements (springs) whose stiffness and mass were typical of the lateral restraint and mass provided by a floor slab. Figure 4-29 shows the finite element mesh.

The linear elastic analysis was performed in segments and the results combined. The static gravity analysis was combined with the results of a dynamic ground-motion analysis. In the dynamic analysis, the equivalent stress level was determined in terms of the principal stresses for each element.

Figure 4-30 shows the vertical static effective stress. Figure 4-31 shows the effective static octahedral normal stress and Figure 4-32 gives a static K (the ratio of minor to major principal stress). Figure 4-33 shows the static shear stress on the former principal plane, and Figure 4-34 shows the dynamic shear stress level. Figure 4-35 shows the dynamic shear stress computed by the methodology discussed in Chapter 2; i.e., the shear stress determined on the principal plane orientation before application of the dynamic load. Thus, this stress rotation eliminates the complexities of considering initial shear stress level and, hence, nonsymmetric stress reversals. Figure 4-36 shows a plot of equivalent shear stress ratio and Figure 4-37 gives the relative number of cycles to cause liquefaction using the modified approach. The specific numbers are not as important as the general shape of the contour lines, since the specific numbers represent the selection of earthquake record amplitude and frequency and the choice of soil material properties. The shape of the general contours appear independent of earthquake loading or soil parameters.

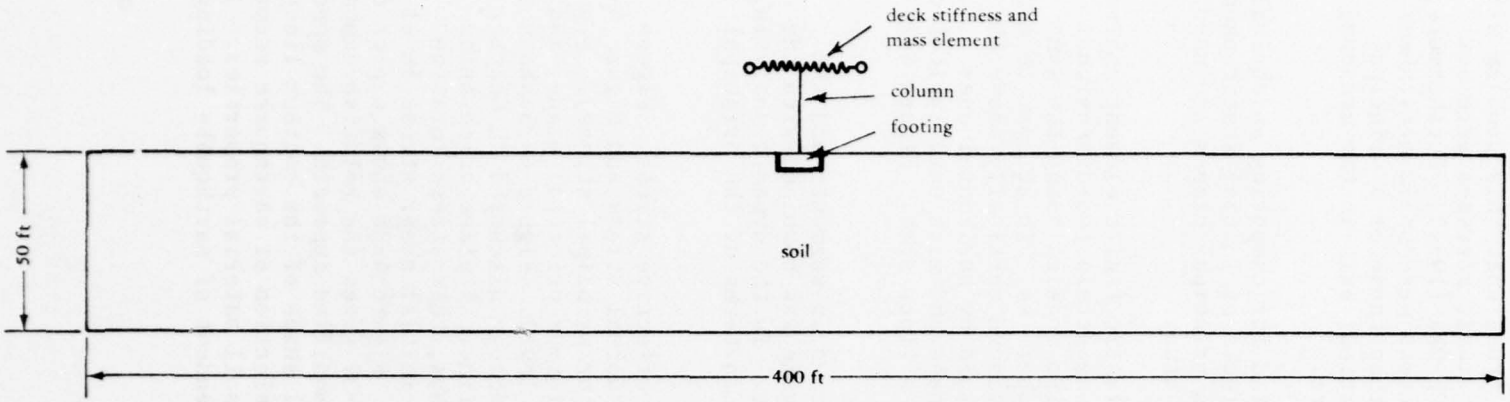

(a) Soil cross section.

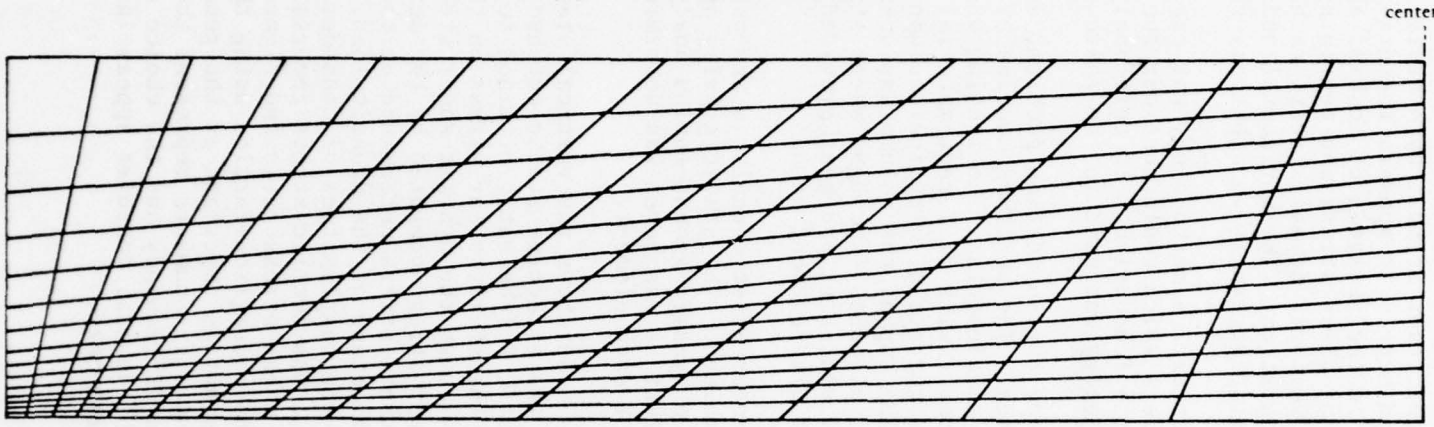

(b) Half of finite element mesh of soil field.

Figure 4-29. Finite element analysis of soil field.

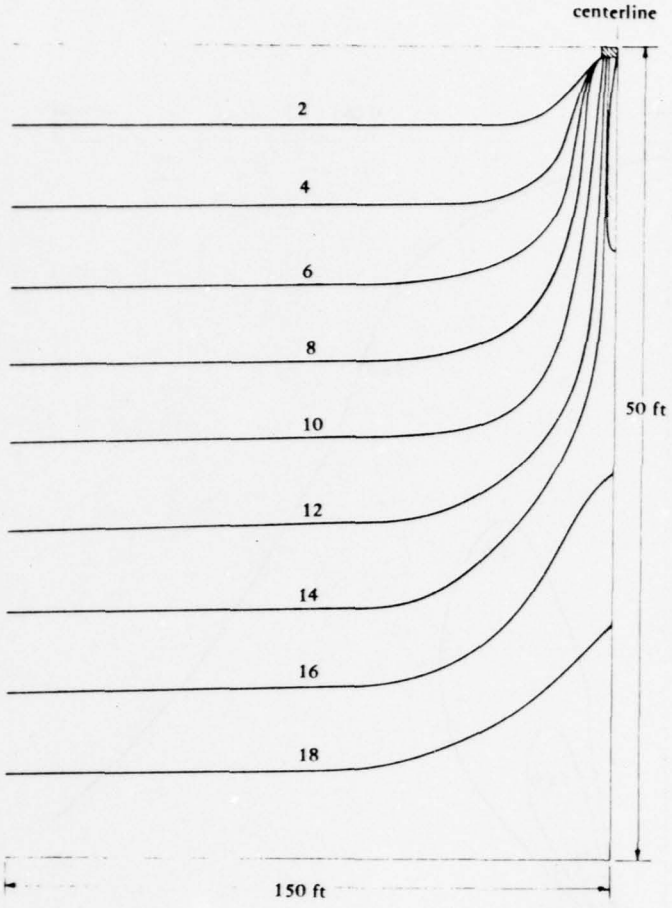

Figure 4-30. Vertical static stress σ_v.

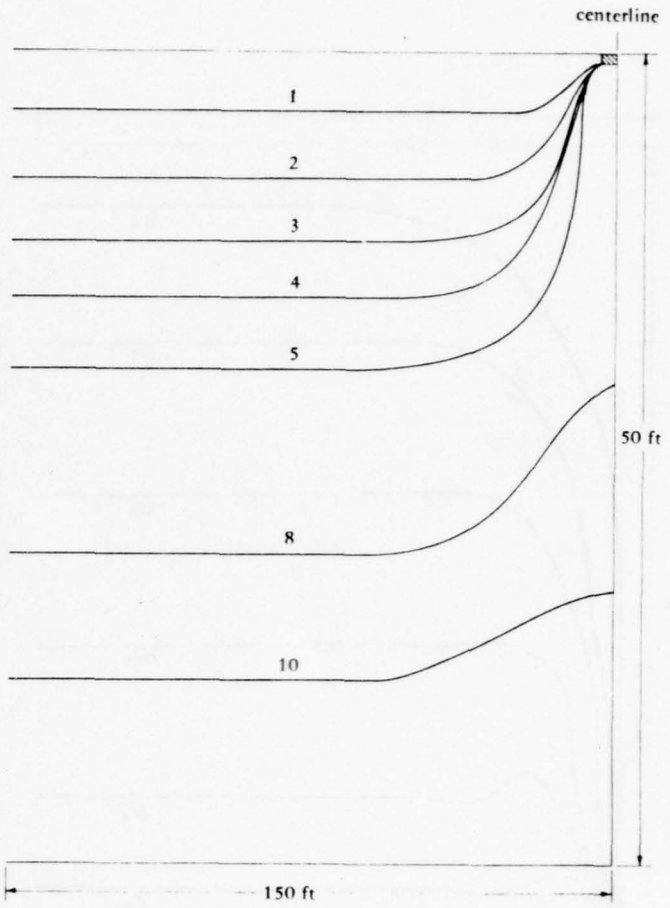

Figure 4-31. Octahedral normal static stress σ_o.

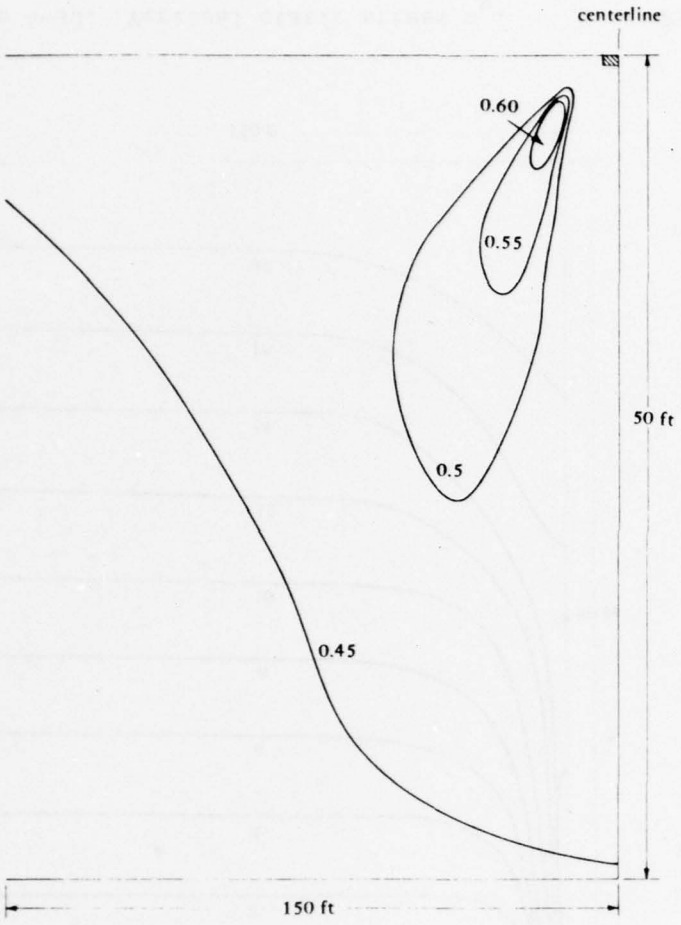

Figure 4-32. Ratio of principal stresses K_o.

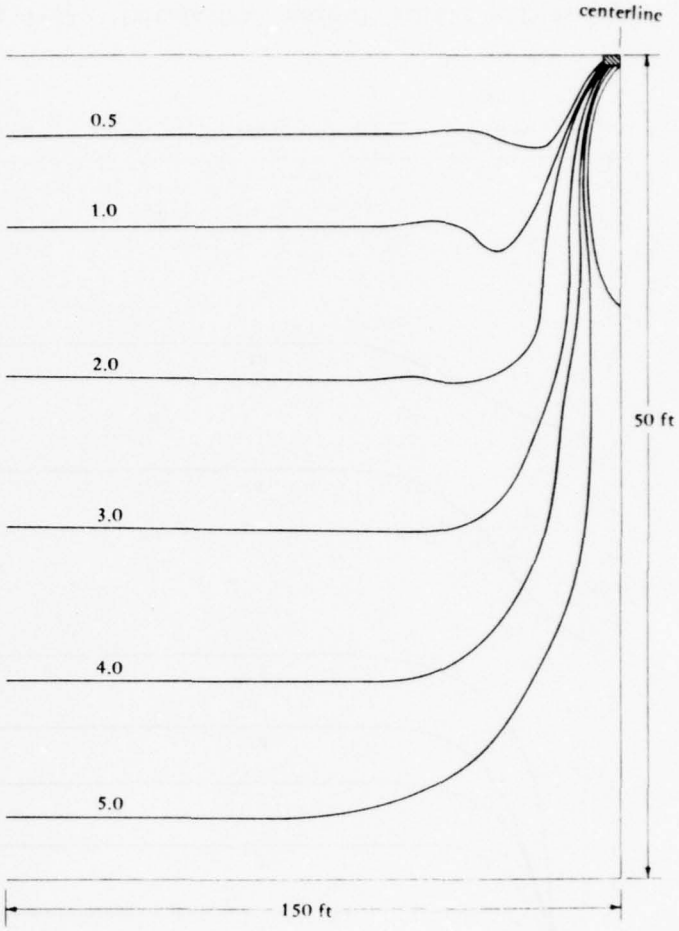

Figure 4-33. Static shear stress τ_{static} on what was formerly the principal plane.

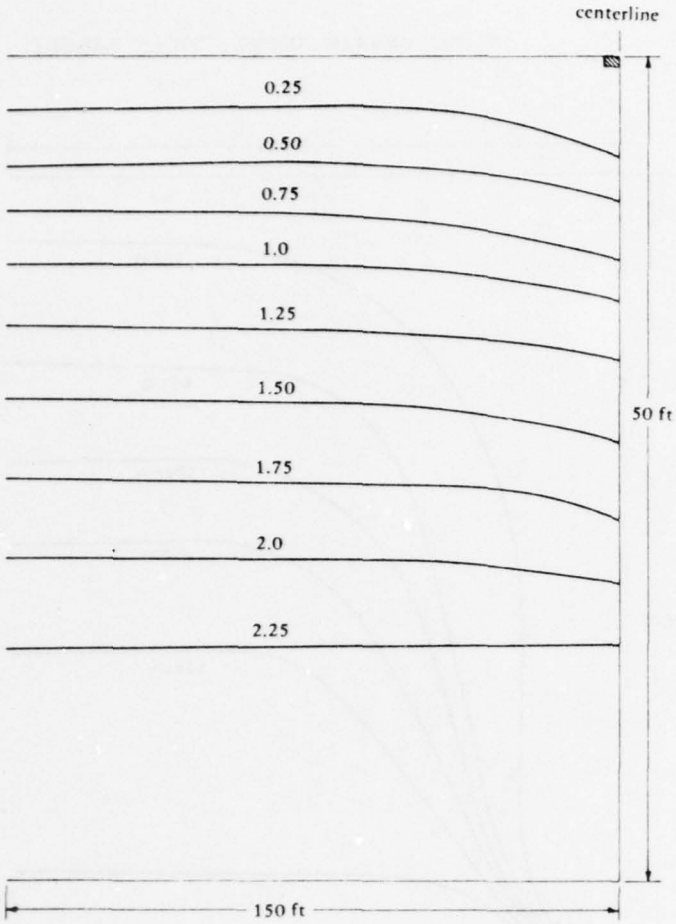

Figure 4-34. Dynamic shear stress $\tau_{dynamic}$.

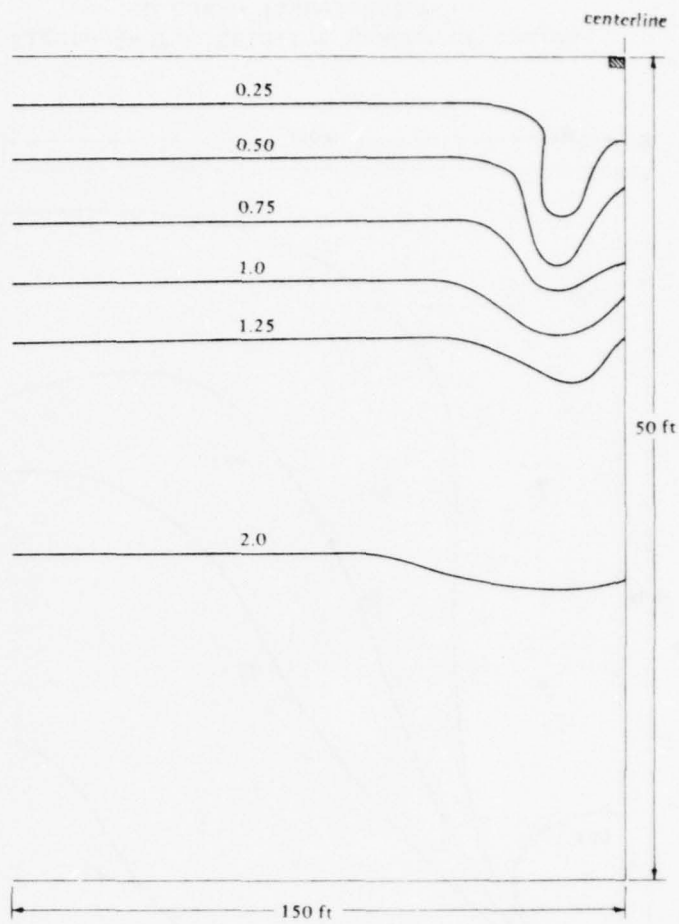

Figure 4-35. Dynamic shear stress on what was the principal plane prior to dynamic loading.

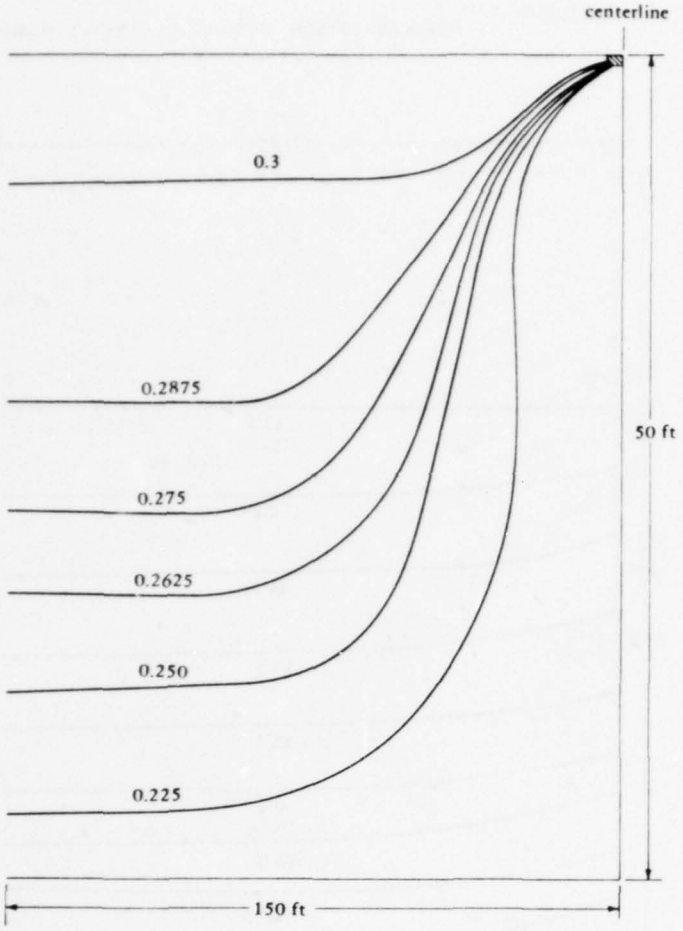

Figure 4-36. Shear stress ratio.

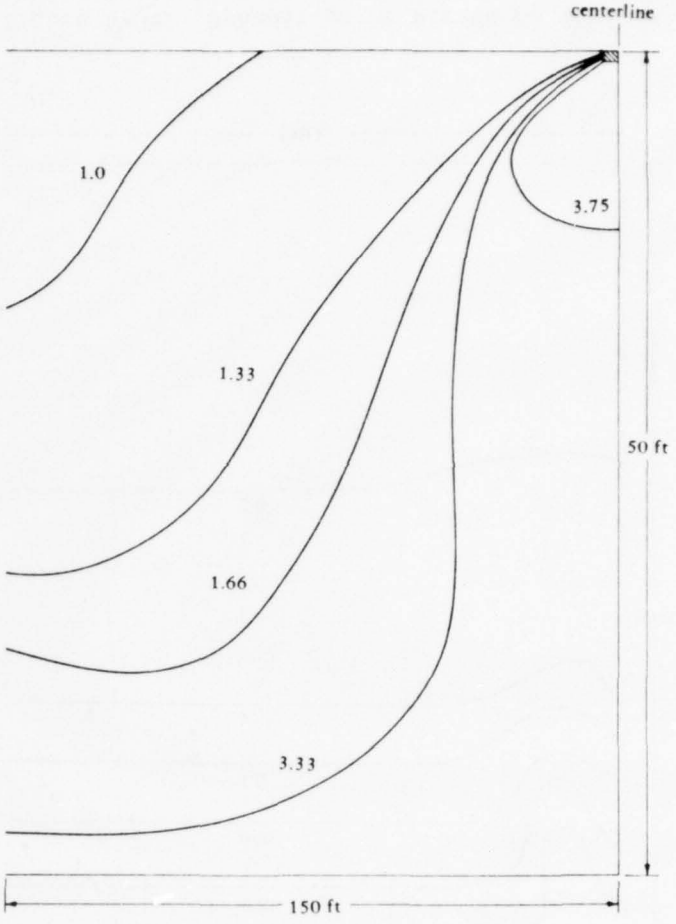

Figure 4-37. Relative number of cycles to cause liquefaction.

The significant conclusion is that, based upon a more realistic assessment of the actual stress conditions, it appears that the area beneath a foundation is less sensitive to liquefaction that the free-field area (the opposite of what Yoshimi and Oh-Oka, 1974, concluded). Thus, liquefaction analysis techniques which are based on free-field conditions are conservative when applied to areas beneath footings. The present state-of-the-art of direct computation of pore pressure is very limited. The present two-dimensional stress-analysis, finite-element programs only attempt to answer the problem of pore pressure distribution indirectly in terms of the shear-stress/confining-stress ratio.

REDUCTION IN FOUNDATION CAPABILITY DUE TO LIQUEFACTION

There is essentially no quantitative experimental data available for evaluating reductions in foundation load-carrying capability due to partial liquefaction of subfoundation soils. It has been tacitly assumed in most instances that foundation load support is not critical up until the point at which initial liquefaction has occurred in the free-field regions. Limited test data on small scale model footings by DeAlba, Chan, and Seed (1975) has tended to support this assumption, at least for homogeneous sands under undrained conditions. The analysis of liquefaction beneath load discontinuities, discussed earlier further suggests the noncritical nature of the subfoundation material response (again for homogeneous soils).

It is generally agreed that structures on homogeneous deposits of sand fail because of excessive settlement rather than by bearing capacity failure. However, in many cases typical soil profiles contain layers of different material, significant parts of which may exhibit cohesive behavior. Bearing capacity failures are common modes of failure in cohesive soils. It is also conceivable that situations could be encountered in the field where strongly stratified soil profiles have horizontal permeabilities many times greater than those in the vertical direction (see Terzaghi and Peck, 1967, page 334). Under such cases it is possible that rapid horizontal equalization of excess pore water pressure might permit settlement or even failure of the foundation following the cessation of earthquake motion under somewhat quasi-static conditions.

Under such conditions, it might be desirable to consider a reduced-foundation capability in order to avoid either foundation failure (outright collapse or shear failure) or unacceptable settlement.

For granular soils, the static-load factor of safety against collapse is generally well over 3, and allowable bearing capacity is generally governed by permissible settlement of the supported structure. In some cases of earthquake-induced loading, a high degree of foundation damage

due to settlement might be considered tolerable provided total collapse of the structure did not occur. In these cases ultimate bearing capacity might become a limiting design factor.

The ultimate bearing capacity of a foundation resting upon soil may be approximated by relationships such as the following proposed by Terzaghi and Peck (1967), for continuous footings:

$$q = c\,N_c + \gamma' D_f N_q + \gamma' B N_\gamma \qquad (1)$$

where

q = bearing capacity of a footing per unit of footing area

c = cohesion of the soil

D_f = depth of embedment of the footing below the ground surface

B = one-half the minimum footing dimension

γ' = effective weight of the soil (i.e., buoyant weight below the water table)

N_c, N_q, N_γ = bearing capacity factors, defined as a function of the frictional resistance of the soil (see Terzaghi and Peck, 1967)

Since the type of liquefaction of interest herein is limited to cohesionless soils, the factor N_c may be neglected and the bearing capacity expressed in the form

$$q = \gamma' D_f N_q + \gamma' B N_\gamma \qquad (2)$$

The factor N_q is intended to account for the strength contribution due to the confinement offered by the surcharge, or the soil above the foundation base level $\gamma' D_f$. The factor N_γ accounts for the frictional resistance of the soil beneath the base of the footing represented by the term $\gamma' B$. A reduction in either N_γ or $\gamma' B$ caused by generation of excess pore water pressure would then cause a reduction in ultimate bearing capacity. Thus, the allowable load following generation of a pore water pressure increment u might be approximated by:

$$q = (\gamma' D_f - \Delta u) N_q + (\gamma' B - \Delta u) N_\gamma \qquad (3)$$

where the unit load reduction is $\Delta u(N_q + N_\gamma)$. The increase in pore pressure may be estimated by use of the program GADFLEA cited earlier in this chapter. To maintain the same factor of safety as under nonearthquake loading, the allowable bearing capacity must be reduced by multiplying it by the factor:

$$R = \frac{(\gamma' D_f - \Delta u)N_q + (\gamma' B - \Delta u)N_\gamma}{\gamma' D_f N_q + \Delta' B N_\gamma} \tag{4}$$

Defining Δu in terms of the ratio of excess pore pressure generated, to initial effective stress, $\Delta u/\sigma'$, Equation 4 may be written as:

$$R = \frac{\gamma' D_f \left(1 - \frac{\Delta u}{\sigma'} N_q\right) + \gamma' B \left(1 - \frac{\Delta u}{\sigma'}\right) N_\gamma}{\gamma' D_f N_q + \gamma' B N_\gamma} \tag{5}$$

where the critical region for $\Delta u/\sigma'$ could be taken as that beneath the foundation base within a depth of one and one-half times the foundation width. Equation 5 may be further simplified by the assumptions:

(1) Water table at the surface (i.e, $\gamma' = \gamma_b$)

(2) $N_q \approx N_\gamma$

(3) $h = \Delta u/\gamma_w$ (where γ_w is the weight of water)

Hence, the reduction factor may be roughly estimated as:

$$R = \frac{(D_f - h) + (B - h)}{D_f + B} \tag{6}$$

The ultimate bearing capacity of a pile group in cohesionless soils may be estimated in terms of that of a pier of similar dimensions. Thus, the bearing capacity is the same as for a footing plus the contribution of skin friction along the sides of the equivalent pier (of depth D). The D-term contributes to ultimate load capacity as a diminishing multiple of D for values of D greater than five times the foundation width, 15 x (2B)1. For D values beyond 15 x (2B), this contribution becomes essentially constant. Thus, an increase in unit bearing capacity due to this latter term may be estimated as:

$$\frac{D^2\gamma'}{2A} P \tan \psi \tag{7}$$

where D = pile group length

γ' = soil effective weight

P = perimeter of the pile group

A = plan area of pile group

ψ = friction angle between the pile group and the surrounding soil

Under this situation the load reduction factor would be roughly equal to

$$R = \frac{(\gamma'D - \Delta u)N_q + (\gamma'B - \Delta u)N_\gamma + \frac{D}{2}(\gamma'D - \Delta u)\frac{P}{A}(\tan \psi)}{DN_q + BN_\gamma + D^2 \tan \psi} \tag{8}$$

or in terms of the ratio $\Delta u/\sigma'$ and assuming $P/A = 8B/4B = 2$;

$$R = \frac{D\left(1 - \frac{\Delta u}{\sigma'}\right)N_q + B\left(1 - \frac{\Delta u}{\sigma'}\right)N_\gamma + D\left(1 - \frac{\Delta u}{\sigma'}\right)\tan \psi}{DN_q + BN_\gamma + D^2 \tan \psi} \tag{9}$$

Settlements of foundations on granular materials are commonly assumed to be roughly proportional to the applied loading. Thus, a prescribed reduction in allowable load capacity due to partial liquefaction could serve to maintain settlement levels within acceptable limits.

To provide a slightly more detailed treatment of the effect of partial liquefaction on allowable settlements, it will be interesting to consider work by Schimming (1962) dealing with the settlement of footings on cohesionless soils. With the use of dimensional analysis combined with model test data, a relationship has been developed between $q/\gamma B$ and δ/B for circular footings resting upon the surface of a cohesionless soil. This relationship when plotted in the hyperbolic form outlined by Kondner (1962) provides the relationship,

$$\delta_1 = \frac{q_1 aB}{\gamma B - bq_1} \tag{10}$$

where q = unit loading

B = footing radius

γ = effective weight of the soil

δ = settlement

a = constant

b = constant

Under an increase in dynamic pore pressure Δu, the revised settlement δ_2 may be estimated in terms of:

$$\delta_2 = \frac{q_2\ aB}{(\gamma B - \Delta u) - bq_2} = \frac{q_2\ aB}{\gamma B\left(1 - \frac{\Delta u}{\sigma'}\right) - bq_2} \tag{11}$$

Assuming it is necessary to permit no increase in settlement under partial liquefaction (δ_2) over that permitted for the normal case of no earthquake loading, then,

$$\delta_2 = \delta_1 \quad \text{or} \quad \frac{q_1\ aB}{\gamma B - bq_1} = \frac{q_2\ aB}{\gamma B\left(1 - \frac{\Delta u}{\sigma'}\right) - bq_2} \tag{12}$$

Therefore,

$$q_2 = q_1\left(1 - \frac{\Delta u}{\sigma'}\right) \tag{13}$$

or the reduction in allowable load to provide no increase in settlement under partial liquefaction is seen to be merely:

$$R = \frac{q_2}{q_1} = 1 - \frac{\Delta u}{\sigma'} \tag{14}$$

(i.e., proportional to the reduction in initial effective confining stress).

DISCUSSION

A designer should have an estimate of the magnitude of ground displacement that might be expected if liquefaction were to occur; however, the information available to date is extremely limited. The methods for estimating displacements given in this chapter are crude and approximate. Further work in this area may show their need for modification; they are presented here as a first guess to alert the designer to a potential hazard. CEL is presently investigating this problem by several approaches, one of which is the two-phase finite element program described in Chapter 3. Hopefully, the results of this work can yield better estimates of ground displacement.

REFERENCES, CHAPTER 4

Ambraseys, N. and Sarma, S. (1969) "Liquefaction of soils induced by earthquake," Bulletin of the Seismological Society of America, vol 59, no. 2, Apr 1969, pp 651-664.

Booker, J. R., Rahman, M. S. and Seed, H. B. (1976) GADFLEA: A computer program for the analysis of pore pressure generation and dissipation during cyclic or earthquake loading, University of California, Earthquake Engineering Research Center, EERC Report No. 76-24. Berkeley, Calif., Oct 1976.

Crandall, R. (1908) The San Francisco peninsula in the California earthquake of 1906, vol 1. Washington, D. C., Carnegie Institute, pp 246-254.

DeAlba, P., Chan, C. and Seed, H. B. (1975) Determination of soil liquefaction characteristics by large-scale laboratory tests, University of California, Earthquake Engineering Research Center, EERC Report No. 75-14. Berkeley, Calif., May 1975.

Kishida, H. (1969) "Characteristics of liquefied sands during Mino-Owari, Tohnankai, and Fukui earthquakes," Soils and Foundations (Japan), vol 9, no. 1, Mar 1969.

Kondner, R. L. (1962) "Hyperbolic stress-strain response, cohesive soils," Journal of the Soil Mechanics and Foundations Division, ASCE, vol 89, no. SM1, Feb 1963, pp 115-143.

Lee, K. L. and Albasia, A. (1974) "Earthquake induced settlements in saturated sands," Journal of the Geotechnical Division, ASCE, no. GT4, Apr 1974.

Martin, P. P. (1975) Non-linear methods for dynamic analysis of ground response, Ph.D. thesis, University of California. Berkeley, Calif., Jun 1975.

McCulloch, D. S. and Bonilla, M. G. (1970) Effects of the earthquake of March 27, 1964, on the Alaska railroad, U. S. Geological Survey, Professional Paper 545-D. Washington, D.C., 1970, 161 pp.

Oldham, R. D. (1899) Report on the great earthquake of 12th June 1897, Memorandum Geological Survey, India, vol 49, 379 pp.

Richter, C. F. (1958) Elementary seismology. San Francisco, Calif., W. H. Freeman, 1958, 786 pp.

Robinson, R., et al. (1975) Structural analysis and retrofitting of existing highway bridges subjected to strong motion seismic loading, Illinois Institute of Technology, Research Institute Report J-6320. Chicago, Ill., May 1975.

Schimming, B. B. (1962) An analytic and experimental study of footings resting on a cohesionless soil, Ph.D. thesis, Northwestern University. Evanston, Ill., 1962.

Seed, H. B. (1968) "Landslides during earthquakes due to soil liquefaction," Journal of the Soil Mechanics and Foundations Division, ASCE, vol 93, no. SM5, May 1968, pp 1053-1122.

Seed, H. B. and Idriss, I. M. (1967) "Analysis of soil liquefaction, Niigata earthquake," Journal of the Soil Mechanics and Foundations Division, ASCE, vol 93, no. SM3, May 1967.

Seed, H. B. and Idriss, I. M. (1971) "A simplified procedure for evaluating soil liquefaction potential," Journal of the Soil Mechanics and Foundation Division, vol 97, no. SM6, Sep 1971.

Seed, H. B., Martin, P. P. and Lysmer, J. (1975) The generation and dissipation of pore water pressures during soil liquefaction, University of California, Earthquake Engineering Research Center, EERC Report No. 75-26. Berkeley, Calif., Aug 1975.

Terzaghi, K. and Peck, R. B. (1967) Soil mechanics in engineering practice. New York, N.Y., John Wiley and Sons, 1967.

Yoshimi, Y. and Kuwakara, F. (1973) "Effect of sub-surface liquefaction on the strength of surface soil," Soils and Foundations (Japan), vol 13, no. 2, Jun 1973.

Yoshimi, Y. and Oh-Oka, H. (1974) "Influence of degree of shear stress reversal on the liquefaction of potential of saturated sand," Soils and Foundations (Japan), vol 15, no. 3, Sep 1974.

Youd, T. L. (1973a) Liquefaction, flow and associated ground failure, U.S. Geological Survey, Circular 688. Reston, Va., 1973, 12 pp.

Youd, T. L. (1973b) Ground movements in the Van Norman Lake vicinity during San Fernando, California, earthquake of February 9, 1971, in San Fernando, California, Department of Commerce, National Oceanic and Atmospheric Administration, vol 3. Washington, D.C., 1973, pp 197-206.

Youd, T. L. (1975) "Liquefaction, flow and associated ground failure," in Proceedings of the U. S. National Conference on Earthquake Engineering, Ann Arbor, Mich., Jun 1975. Earthquake Engineering Research Institute, Oakland, Calif., 1975, pp 146-155.

Chapter 5

RECOMMENDATIONS FOR CONSIDERATION BY PLANNERS AND DESIGN ENGINEERS

RISK ASSESSMENT

A dictionary definition of the term "calculated risk" states: "A hazard or chance of failure whose degree of probability has been estimated before some undertaking is entered upon." Casagrande (1965), in a study of the role of risk in soil mechanics, states that the calculated risk is the type of risk that nobody knows how to calculate, bringing out the ambiguity of the adjective "calculated." He defines the term calculated risk as: the use of imperfect knowledge guided by judgment and experience to estimate the probable ranges for all pertinent quantities that enter into the solution of a problem and to base a decision on an appropriate margin of safety.

The margin of safety that we use should bear a direct relationship to the magnitude of the potential losses and the range of uncertainties at a site. Projects with the potential for catastrophic loss of lives and property should always be planned with an awareness of the responsibility involved. Therefore, the best knowledge and judgment, coupled with the most sophisticated techniques, must be used to ensure the best design. Detailed site investigations should be undertaken to provide all the required information for an analysis. This, along with conservative factors of safety, minimizes the risk. However, when failure of smaller projects involves a tolerable financial loss and no loss of life, the extent or degree of risk must take into consideration economic factors and magnitude of losses that would result from failures. The effort spent in the design is obviously reduced. It is in these routine projects where the calculated risk is greatest. Obviously, the extent of site definition is more limited for smaller projects. It is in these areas that this report attempts to provide most guidance.

Casagrande (1965) divides risk into two groups: engineering risk and human risk. He further divides engineering risk into two groups, unknown risks and calculated risks. Unknown risks are, by definition, those risks which cannot be identified until they reveal themselves by

failure. Calculated risks are areas where the state of knowledge is limited, requiring judgment. Significant progress has been made in our understanding of the seismic liquefaction phenomenon. However, uncertainties exist in the determination of site motion, the determination of site soil profile and parameters, and the evaluation of the soil strength. Table 5-1 summarizes the design philosophy suggested.

Table 5-1. Philosophy of Earthquake-Resistant Design

Structural Criteria	Liquefaction Behavior
1. Prevent nonstructural damage in minor earthquake ground shakings which may frequently occur in the service life of the structure.	1. No liquefaction. Factor of safety >1.3.
2. Prevent structural damage and minimize nonstructural damage in moderate earthquake ground shaking which may occur occasionally.	2. No liquefaction. Factor of safety >1.1.
3. Avoid collapse or serious damage in severe earthquake ground shakings which may rarely occur.	3. Liquefaction limited to confined subsurface layer which does not propagate to surface to cause bearing failure. Horizontal flow potential limited to acceptable level.

SITE INVESTIGATION

Ferritto (1978) presents a method for evaluating a potential site to determine the design earthquake ground motion. Detailed surface and subsurface geological information, when available, can aid in evaluation of a site by giving evidence of fault offset, earthquakes associated with faults, determination of age of most recent movement on faults, determination of relationships between site area faults and regional faults, and the identification and description of the faults capable of producing an earthquake. Use should be made of all available geologic maps and data. The time period for active faults should include the Holocene period and perhaps as much as several hundred thousand years in areas of low seismicity to ensure recognition of all potentially active faults.

The detailed site investigation must, as a minimum, provide information on the type and in situ condition of the soil with depth and the location of the water table so that a soil profile may be constructed. The extent of the investigation is controlled by the importance of the structure. For conventional structures of normal importance where large-scale soil-test programs are not possible, it is suggested that at least standard penetration tests be used in conjunction with the recovery and classification of borings.

Since the amount of money that might be spent on a site investigation may be limited for a simple structure, the emphasis should be placed on field tests rather than laboratory tests. Also to be considered is that although the structure by itself might not be costly, it may represent a link in a network which would become useless if it should fail.

SITE MOTION

The ground motion should be determined based on a design level earthquake as described by Ferritto (1978). A design magnitude should be selected in relation to a probability of occurrence during the life of the structure. In most cases, historical data is limited and additional data from the fault slip rates (see Ferritto, 1978) may be needed to provide guidance in selecting design level earthquakes. The design level earthquake should be checked with design earthquake levels assigned to specific faults that have occurred in the past and were thought possible for the future. The present state-of-the-art of liquefaction analysis is limited to ground-motion analysis represented by shear waves.

CONSTRUCTION IN AREAS OF POTENTIAL LANDSPREADING

Regional land movement - landspreading - may occur during earthquakes as a result of increased pore pressures and reduced soil strength. Structures which cannot undergo differential settlements of high magnitudes should not be built where landspreading is expected, such as on topographically low areas where the water table is high. The process of site selection should give preference to areas where soils are at higher relative densities and unconsolidated sediments are thinnest. Landspreading may be reduced by elimination of surface depressions. The practice of side borrowing to build embankments increases lateral spreading and should be avoided. Narrow fills, even on well-compacted areas, can settle as a result of ground cracks. Outward flow of soils on the embankment can be expected if the underlying native soils undergo limited flow from liquefaction. Then settlements of embankments will occur: the wider the fill, the less chance of damage.

In site selection the toes of alluvial fans and deltas should be avoided. Sites should be limited to older, higher, better drained upper segments of fans and deltas, which are probably more stable.

PRELIMINARY EVALUATION OF LIQUEFACTION POTENTIAL

A preliminary analysis should be made to determine if a liquefaction problem exists and to what extent a site investigation should be planned. Figure 5-1 outlines the decision process, and the following information is required: (1) design earthquakes and (2) a preliminary soil profile and an estimate of in situ soil conditions.

The site profile may be estimated from standard penetration test results. The simplified hand-computation procedures described in Chapter 3 should be used to define the liquefiable region. For typical soils the soil strength may be estimated from Ferritto and Forrest (1978). The extent of the investigation is controlled by the magnitude of the project; a structure might not justify a large exploration and testing program unless it is of key importance. Generally, a moderate program of standard penetration field tests and cyclic triaxial laboratory tests may cost $10,000 to $15,000 (in 1978 dollars) by the time the samples are collected and data reduced, evaluated, and presented in a usable form, provided the site is easily accessible to a local soils laboratory.

DETAILED ANALYSIS OF VULNERABILITY TO LIQUEFACTION

The methods for predicting the occurrence of liquefaction have been described in Chapter 3. By use of either the simplified hand computation or the more complex computer one-dimensional or two-dimensional method, the number of cycles to cause liquefaction at various depths is determined. The soil information required to accomplish this includes a detailed soil profile of the site with estimates of layer density, shear modulus, and strength. Having established a pore pressure generation parameter in terms of the number of cycles to liquefy (N_L), the pore pressure generation/dissipation equation (see Chapter 4) may be solved by the computer programs APOLLO or GADFLEA resulting in a time history of the bearing capacity of the soil, or approximated by Figures 4-9 and 4-10. Estimates of soil compressibility and permeability are required. The adequacy of support in bearing may now be estimated. Using consolidation analysis and viscous flow, support motions may be estimated. These support motions may be evaluated by a static structural displacement analysis. The structure should have the design dead weight and live load acting on it in conjunction with the displacements. A static

displacement analysis is satisfactory since the occurrence of liquefaction isolates the structure from ground motion and the support displacements are delayed until the liquefaction has time to propagate to the surface.

MINIMIZATION OF DAMAGE

Three basic ingredients are available to reduce the possible damage from liquefaction: (1) site selection, (2) site improvement, and (3) structure design.

Site Selection

As noted in the Alaskan earthquake, located on bedrock suffered least while those on deep fine-grained soils suffered most. The geologic and engineering characteristics of a site should be thoroughly investigated and evaluated. In some cases, geologic and hydrologic factors may dictate a selection that may initially be more expensive than an alternate one on liquefiable soils. However, if repair costs after an earthquake are considered, the overall cost may be less for the more expensive site. Whenever possible, sites should be selected that avoid areas where thick, unconsolidated, young, water-laid, noncohesive sediments occur. Liquefaction requires a high water table; the probability of occurrence can be reduced be selecting an area with a water table below 10 or 20 feet, if possible. Areas where the ground is sloping offer the possibility of horizontal flow if liquefaction occurs. As noted in Chapter 4, slopes of only a few degrees are capable of creating flows of several feet. Sites with sloping ground and topographically low areas should be avoided as much as possible.

Specifically, the propagation of liquefaction must be evaluated. If the region in which liquefaction occurs propagates to the surface from an earthquake, large motions can be expected and the site should not be considered as satisfactory. If the region in which liquefaction occurs is limited and confined to subsurface layers which do not affect the bearing of the foundation, the site may be considered acceptable if regional subsidence is not large.

Sites where calculations for horizontal and vertical movement must be made using viscosity calculations are probably not well-suited for structures since large deformations would be expected.

As shown in Chapter 4, soils with relative densities less than 45% can undergo unlimited flow and should be avoided. Soils with relative densities of 80% or greater will probably have limited displacements if

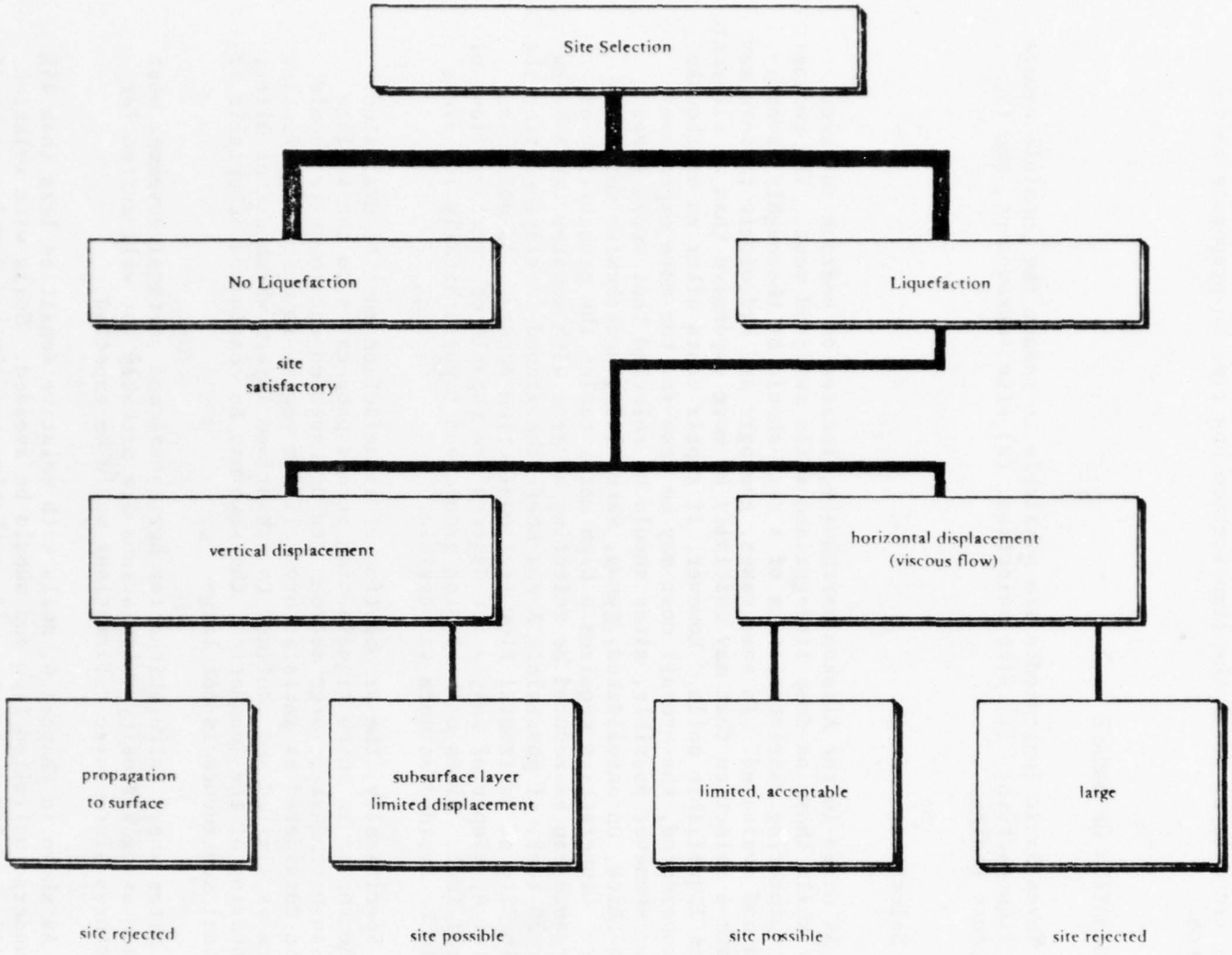

Figure 5-1. Outline of decisions for site selection.

liquefaction occurs. Structures which are sited on these soils must be designed to withstand the displacements expected. Soils with relative densities between 45% and 80% may or may not be suitable sites; therefore, an extensive analysis should be performed to estimate the potential soil strain which might occur.

Site Improvement

It has been noted previously that a high groundwater table contributes markedly to liquefaction potential. Lowering the water table has a twofold effect: first, it lowers the region in which liquefaction can be initiated; second, it increases the effective confining stress on the potentially liquefiable soil zone. From a practical point of view, it may not be economical to permanently lower the water table at a site.

Next to lowering the groundwater table, the most important method of reducing the liquefaction potential is by increasing the relative density of the soil. Densification increases the initial shear strength of the soil; however, as pointed out in Chapter 4, densification may cause a reduction in permeability of the top layer of soil resulting in an unfavorable condition. Increasing the permeability of the near surface soil improves it. Vibroflotation or sand compaction piles both densifies the soil and improves drainage when porous material is used. Thus, these methods should be more effective than other densification methods in which density alone is increased. Increased confinement through use of highly porous surcharges such as coarse backfill are also extremely effective in reducing liquefaction potential.

Structure Design

Both structurally indeterminant and determinant structures can be designed to withstand stresses and displacements without failure. However, the more indeterminant a structure is, the more the stresses in the structure are influenced by support displacement. A typically designed indeterminant structure is limited to significantly less displacement than a corresponding determinant structure. However, loss of the support capacity of a column bent for either structure will probably result in damage of the structure. In general, structures should be designed to be articulated to maintain static determinancy. This is not meant to require expansion joints or other similar devices which have given designers problems in earthquakes; the intent is to make superstructure component stress levels independent of support displacements.

In areas where bedrock is near the surface, caissons to rock provide the most reliable, although probably the most expensive, type of foundation. In regions where liquefaction will occur, vertical piles have

been found to have insufficient lateral stability. When the soil becomes liquefied, the horizontal restraint is lost, and the pile may experience large lateral displacements. This is not surprising considering the long unbraced length of the pile and its load. Thus piles, even though driven into competent material below a potentially liquefiable zone and designed not to rely on friction in the liquefiable zone, may still fail because of excessive horizontal motion or from buckling over its unsupported length.

In the Alaskan earthquake, heavy objects (automobiles, structures, etc.) gradually settled into the quicksand. In several cases, lightweight buried structures floated to the surface. This may be a problem for Navy drydocks, sewage treatment tanks, and similar structures which displace large amounts of soil but have relatively light weight.

Waterfront bulkheads are especially vulnerable to liquefaction of the backfill since they are often backfilled with loose sand. It is difficult to compact the backfill below the water level. The quay walls and bulkheads in dock areas often suffer major damage during earthquakes from the liquefied backfills which exert higher pressures than those for which the walls are designed.

Shallow, low pressure footings might be suited for liquefaction which does not propagate to the surface and cause bearing failure. The engineer must make foundation choice based on the specifics of the site, the types of structure, and loads. In any case, the structure must be designed such that the combination of dead and live load and liquefaction displacement do not result in overstressing at any point.

PROBABILITY OF OCCURRENCE

To evaluate the risk of liquefaction at a site, both the damage from liquefaction and the probability of occurrence must be reviewed together. To accomplish this, the designer should prepare a list of magnitudes of earthquakes from results of liquefaction analyses showing: (1) no liquefaction, (2) liquefaction of subsurface layer without widespread propagation, (3) liquefaction of subsurface layer with propagation to foundation support level, and (4) liquefaction propagating to surface. These levels of liquefaction should then be correlated to the probability that a specific magnitude earthquake occurs. Depending on the method for analysis, uncertainties in acceleration, relative density, and soil strength may be included.

An example of this will be shown. Let us consider a site at a known distance from a fault. The site acceleration and standard deviation may be estimated from Ferritto (1978). The number of earthquake cycles and standard deviation may be estimated from Figure 3-24. The soil's relative density and standard deviation may be determined, as

discussed in Chapters 2 and 3, from laboratory or field tests, and the soil strength and standard deviation, in the absence of actual data, may be estimated from Ferritto and Forrest (1978). Using the simplified calculation procedure, a factor of safety may be determined directly. However, a Monte Carlo simulation can be performed taking the four variables (soil strength, relative density, site acceleration, and number of earthquake cycles) as random, normally distributed values, shaped by their means and standard deviations.

Consider the following case where the distance to the fault is 40 miles; then the ground motion for various magnitude earthquakes is given in Table 5-2.

Assume a case where the relative density is 0.60 with standard deviation of 0.06 and the soil strength as indicated in Figure 3-7; then, by using simple Monte Carlo simulation (see Appendix), the probability of liquefaction may be determined as a function of earthquake magnitude, as shown in Table 5-3. The probability of an earthquake occurring and causing liquefaction may be estimated by use of recurrence data for a fault (usually expressed as a number of events per year for magnitude greater than or equal to M). The recurrence data are used to determine the number of events expected between a magnitude increment, M_i to $M_i + 1$. The expected number of earthquake events per year is multiplied by the number of years for the life of the structure and by the average probability of liquefaction occurring for the magnitude range M_i to $M_i + 1$ to yield the expected number of earthquakes causing liquefactions for the fault, time period and magnitude increment. The expected number of earthquakes causing liquefaction, λ, is used to compute the probability of an earthquake occurring and causing liquefaction by a Poisson's distribution

$$P_{LE} = 1 - e^{-\lambda}$$

Assuming the fault to be a typical fault system in California with specific recurrence intervals (number of earthquakes per year), the probability of an earthquake occurring and causing liquefaction is shown in Table 5-4.

For this example the highest probability of liquefaction in the 50-year span is 0.046 from a magnitude 8 earthquake. The most probable earthquake causing liquefaction may occur at any magnitude and is a function of fault activity and site conditions. The consequences and extent of liquefaction for the most probable magnitude earthquake should be determined. (Although the consequences from other magnitude earthquakes will be greater, the probability is lower.) Thus, levels of damage and extent of propagation of liquefaction can be determined as a function of magnitude and probability of occurrence.

Table 5-2. Ground Motion

Earthquake Magnitude	Number of Cycles	Number of Cycles Standard Deviation	Acceleration (g)	Acceleration Standard Deviation (g)
5.0	3.67	3.64	0.005	0.0056
5.5	4.86	3.92	0.0143	0.0146
6.0	6.43	4.11	0.0303	0.0309
6.5	8.51	4.14	0.0516	0.0527
7.0	11.27	5.81	0.0711	0.0725
7.5	14.92	8.19	0.0790	0.0806
8.0	19.76	11.52	0.0790	0.0806

Table 5-3. Probability of Liquefaction

Earthquake Magnitude, M	Probability of Liquefaction, $P_L(M)$	Median Factor of Safety
5.0	0.000	>10
5.5	0.000	>10
6.0	0.007	5.38
6.5	0.047	3.06
7.0	0.097	2.22
7.5	0.165	1.81
8.0	0.218	1.67

Table 5-4. Probability of Earthquake Causing Liquefaction

Magnitude	Recurrence Interval, U(M)[a]	Number of Events/Yr, U(M)	Expected Events 50 Years	P_L	Expected Events Causing Liquefaction	P_{LE}
5.0	0.26	0.13	6.5	0	0	0
5.5	0.13	0.063	3.15	0	0	0
6.0	0.067	0.033	1.65	0.007	0.01155	0.011
6.5	0.034	0.017	0.85	0.047	0.03995	0.039
7.0	0.017	0.0076	0.38	0.097	0.03686	0.036
7.5	0.0094	0.0050	0.25	0.165	0.04125	0.040
8.0	0.0044	0.0044	0.22	0.218	0.04796	0.046

[a] Number of events per year $\geq$M and assumed that t = 50 years.

The overall risk to a structure may be determined based on the probability of occurrence of liquefaction and the consequences should it occur. It is also obvious that the uncertainty associated with the ability to predict earthquake motion and to determine site properties results in some probability of liquefaction even though the median factor of safety is greater than 1.0. Thus, a degree of conservatism must be exercised until more accurate site definition and earthquake-motion data become available.

Using the Monte Carlo simulation technique, graphs may be developed which show the factor of safety and probability of liquefaction as a function of earthquake magnitude, distance from the fault, and relative density of the soil at the site (Figures 5-2 through 5-6). The groundwater table is assumed to be at a depth of 5 feet and the occurrence of liquefaction at a depth of 20 feet. Figure 5-2 shows the factor of safety for various confidence limits.

CRITERIA FOR SITES

The criteria for selection of sites should be based on earthquakes with the following magnitudes:

M_A = recurrence, once in 10 years

M_B = recurrence, once in 25 years

M_C = recurrence, once in 50 years, or design level earthquake

M_D = recurrence, once in 200 years, or the maximum credible earthquake

Under the proposed criteria the site is considered acceptable if the mean-minus-one-standard-deviation factor of safety $FS_{m-\sigma}$ (84% confidence limit) and the probability of an earthquake causing liquefaction P_{LE} are as shown in Table 5-5. Note that the probability includes the occurrence of an earthquake and is not simply the probability of liquefaction.

It should be noted that in the proposed criteria liquefaction is allowed to occur for the M_D earthquake (maximum credible earthquake) as long as it remains confined to subsurface layers, does not cause bearing failures, or produce unacceptable horizontal and vertical displacements. Since the displacements would be limited, acceptable levels of damage would be imposed on the structures, and collapse would not occur.

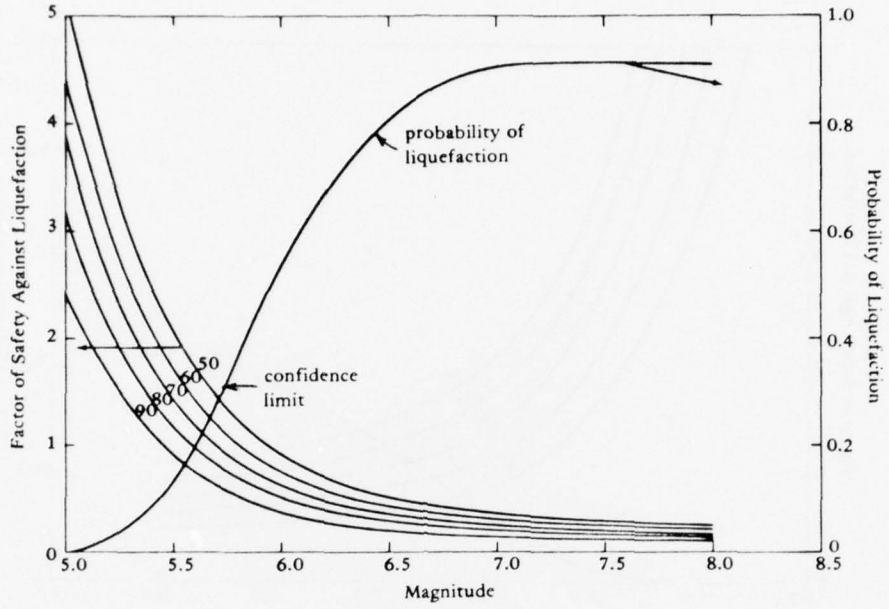

(a) Distance to fault - 20 miles.

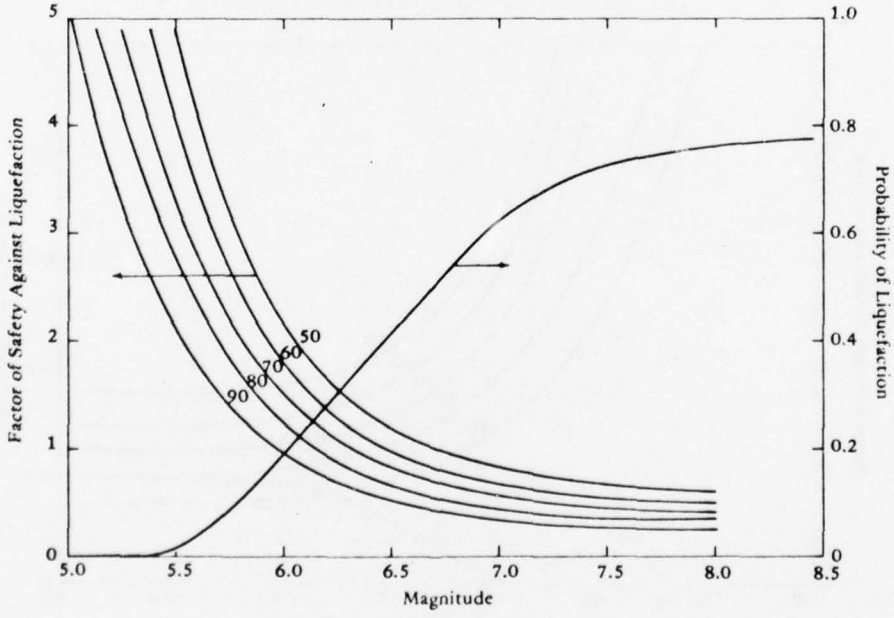

(b) Distance to fault - 30 miles.

Figure 5-2. Factor of safety for various confidence limits and probability of liquefaction at relative density of 0.4.

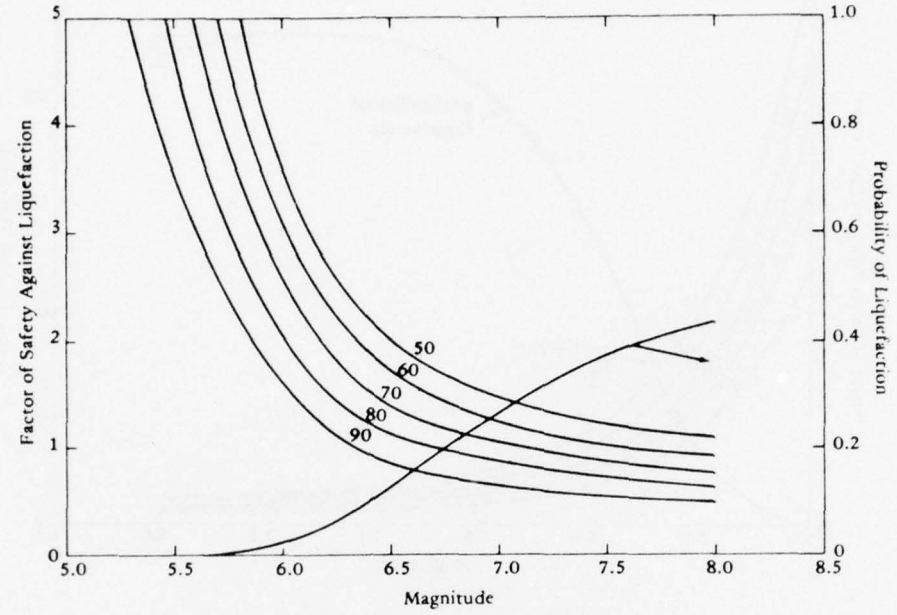

(c) Distance to fault - 40 miles.

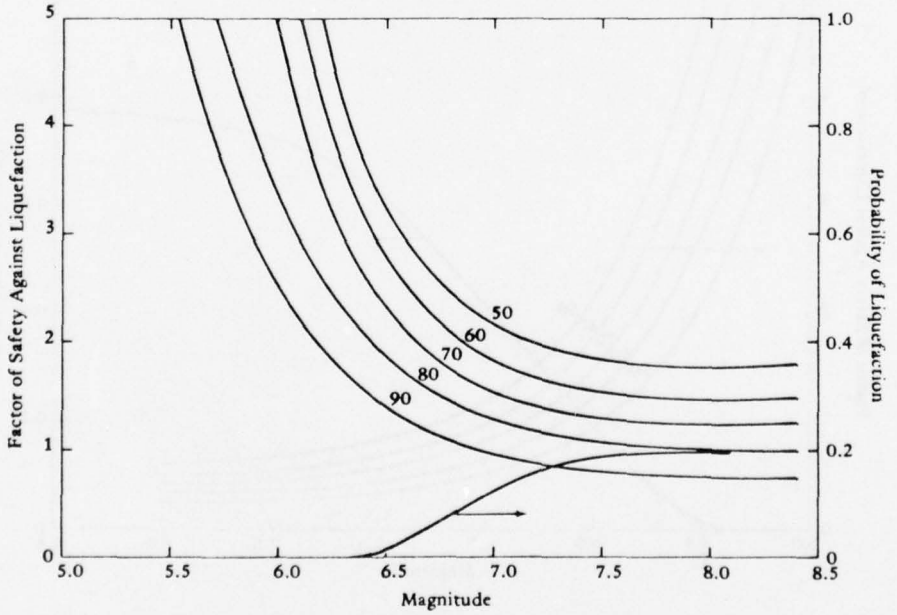

(d) Distance to fault - 50 miles.

Figure 5-2. Continued

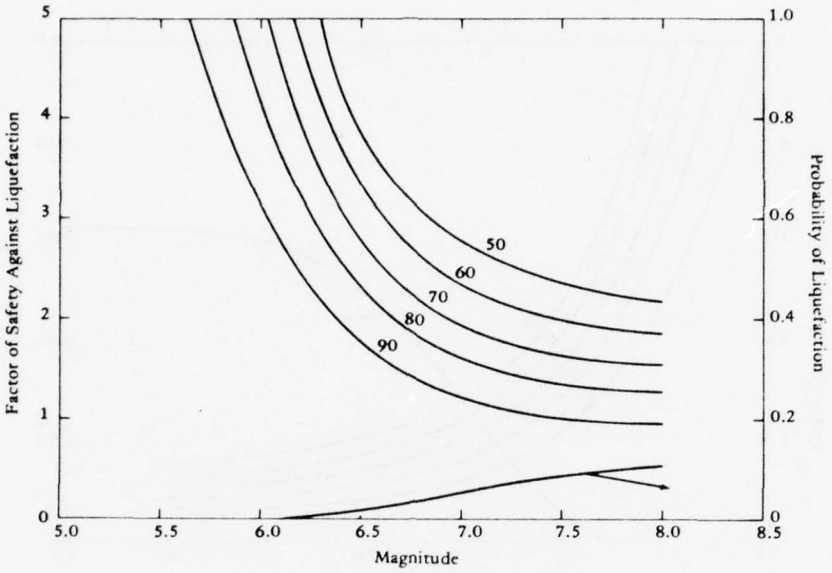

(e) Distance to fault - 60 miles.

Figure 5-2. Continued

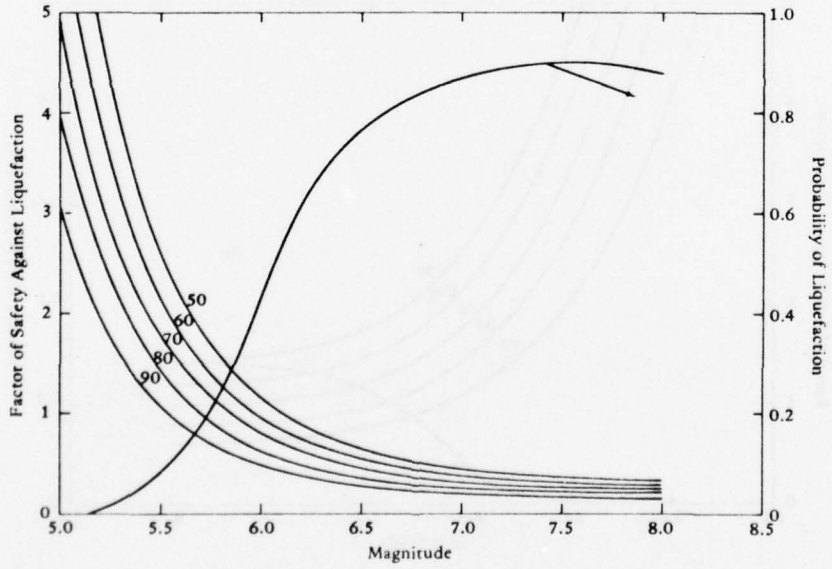

(a) Distance to fault - 20 miles.

Figure 5-3. Factor of safety for various confidence limits and probability of liquefaction at relative density of 0.5.

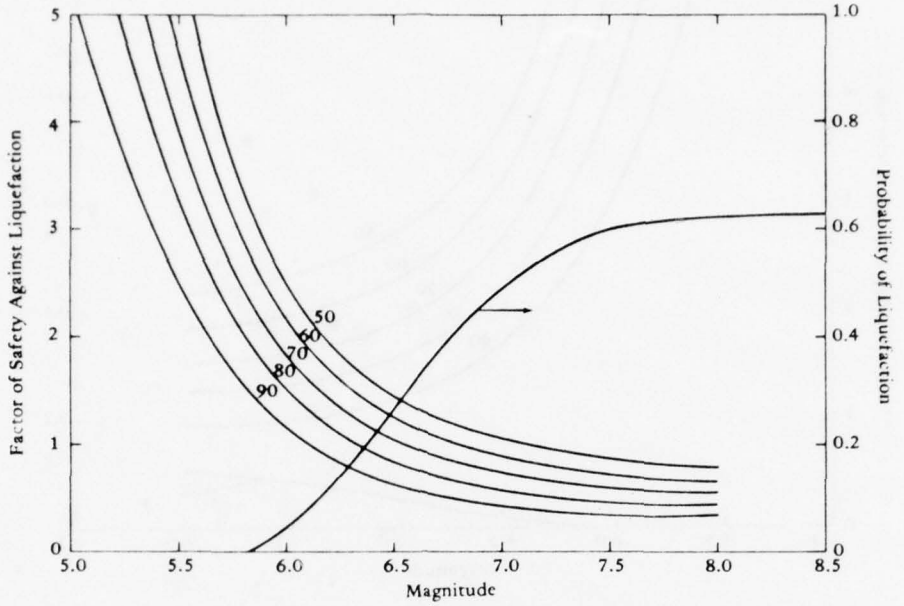

(b) Distance to fault - 30 miles.

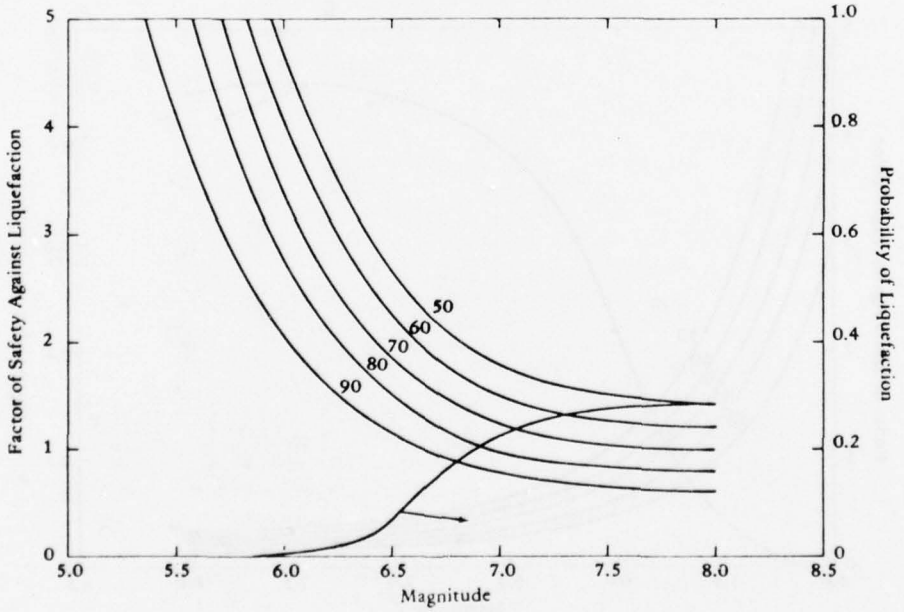

(c) Distance to fault - 40 miles.

Figure 5-3. Continued

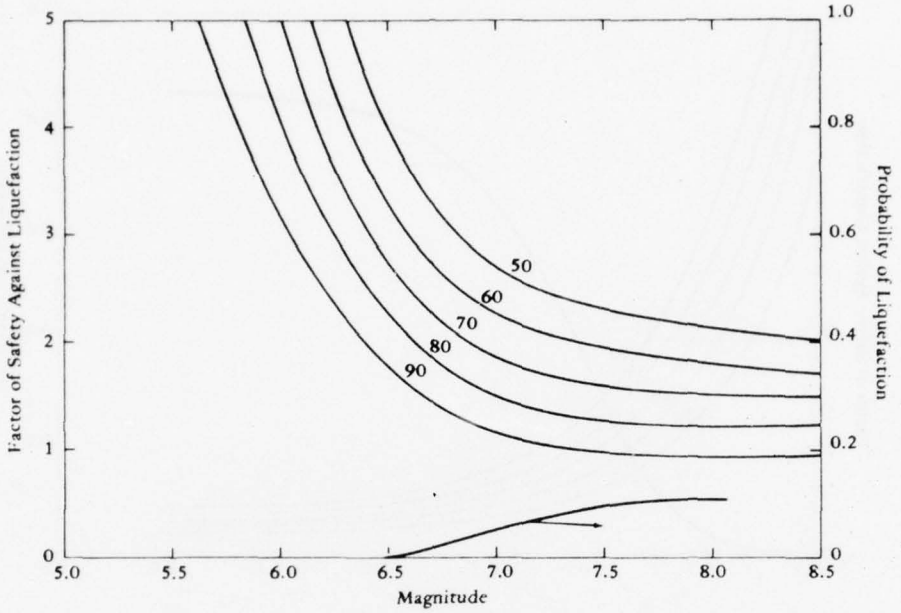

(d) Distance to fault - 50 miles.

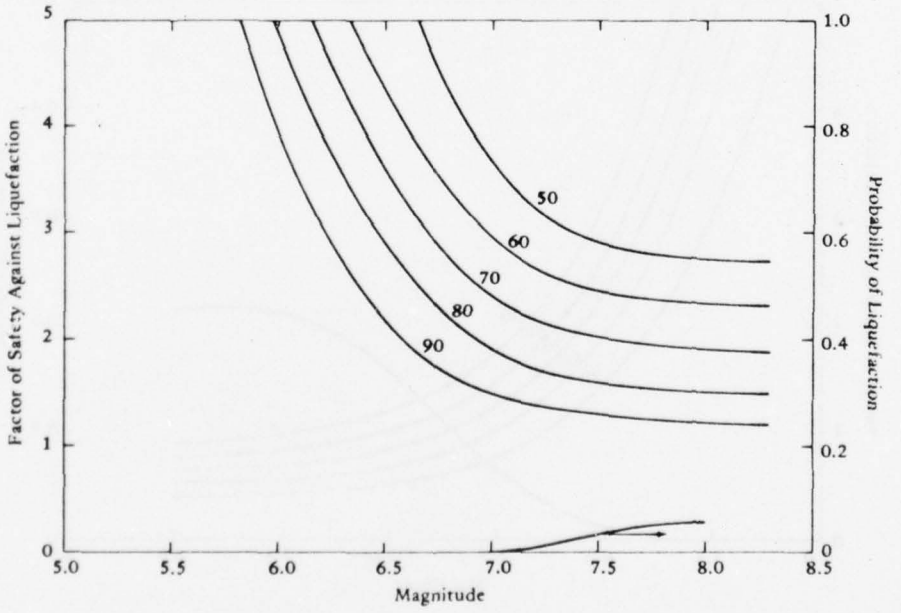

(e) Distance to fault - 60 miles.

Figure 5-3. Continued

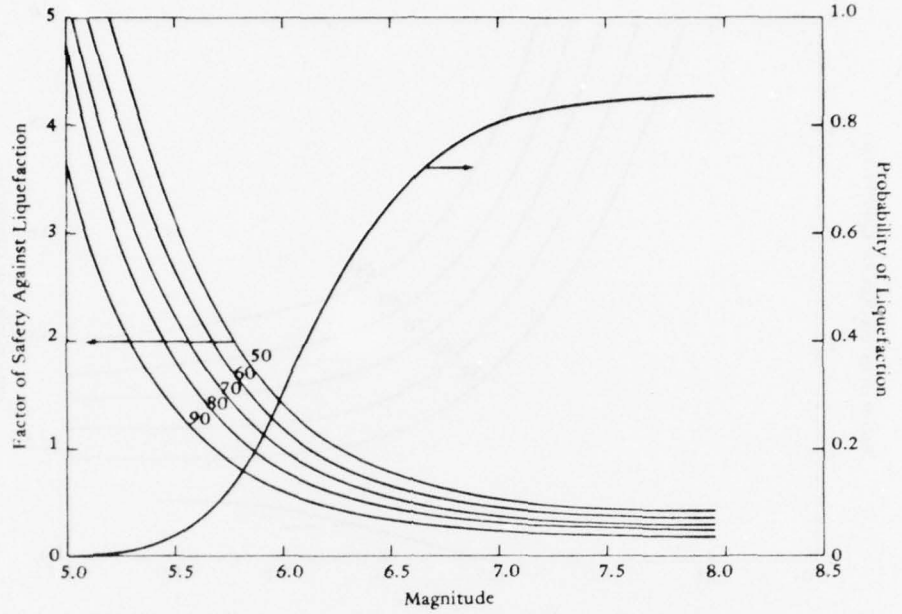

(a) Distance to fault - 20 miles.

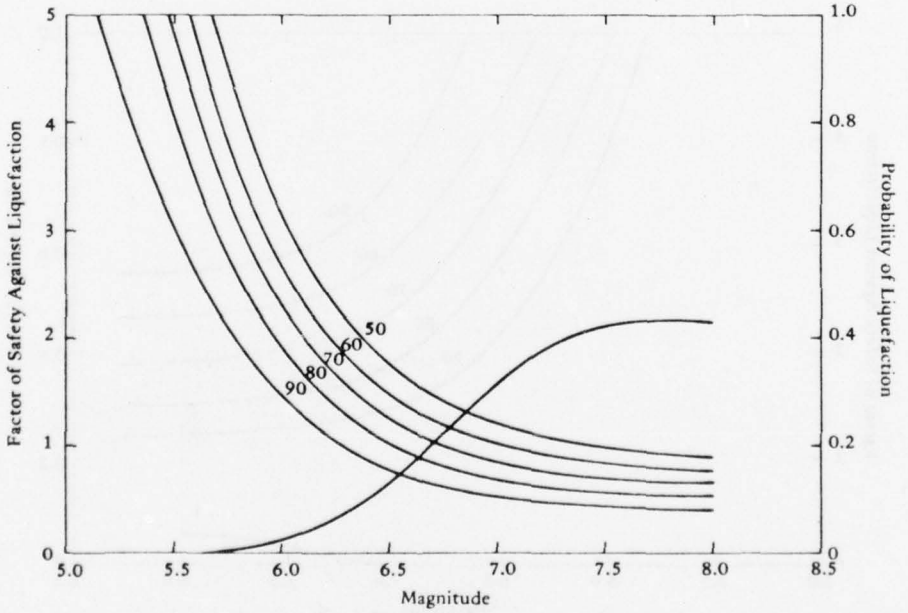

(b) Distance to fault - 30 miles.

Figure 5-4. Factor of safety for various confidence limits and probability of liquefaction at relative density of 0.6.

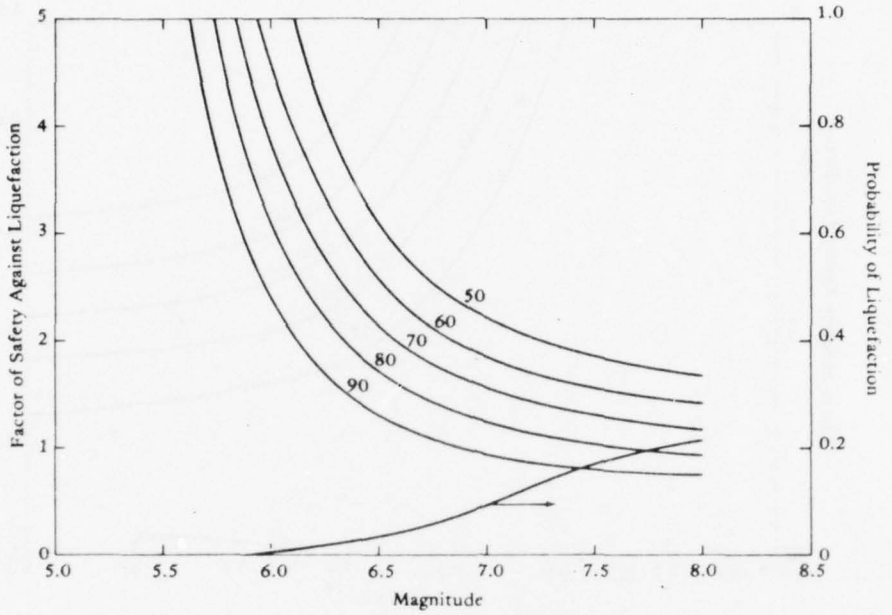

(c) Distance to fault - 40 miles.

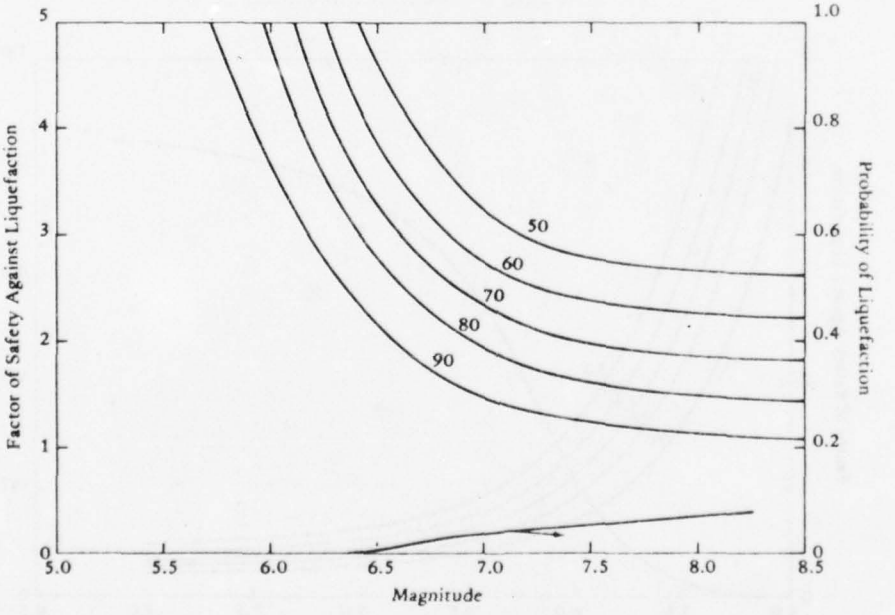

(d) Distance to fault - 50 miles.

Figure 5-4. Continued

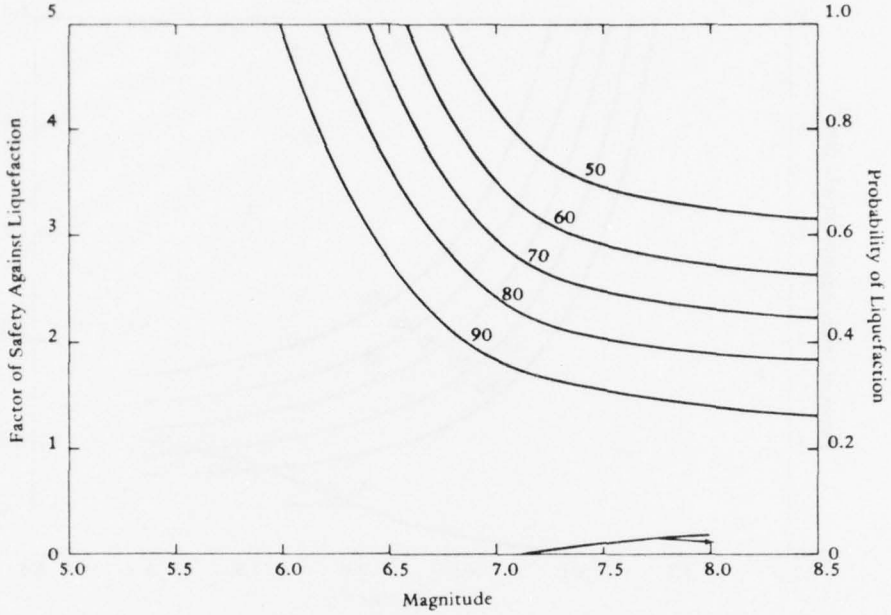

(e) Distance to fault - 60 miles.

Figure 5-4. Continued

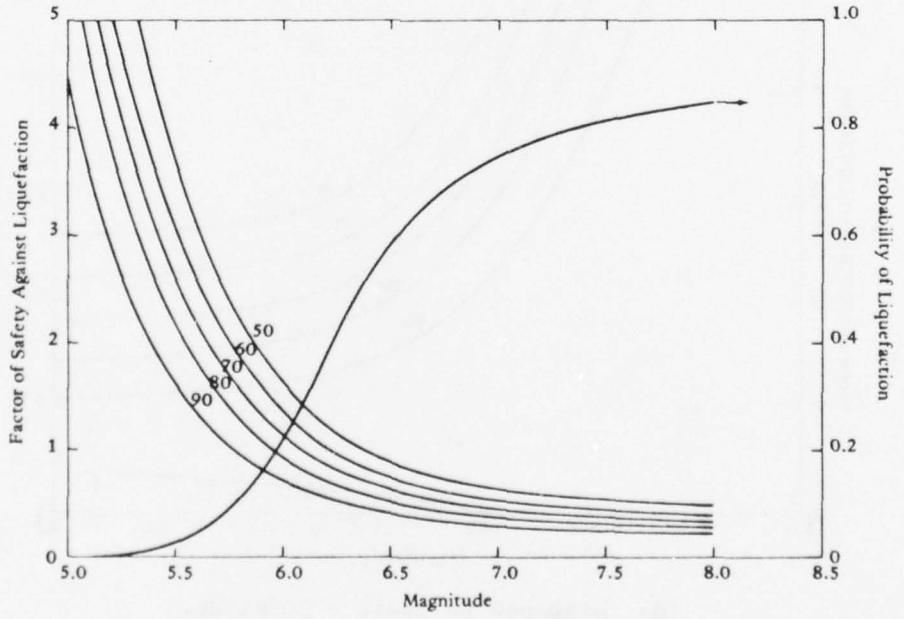

(a) Distance to fault - 20 miles.

Figure 5-5. Factor of safety for various confidence limits and probability of liquefaction at relative density of 0.7.

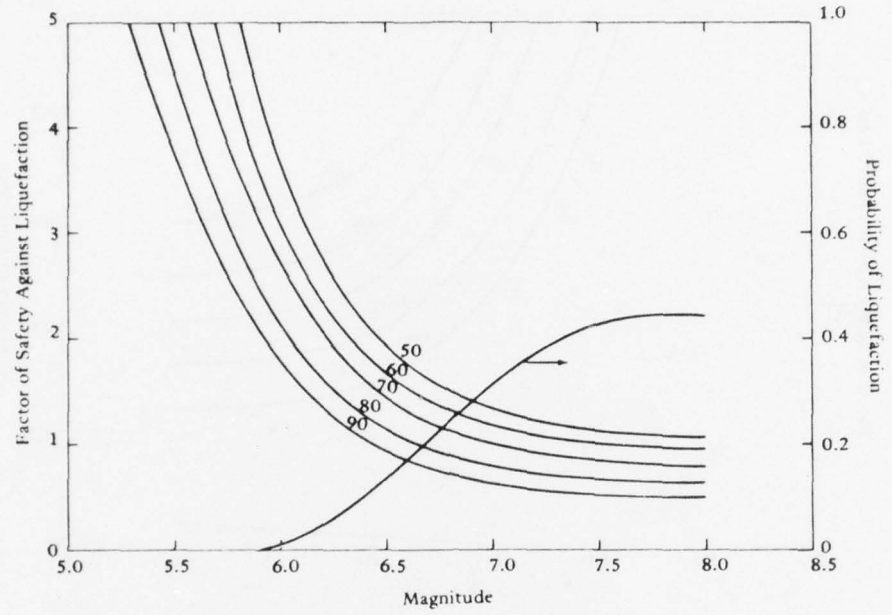

(b) Distance to fault - 30 miles.

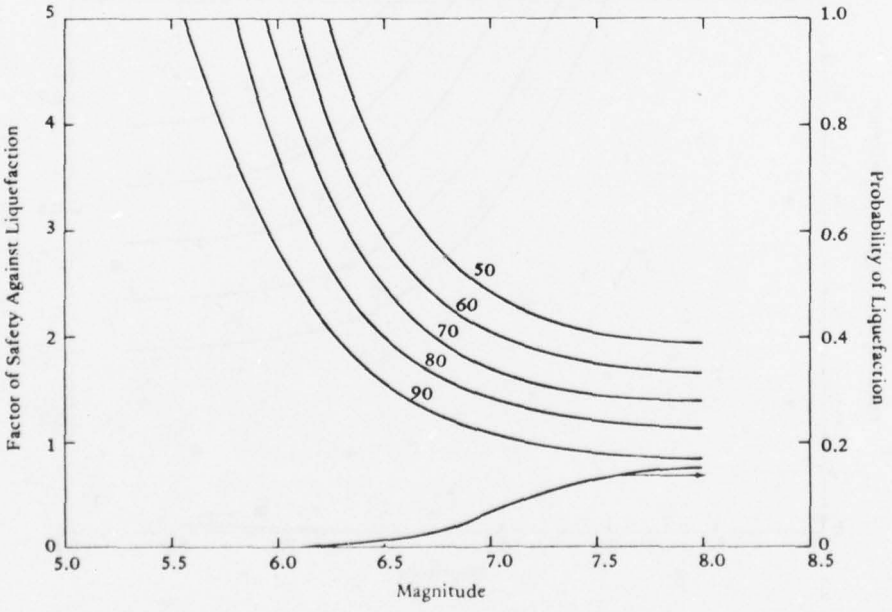

(c) Distance to fault - 40 miles.

Figure 5-5. Continued

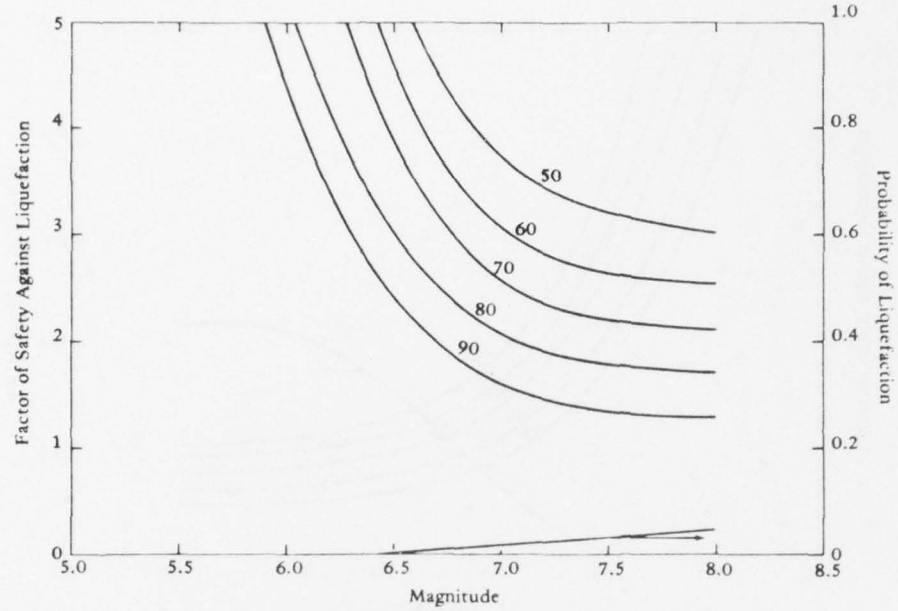

(d) Distance to fault - 50 miles.

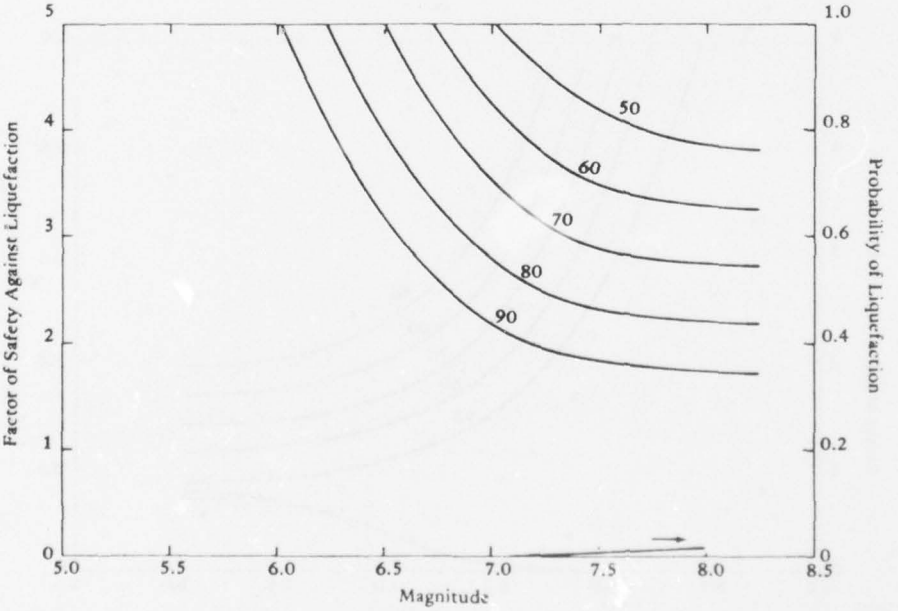

(e) Distance to fault - 60 miles.

Figure 5-5. Continued

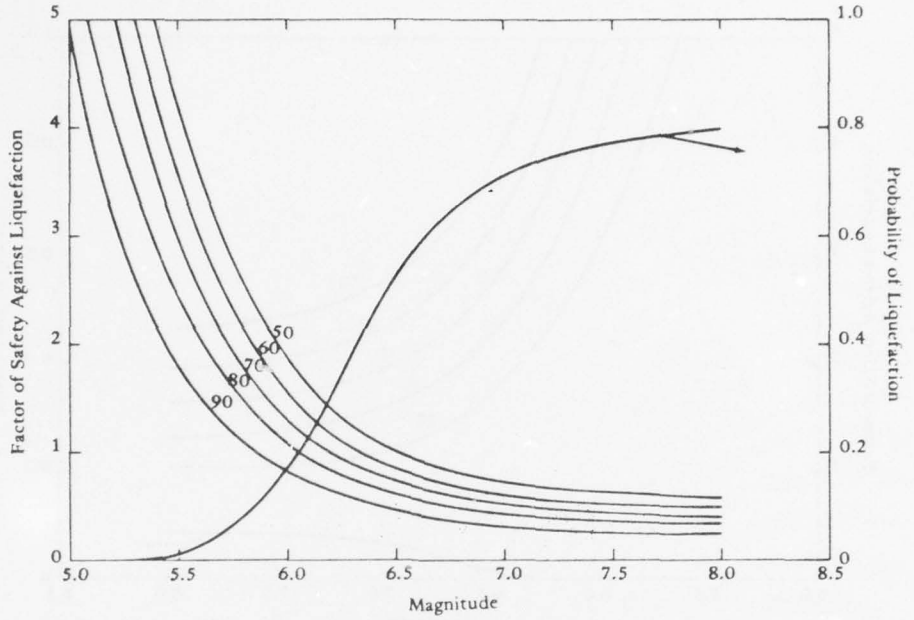

(a) Distance to fault - 20 miles.

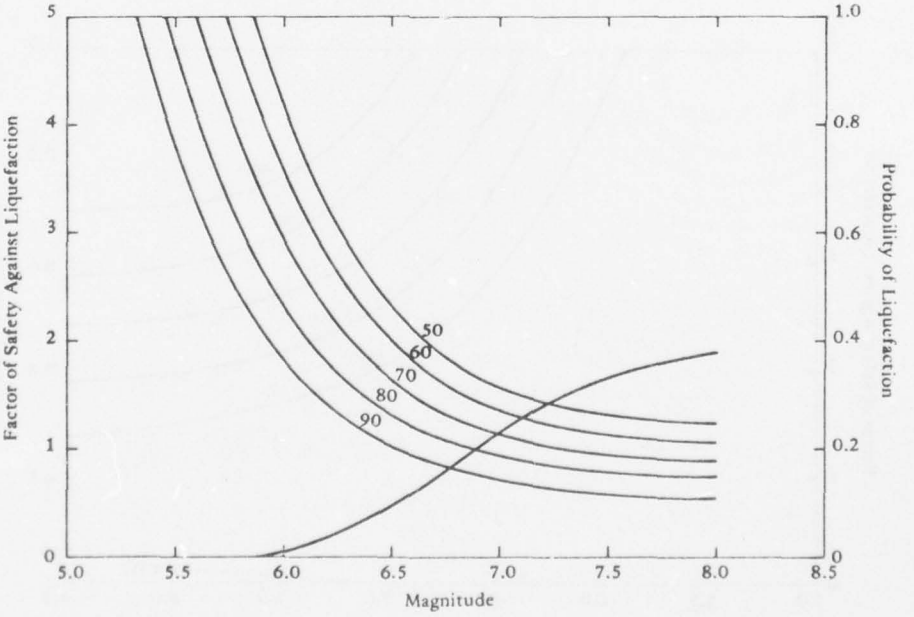

(b) Distance to fault - 30 miles.

Figure 5-6. Factor of safety for various confidence limits and probability of liquefaction at relative density of 0.8.

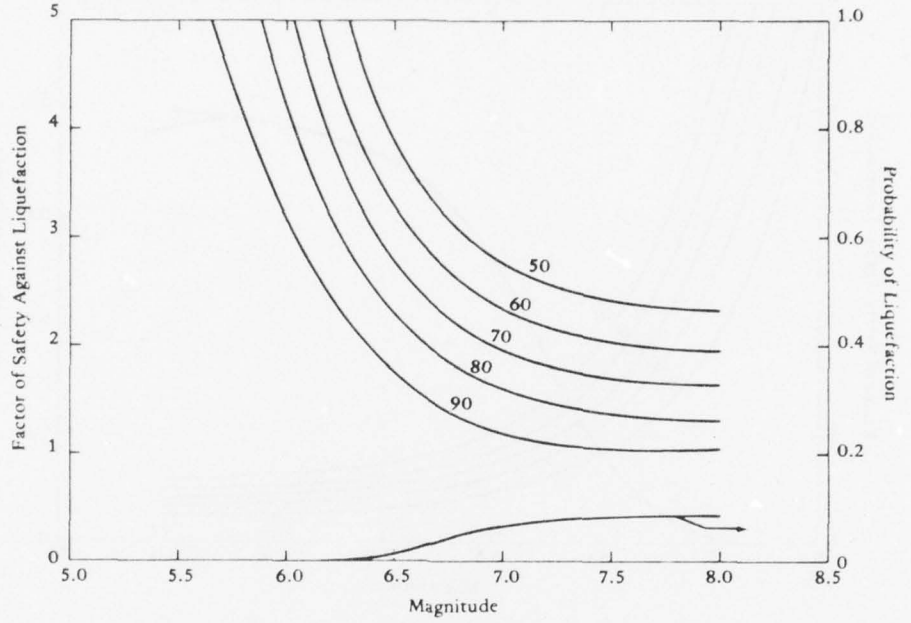

(c) Distance to fault - 40 miles.

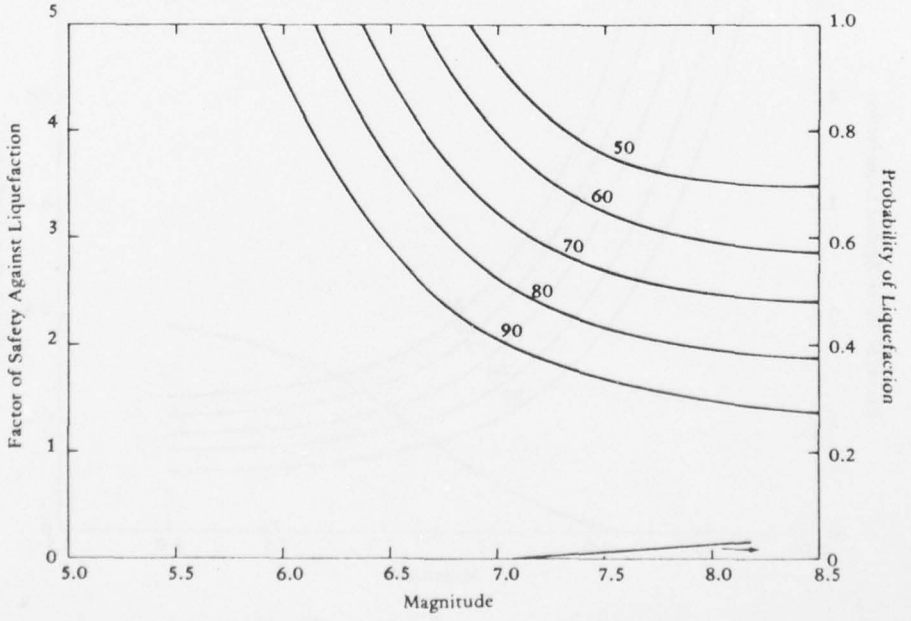

(d) Distance to fault - 50 miles.

Figure 5-6. Continued

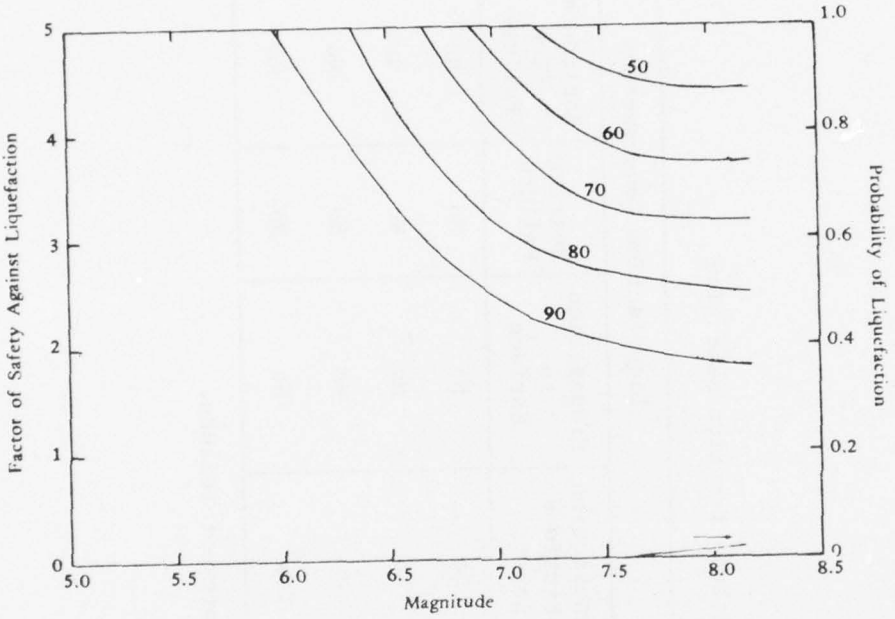

(e) Distance to fault - 60 miles.

Figure 5-6. Continued

Table 5-5. Criteria for Site Selection

Earthquake	Factor of Safety, $FS_{m-\sigma}$	Liquefaction Probability, P_{LE}	Liquefaction Consequences				
			Liquefaction Subsurface Layer	Propagation to Surface	Bearing Failure	Horizontal Flow Failure	Vertical Settlement Failure
M_A	≥ 1.5	≤ 0.1	No	No	No	No	No
M_B	≥ 1.3	≤ 0.1	No	No	No	No	No
M_C	≥ 1.1	≤ 0.1	No	No	No	No	No
M_D	—	—	Yes[a]	No	No	No	No

[a] Upper region pore pressure limited to prevent failure.

In the proposed siting criteria, the acceptability of a site depends on whether the value of the probability of a design level earthquake causing liquefaction is ≤ 0.10. This value is based solely on engineering judgment. By comparison, the Naval Facilities Engineering Command, as a basis for structural design, uses an earthquake with a probability of occurring, or being exceeded, of 0.1 in 25 years (the approximate design life of typical Naval structures). The criterion proposed here is somewhat more conservative in that it suggests use of 50 years. Further, the occurrence of liquefaction does not always result in collapse of the structure. It is very difficult to quantify the dollar value of a functioning structure. The value of human life has always been of highest importance in the United States. Engineers are often faced with problems asking, "How safe is safe enough?" An economic analysis may be of use in comparing alternatives to produce the best return.

In the proposed criteria it should be pointed out that the total probability of liquefaction is the sum of the individual probabilities of liquefaction for a given magnitude earthquake, P_{LE}, taken over all the magnitudes. However, this value is misleading since the consequences if liquefaction were to occur would be very different from a brief period of liquefaction caused by a magnitude 5 earthquake than from a prolonged period with a magnitude 8 earthquake. The criterion attempts to limit overall exposure by limiting the function at several selected points representing a design earthquake. Note the dual criteria of factor of safety and probability. Table 5-5 is intended to present a procedure whose numerical values can only be determined from experience. The numbers used in the table are intended to represent the approximate level of conservatism which is compatible with present engineering practice and should not result in major construction cost increases.

If the earthquake motions are specified at the ground surface, then the stresses developed in, say, the upper 40 feet of a soil deposit can be assessed. The preceding pages have discussed at length the procedures required to make a good assessment of the stresses required to cause initial liquefaction or a given degree of strain. The final acceptable factor of safety will clearly depend on the accuracy with which each of these individual assessments can be made in any given case.

A further consideration which must be taken into account in determining what value constitutes an acceptable factor of safety is the consequences arising, if for some reason the actual factor of safety should be reduced to unity. Clearly, this is very different in the case of a loose sand with a relative density of about 54% as opposed to the same sand in a dense condition, say with a relative density of 82%. Seed (1976) reports in his studies that the limiting strain for Monterey No. 0 sand at 54% relative density is $\pm 30\%$, while the limiting strain for the same sand at 82% relative density is only $\pm 10\%$. The stress

conditions producing these conditions are shown graphically in Figure 5-7. Seed (1976) shows that if the stress ratio causing 5% strain at a relative density of 54% is even slightly exceeded, then the sand will undergo strains up to ±30% with almost certain catastrophic consequences. However, if the stress ratio causing 5% strain at a relative density of 82% is slightly exceeded, the only result would be to cause a strain of perhaps 6%, and no more than 10%, even if the factor of safety should drop to 0.5 or even lower.

DISCUSSION

This report is intended to provide guidance to an engineer with a problem of siting a structure in an area where potentially liquefiable soils exist. The range of methods for predicting the occurrence of liquefaction has been given. The choice of a method is a function of the available information and size of the study. Methods were given to estimate soil displacement. Although these are admittedly crude, some means of determining the consequences of liquefaction must be used. It is in this area that existing knowledge is most limited and to which future research should be directed.

REFERENCES, CHAPTER 5

Casagrande, A. (1965) "The role of the calculated risk in earthwork and foundation engineering," Journal of Soil Mechanics and Foundations Division, ASCE, vol 91, no. SM4, Jul 1965.

Ferritto, J. M. (1978) "A Probabilistic Procedure for Estimating Seismic Loading Based On Historic and Geologic Data." Civil Engineering Laboratory, Port Hueneme, Calif. (in publication).

Ferritto, J. M. and Forrest, J. B. (1977) FHWA-RD-77-127, Determination of seismically induced soil liquefaction potential at proposed bridge sites, Department of Transportation. Washington, D.C., Aug 1977.

Seed, H. B. (1976) "Evaluation of soil liquefaction effects on level ground during earthquakes," ASCE Preprint 2752 (Liquefaction Problems in Geotechnical Engineering), American Society of Civil Engineers Annual Convention, Philadelphia, Pa., 27 Sep-1 Oct 1976.

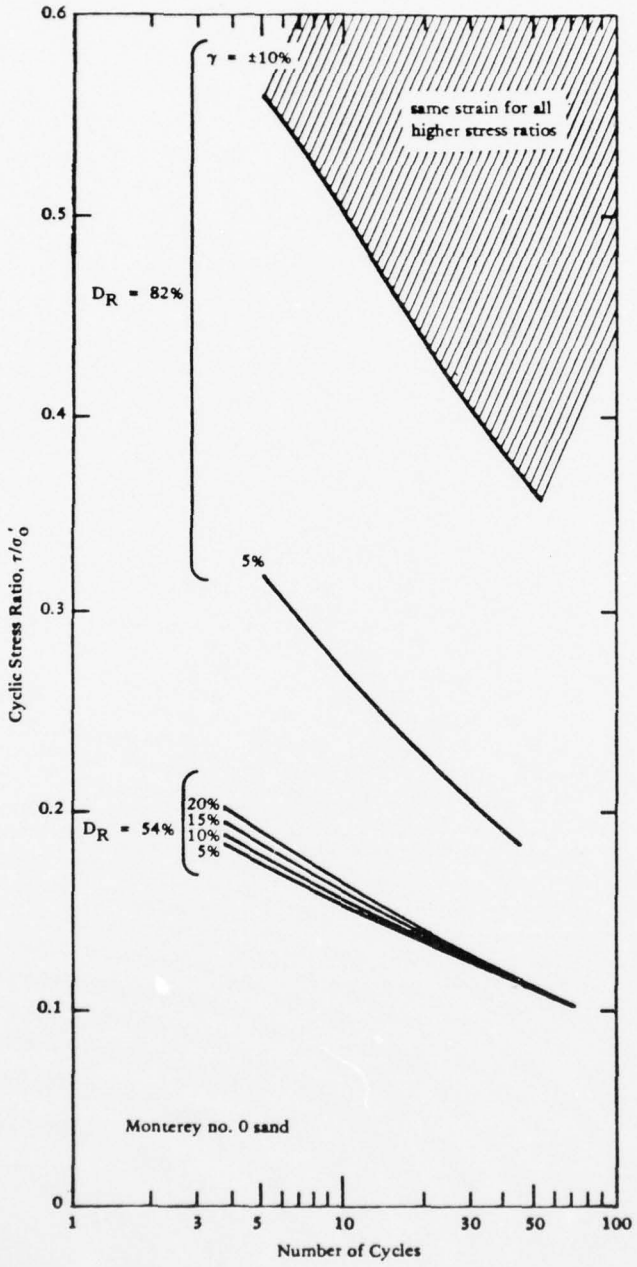

Figure 5-7. Relationship between τ/σ_o' and number of cycles causing different strain levels (from H. B. Seed, I. Arango, and C. K. Chan, 1975).

Appendix

MONTE CARLO SIMULATION

COMPUTATION PROCEDURE

This section will describe the Monte Carlo methodology developed to compute the probability of liquefaction of a soil profile composed of a series of horizontal layers. The methodology has been programmed on a computer and is most easily explained in terms of the computational steps in the program. The computer program is composed of a main program and eight subroutines. The basic input information consists of the magnitude of the earthquake under consideration, the horizontal distance of the closest point on the associated fault to the site, the number of soil layers in the profile, the material properties of each layer and location of the water table. The material properties consist of the total and effective unit weights of the layer, the layer thickness, and the layer relative density.

The main program calls the Subroutine ACC which computes the site acceleration and its standard deviation using a ground motion attenuation relationship and the input magnitude and site distance. The specific relationship used is that developed by Trifunac and Brady (1975) although any other could have been used. The main program calls Subroutine CYC, which computes the number of equivalent uniform cycles and its standard deviation using a relationship based on data by Seed, et al. (1975) and the magnitude of the earthquake. The main program computes the total and effective stress for each layer of the profile using the unit weight input for each layer. Having developed all the above preliminary information the main program calls the Subroutine PRLIQ where the Monte Carlo process is carried out.

Subroutine PRLIQ essentially consists of a looping sequence in which specific values of each of the four variables (acceleration, number cycles, relative density, soil strength) are selected and combined to compute a specific factor of safety against liquefaction. The Subroutine RFU is called for each variable; this subroutine returns a random, normally distributed variable using the direct method for generation of normally distributed numbers. Subroutine TTS is called by Subroutine

PRLIQ; this subroutine computes the soil stress ratio and its standard deviation using a generalized expression for soil strength based on data and the specific value of the number of cycles of excitation. A random normal distribution value for stress ratio is then determined.

Having the specific values for acceleration, number of cycles, relative density and soil stress ratio the factor of safety is computed by the method developed by Seed and Idriss (1970). The factor of safety is computed for each iteration; although each variable has been obtained from a normal distribution the resulting distribution for the factor of safety is not a normal distribution. The process is repeated 1,000 times. Subroutine SORT is called to sort the array consistng of factor of safety values. The last is evaluated and the number of values less than 1.0 forms the basis for computation of probability of liquefaction. The array of factor of safety values is plotted as a histogram to show its distribution. This program has been used with Program APOLLO described in Chapter 4 to compute pore pressure histories in each layer.

USER'S GUIDE

The program is intended as a first approximation for evaluation of sites using standard penetration data. As such, triaxial test data would not be available (such as for routine structures) and data is based on a report by Ferritto and Forrest (1977).

User's Guide

Card 1 Format 2F10.2
- Magnitude
- Distance, miles

Card 2 Format I10
- Number layers

Card 3 Format 8F10.2
- One card for each layer
- Layer number
- Effective Unit Weight, lb/ft^3
- Total Unit Weight, lb/ft^3
- Layer thickness, ft
- Relative density, . xx .
- Standard deviation relative density, . xx .

REFERENCES

Ferritto, J. M. and Forrest, J. B. (1977) FHWA-RD-77-127, "A compilation and analysis of cyclic triaxial test data," Department of Transportation. Washington, D.C., Aug 1977.

Seed, H. B. and Idriss, I. M. (1970) "A simplified procedure for evaluating soil liquefaction potential," University of California, Earthquake Engineering Research Center, EERC Report No. 70-9. Berkeley, Calif., Nov 1970.

Seed, H. B., Idriss, I. M., Makdisi, F., and Baneyee, N. (1975) "Representation of irregular stress time histories by equivalent uniform stress series in liquefaction analysis," University of California, Earthquake Engineering Research Center, EERC Report No. 75-29. Berkeley, Calif., Oct 1975.

Trifunac, M. D. and Brady, A. G. (1975) "On the correlation of peak acceleration of strong motion with earthquake magnitude epicentral distance and site condition," in Proceedings of the U.S. National Conference of Earthquake Engineering, Ann Arbor, Mich, Jun 1975. Earthquake Engineering Research Institute, Oakland, Calif., 1975.

DISTRIBUTION LIST

AF HQ Prees Washington DC (R P Reid)
AFB AFCEC/XR,Tyndall FL; CESCH, Wright-Patterson; MAC/DET (Col. P. Thompson) Scott, IL; SAMSO/MNNF, Norton AFB CA; Stinfo Library, Offutt NE
ARCTICSUBLAB Code 54T, San Diego, CA
ARMY BMDSC-RE (H. McClellan) Huntsville AL; DAEN-MCE-D Washington DC; Tech. Ref. Div., Fort Huachuca, AZ
ARMY COASTAL ENGR RSCH CEN Fort Belvoir VA; R. Jachowski, Fort Belvoir VA
ARMY CORPS OF ENGINEERS MRD-Eng. Div., Omaha NE; Seattle Dist. Library, Seattle WA
ARMY ENG DIV HNDED-CS, Huntsville AL; Hnded-Sr, Huntsville, AL
ARMY ENG WATERWAYS EXP STA Library, Vicksburg MS
ARMY ENGR DIST, Library, Portland OR
ARMY ENVIRON, HYGIENE AGCY Water Qual Div (Doner), Aberdeen Prov Ground, MD
ARMY MATERIALS & MECHANICS RESEARCH CENTER Dr. Lenoe, Watertown MA
ARMY MOBIL EQUIP R&D COM Mr. Cevasco, Fort Belvoir MD
ASST SECRETARY OF THE NAVY Spec. Assist Energy (P. Waterman), Washington DC
CINCLANT Civil Engr. Supp. Plans, Ofr Norfolk, VA
CNM NMAT 08T246 (Dieterle) Wash, DC
CNO Code NOP-964, Washington DC; OP987J (J. Boosman), Pentagon
COMOCEANSYSPAC SCE, Pearl Harbor HI
DEFENSE DOCUMENTATION CTR Alexandria, VA
DEFENSE INTELLIGENCE AGENCY Dir., Washington DC
DNA STTL, Washington DC
DOD Explosives Safety Board (Library), Washington DC
FLTCOMBATTRACENLANT PWO, Virginia Bch VA
HEDSUPPACT PWO, Taipei, Taiwan
MARINE CORPS BASE M & R Division, Camp Lejeune NC; PWO, Camp S. D. Butler, Kawasaki Japan
MARINE CORPS DIST 9, Code 043, Overland Park KS
MARINE CORPS HQS Code LFF-2, Washington DC
MCAS Facil. Engr. Div. Cherry Point NC; Code PWE, Kaneohe Bay HI; Code S4, Quantico VA; J. Taylor, Iwakuni Japan; PWO Kaneohe Bay HI
MCDEC P&S Div Quantico VA
MCLSBPAC B520, Barstow CA
MCRD PWO, San Diego Ca
NAD Engr. Dir. Hawthorne, NV
NAF PWO Sigonella Sicily; PWO, Atsugi Japan
NAS CO, Guantanamo Bay Cuba; Code 114, Alameda CA; Code 183 (Fac. Plan BR MGR); Code 187, Jacksonville FL; Code 18700, Brunswick ME; Code 70, Atlanta, Marietta GA; Dir. Util. Div., Bermuda; ENS Buchholz, Pensacola, FL; Lead. Chief. Petty Offr. PW/Self Help Div, Beeville TX; PW (J. Maguire), Corpus Christi TX; PWD Maint. Div., New Orleans, Belle Chasse LA; PWD, Willow Grove PA; PWO (M. Elliott), Los Alamitos CA; PWO Belle Chasse, LA; PWO Chase Field Beeville, TX; PWO Key West FL; PWO, Dallas TX; PWO, Glenview IL; SCE Lant Fleet Norfolk, VA; SCE Norfolk, VA; SCE, Barbers Point HI
NATL RESEARCH COUNCIL Naval Studies Board, Washington DC
NATPARACHUTETESTRAN PW Engr, El Centro CA
NAVACT PWO, London UK
NAVAEROSPREGMEDCEN SCE, Pensacola FL
NAVAL FACILITY PWO, Barbados; PWO, Brawdy Wales UK; PWO, Cape Hatteras, Buxton NC
NAVCOASTSYSLAB Code 423 (D. Good), Panama City FL; Library Panama City, FL
NAVCOMMAREAMSTRSTA PWO, Norfolk VA; PWO, Wahiawa HI; SCE Unit 1 Naples Italy
NAVCOMMSTA Code 401 Nea Makri, Greece; PWO, Adak AK; PWO, Exmouth, Australia
NAVEDTRAPRODEVCEN Tech. Library
NAVEDUTRACEN Engr Dept (Code 42) Newport, RI
NAVFACENGCOM Code 043 Alexandria, VA; Code 044 Alexandria, VA; Code 0451 Alexandria, VA; Code 0453 (D. Potter) Alexandria, VA; Code 0454B Alexandria, Va; Code 04B5 Alexandria, VA; Code 101 Alexandria, VA; Code 10133 (J. Leimanis) Alexandria, VA; Code 1023 (T. Stevens) Alexandria, VA; Code 2014 (Mr. Taam), Pearl Harbor HI; Morrison Yap, Caroline Is.; P W Brewer Alexandria, VA; PC-22 (E. Spencer) Alexandria, VA

NAVFACENGCOM - CHES DIV, Code 101 Wash, DC; Code 405 Wash, DC; Code FPO-1 (C. Bodey) Wash, DC; Code FPO-1 (Ottsen) Wash, DC; Code FPO-1SP (Dr. Lewis) Wash, DC; Code FPO-1SP13 (T F Sullivan) Wash, DC; Code FPO-IP12 (Mr. Scola), Washington DC; Scheessele, Code 402, Wash, DC
NAVFACENGCOM - LANT DIV.; Eur. BR Deputy Dir, Naples Italy; RDT&ELO 09P2, Norfolk VA
NAVFACENGCOM - NORTH DIV, (Boretsky) Philadelphia, PA; Code 09P (LCDR A.J. Stewart); Code 1028, RDT&ELO, Philadelphia PA; Design Div. (R. Masino), Philadelphia PA; ROICC, Contracts, Crane IN
NAVFACENGCOM - PAC DIV, Code 402, RDT&E, Pearl Harbor HI; Commander, Pearl Harbor, HI
NAVFACENGCOM - SOUTH DIV, Code 90, RDT&ELO, Charleston SC; Dir., New Orleans LA
NAVFACENGCOM - WEST DIV, Code 04B; RDT&ELO Code 2011 San Bruno, CA
NAVFACENGCOM CONTRACT AROICC, Point Mugu CA; Eng Div dir, Southwest Pac, Manila, PI; OICC, Southwest Pac, Manila, PI; OICC/ROICC, Balboa Canal Zone; ROICC LANT DIV., Norfolk VA; ROICC, Diego Garcia Island; ROICC, Keflavik, Iceland
NAVHOSP LT R. Elsbernd, Puerto Rico
NAVMAG SCE, Guam
NAVOCEANSYSCEN Code 409 (D. G. Moore), San Diego CA
NAVPETOFF Code 30, Alexandria VA
NAVPGSCOL Code 61WL (O. Wilson) Monterey CA
NAVPHIBASE CO, ACB 2 Norfolk, VA; Code S3T, Norfolk VA; OIC, UCT ONE Norfolk, Va
NAVREGMEDCEN SCE (D. Kaye); SCE, Camp Pendleton CA
NAVSCOLCECOFF C35 Port Hueneme, CA; C44A (R. Chittenden), Port Hueneme CA; CO, Code C44A Port Hueneme, CA
NAVSEASYSCOM Code OOC (LT R. MacDougal), Washington DC
NAVSECGRUACT PWO, Torri Sta, Okinawa
NAVSHIPYD Code 404 (LT J. Riccio), Norfolk, Portsmouth VA; Code 410, Mare Is., Vallejo CA; Code 440 Portsmouth NH; Code 440, Norfolk; Code 440, Puget Sound, Bremerton WA; Code 440.4, Charleston SC; L.D. Vivian; PWO, Mare Is.; Tech Library, Vallejo, CA
NAVSTA CO Naval Station, Mayport FL; CO Roosevelt Roads P.R. Puerto Rico; Engr. Dir., Rota Spain; Maint. Div. Dir/Code 531, Rodman Canal Zone; PWD (LTJG.P.M. Motolenich), Puerto Rico; PWO Midway Island; PWO, Keflavik Iceland; PWO, Mayport FL; ROICC, Rota Spain; SCE, Guam; SCE, Subic Bay, R.P.; Utilities Engr Off. (LTJG A.S. Ritchie), Rota Spain
NAVSUBASE LTJG D.W. Peck, Groton, CT
NAVSUPPACT CO, Seattle WA; Code 413, Seattle WA; LTJG McGarrah, Vallejo CA
NAVSURFWPNCEN PWO, White Oak, Silver Spring, MD
NAVTECHTRACEN SCE, Pensacola FL
NAVWPNCEN Code 2636 (W. Bonner), China Lake CA; PWO (Code 26), China Lake CA; ROICC (Code 702), China Lake CA
NAVWPNSTA EARLE ENS G.A. Lowry, Fallbrook CA; PW Office (Code 09C1) Yorktown, VA
NAVWPNSUPPCEN Code 09 Crane IN
NCBU 405 OIC, San Diego, CA
CEC Petersen, Norman W., CAPT
NCBC CEL AOIC Port Hueneme CA; Code 155, Port Hueneme CA; Code 156, Port Hueneme, CA; PW Engrg, Gulfport MS
NCBU 411 OIC, Norfolk VA
NCR 20, Commander
NMCB 133 (ENS T.W. Nielsen); 5, Operations Dept.; Forty, CO; THREE, Operations Off.
NORDA Code 440 (Ocean Rsch Off) Bay St. Louis MS
NRL Code 8400 (J. Walsh), Washington DC; Code 8441 (R.A. Skop), Washington DC; Rosenthal, Code 8440, Wash. DC
NSD SCE, Subic Bay, R.P.
NUSC Code 131 New London, CT; Code EA123 (R.S. Munn), New London CT
ONR Code 700F Arlington VA; Dr. A. Laufer, Pasadena CA
PHIBCB 1 P&E, Coronado, CA
PMTC Pat. Counsel, Point Mugu CA
PWC ACE Office (LTJG St. Germain) Norfolk VA; CO Norfolk, VA; CO, Great Lakes IL; Code 116 (LTJG. A. Eckhart) Great Lakes, IL; Code 120C (Library) San Diego, CA; Code 128, Guam; Code 200, Great Lakes IL; Code 200, Oakland CA; Code 220 Oakland, CA; Code 220.1, Norfolk VA; Code 30C (Boettcher) San Diego, CA; Code 400, Pearl Harbor, HI; Code 680, San Diego CA; Library, Subic Bay, R.P.; OIC CBU-405, San Diego CA; Utilities Officer, Guam; XO Oakland, CA

SPCC Code 122B, Mechanicsburg, PA; PWO (Code 120) Mechanicsburg PA
U.S. MERCHANT MARINE ACADEMY Kings Point, NY (Reprint Custodian)
US DEPT OF INTERIOR Bureau of Land MNGMNT - Code 733 (T.E. Sullivan) Wash, DC
US GEOLOGICAL SURVEY Off. Marine Geology, Piteleki, Reston VA
USCG (G-ECV/61) (Burkhart) Washington, DC; G-EOE-4/61 (T. Dowd), Washington DC
USCG ACADEMY LT N. Stramandi, New London CT
USCG R&D CENTER D. Motherway, Groton CT
USNA Ocean Sys. Eng Dept (Dr. Monney) Annapolis, MD; PWD Engr. Div. (C. Bradford) Annapolis MD
CALIF. DEPT OF NAVIGATION & OCEAN DEV. Sacramento, CA (G. Armstrong)
CALIFORNIA STATE UNIVERSITY LONG BEACH, CA (CHELAPATI); LONG BEACH, CA (YEN)
COLORADO STATE UNIV., FOOTHILL CAMPUS Fort Collins (Nelson)
CORNELL UNIVERSITY Ithaca NY (Serials Dept, Engr Lib.)
DAMES & MOORE LIBRARY LOS ANGELES, CA
DUKE UNIV MEDICAL CENTER B. Muga, Durham NC; DURHAM, NC (VESIC)
FLORIDA ATLANTIC UNIVERSITY BOCA RATON, FL (MC ALLISTER); Boca Raton FL (Ocean Engr Dept., C. Lin)
FLORIDA ATLANTIC UNIVERSITY Boca Raton FL (W. Tessin)
FLORIDA TECHNOLOGICAL UNIVERSITY ORLANDO, FL (HARTMAN)
GEORGIA INSTITUTE OF TECHNOLOGY Atlanta GA (B. Mazanti)
IOWA STATE UNIVERSITY Ames IA (CE Dept, Handy)
VIRGINIA INST. OF MARINE SCI. Gloucester Point VA (Library)
LEHIGH UNIVERSITY BETHLEHEM, PA (MARINE GEOTECHNICAL LAB., RICHARDS); Bethlehem PA (Fritz Engr. Lab No. 13, Beedle); Bethlehem PA (Linderman Lib. No.30, Flecksteiner)
LIBRARY OF CONGRESS WASHINGTON, DC (SCIENCES & TECH DIV)
MICHIGAN TECHNOLOGICAL UNIVERSITY Houghton, MI (Haas)
MIT Cambridge MA; Cambridge MA (Rm 10-500, Tech. Reports, Engr. Lib.); Cambridge MA (Whitman)
NORTHWESTERN UNIV Z.P. Bazant Evanston IL
NY CITY COMMUNITY COLLEGE BROOKLYN, NY (LIBRARY)
UNIV. NOTRE DAME Katona, Notre Dame, IN
OREGON STATE UNIVERSITY (CE Dept Grace) Corvallis, OR; CORVALLIS, OR (CE DEPT, BELL); Corvalis OR (School of Oceanography)
PENNSYLVANIA STATE UNIVERSITY UNIVERSITY PARK, PA (GOTOLSKI)
PURDUE UNIVERSITY Lafayette IN (Leonards); Lafayette, IN (Altschaeffl); Lafayette, IN (CE Engr. Lib)
SAN DIEGO STATE UNIV. I. Noorany San Diego, CA; Dr. Krishnamoorthy, San Diego CA
SEATTLE U Prof Schwaegler Seattle WA
STANFORD UNIVERSITY Engr Lib, Stanford CA
TEXAS A&M UNIVERSITY COLLEGE STATION, TX (CE DEPT); College Station TX (CE Dept. Herbich)
UNIVERSITY OF CALIFORNIA BERKELEY, CA (CE DEPT, MITCHELL); DAVIS, CA (CE DEPT, TAYLOR); LIVERMORE, CA (LAWRENCE LIVERMORE LAB, TOKARZ); La Jolla CA (Acq. Dept, Lib. C-075A); M. Duncan, Berkeley CA; SAN DIEGO, CA, LA JOLLA, CA (SEROCKI)
UNIVERSITY OF DELAWARE Newark, DE (Dept of Civil Engineering, Chesson)
UNIVERSITY OF HAWAII HONOLULU, HI (SCIENCE AND TECH. DIV.)
UNIVERSITY OF ILLINOIS Metz Ref Rm, Urbana IL; URBANA, IL (DAVISSON); URBANA, IL (LIBRARY); URBANA, IL (NEWARK); Urbana IL (CE Dept, W. Gamble)
UNIVERSITY OF MASSACHUSETTS (Heronemus), Amherst MA CE Dept
UNIVERSITY OF MICHIGAN Ann Arbor MI (Richart)
UNIVERSITY OF NEBRASKA-LINCOLN Lincoln, NE (Ross Ice Shelf Proj.)
UNIVERSITY OF NEW MEXICO J Nielson-Engr Matls & Civil Sys Div, Albuquerque NM
UNIVERSITY OF TEXAS AT AUSTIN Austin TX (R. Olson)
UNIVERSITY OF WASHINGTON SEATTLE, WA (MERCHANT); SEATTLE, WA (OCEAN ENG RSCH LAB, GRAY); Seattle WA (E. Linger); Seattle, WA Transportation, Construction & Geom. Div
ATLANTIC RICHFIELD CO. DALLAS, TX (SMITH)
AUSTRALIA Dept. PW (A. Hicks), Melbourne
BECHTEL CORP. SAN FRANCISCO, CA (PHELPS)
BELGIUM HAECON, N.V., Gent
BETHLEHEM STEEL CO. Dismuke, Bethelehem, PA
BROWN & CALDWELL E M Saunders Walnut Creek, CA
BROWN & ROOT Houston TX (D. Ward)

CANADA Mem Univ Newfoundland (Chari), St Johns; Surveyor, Nenninger & Chenevert Inc., Montreal; Warnock Hersey Prof. Srv Ltd, La Sale, Quebec
CF BRAUN CO Du Bouchet, Murray Hill, NJ
CHEVRON OIL FIELD RESEARCH CO. LA HABRA, CA (BROOKS)
DRAVO CORP Pittsburgh PA (Giannino)
NORWAY DET NORSKE VERITAS (Library), Oslo
FRANCE Dr. Dutertre, Boulogne; L. Pliskin, Paris; P. Jensen, Boulogne
GEOTECHNICAL ENGINEERS INC. Winchester, MA (Paulding)
GLIDDEN CO. STRONGSVILLE, OH (RSCH LIB)
HALEY & ALDRICH, INC. Cambridge MA (Aldrich, Jr.)
HONEYWELL, INC. Minneapolis MN (Residential Engr Lib.)
ITALY M. Caironi, Milan; Sergio Tattoni Milano; Torino (F. Levi)
LAMONT-DOHERTY GEOLOGICAL OBSERV. Palisades NY (McCoy); Palisades NY (Selwyn)
LOCKHEED OCEAN LABORATORY San Diego CA (F. Simpson)
MARATHON OIL CO Houston TX (C. Seay)
MC CLELLAND ENGINEERS INC Houston TX (B. McClelland)
MEDALL & ASSOC. INC. J.T. GAFFEY II SANTA ANA, CA
MOBIL PIPE LINE CO. DALLAS, TX MGR OF ENGR (NOACK)
MUESER, RUTLEDGE, WENTWORTH AND JOHNSTON NEW YORK (RICHARDS)
NEW ZEALAND New Zealand Concrete Research Assoc. (Librarian), Porirua
NORWAY DET NORSKE VERITAS (Roren) Oslo; I. Foss, Oslo; J. Creed, Ski; Norwegian Tech Univ (Brandtzaeg), Trondheim
PORTLAND CEMENT ASSOC. Skokie IL (Rsch & Dev Lab, Lib.)
PRESCON CORP TOWSON, MD (KELLER)
RAND CORP. Santa Monica CA (A. Laupa)
RAYMOND INTERNATIONAL INC. E Colle Soil Tech Dept, Pennsauken, NJ
SANDIA LABORATORIES Library Div., Livermore CA
SEATECH CORP. MIAMI, FL (PERONI)
SHELL DEVELOPMENT CO. Houston TX (E. Doyle)
SHELL OIL CO. HOUSTON, TX (MARSHALL)
SWEDEN GeoTech Inst
TIDEWATER CONSTR. CO Norfolk VA (Fowler)
TRW SYSTEMS REDONDO BEACH, CA (DAI)
UNITED KINGDOM D. New, G. Maunsell & Partners, London; Shaw & Hatton (F. Hansen), London; Taylor, Woodrow Constr (014P), Southall, Middlesex
WOODWARD-CLYDE CONSULTANTS (A. Harrigan) San Francisco; PLYMOUTH MEETING PA (CROSS, III)
AL SMOOTS Los Angeles, CA
BARA, JOHN P. Lakewood, CO
BROWN, ROBERT University, AL
BULLOCK La Canada
F. HEUZE Boulder CO
R.F. BESIER Old Saybrook CT
T.W. MERMEL Washington DC

END
3-79